Characterisation of novel culturing systems for the *in vitro* expansion of haematopoietic stem cells

Fiona Bain

PhD

University of York
Biology
September 2024

Abstract

Haematopoietic stem cell (HSC) self-renewal is essential for the development and homeostasis of the blood system. Self-renewal expansion divisions where one HSC makes two equally potent daughter HSCs can be harnessed to create large numbers of HSCs for cell and gene therapies.

Although mouse and human HSCs can be expanded *in vitro* to unprecedented levels using recently developed expansion cultures, not all cells in culture maintain stem cell properties. Chapter 4 of this thesis focused on refining the identification of functional expanded HSCs by using ESAM as a novel marker and replacing the need for the $Fgd5^{ZsGreen\cdot ZsGreen/+}$ reporter, which in turn averts the need to cross genetically modified mice onto the Fgd5 background in order to permit HSC identification.

Successive chapters (5 and 6) focused on the newly described expansion system for human HSCs - focusing initially on establishing this system for cord blood samples and testing further refinements to this expansion protocol via the supplementation of additional molecules to the culture media to increase HSC frequency. Chapter 5 of this thesis successfully applied this culture system to expansion of previously difficult to culture peripheral blood samples from healthy individuals and patients with early-stage blood cancers.

This thesis then aimed to unpick the specific roles of cytokine agonists used in the human HSC culture media, specifically the thrombopoietin-mimetic butyzamide - a strong candidate for culture refinement which could alter downstream signalling and therefore culture success. To elucidate the effects of butyzamide versus alterative thrombopoietin (TPO) mimetics, in Chapter 6, receptor internalisation assays, fluorescent cell barcoding with phospho-flow cytometry, and phosphoprotomics were used on cell lines expressing either wild-type TPO-receptor (MPL), or $JAK2^{V617F}$ mutated MPL, and have identified key differences which may be exploitable for further improving and modulating cultures for therapeutic purposes

Author declaration

I declare that this thesis is a presentation of original work and I am the sole author. This work has not previously been presented for a degree or other qualification at this University or elsewhere. All sources are acknowledged as references.

Sections of the introduction are based off of my first author review, “Lessons from early life: understanding development to expand stem cells and treat cancers”, Bain et al., Development, 2022. ESAM as a novel marker for functional expanded HSCs was published in “Identification and characterization of in vitro expanded hematopoietic stem cells”, Che and Bode, EMRO Rep. 2022.

Experiments performed in collaboration with others are noted below:

Results chapter 1

All work was conducted under the supervision of Dr David Kent. Sorting of mouse ESLAM cells was performed by Karen Hogg and Graeme Park at the University of York Technology Facility. HSC transplantation and peripheral blood bleeds throughout this chapter were performed by Grace Boyd, Ellie Bennett, and Joanna Milek. Culturing and phenotyping of cells before transplantation, and flow cytometric analysis to determine chimerism was performed by myself. One of the ESAM transplantations (Figure 4.4) was performed in collaboration with Maria Jassinskaja. CD321 flow cytometric data was analysed via Maria Jassinskaja (Section 4.3). Split culture data was generated in collaboration with Juan Rubio-Lara (Section 4.6), and schematic Figure 4.12a was created by Juan Rubio-Lara. Full length versus truncated TPO screens (Section 4.9), and MPL^+ versus MPL^- mouse PVA expansion cultures (Section 4.10) were performed in collaboration with Katie West and Lucie Moss, members of the Hitchcock Lab at York. Picowell development and fabrication was taught to me, and originally performed by Christopher Reardon.

Results chapter 2

All work was conducted under the supervision of Dr David Kent. Sorting of human $CD34^+$ cells was performed by Karen Hogg and Graeme Park at the University of York Technology Facility. Initial direct comparison between 3a and StemSpan cultures was performed in collaboration with Juan Rubio-Lara, and William Grey (Section 5.1). The testing of human cord blood expansion in gels versus on plastic, and comparisons between Soluplus and Dextran were performed in collaboration with Juan Rubio-Lara. Experiments involving sorting healthy donor and MPN patient samples for $MPL^{+/-}$ and successive expansion /

imaging / MPL quantification were performed in collaboration with Katie West (Sections 5.3, 5.5, 5.6, 5.7).

Results chapter 3

All work was conducted under the supervision of Dr David Kent. Initial 3a expansion culture screens comparing butyzamide to TPO and alternative TPO mimetics, and testing Flt3L in 3a cultures were performed in collaboration with Juan Rubio-Lara (Sections 6.1, 6.2). TPO internalisation assays were taught to my by Katie West, and 1 of the 3 repeats included in the data was performed by me (Section 6.3). Fluorescent barcoding and phosphoflow of TPO/TPO mimetic stimulated UT7 cells was taught to me by Katie West, and independent repeats performed by myself and Katie West comprised the final data (Section 6.4). Phosphoroteomic data, and low cell number proteomic samples were prepared in collaboration with Katie West, and samples were run on the TimsTOF by Adam Dowle, Chloe Baldreki in the Technology Facility at the University of York (Section 6.5, 6.6, 6.7)

Acknowledgements

I am so grateful for all of the support from my family, friends, and colleagues over the course of my PhD.

I would first like to thank Dr David Kent for being such an amazing and inspiring supervisor. He has taught me so much, both as a scientist and as a professional away from the bench – getting to complete a PhD in the Kent lab has truly shaped me as a person.

I would also love to thank all of my friends and colleagues at the University of York, past and present, in particular Katie West, Monika Gonka, Alyssa Cull, Lily Cabrera Cosme, Maria Jassinskaja, Lizzy Morritt, Zoe Ingold, Ellie Bennett, Joanna Milek, Lucie Moss, Razan Alhefzi, Juan Rubio-Lara, Jillian Barlow, Sam Elberfeld, Grace Boyd, Alex Hogg, Sophie Davies, Leah Etheridge, Ian Hitchcock and Rasha Rezk. I have learnt so much from you all, it has been a true collaborative effort, and I have made some really great friends.

On top of that, I would like to thank the Technology Facility staff at the University of York, without which this project would not have been possible, in particular Karen Hogg, Graeme Park, Karen Hodgkinson, Sukhveer Mann, Adam Dowle, Chloe Baldreki and Chris Taylor – thank you all so much!

I would finally like to thank my brother, Tom, and my parents Joanne and John who have been cheering me on throughout , and my partner Patrick who has been there to support me all the way.

Abbreviations

AGM; aorta-gonad-mesonephros

ALCAM; activated leukocyte cell adhesion molecule

ALL; acute lymphoblastic leukaemia

AML; acute myeloid leukaemia

ANGPT1; angiopoietin-1

AP2; adaptor protein 2

ATAC-Seq; assay for accessible chromatin with sequencing

BCA; bicinchoninic acid assay

BM; bone marrow

BMT; bone marrow transplant

BrdU; Bromodeoxyuridine

CAFC; cobblestone area-forming cell assay

CALR; calreticulin

CB; cord blood

CFU-S; colony forming unit - spleen

CH; clonal haematopoiesis

ChIP-seq; chromatin immunoprecipitation sequencing

CLASP1; cytoplasmic linker associated protein 1

CLL; chronic lymphoblastic leukaemia

CLP; common lymphoid progenitor

CML; chronic myeloid leukaemia

CMP; common myeloid progenitor

CXCL12; chemokine (C-X-C motif) ligand-12

cyTOF; cytometry by time of flight

DDA; data dependent acquisition

DIA; data independent acquisition

DMR; differentially methylated region

DNMT; DNA methyltransferase

E; embryonic day

ECM; extracellular matrix

ELSK; $EPCR^{+}Lineage^{-}Sca1^{+}cKit^{+}$

EELSK; ESAM^{+}EPCR^{+}Lineage^{-}Sca1^{+}cKit^{+}

EHT; endothelial to haematopoietic transition

EMPs; erythro-myeloid progenitors

ESAM; endothelial selective adhesion molecule

ET; essential thrombocytopenia

FACS; fluorescence activated cell sorting

FBS; foetal bovine serum

FDR; false discovery rate

FELSK; Fgd5+EPCR^{+}Lineage^{-}Sca1^{+}cKit^{+}

FL; foetal liver

Flt3; fms like tyrosine kinase 3

Flt3L; Flt3-ligand

G-CSF; granulocyte colony-stimulating factor

GEF; guanosine exchange factor

GFP; green fluorescent protein

GM; granulocyte macrophage

GMPs; granulocyte-monocyte progenitors

GRN; gene regulatory network

HIF-1α; hypoxia-inducible factor 1-α

HLA; human leukocyte antigen

HSC; haematopoietic stem cell

HSCT; haematopoietic stem cell transplantation

HSPC; haematopoietic stem and progenitor cell

IFN; interferon

IL: interleukin

iNKT cell: innate natural killer T-cell

IT-HSC; intermediate term HSC

JAK; janus kinase

LDA; limiting dilution assay

Lin; lineage

LMPP; lymphomyeloid primed progenitors

lncRNA; long non-coding RNA

LSK; Lineage^{-}Sca1^{+}cKit^{+}

LTC-IC; long term culture initiating cell

LT-HSC; long term HSC

MACS; magnetic cell separation

MAPK; mitogen-activated protein kinase

MERPs; megakaryocyte erythroid restricted progenitors

MEPs; megakaryocyte erythroid progenitors

MF; myelofibrosis

MFI; mean fluorescent intensity

miRNA; micro RNA

MkRPs; megakaryocyte restricted progenitors

MNC; mononuclear cell

MolO; molecular overlap

MPL; myeloproliferative leukaemia protein

MPN; myeloproliferative neoplasm

MPP; multipotent progenitor

MTG; monothioglycerol

NK; natural killer

NO; nitric oxide

P; postnatal day

PASEF; parallel accumulation-serial fragmentation

PASEF-DDA; parallel accumulation-serial fragmentation with data dependent acquisition

PB; peripheral blood

PcG; polycomb group

PCL; polycaprolactone

PDMS; polydimethylsiloxane

PET; polyethylene terephthalate

pHSC; phenotypic HSC

PU; polyurethane

PV; polycythaemia vera

PVA; polyvinyl alcohol

qPCR; quantitative PCR

ROS; reactive oxygen species

SCF; stem cell factor

scRNA-seq; single cell RNA-sequencing

SLAM; Signalling Lymphocyte Activation Molecules

SPRED1; sprout-related EVH1 domain-containing protein 1

SR1; StemRegenin1

ST-HSC; short term HSC

TCR; t-cell receptor

TF; transcription factor

TMT; tandem mass tag

TR; truncated

TPO; thrombopoietin

VEGF; vascular endothelial growth factor

VF; $JAK2^{V617F}$ mutated

WT; wild-type

Table of Contents

Table of Figures

List of Tables

1 Introduction

1.1 Haematopoiesis

The blood system is an incredibly productive tissue, with estimates of 1 trillion blood cells being produced and destroyed by the body each day (Johnson et al., 2024). Blood is a liquid tissue, consisting of an aqueous plasma and several specialised cell populations, each with specific biological roles. The two key functions of the blood system are firstly, to produce all of the immune cells in the organism, and secondly, to facilitate the transport of various nutrients, signalling molecules, gases such as oxygen and carbon dioxide, as well as several essential hormones around the body. The process of blood development is known as haematopoiesis and it is a hierarchically organised process. At the apex of this hierarchy sit the haematopoietic stem cells (HSCs), a population of rare cells that exist predominantly in the bone marrow (BM). HSCs are generally quiescent until called upon to divide in response to stimuli such as bleeding or infection, where an increase in mature blood cell output is required. This quiescent state, known as G_0, protects HSCs from spontaneous DNA damage acquired naturally through cell division, and is one mechanism hypothesised to increase their longevity and genome stability (Walter et al., 2015).

HSCs have two hallmarks features – firstly they are able to undergo self-renew expansion divisions, a process whereby one parent HSC produces two functionally identical and equally undifferentiated daughter cells. Secondly, they have the capacity to differentiate into all of the mature cell types of the blood system. The capacity of HSCs to divide either symmetrically or asymmetrically, generating either 0, 1, or 2 daughter HSCs from one parent HSC, is important to the stability of the haematopoietic system and the maintenance of the HSC pool. This balance is therefore tightly controlled. Unrestrained HSC self-renewal coupled with a block in differentiation can lead to the development of a range of haematological diseases and, in extreme cases where this unregulated growth is maintained, the development of leukaemias. On the other hand, excessive differentiation coupled with insufficient self-renewal will result in the exhaustion of the HSC pool (Eaves, 2014). Fundamental to the regulation of this system is a decrease in self-renewal capacity in the progeny of HSCs whereby gradual fate restriction occurs as cells differentiate into highly proliferative progenitor intermediaries, which in turn undergo further differentiation into terminally differentiated mature blood cells (Doulatov et al., 2012, Seita and Weissman., 2010).

The mature haematopoietic cells, at the base of the haematopoietic hierarchy, can be broadly subdivided into either myelo-erythroid or lymphoid cells. Historically, these cells were

proposed to originate from intermediary progenitors – either common myeloid progenitors (CMPs) or common lymphoid progenitors (CLPs), both of which are more specific in terms of their differentiation capacity than HSCs, but are still multipotent cells (Akashi et al., 2000, Eaves, 2014). However, more recently, questions over the existence of a definitive CLP have shifted the field towards the use of multipotent progenitor (MPP) and lympho-myeloid primed progenitor (LMPP) terminology. LMPPs are originally multi-lineage primed, and express low levels of both lymphoid and myeloid lineage mRNAs (Pooter et al., 2019). However, over time a fraction of the LMPP pool will lose their myeloid lineage potential, become limited to lymphoid differentiation - a process linked to positive regulation of lymphoid gene expression programs by key transcription factors *E2A*, *HEB*, *Tal1* and *Ly11* (Zohren et al., 2013, Dias et al., 2008, de Pooter et al., 2019).

Myeloid cell types include erythrocytes, monocytes, granulocytes, megakaryocytes, thrombocytes, mast cells and macrophages, whilst lymphoid cell types include T- cells, B-cells, innate lymphoid cells, and dendritic cells (Kondo et al., 2010). Each of these cell types are specialised to their specific roles in either nutrient supply or the body's response to infection, and are discussed in detail in Table 1.

Cell type	Function	References
Erythrocyte	The most common cell type present in the blood – these anucleate cells are essential for oxygen transport and comprise approximately 40-45% of the total blood volume	Pretini et al., 2019
Monocyte	Monocytes generate both macrophages and a subtype of dendritic cells arising from the myeloid lineage.	Karlmark et al., 2012
Granulocyte	Granulocytes, the most common leukocytes, can be subdivided into three classes – eosinophils, neutrophils and basophils. Basophils release granules containing histamine, cytokines, and leukotrienes, and therefore have key roles in the allergic response . Neutrophils and eosinophils are both involved in the phagocytosis of pathogenic bacteria and parasites, whilst neutrophils are additionally capable of NETosis – the reactive oxygen species (ROS) dependent release of modified chromatin coated in bactericidal proteins.	Shah et al., 2021 Vorobjeva et al., 2020

Megakaryocyte	The largest of the mature blood cells, megakaryocytes are essential for the production of thrombocytes (platelets) and therefore are essential in the processes of haemostasis and thrombosis.	Geddis, 2010
Thrombocyte	Thrombocytes (or platelets) are able to bind to each other and the exposed endothelium below injured vascular walls, allowing them to form a platelet plug – protecting the organism from blood loss.	Holinstat, 2017
Macrophage	Macrophages are innate immune cells and use phagocytosis as a first line of defence to protect the host from pathogens, infected cells, and tumour cells.	Luo et al., 2018 Lundeckel et al., 2022
Mast cell	Mast cells are innate immune cells which degranulate to release a range of molecules such as histamine, pro-angiogenic factors such as vascular endothelial growth factors (VEGF) Interleukin 8 (IL-8), and inflammatory cytokines such as IL-4. As a result, they have been shown to regulate vasodilation as well as the immune response.	Krystel-Whittemore et al., 2015 Gilfillan and Beaven, 2011
T-cell	T-cells are adaptive immune cells, and can be classified further into T-helper, and cytotoxic T-cells. T-Killer cells induce apoptosis in cells capable of binding to the T-cell receptor (TCR), whilst T helper cells secrete the required cytokines to facilitate this process. Additionally, secretions from T-helper cells support the activity of macrophages and B-cells. A rare subtype of T-cells are the specialised innate natural killer T-cells (iNKT cells), which bridge the gap between natural killer (NK) cells and T-cells.	Raskov et al., 2021 Saravia et al., 2019 Brennan et al., 2013
B-cell	B-cells are adaptive immune cells, which upon stimulation by a foreign antigen or pathogenic secreted molecule, undergo clonal selection and expansion, before differentiating into plasma cells. As plasma cells they are able to release antibodies, capable of binding to and neutralising pathogenic antigens.	Hoffman et al., 2016 LeBien and Tedder, 2008

Innate lymphoid cells (ILCs)	Cytotoxic natural killer cells are a subset of ILCs and are rapidly responding lymphoid cells essential in protecting the host from viral infections and tumour cells. Unlike T and B cells, they do not depend on the expression of an antigen to respond to infection.	Vivier et al., 2011
Dendritic	Dendritic cells are essential for antigen presentation to T- and B-cells in order to orchestrate an efficient immune response. They have roles in moderating the immune response – ensuring tolerance of harmless antigens. Dendritic cells are dual origin - with subtypes arising from both lymphoid and myeloid precursors and provide a link between the innate and adaptive immune systems.	Manz et al., 2001 Zink et al., 2021

Table 1.1 **Function of cell types present in the blood.** Mature blood cells can be broadly categorised into two lineages – myeloid and lymphoid. Here, cell types are coloured based on the classification. Blue = myeloid, Yellow = lymphoid, Green = both myeloid and lymphoid origin.

1.1.1 Haematopoietic homeostasis and fate choice

The haematopoietic system relies on tight regulation to protect against the development of haematological malignancies or the exhaustion of the stem cell pool. Yet, it must also meet the body's need to adapt to external environmental changes and stimuli such as infection (Haas et al., 2015), blood loss (Walter et al.,2015), or drug-induced stresses such as chemotherapy (Batsivari et al., 2020). The ability of a single transplanted HSC to repopulate the entire blood system of an irradiated recipient is a prime example of this ability to respond to external stresses, and the direct effect of environmental stimuli on the activity of these cells (Osawa et al., 1996). The "fate choice" to self-renew and maintain their own pool, to differentiate into several potential alternative cell lineages, or to undergo apoptosis, made by haematopoietic stem and progenitor cells (HSPCs) as they progress through the haematopoietic hierarchy, is therefore tightly regulated by several key intrinsic and extrinsic signals. This ensures the correct production of the required cell types in the necessary quantity (Wilkinson et al., 2020). These regulatory mechanisms will be discussed in detail later in this thesis.

1.2 Haematopoietic Stem Cells (HSCs)

1.2.1 Discovery of HSCs

The first bone marrow transplantation (BMT) in human patients was performed in 1959 and demonstrated the capacity of BM cells to successfully sustain lifelong haematopoiesis in the recipient (Thomas et al., 1959, Thomas et al., 1957). Quickly following this, the first formal evidence for the existence of a single progenitor possessing both multi-lineage differentiation and the capacity to self-renew was collected in the 1960s in seminal experiments performed by Till and McCulloch (Till and McCulloch, 1961, Till et al., 1964). These quantitative spleen colony-forming assays demonstrated the capacity of transplanted BM samples to generate multi-lineage and serially transplantable macroscopic colonies of single cell origin on the spleens of irradiated recipient mice. The ability of these colonies, containing multiple cell types originating from a single common parent cell, to successfully transplant into a secondary mouse demonstrated that these cells were capable of self-renewal. Taken together, data from these key experiments identify the presence of a functional multipotent, and self-renewing cell population in the bone marrow, and calculated their frequency at approximately 1 in 10,000 BM cells (Till and McCullcoh., 1961, Abramson et al., 1977). Furthermore, these early experiments highlighted the heterogeneity within this pool of cells, with differences in proliferation rates and differentiation potential noted between cells capable of forming these colonies.

Following on from these key discoveries, the field of haematopoiesis turned to focus on the identification and purification of functional HSC populations, and by 1996 the first single HSC transplantation was performed using a $CD34^{-/low}$ $cKit^{+}$ Stem cell antigen-1 $(Sca1)^{+}$ Lineage $(Lin)^{-}$ cell (Osawa et al., in 1996). This transplantation highlighted the capacity of a single cell to perform these repopulating functions on its own, allowing researchers to differentiate between true HSCs and progenitors which retained multilineage potential but were not capable of long-term reconstitution. This led to the discovery and classification of both long term (LT) HSCs and, transiently repopulating but still multi-lineage, short term (ST) HSCs.

1.2.2 The haematopoietic hierarchy

Since the idea of a hierarchically organised haematopoietic system was theorised, this concept has been developed and re-evaluated several times. The earliest models for the haematopoietic hierarchy described a bifurcation model, where LT-HSCs at the peak of the hierarchy progress to ST-HSCs, before reaching a MPP stage (Woolthius and Park, 2016). Here, at a key bifurcation point, MPPs differentiate into either CMPs, capable of differentiating into all mature myeloid cells, or into CLPs capable of generating mature

lymphoid cells (Akashi et al., 2016, Kondo et al., 1997). Despite this classical model for haematopoiesis presenting a clear and simple description of this complex system, and useful for understanding the premise of differentiation, it was based on bulk transplantation and *in vitro* data, and broadly assumed that each individual cell expressing the same surface marker combination was functionally identical. Developments in technology, especially single cell approaches, have allowed HSC heterogeneity and the hierarchy of haematopoiesis to be considered and further refined (Cheng et al., 2020).

Over time, these models have become increasingly complex, in order to reflect more recently discovered mature cell biases that exist within the phenotypic HSC fraction (Sanjan-Pla et al., 2013, Dykstra et al., 2007, Muller-Sieburg et al., 2002, Muller-Sieburg et al., 2004). This bias has been highlighted in genetic barcoding experiments, combined with high-throughput sequencing, which revealed the extent of this heterogeneity, and showed that HSCs do not contribute equally to all lineages (Lu et al., 2011). Additional single cell transplantation studies revealed that lineage-restricted progenitors capable of self-renewal exist within the phenotypic HSC fraction, specifically the existence of uni-, bi-, and oligo-potent cells within this population (Yamamoto et al., 2013). Taken together, this accumulation of data implies that significant overarching lineage decisions may be occurring at the very first stages of development, rather than at the progenitor level (Woolthius and Park, 2016).

An important example of this early-stage priming of differentiation is the discovery of megakaryocyte-biased HSCs, which proved capable of generating megakaryocyte progenitors directly, bypassing the intermediary progenitors entirely (Sanjuan-Pla et al., 2013). However, rebuttals to this study argue that this finding results from contamination within the HSC compartment with megakaryocyte progenitors capable of transient self-renewal (Roch et al., 2015). Despite this, more recent studies in mice have demonstrated the existence of a distinct stem cell pool capable of exclusively platelet differentiation, which do not rely on the typical haematopoietic differentiation hierarchy to produce molecularly unique megakaryocyte-restricted progenitors (Carrelha et al., 2024). This study defined two differentiation pathways downstream of these restricted stem cell populations - a slower multipotent pathway, and a rapid, so called “emergency-activated” platelet differentiation pathway. Using single cell transplantations and paired daughter cell assays Yamamoto et al., 2013 also identified megakaryocyte and megakaryocyte-erythroid restricted progenitors (MkRPs, MERPs), within the HSC pool, and confirmed that phenotypic HSCs are capable of dividing asymmetrically in order to directly generate HSC-MkRP and HSC-MERP cell outputs. Additional studies utilising molecular barcoding approaches and sequential single cell RNA-seq of human bone marrow HSCs (BM-HSCs) following xenograft, confirmed the

existence of a platelet-biased HSC fraction, which increases in prevalence with HSC age (Aksöz et al., 2024).

The advancement of novel single-cell approaches to study the hematopoietic hierarchy, such as single-cell transcriptomics, has enabled a more thorough examination of the varying molecular states that accompany HSC differentiation throughout all stages of the haematopoietic hierarchy (Nestorowa et al., 2016). These approaches shine light on the significant heterogeneity within the HSPC pool and revealed the hierarchy to be a gradual continuum between increasingly differentiated cells, rather than set, distinctive populations (Laurenti and Gottgens, 2018). In line with this, over the course of differentiation, incremental changes in the transcriptome of the cells occur as lineage-specific traits are acquired (Velten et al., 2017, Macaulay et al., 2016, Laurenti and Gottgens, 2018). An illustration outlining the discrete and continuous haematopoietic models is shown in Figure 1.1.

Overall, despite our ever increasing understanding of heterogeneity within the stem cell pool, haematopoiesis is still generally considered a hierarchical continuum, with HSCs sitting at the apex of the hierarchy, and being the original source of all mature cells of the blood system. Whilst exceptions to the more generalised hierarchical structure are coming to light, such as the existence of platelet and megakaryocyte-restricted fractions within the HSC compartment, and the likely discovery of more lineage-biased populations within this fraction in the future, the hierarchy model still largely remains relevant.

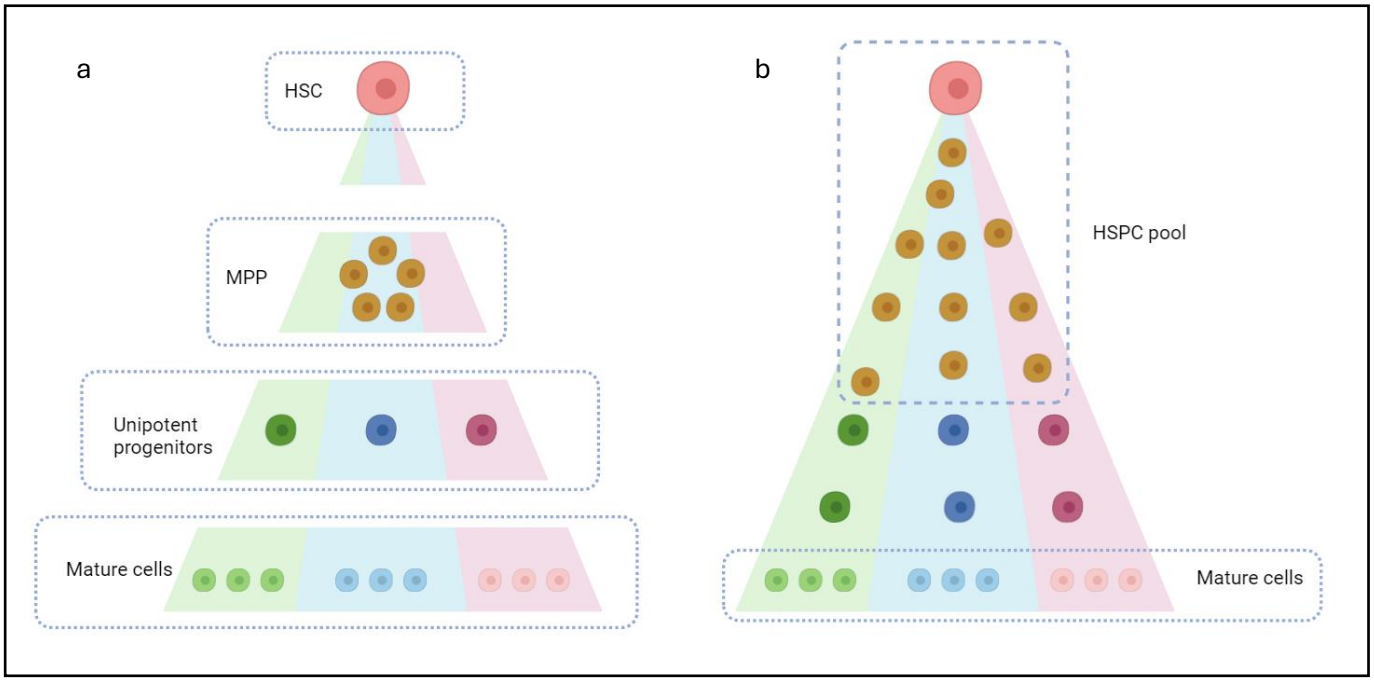

Figure 1.1 **Discrete versus continuous haematopoietic hierarchy.** Adapted from Cheng et al., 2020. a) A discrete model for the haematopoietic hierarchy shows the stepwise differentiation from immature, undifferentiated HSC to mature, terminally differentiated cell via discrete, defined cell populations of MPPs and unipotent progenitors. b) The continuous model for differentiation blurs the boundaries in the hierarchy, where cells acquire lineage traits and biases in a gradual, continuous process, matched by incremental changes in the transcriptome of the cells. Made in BioRender.

1.2.3 HSCs in development

Developmental haematopoiesis in mice occurs in separate waves, referred to as primitive and definitive (Dzierzak et al., 2018, Ottersbach et al., 2010). Primitive, HSC-independent, haematopoiesis is first observed around embryonic day (E) 7.5 in mice (E17 in humans) in the yolk sac blood islands. In this wave, erythro-myeloid progenitors (EMPs) are formed in order to provide the early embryo with red blood cells and macrophages, the latter of which persist in adult life as tissue-resident immune cells (e.g. microglia, Langerhans cells, and Kupffer cells) (Dzierzak and Medvinsky 1995, Mirshekar-Syahkal et al., 2014). EMPs are now considered definitive embryonic progenitors, presenting with a marked difference in immunophenotype and function compared with primitive haematopoietic progenitor populations (Frame et al., 2016, McGrath et al., 2015).

The second primitive wave produces some early myeloid and lymphoid cell types, including IL-7RA expressing lymphomyeloid primed progenitors (LMPPs) (Böiers et al., 2013). However, because these primitive cells lack long-term self-renewal capacity, the primitive

wave is considered transient (Orkin and Zon, 2008). Definitive haematopoiesis begins subsequently at E10.5 (E21 in human) in the aorta gonad mesonephros (AGM) region, generating the first transplantable, definitive HSCs (Mikkola et al., 2005, Dzierzak et al., 2002, Buckley et al., 2011). These rare, multipotent cells are produced from the haemogenic endothelium via endothelial to haematopoietic transition (EHT). This involves a series of controlled morphological changes occurring in the vascular wall of the main embryonic arteries. This process is triggered by the onset of circulation and has been experimentally shown to be dependent on both *Runx1* and *Tal1* (Shivdasani et al.,1995, Okuda et al., 1996). The onset of circulation and the associated production of nitric oxide (NO) from closely associated vascular endothelial cells have been shown to be essential regulators of haematopoiesis, with their influence beginning as early as the initiation of HSC formation in the AGM (North et al., 2009; Adamo et al., 2009). Exemplifying this, HSCs in *Ncx*$^{-/-}$ (also known as *Slc8a1*) mice, which completely lack a circulation, are unable to develop past the pro-HSC stage, remaining functionally impaired with a dysregulated metabolism and an inability to activate the *Runx1* pathway (Azzoni et al., 2021).

Alternative sites of definitive haematopoiesis have also been described, including the placenta (Mikkola et al., 2005; Gekas et al., 2010); however, some controversy around the magnitude of this contribution remains (Huang et al., 2007). The extravasation of HSCs into circulation enables them to migrate to the upcoming haematopoietic sites (Horton et al., 2021). Following a brief HSC expansion period in the placenta (Gekas et al., 2010), the foetal liver (FL) becomes the main site of definitive haematopoiesis by E11 and E12, with the most rapid phase of HSC expansion occurring at approximately E14.5, until HSCs migrate to the spleen (Christensen et al., 2004) and the BM just before birth. Splenic haematopoiesis remains active until approximately two weeks after birth; from then on, and throughout adulthood, the BM is the primary site of HSCs and haematopoiesis (Rowe et al., 2016) with HSCs largely acting as a dormant reservoir of non-dividing cells.

Postnatally, there is a dramatic switch in HSC characteristics that occurs between 3-4 weeks in mice (Bowie et al., 2007, Copley et al., 2013, Kim et al., 2007). Multiple foetal specific characteristics are lost, and an adult HSC phenotype is established. This includes entering a state of quiescence with reduced rates of translation (Kohli et al., 2014), a shift from oxidative phosphorylation to anaerobic, glycolytic based metabolism (Kohli et al., 2014, Manesia et al., 2015, Yu et al., 2013), a shift in the expression of key HSC regulators (Bowie et al., 2007, Kim et al., 2007, Copley et al., 2013, Jassinskaja et al., 2017), and a re-balancing of mature cell outputs (Signer et al., 2014). This is further accompanied by a switch from the production of an innate-like lymphoid compartment (Ikuta et al., 1990; Hardy

and Hayakawa, 1991) towards the production of adaptive T- and B- cells (Gilfillan et al., 1993) and, during the final stages of the foetal-to-adult switch at 3-4 weeks, bone mineralisation significantly increases, perhaps indicative of a larger organismal transition period (Ferguson et al., 2003). Interestingly, there is also a metabolic switch that developing HSCs undergo and this is additionally associated with a decrease in ROS levels (Pimkova et al., 2022), and maintenance of a ROS^{low} state which is essential for adult HSC function (Ito et al., 2004; Ito et al., 2006). Importantly, as adult HSCs initiate differentiation, they undergo a further metabolic switch back to oxidative phosphorylation which becomes the primary energy source for downstream progenitors, enabling a larger energy output (Figure 1.2).

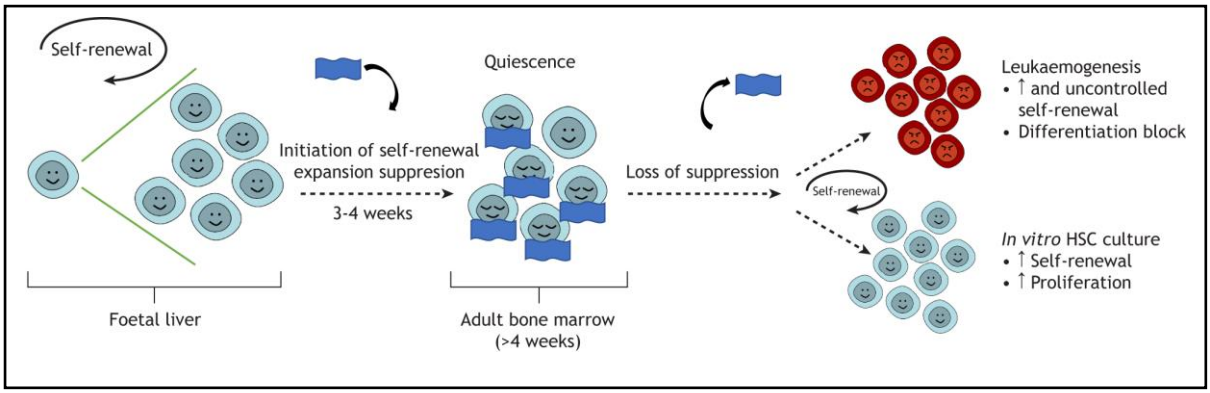

Figure 1.2 **Regulation of HSC self-renewal during life.** Taken from Bain et al., 2022. During development, particularly in the foetal liver, HSC self-renewal expansion divisions occur in order to produce HSCs to sustain lifelong haematopoiesis. Postnatally, at approximately 3-4 weeks of age in mice, this self-renewal expansion is suppressed (represented by the blue blanket) as HSCs transition to a largely quiescent population. The loss of this suppression of proliferation can result in the aberrant accumulation of immature HSC-like cells (e.g. in leukaemia), but may also be harnessed to expand HSCs transiently outside the body for clinical utility. Made in BioRender.

Recent work has shown that although most molecular changes in developing HSCs are uncoordinated at a single-cell level, nearly all HSCs show a transient spike in type I interferon (IFN) signalling and expression of associated genes between E16.5 and postnatal day (P) 0 (Li and Magee, 2021). These findings correspond with previous work showing that differential expression of type I IFN-associated transcripts and proteins is one of the key molecular differences between FL and adult HSCs (McKinney-Freeman et al., 2012; Kim et al., 2016; Jassinskaja et al., 2017), and other studies identify type I IFN signalling as a driver of AGM HSC generation and maturation (Kim et al., 2016; Li et al., 2014).

Several genes have been linked directly to the regulation of FL or adult HSCs. The Lin28b-let7-Hmga2 axis has been shown to be a key pathway, and master regulator, of the FL state (Copley et al., 2013; Rowe et al., 2016a,b). In FL HSCs, *Lin28b* and *Igf2bp3* maintain the foetal HSC phenotype by forming a complex that stabilises the expression of key FL HSC genes (including *Hmga2* and *Arid3a*). Importantly, both *Lin28b* and *Igfb3* are downregulated postnatally and so are effectively foetal specific. Inducing ectopic expression of *Lin28b and Igf2bp3* is enough to revert adult HSCs to a phenotypically foetal state, and this is accompanied by an associated increase in proliferation and erythroid bias. These induced foetal-like cells are also able to generate foetal-specific IL-7RA-expressing LMPPs and have an increased capacity to generate innate-like B-cell subsets (Rowe et al., 2016a,b; Wang et al., 2019; Kristiansen et al., 2016). A number of other genes have been identified to be exclusively important for embryonic HSCs, such as *Runx1* (Okuda et al., 1996; Chen et al., 2009; Wilson et al., 2011; Wilkinson and Gottgens, 2013) and *Ezh2* (Mochizuki-Kashio et al., 2011), whilst a further gene set specific for adult HSCs, such as *Bmi1* (Park et al., 2003), *Gfi1* (Wilson et al., 2010) and *Cebpa* (Ye et al., 2013) has also been identified. Perhaps the most comprehensive study of the foetal-to-adult transition revealed *Sox17* as a foetal and neonatal HSC-specific gene, with little to no expression detected in adult HSCs (Kim et al., 2007). Here, an induced germline deletion of *Sox17* resulted in the lack of any detectable HSCs, whereas conditional deletion of *Sox17* from the endothelial cell and embryonic HSC compartments using a *Tie2-Cre* floxed allele of *Sox17* (*Tie2-Cre*$^{+}$*Sox17*$^{fl/GFP}$) resulted in the loss of foetal and neonatal, but not adult HSCs (Kim et al., 2007). *Tie2* was selected here as a appropriate promotor due to its restriction to the endothelial and haematopoietic pools of interest, limiting Cre expression to these cell types. As a site-specific DNA recombinase, once the Cre is expressed within a cell, it will target specific lox-P sites within the DNA that flank the gene of interest, in this case *Sox17,* and will cut at these points, removing the gene. It is possible, however, that Cre recombinases under the control of promotors other than *Tie2* may not give the same result. Importantly, the reduction of *Sox17* expression aligns with the 3-4 week developmental switch and corresponds to reduced self-renewal and proliferation, and the acquisition of the adult HSC phenotype.

One of the key distinguishing properties between FL and adult HSCs is their cell cycle status: FL HSCs are actively cycling whereas adult HSCs are mostly quiescent. Therefore, another important developmental transition is the switch between these two states. Specifically, in a process initiated before birth, and lasting until approximately 3-4 weeks postpartum in mice, a gradual shift in the cellular and molecular properties of HSCs occurs (Bowie et al., 2007a,b, Copley and Eaves, 2013; Kim et al., 2007; Li et al., 2020).

As a result of the foetal-to-adult switch, several differences between FL and adult HSCs are evident, especially with regard to their expansion rates and developmental potential. During development, FL HSCs undergo massive expansion, increasing in numbers by 10-30 fold within 4 days (Ema and Nakauchi, 2000). Although there is evidence of some seeding of HSCs generated from, and/or expanded in, the placenta (Rhodes et al., 2008; Ottersbach and Dzierzak, 2005), most of the increase in FL HSCs is due to their frequent execution of symmetrical self-renewal divisions (Bowie et al., 2006; Morrison et al., 1995). This higher rate of expansion was foreshadowed by early experiments using FL HSCs, where it was shown that spleen colony-forming units (CFU-S) from FL-HSCs were a more rapidly regenerating stem/progenitor population than adult spleen and bone marrow HSCs (Becker et al., 1965). FL HSCs also exhibit faster cycling rates compared with adult HSCs; nearly all FL HSCs are cycling whereas >75% of adult HSCs are quiescent (Cheshier et al., 1999). Despite this, the cell cycle transit time of FL HSCs is similar to that of adult HSCs once the latter have fully exited quiescence (Bowie et al., 2007a,b). The switch in cycling is an intrinsically regulated process, with the site change from the FL to the developing BM not inducing HSC quiescence until 3-4 weeks later (Bowie et al., 2007a,b).

FL HSCs possess a similar developmental potential to adult HSCs with respect to the types of cells that they can give rise to in bone marrow transplantation experiments (Bowie et al., 2007a), with the exception of some distinct developmental T-cell lineages (Ikuta et al., 1990). However, their stepwise progression through progenitor stages is much less well defined. At the population level, FL HSCs are more likely to be balanced in their mature cell output in functional assays (e.g. they contribute equally to myeloid and lymphoid lineages) compared with adult HSCs, which become more lymphoid deficient with age (Benz et al., 2012). Relative to adult HSCs, FL HSCs additionally show an erythroid-over-myeloid bias in both mice and humans (Rowe et al., 2016a,b, Popescu et al., 2019). Recent work has also shown a developmental switch in the megakaryocyte production capacity of HSCs, with foetal HSCs being considerably less primed towards the megakaryocytic lineage compared with adult HSCs (Kristiansen et al., 2022). Using the HSC subtypes described by Dykstra et al. 2007, each cell can be categorised based on its mature cell production in single-cell transplantation assays as alpha, beta, gamma or delta. Interestingly, in line with the 3-4 week switch, ratios of the HSC subtypes present at this timepoint shift, suggesting a wider change in HSC functionality (Benz et al., 2012, Copley et al., 2013). In functional assays, in particular during the early stages following transplantation, FL HSCs repopulate recipients more quickly than their adult counterparts and generate more HSCs through symmetric self-renewal (Bowie et al., 2007a,b, Pawliuk et al., 1996). Around 6 weeks after transplantation, FL HSCs adopt a more adult-like self-renewal capacity, resembling the natural transition that occurs between 3 and 4 weeks after birth (Bowie et al., 2007a,b).

1.2.4 HSCs in ageing

Over the course of ageing, HSCs gradually lose their ability to self-renew and to differentiate into the required mature cells (López-Otín et al., 2013). Therefore, haematopoietic function generally declines with age and is often accompanied by an exhaustion of the stem cell pool (Mejia-Ramirez et al., 2020). As a result, haematological diseases are highly age-dependent (Winter et al., 2024). The exhaustion of the HSC pool noted in the elderly develops gradually, and limits the homeostatic capacity of the blood system. Several fundamental intrinsic and extrinsic mechanisms have been linked to this phenomenon.

In order to elucidate the fundamental differences between young HSCs and old HSCs, transplantation experiments were performed - transplanting either young or old donor HSCs into their counterpart recipient mice (Dykstra et al., 2011, Harrison et al., 1982, Rossi et al., 2005, Van Zant et al. 1990). In these seminal experiments, old HSCs remained functionally impaired even when transplanted into young mice, implying that the shift in characteristics observed in old HSCs is intrinsically regulated. In these experiments, HSC function is determined by mature cell counts originating from the transplanted sample, and the balance of myeloid to lymphoid lineages (Beerman et al., 2010, Dykstra et al., 2011). Although convincing, these experiments somewhat negate the consideration that environmental stimuli induced the intrinsic molecular changes themselves. Such stimuli include mechanical and cellular changes in the bone marrow microenvironment which are well studied components of inflamm-ageing (Kovtonyuk et al., 2016). Further studies reveal that aged HSCs present with a skewed mature cell production towards the myeloid lineage – a result of a deficiency in lymphoid lineage production, rather than a myeloid overproduction (Kuranda et al., 2011, Yamamoto et al., 2018b).

In terms of the intrinsic mechanisms linked to HSC ageing, these include, but are not limited to, reduced mitochondrial function, reduced autophagy, increased ROS, mTOR activation, and the accumulation of sporadic and random DNA damage (de Haan et al., 2018). A further example of an intrinsic mechanism regulating HSC ageing and decline is the gradual shortening of telomeres with time, despite telomerase expression within HSCs. This phenomenon has been linked in several studies to relate to HSC functional decline (Allsop et al., 2003, Mejia-Ramirez and Florian, 2020, de Haan and Lazare, 2020). The acquisition of mutations leading to the decline of the DNA damage repair response in HSCs has also been correlated with premature ageing in both mouse models and human patients (Rossi et al., 2007). Additionally, replicative stress which enhances the rate of random mutation acquisition through an increased rate of cell division amplifies this loss of robust stem cell

activity in individuals (Flach et al., 2014, Herr et al., 2024). Alongside the accumulation of random mutations over time, the accumulation of specific driver mutations in key proteins such as *Jak2*, *Tet2*, and *Dnmt3a* is known to be specifically linked to the development of clonal haematopoiesis (CH) (Jaiswal et al., 2014, Zink et al., 2017), an age-related condition which contributes to a loss of a functional HSC compartment.

Furthermore, the role of mitochondria in retaining HSC functionality is essential. The natural increase in mitochondria observed in HSCs as they age, a result of impaired autophagy within the cells, induces a state of metabolic stress and increased intracellular levels of ROS (Mansell et al., 2021, Morcos et al., 2020, Mohrin et al., 2015). ROS itself is theorised to induce mitochondrial DNA damage, furthering the severity of this metabolic stress, as mitochondrial DNA mutations are shown to increase with age (Norddahl et al., 2011).
CH is a phenomenon that has been suggested as a “pre-leukaemic” state, with CH patients presenting with a higher, albeit still very small, predisposition to leukaemic transformation. CH is caused by a relative outgrowth of a specific HSC clone within the HSC pool, carrying a somatic mutation conferring a survival or self-renewal advantage (Winter et al., 2024). As a result of CH, the aged haematopoietic system is comprised of a smaller number of clones than the younger haematopoietic system and a single HSC derived clone often drives this phenomenon. This results in a significant reduction in the genetic diversity of this tissue within both HSC and mature cell populations (Mitchell et al., 2022). Whilst occurring often spontaneously, key driver mutations are known to be highly correlated to the development of CH. These include *TET2*, *JAK2*, *DNMT3A*, and *ASXL1* (Xie et al. 2014, Jaiswal et al., 2014, McKerrell et al., 2015, Pich et al., 2022, Zink et al., 2017), and provide the affected cells with a strong survival advantage. Additionally, coordinated changes to the BM microenvironment observed with ageing have been proposed to correlate to both CH and malignant transformation into leukaemia, possibly providing evidence that the physical environment provides a selection pressure that enables certain clones to thrive over others (Ho et al., 2019, Winter et al., 2024, Hormaechea-Agulla et al., 2021, Pinho and Frenette, 2019, Sacma et al., 2019).

1.2.5 The HSC niche

First proposed as a concept by Dr Ray Schofield in 1978, the haematopoietic niche within the BM has since been studied in depth for its important role in HSC regulation, and its maintenance of HSC self-renewal capacity. Dr Schofield discovered that, in the context of HSC transplantation, the outcome of transplantation as determined by CFU-S recovery was highly dependent on the cytotoxic agent or regime used to deplete the recipients’ bone

marrow ahead of receiving the transplanted cells (Schofield, 1978). Dr Schofield concluded that HSCs rely on neighbouring cells to govern their own behaviour – both in terms of proliferation and quiescence (Schofield, 1978).

In mammalian tissues, the cortical bone is the outermost layer of the bone, with the endosteum lying just below - separating the cortical bone from the underlying BM. The BM is a significantly softer, highly vascular tissue with an extensive sympathetic nervous network (Boulais and Frenette, 2015, Pinho and Frenette, 2019, Yamazaki and Allen, 1990). At the base of the bone tissue, in close proximity to the endosteum, osteoblasts and osteoclasts regulate the formation and remodelling of the bone. In contrast to more simple organisms such as *Drosophila* and *Caenorhabditis elegans* where the importance of the niche had been previously described (Crozatier and Vincent, 2011, Joshi et al., 2010), in mammals, and specifically within the haematopoietic system, the niche is significantly more complex. Cell populations present in the broader BM niche are not only heterogenous, which may require varying niches for each subpopulation, but are also capable of circulating and moving within the BM, making it an increasingly dynamic environment (Kunisaki et al., 2013, Itkin et al., 2016, Pinho et al., 2018).

In order to study the HSC niche in more detail, it was vital to determine with greater specificity where the HSCs reside within the BM microenvironment. Several different approaches have been used to tackle this issue. Initially, the use of surface marker staining for the well known SLAM markers (Signalling Lymphocyte Activation Molecules) used to identify mouse HSCs ($CD150^{+}CD48^{-}CD244^{-}$) enabled visualisation of HSCs within bone tissue sections (Kiel et al., 2005). More recent approaches have utilised confocal imaging and two-photon imaging of single HSCs in live recipient mice in a post-transplantation setting. Data from these experiments revealed that subsets of haematopoietic cells home to different locations within the endosteal niche, dependent on their degree of differentiation, with the repopulating HSC fraction typically found in close association to the endosteal surface (Lo Celso et al., 2009). Furthermore, it was shown that this initial seeding of primitive HSCs is both intrinsically and extrinsically regulated (Lo Celso et al, 2009). Most recently, confocal imaging of hundreds of entire mouse sternums, aided by computational analysis and modelling, revealed an increased density of the most quiescent, most primitive, HSCs near to bone marrow arterioles present within the endosteal niche (Kunisaki et al., 2013). Additionally, Leptin receptor positive, and Nestin positive, perivascular cells have been shown to highly express key HSC niche factors including chemokine (C-X-C motif) ligand-12 (CXCL12), stem cell factor (SCF), IL-7 and angiopoietin-1 (ANGPT1) (Mendez-Ferrer et al.,

2010). When functionally validated via the deletion of CXCL12 and SCF from perivascular cells, HSC numbers were depleted and haematopoiesis was disrupted (Ding et al., 2012)

Within the niche, extensive, complex, and dynamic crosstalk between cells regulates both the activity of the HSC fraction, and the differentiated progeny (Lo Celso and Scadden, 2011). Within the axial bone marrow, where the vast majority of HSCs reside postnatally, the endosteal tissue close to the bone surface and its associated osteoblastic cells has been shown to be a fundamental element of the HSC niche (Kent et al., 2008a). Specifically, within the heterogenous osteoblastic populations, osteoblasts expressing key markers activated leukocyte cell adhesion molecule (ALCAM) (Nakamura et al., 2010) and Osteopontin (Nilsson et al., 2005), were shown to be supportive of HSCs within this niche, enhancing long-term reconstitution via associated upregulations of genes linked to HSC homing and cell-adhesion (Nakamura et al., 2010). Furthermore, the N-cadherin/β-catenin adhesion complex, regulated by c-Myc, has been shown to be essential in the interactions between HSCs and their niche (Wilson et al., 2004). Conditional knock-out models of c-Myc result in the increase of N-cadherin expression and associated increase in HSC retention within the BM niche (Wilson et al., 2004). Interestingly, alterations in HSC fate choice in these conditional c-Myc knock-out mice were noted, with HSCs failing to robustly differentiate, and LT-HSCs instead accumulating within the BM microenvironment. These pioneering experiments directly link the BM niche to the fundamental balance between HSC self-renewal and differentiation.

1.2.6 Key characteristics of HSC metabolism

The haematopoietic system, partially due to its accessibility, is one of the best studied tissues and therefore HSCs, at the peak of the hierarchy, are some of the best studied stem cell populations (Orkin et al., 2008). As discussed previously in this thesis, the ability of HSCs to both self-renew and to differentiate into all mature cells of the blood is fundamental to the function and lifelong maintenance of the haematopoietic system. Furthermore, the protective G_0 state that HSCs typically reside in is essential for their longevity and DNA integrity preservation. The ability of HSCs to rapidly alter their metabolic state and exit quiescence in order to respond to stimuli, and then re-enter once they are no longer required to be actively dividing, is an efficient protective mechanism for this rare cell type, but is also a highly regulated process (Xie et al., 2019).

Coupled with low rates of cell division due to their quiescent state, transcriptomic analyses revealed increased levels of DNA protective mechanisms – including both cytoprotective and

DNA damage repair genes within the HSC population (Bryder et al., 2006). In order to quantify the frequency of HSC cell divisions in both of the previously discussed LT-HSC and ST-HSC populations, label retaining studies utilising Bromodeoxyuridine (BrdU) were performed. These studies revealed that unstimulated LT-HSCs (as defined by Lineage$^-$ cKit$^+$Sca1$^+$CD48$^-$CD150$^+$) undergo cellular divisions rarely, with 20% of HSCs tested being especially quiescent, dividing at rates of just 0.8%-1.8% per day, and the remaining larger population entering the cell cycle and dividing at 5.3-11% per day (Foudi et al., 2009). On average, the entire LT-HSC population tested divided approximately once every 55-145 days whilst ST-HSCs generally divided 4 times more frequently. Interestingly, heterogeneity was observed within the LT-HSC population measured, however the study suggests this may result from progenitor contamination within this pool (Foudi et al., 2009). Additionally, upon stimulation, LT-HSCs were much slower to respond than ST-HSCs – in terms of exiting the quiescent state and initiating the process of DNA replication and cell division (Laurenti et al., 2015, Müller-Sieburg et al., 2002). Further quantitative cellular labelling assays showed that transition from LT-HSC to ST-HSC occurs in approximately 1 in 110 LT-HSCs each day (Busch et al., 2015).

Furthermore, multiple metabolic studies reveal that HSCs exist in a low metabolic state, with low levels of mitochondrial activity mediated by autophagy (Ho et al., 2017, Dellorusso et al., 2024). In line with this, HSCs typically rely on glycolysis rather than oxidative phosphorylation as a source of energy (Ito and Suda, 2014). As well as limiting the levels of damaging ROS produced as a by-product of the lesser used oxidative phosphorylation pathway in these cells (Ludin et al., 2014, Cabezas-Wallschied et al., 2017), the reliance of HSCs on glycolysis is a helpful adaptation to the hypoxic areas present in the BM niche in which they may reside (Zhang and Sadek, 2014). On the other hand, downstream progenitors are significantly more metabolically active, instead relying on oxidative phosphorylation to meet their increased energy requirements (Ito and Suda, 2014, Vannini et al., 2016).

1.2.7 Heterogeneity in HSCs

HSCs are well known to be a highly heterogeneous population, with multiple studies revealing high variability in molecular and functional characteristics all existing within the same phenotypic HSC pool. These distinct HSC subtypes can be linked to variations in self-renewal capacity, quiescence, cell cycle status, differentiation capacity, and lineage bias (Ema et al., 2014, Yamamoto et al., 2013, Seiburg et al.,2006).

Initially, this heterogeneity was identified through variation in CFU-S studies, where single cell initiated colonies vary in extent of proliferation (colony size), and phenotype of cells present in the colonies (Till et al., 1964). The first demonstration of lineage bias within individual HSCs was noted in pioneering experiments by Muller-Sieburg et al, where the use of HSC transplantations coupled with limiting dilution assays revealed a skewing to either a myeloid or lymphoid bias, which was sustained in serial transplantations. 3 basic categories of HSC were defined as a result of these seminal experiments – balanced output, myeloid biased, and lymphoid biased (Muller Sieburg et al., 2002). Following this, Benz et al, in 2012 showed that myeloid biased HSCs have the capacity to produce daughter HSCs with a balanced output, and vice versa in rarer situations (Pinho et al., 2018, Itkin et al., 2016)

This strategy of categorising HSCs based on lineage output was supported, but also further refined, in 352 independent single cell transplantations of either fresh or cultured HSCs (Dykstra et al., 2007). In the 93 mice that presented with a donor derived chimerism contribution for at least 4 months post-transplant, 4 key trends in HSC reconstitution potential and relative lineage contribution were noted, labelled α, β, γ and δ. Two of these patterns (α and β) correlated with long-term self-renewal in serial transplantation experiments as determined by sustained secondary and tertiary contributions to the white blood cell pool of >1% at 16-weeks post-transplant (Dykstra et al., 2007). These patterns were shown to likely be intrinsically regulated, and predetermined before these cells were transplanted. Within these two categories, α HSCs were myeloid-biased whilst β HSCs presented with a more balanced lineage output, more reminiscent of a classical LT-HSC. On the other hand, γ and δ HSCs became exhausted over the course of serial transplantations, and tended to be lymphoid biased, representing the broader ST-HSC pool. γ HSCs, whilst remaining multipotent and contributing significantly to mature cell populations for 4 months post-transplant, were unable to sustain self-renewal beyond the 6-7 month time point. It is thought that this category represents a transiently repopulating intermediary, rather than a traditional LT-HSC. Interestingly, whilst γ HSCs are capable of generating myeloid progeny, δ HSCs are entirely restricted to the lymphoid lineage, and produce no myeloid cells. The relative frequencies of these four subtypes shift as the host ages – with β HSCs dominating the foetal liver, but becoming replaced by α HSCs for the majority of adult life. In old age, a shift towards lymphoid-deficient HSC subtypes is observed (Sudo et al., 2000, Cho et al., 2008). It is not yet understood if α and β HSCs are entirely independent populations, or whether the α HSCs that arise postnatally derive directly from the initial β cell pool. A 2022 study by Ganuza et al., investigated the contribution of foetal liver HSCs to adult haematopoiesis and concluded that many FL-HSCs are biased towards differentiation over self-renewal, in order to support the needs of the developing embryo. Furthermore, they

observed only a modest 2-fold expansion of HSPCs that contribute to the adult blood during the FL stage of development, implying that the FL acts more as a site for pre-HSC maturation, rather than expansion (Ganuza et al., 2022). Additionally, another paper by the same group (Hall et al., 2022) compared foetal BM-HSCs at E15.5 to their FL counterparts and determined they are functionally and phenotypically distinct populations. Moreover, transcriptional analysis of foetal BM populations uncovered that HSPCs present in this location lack expression of robust intrinsic self-renewal signatures.

One of the key surface proteins used to separate LT- (α and β), from ST- (γ and δ) HSCs is CD150. An easily accessible surface protein with readily available antibodies, high CD150 expression is an efficient method of refining the HSC pool to enrich for long-term repopulating capacity more than 10-fold (Kent et al., 2009, Yamamoto et al., 2013, Schulte et al., 2015, Beerman et al., 2010). Furthermore, high expression of surface protein CD299, low expression of CD49b, and extent of Hoechst 33343 efflux enable identification of exclusively lymphoid biased HSCs (Challen et al., 2010, Oguro et al., 2013). Taken together, these approaches are valuable for removing unwanted HSCs that are lymphoid biased and/or lack long-term self-renewal, but do not enable complete identification of balanced output LT-HSCs.

The advent of novel technologies enabling single cell analysis of HSCs such as single cell quantitative PCR (qPCR), refined identification strategies for HSCs, and single cell transplantation, has helped us to refine our knowledge of subtypes within the HSC pool and even enables prospective isolation of different categories of HSC (Crisan and Dzierzak, 2016). The first study performing single cell qPCR on LT- HSCs twinned with functional assays was performed by Wilson et al., 2015. This experiment targeted 48 genes previously linked to HSC function and lineage bias and enabled the identification of a common molecular profile between 5 defined phenotypic LT-HSC populations – the Molecular Overlap (MolO) gene signature. Retrospective analysis allowed identification of the cells that fell within this MolO cluster and revealed that these cells expressed high levels of *Sca-1*, and hence could be prospectively isolated through the use of this marker. Functional studies have again linked *Sca-1* expression to repopulation capacity and to a high MolO score. As a result, the MolO gene signature, and score, has since gone on to be widely used as a surrogate marker for durable self-renewal capacity. However, a more recent study utilising scRNA-seq datasets found that whilst average MolO gene set expression could crudely identify the HSPC population, MolO expression was not entirely uniform throughout this pool (Hamey and Gottgens, 2019). Additional studies following this work used single cell approaches to identify key transcription factors regulating myeloid differentiation in HSC and

progenitor populations, and those involved in changes to metabolism and cell cycle linked to early differentiation (Paul et al., 2015, Nestorowa et al., 2016).

The identification of novel pathways and genes involved in HSC regulation and differentiation highlights the heterogeneity within this population originally thought to be a homogenous pool and helps us unpick key regulators of HSC fate and potential.

1.2.8 Intrinsic self-renewal regulation in HSCs

Tight regulation of HSC self-renewal is essential for a balanced homeostatic haematopoietic system. Intrinsic molecular regulators of HSC self-renewal in both the FL and adult BM have been studied for over 30 years, with hopes to unpick these mechanisms and apply it to the *in vitro* culture and expansion of HSCs (Wilkinson et al., 2019).

Decades of study, and more recent transcriptomic analysis of the LT-HSC pool, brought to light complex gene regulatory networks (GRNs) which determine LT-HSC fate.
An example of such regulation, key transcription factors (TFs) *Gata2 and Scl* have both been studied extensively for their roles in haematopoiesis. These TFs form an essential haematopoietic regulatory triad with a third TF, *Fli1,* with each TF binding to the cis-regulatory regions of the others and influencing their expression *(*Pimanda et al., 2007*).* Additionally, many more TFs have been linked directly to intrinsically regulating HSC function. These include *CEBPα, RUNX1, HOXB4, GFI1, Myc, Meis1*, and *β-catenin* (Pawliuk et al., 1996, Wilson et al., 2010, Reya et al., 2003, , Murphey et al., 2005, Iwasaki et al., 2005, Bowie et al., 2007*),* as well as cell cycle regulators *Cdkn1a* and *Cdkn2c* (Cheng et al., 2000, Yuan et al., 2004). However, as discussed previously in Section 1.2.3 of this thesis, the GRNs and TFs regulating HSC self-renewal and fate choice in generally quiescent adult HSCs differ significantly from those in actively cycling FL HSCs. Some of the most striking differences are *Sox17* (Kim et al., 2007), *Hmga2*, and *Arid3a* (Copley et al., 2013), all of which are essential FL-HSC specific TFs.

Despite the importance of TF regulation on HSC fate, it is equally important to consider the wider epigenetic state of the HSC genome in order to understand the complex interplay regulating gene expression – especially as epigenetic reprogramming is observed over the course of HSC differentiation (Rodrigues et al., 2011). A pioneering study by Cabezas-Wallscheid et al. integrated transcriptomic, proteomic, and methylation data sets from quiescent HSCs and four MPP subsets. From here, they were able to identify several continuous changes in the proteome, transcriptome, and methylome that accompany the

early stages HSC differentiation, including 493 TFs and 682 long non-coding RNAs (lncRNAs) that form core signalling nodes (Cabezas-Wallscheid et al., 2014). Clinically, lncRNAs have been linked in over 4000 studies to the development and maintenance of various cancers, including leukaemias (Wong et al., 2018). For example, lncRNA UCA1is known to be overexpressed in AML, and induces excessive cell proliferation via the suppression of $p27^{kip1}$, a cell cycle regulator (Hughes et al., 2015).

Furthermore, several DNA methyltransferases including DNMT3a/DNMT3b (Sharma and Gurudutta, 2016, Wallace et al., 2023, Avgustinova and Benitah., 2016), and the TET family of enzymes (Moran-Crusio et al., 2001, Vanner et al., 2023) are essential in the regulation of HSC self-renewal. Loss of function mutations in these proteins induce a sustained self-renewal advantage for the affected cell, therefore resulting in the selective outgrowth of these HSCs and eventually the development of clonal haematopoiesis. As a result, these mutations are frequently observed in myeloproliferative diseases and haematological malignancies (Schaub et al., 2010, Schiroli et al., 2024, Wang et al., 2024).

BMI1 and *EZH2*, both Polycomb group (PcG) chromatin modifiers, have been decisively linked to the adult HSC self-renewal program (Lessard and Sauvageau, 2003, Park et al., 2003), as well as being fundamental to preventing excess differentiation and exhaustion of the stem cell population. *Bmi1* is specifically expressed in the most immature HSCs, with loss of function mutations in this protein resulting in impaired HSC self-renewal and reconstitution capacity (Klauke et al., 2013, Hidalgo et al., 2022). Interestingly, in low SCF culture conditions, a striking reduction in both *Bmi1* and *Ezh2* transcripts was noted (Kent et al., 2008a). Utilising a retroviral overexpression system, overexpressing *Ezh2* bypasses HSC senescence, and mitigates against the usual levels of HSC exhaustion noted over serial transplantation experiments (Kamminga et al., 2006). In terms of clinical impact, *EZH2* has been shown to have a dual purpose – with potential to act as both an oncogene and a tumour suppressor in differing types of leukaemia. Whilst lower levels of *EZH2* expression have been noted in CML and ALL compared to healthy controls, overexpression of EZH2 has been reported in T-ALL, CLL and CML (Kempf et al.,2021). Furthermore, a study by Basheer et al identified opposing effects of EZH2 in AML induction and maintenance, where it acts as a tumour suppressor, and oncogene accordingly (Basheer et al., 2019).

MicroRNAs (miRNAs) are small noncoding RNAs which regulate expression of target genes post-transcriptionally (Luinenburg et al., 2021). Their role in HSCs has been widely implicated in the regulation of HSC self-renewal and fate choice (Vasilatou et al., 2010).

Specifically, miR125 is highly expressed in both human and mouse HSCs, and is essential for inducing HSC and MPP self-renewal both *in vivo* and *in vitro* (Luinenburg et al., 2021*)*. As a result, long-term overexpression of miR125 results in enhanced MPP self-renewal and has been linked to the development of haematological malignancies. Quantitative proteomic studies reveal that constituent overexpression of miR125 deregulates the complex downstream target network, including the mitogen-activated protein kinase (MAPK) signalling pathway, which in healthy conditions acts to limit self-renewal in less primitive cells (Wojtowicz et al., 2016). Additionally, miR125 is involved in the regulation of apoptosis within the HSPC fraction – again essential to maintain the health of the HSC pool and therefore the wider haematopoietic system (Guo et al., 2010). Furthermore, miRNA-29a is expressed at the highest levels in HSCs, and expression tails off as differentiation occurs. Induced overexpression of miRNA-29a was found to instigate aberrant self-renewal in myeloid biased MPPs, and therefore can promote the development of myeloproliferative diseases, which hold the capacity to develop into acute myeloid leukaemia (Han et al., 2010).

Ultimately, strict intrinsic regulation of HSCs, from TFs, chromatin remodelers, noncoding RNAs, and additional regulatory proteins, is essential for ensuring stability within the haematopoietic system, and preventing the development of haematological disease.

1.2.9 Extrinsic self-renewal regulation in HSCs

As outlined above, intrinsic regulators form complex networks, ensuring the balance of self-renewal and differentiation is maintained within the HSC pool, and the downstream progenitors. However, HSCs do not exist alone in the BM niche, and therefore extrinsic regulators also control HSC fate, and impact the intrinsic regulatory systems directly (Mayani, 2016). A huge range of extrinsic stimuli act within the BM, including the mechanical microenvironment (Pinho and Frenette, 2019, Li et al., 2021, Lee et al., 2013, Huang et al., 2019), inflammation (Pietras et al., 2016), haematopoietic cytokines (Lee et al., 2017), and the hypoxic nature of this niche (Zhang and Sadek, 2014, Takubo et al., 2010).

Immune cytokines, chemokines, and growth factors are key components of the BM and are fundamental to the maintenance of HSC self-renewal capacity, and differentiation into mature cell populations. As a result, they are widely used in *in vitro* culture systems to support the expansion of HSCs. As expected, dysregulation of these key molecules and their cognate receptors has been linked to a range of inflammatory conditions and malignancies (Camacho et al., 2017, Multhoff et al., 2011). In particular, chronic inflammation is associated with a sustained increase in pro-inflammatory cytokine release. In turn, this

results in genomic damage and instability, development of pre-malignant conditions such as myeloproliferative neoplasms, and an increased risk of malignant transformation (Chen et al., 2024, Koschmieder et al., 2016, Soyfer and Fleischman, 2023, Hasselbalch and Bjorn, 2015). Furthermore, increased serum concentrations observed in leukaemia patients of IL-10, IL-12, IL-6, IFNα, and TNF- α have been linked to patient survival and outcomes (Yan et al., 2011, Stevens et al., 2017, Fitch et al., 2022).

Stem cell factor (SCF), also known as steel factor, is a haematopoietic cytokine involved in regulating HSC self-renewal within the BM niche, and elicits its effects via binding to its receptor c-Kit, a receptor tyrosine kinase expressed on the membrane of all HSCs. SCF exists in both a soluble form and as a transmembrane bound protein, with these variants generated through alternative splicing (Flanagan et al., 1991, Huang et al., 1992). SCF is released by a wide range of supportive cells, including perivascular cells, endothelial cells, and fibroblasts present in the BM niche (Ding et al., 2012, Xu et al., 2018). Highlighting the necessity of consistent SCF release in order to maintain functional haematopoiesis, mice treated *in vivo* with neutralising Kit antibodies developed marked decreases in BM cellularity and developed pancytopenias (Ogawa et al.,, 1991, Shin et al., 2014, Heinrich et al., 1993). Furthermore, mutations in SCF impair the ability of supportive niche cells to maintain the HSC population (Ding et al., 2012), whilst mutations in Kit result in reduced HSC counts and decreased CFU formation (Lennartsson and Ronnstrand, 2012, Zhang and Pinho, 2023, Metcalf, 2008). Interestingly, the response to SCF changes over the course of development, with FL HSCs requiring significantly lower levels of SCF than adult HSCs, despite expressing comparable levels of the cognate receptor, Kit (Bowie et al., 2007a,b).

Additionally, haematopoietic cytokine thrombopoietin (TPO) is essential for megakaryocyte and platelet production, whilst also being fundamental in facilitating HSC self-renewal and therefore also HSC *in vitro* expansion (Tsutsumi et al., 2023, Seita and Weissman, 2010). In TPO and TPO receptor (myeloproliferative leukaemia protein (MPL)), knockout mice models, levels of erythroid and myeloid progenitors are half that of wild type. Strikingly, in MPL knockout mice, HSC and MPP function is so impaired that they are unable to successfully rescue a sub-lethally irradiated mouse in an HSC transplantation setting (Kimura et al., 1998). Additionally, loss of function mutations in MPL result in dramatically reduced numbers of early haematopoietic progenitors, and are closely linked to the development of bone marrow failure disorders (de Graaf and Metcalf, 2011, Ballmaier et al., 2003). Both SCF and TPO will be discussed in significantly more detail, particularly in relation to their roles in the *in vitro* expansion of HSCs, later in this thesis.

Alongside haematopoietic cytokines, key signalling pathways including Wnt and Notch have been associated with balancing HSC self-renewal, differentiation, and fate choice (Bigas and Espinosa, 2012). Notch transgenic mice, with a green fluorescent protein (GFP) labelled Notch reporter enabling the identification of cells with active Notch signalling, combined with immunofluorescent flow cytometric analysis, revealed that a large fraction of kit expressing cells were concurrently expressing this Notch reporter. Additionally, the extent of Notch signalling, as determined by expression of this reporter, decreased as cells became increasingly differentiated (Duncan et al., 2005). Furthermore, the influence of Wnt-Notch signalling on HSC function is recapitulated in *in vitro* environments, where Notch-GFP^{+} HSCs retained greater levels of multi-lineage potential post-culture, and inhibition of Notch increased *in vitro* differentiation (Duncan et al., 2005, Honey, 2005). Additional studies have shown inhibition of the Wnt signalling pathway *in vitro* using Wnt5a maintains the HSC population in a largely quiescent state, and increases the repopulation capacity of the post-culture HSCs when transplanted (Nemeth et al., 2007).

The hypoxic nature of the BM microenvironment plays an important role in regulating HSC function, with low oxygen levels in the BM niche, and associated upregulation of HIF-1α (hypoxia-inducible factor 1-α), being shown to have a direct effect on HSC homing and behaviour (Nombela-Arrieta et al., 2014). Typically, the most quiescent HSCs, with the greatest repopulation capacity are found in the most hypoxic areas of the niche, such as the endosteal region (Lee et al., 2017, Suda et al., 2011, Mohyeldin et al., 2010, Eliasson and Jonsson, 2010). Furthermore, when preparing HSCs for transplantation, those harvested and processed in hypoxic conditions have increased success in transplantation, whilst exposure to normoxic air reduces HSC recovery from BM and cord blood samples (Mantel et al., 2015).

Overall, it is clear that a complex network of intrinsic and extrinsic regulators is essential for the regulation of haematopoiesis, and enables HSCs to respond appropriately to the physiological requirements of the body.

1.3 Assays for haematopoietic stem and progenitor cells

1.3.1 HSC transplantation assays

To date, HSC transplantation assays remain the gold standard for determining presence of functional LT-HSCs in the transplanted material; this can be either a bulk sample or a single cell. Often in the case of single cell transplantations, a larger population of supportive "helper" BM cells are transplanted alongside the HSC. These helper cells provide protective

short-term transiently repopulating progenitors, therefore improving recipient survival. These progenitor populations mitigate against the delay from HSC transplantation to mature cell contribution from the HSC (Purton and Scadden, 2007, van den Brink et al., 2015). With a long history of clinical use, HSC transplantation remains the sole curative therapy for a range of haematological diseases, and it is widely understood that the cell dose given to the patient following irradiation correlates directly with likelihood of treatment success (Remberger et al., 2020).

First performed in mice in 1951, these preliminary transplantations highlighted the ability of transplanted BM cells to reconstitute the haematopoietic systems of lethally irradiated recipients (Jacobson et al., 1951). As previously discussed earlier in this thesis, CFU-S assays identified that transplanted cells homed to the spleen and produced quantifiable numbers of macroscopic colonies – each originating from a single cell. Since then, the ability of an HSC to rescue a lethally irradiated recipient has become fundamental to the definition of an HSC. However, with the lengthy lag time (>16 weeks) between the transplantation being performed and a successful outcome being determined, transplantation assays rely on retrospective analysis to study the functional HSCs themselves. Generally, success in HSC transplantation is defined as a >1% contribution to all mature cell lineages at ≥16 weeks in serial transplantation (Purton and Scadden, 2007). Success in serial transplantations enables differentiation between ST- and LT-HSCs as ST-HSCs are capable of providing 16-weeks of chimerism in primary hosts, but will not be able to reconstitute the haematopoietic system in a secondary transplantation setting (Cheng et al., 2020). With success in secondary and tertiary transplants demonstrating long term self-renewal capacity, LT-HSCs are therefore capable of dividing symmetrically into equally potent daughter cells that retain the ability to reconstitute an irradiated recipient (Haas et al., 2018, Suda et al., 1984). In between the two broad categories of ST- and LT-HSCs lie Intermediate-term (IT-) HSCs, capable of prolonged, yet still transient, reconstitution. This is defined by contributing to mature cell chimerism for 6-8 months, before becoming exhausted (Beneveniste et al., 2010).

Early attempts to track progeny arising from the transplanted HSCs, and to therefore chart myeloid and lymphoid lineage outputs and/or bias, used random retroviral integration and labelling (Keller et al, 1985, Jordan and Lemischka, 1990, Dick et al., 1985). However, these methods were complex and time consuming and were blind to smaller donor contributions. Since then, the more refined CD45 congenic system has taken precedence. This method involves utilising two variant alleles of the pan-haematopoietic cell marker CD45 (CD45.1 and CD45.2) which differ in just 5 amino acids within their respective extracellular domains.

Using this approach, CD45.1 and CD45.2 are used to mark either the donor or recipient cells, and can be detected via differing monoclonal antibodies for each isotype. This enables accurate separation of donor-derived cells from the recipients' own cells during flow cytometric analysis, allowing reliable quantification of donor cell contribution post-transplantation (Mercier et al., 2016). Combining CD45.1/.2 antibodies with lineage specific markers on the flow cytometric panels used to analyse peripheral bloods post-transplant enables the determination of chimerism within individual mature cell fractions. Markers commonly included alongside CD45.1/.2 include CD3 (T-cells), B220 (B-cells), Ly6g (monocytes, granulocytes, neutrophils), and Mac1 (Macrophages). However, the main limitation of the CD45 congenic system is that, although CD45 marks stem and progenitor cells, B-cells, T-cells, ILCs, and neutrophil-monocyte derived cells, it is not expressed on platelets or erythrocytes, inhibiting chimerism quantification within these lineages (Yamamoto et al., 2018a). In order to determine contribution to these populations, fluorescently labelled transgenic donor cells for von Willebrand Factor (VWF) or Gata1 to allow the quantification of platelet and erythrocyte chimerism accordingly (Yamamoto et al., 2018a). Additionally, the development of a Kusabira Orange (KuO)-expressing transgenic reporter mouse provides stable expression of KuO in all haematopoietic cellular components, including platelet and erythrocyte populations (Hamanaka et al., 2013, Yamamoto et al., 2018).

1.3.2 In vitro assays

In order to avoid the associated costs and lengthy time courses of transplantation assays, several alternative *in* vitro assays have been developed in order to assess the HSC content of cell populations more efficiently.

CFU assays were originally established by McCulloch and Till in 1964. In these robust quantitative assays, transplanted BM samples generated a quantifiable number of macroscopic colonies in the spleens of the irradiated recipient mice, with each colony originating from a single transplanted cell. To date, colony forming capacity remains widely used as a way to measure multi-potent and self-renewing progenitor cells present in the sample, and as a surrogate for determining the proliferation and differentiation capacity within a population of cells (Purton and Scadden, 2007, Li et al., 2016). In more recently developed *in vitro* forms of these assays, a semisolid media containing key haematopoietic cytokines is used to culture the cells of interest, physically holding individual cells in isolation to enable detection of progeny from each separate cell with the main two systems being methylcellulose and agar-based. The number, and lineages, of colonies is then assessed at

the end of a 14 day culture period. Despite the ease and efficiency of CFU assays to give us insights into multilineage and proliferation capacity, and therefore progenitor content within a population of cells, CFU assays do not enable quantification of the HSC fraction specifically since large proportions of progenitor cells are also capable of generating spleen colonies.

A further refinement of the CFU assay is the long-term culture initiating cells (LTC-IC) system. This assay enables more accurate quantification of the most primitive haematopoietic cells capable of sustained *in vitro* myelopoiesis for many weeks – a fundamental trait of functional HSCs (Sutherland et al., 1990, Lemieux et al., 1995). To combat the inherent myeloid specificity of the CFU assay, LTC-IC assays for lymphoid lineage quantification were developed, and specialised cell lines OP9 and OP9-DL1 have been generated to support the *in vitro* culture of progenitors from B- and T- cell lineages (La Motte-Mohs et al., 2005, Liu et al., 2013). In the context of this assay, these primitive cells are known as LTC-IC. Initially, cells of interest are cultured for 5 weeks *in vitro* on a pre-established supportive layer of feeder stromal cells, typically a human or mouse fibroblastic cell line. Following this period, the sample (now containing just the progeny of the most primitive LTC-IC population, as the more mature cells present in the initial cell suspension would have differentiated *in vitro*) is transferred into a standard CFU assay, where after 14 days colonies are counted, and lineages determined. Cobblestone area-forming cell assay (CAFC) is another co-culture assay developed, much like LTC-IC, to quantify the most primitive cells within the sample (van Os et al., 2004), and is capable of distinguishing LT- and ST- HSC populations (Ploemacher et al., 1989). Combining these assays with a limiting dilution approach is becoming increasingly common for enhancing accuracy of HSC frequencies (Purton and Scadden, 2007). However, due to the reliance on potentially variable supportive cell lines, this remains a concern of these assays.

Most recently, the advent of novel liquid media HSC culture systems and associated flow cytometric panels to analyse post-expansion cell content have superseded both CFU and co-culture assays for quantification of both mouse and human progenitors (Kent et al., 2008, Sakurai et al., 2023, Wilkinson et al., 2019, Laurenti et al., 2015). These expansion systems have been fundamental to this PhD, and will be discussed in detail in Sections 1.4.2 and 1.4.3 of this thesis,

1.3.3 Methods for HSC identification and purification

With HSC heterogeneity originally identified solely by functional assays, the molecular differences that underpin this heterogeneity have historically been more poorly understood.

In order to study the HSC pool in greater detail, identification and purification of this population is essential, and is the first hurdle for any kind of analysis. The latest HSC identification strategies rely on multi-parameter flow cytometric approaches and Fluorescent Activated Cell Sorting (FACS) to isolate populations expressing, or lacking, several specific surface markers. The development of integrated fluorescent molecules onto commercially available antibodies has been a massive step forward in improving the ease and standardisation of this technology. Throughout this thesis, the terms “reporter strategy” and “reporter” are used to refer to cell identification strategies, predominantly flow cytometric panels, which allow isolation of HSCs, and do not specifically refer to the use of reporter genes in genetically modified animals.

Despite HSC biology being largely similar between mice and humans, and a well known high level of conservation between the species (Parekh and Crooks., 2013), the molecular markers used to identify and isolate the HSC populations differ significantly. Initially, the marker combination Thy1^{low}Lineage(Lin)$^{-}$Sca1^{+} was used as a read out for functional mouse HSCs, where Lin represented a cocktail of antibodies against mature lymphoid and myeloid markers (including Mac1, Gr-1, B220, and CD3), Thy1 was a further marker for differentiated cells, and *Sca-1* represented a promising novel marker for the HSC fraction. Using this flow cytometric strategy it was possible to enrich for HSCs within BM samples to a purity of ~10% (Muller-Sieburg et al., 1986, Spangrude et al., 1988). Although still low in comparison to the efficiency of flow cytometric isolation of other cell populations available, this was a marked improvement to the original concentrations of HSCs within the BM samples. Following this, c-Kit, the cognate receptor for haematopoietic cytokine SCF, was identified as a reliable marker on haematopoietic progenitor populations, and the addition of c-Kit^{+} onto the pre-existing Lin^{-}Sca1^{+} panel furthered improved isolation efficiency (Okada et al., 1992). This panel is widely known as the LSK panel, and is a popular surrogate for functional HSC content – however whilst these LSK cells were capable of reconstituting primary mice in a transplantation setting, the lack of secondary transplantations in seminal studies verifying this reporter strategy meant that estimates of HSC purity within this are widely assumed to be overestimated. An alternative isolation strategy for mouse HSCs utilised CD34^{low} expression as a method for enriching for specifically LT-HSCs with single-cell serial repopulating capacity, whilst CD34^{+} fractions contained the ST-HSC, transiently repopulating fraction (Osawa et al., 1996).

These strategies for isolating fresh HSCs are limited by the fact that both HSCs and MPPs reside within the LSK fraction, hence the need for additional differentiating markers to be

considered. The SLAM family of surface proteins, including CD48, CD150, and CD244 have been shown to be differentially expressed within the broader HSPC population, and further refinement revealed that the $CD150^{+}CD48^{-}$ reporter strategy efficiently enriched for LT-HSCs (Kiel et al., 2005), as did endothelial protein C receptor (EPCR, CD201) (Kent et al., 2009, Balazs et al., 2006). Through combining the LSK, EPCR, and SLAM markers it is possible to generate a highly specific reporter strategy for LT-HSCs: $EPCR^{+}CD150^{+}CD45^{+}CD48^{-,}$ which is often additionally combined with $Sca1^{+.}$ The ESLAM marker combination ($CD48^{-}$ $CD150^{+}$ $EPCR^{+}$ $CD45^{+}$) is the current gold standard used to identify freshly isolated mouse HSCs, especially for initiating single cell expansion cultures, and generates a LT-HSC purity of approximately 50%, as determined by single cell serial transplantation assays (Kent et al., 2009, Wilson et al., 2015). To date, the combination of the previously described LSK strategy with the addition of $EPCR^{+}$, (coined the ELSK reporter strategy) ($EPCR^{+}Sca1^{+}cKit^{+}Lineage^{-}$) is the established readout for murine HSCs post-culture (Che and Bode, 2022). The discrepancy in markers used for fresh and expanded HSCs results from the observed shift in surface marker expression over the course of *in vitro* culture (Zhang and Lodish, 2005).

On the other hand, for human HSCs, the most efficient and regularly used post-culture identification strategy utilises the following combination of surface markers: $CD34^{+}EPCR^{+}CD90^{+}CD45RA^{-}$, which enriches to purities of approximately 10% HSC (Notta et al., 2011, Anjos-Afonso et al., 2022, Fares et al., 2017, Sakurai et al., 2023). Isolating fresh human HSCs remains a challenge too, as whilst $Lin^{-}CD34^{+}CD38^{-}CD45RA^{-}$ $CD90^{+}CD49f^{+}$ can be used to crudely isolate HSCs from cord blood samples (to purities of approximately 9.5% long-term, multilineage repopulating cells, of which 69% could be serially transplanted Notta et al., 2011), peripheral blood and BM samples are significantly harder to enrich (Anjos-Afonso et al., 2022, Rix et al., 2022). This is in part due to the extremely high variance of human samples (Doulatov et al., 2012). Despite these marker combinations being the gold standard and frequently used, there is still much room for improvement in human HSC identification strategies that provide increased specificity. Currently, the low purities achieved with existing strategies prevent scientists performing single cell assays on these crudely isolated human cell populations. The identification of novel protein markers for human HSC populations, and the associated development of efficient flow cytometric strategies that would facilitate the isolation of these fractions would be a huge breakthrough in the field of experimental haematology, as assays developed in the murine system, such as single cell proteomics, are ready and waiting for human translation, and would massively aid the study of human HSC heterogeneity and molecular

profiling. This in turn would enable a significantly deeper understanding of the therapeutic potential of human HSCs.

1.3.4 Reporter mice for HSC identification

Despite surface marker reporter strategies such as ESLAM and ELSK enriching HSCs to approximately 50% purity, these are far from perfect, hence the importance of utilising additional HSC identification strategies. Alongside surface protein analysis, further tools we have at our disposal for murine HSC identification include several reporter mice, which have primarily been developed with aims to label and study HSCs in their bone marrow niche.

A huge range of reporter mice have been developed which enrich for the HSC population, including *Abcg2* (Fatima et al., 2012), *Fgd5* (Gazit et al., 2014)*, Vwf* (Sanjuan-Pla et al., 2013), *Hoxb5 (Chen et al., 2016, Kucinski et al., 2024) ,* and *Ctnnal1* (Acar et al., 2015). The reliability of these reporter mice has been validated through primary transplantation experiments where *Ctnnal1* and *Fgd5* reporters have enriched for HSCs at a frequency of 14.9% and 31.2% respectively. Furthermore, single cell RNA-sequencing (scRNA-seq) of LT-HSCs, LMPPs, MPPs, MEPS, CMPs and GMPs has generated expression maps representing transcriptional changes associated with differentiation in pseudo time. This facilitated the grouping of tested cells into 4 clusters, of which retrospective analysis determined that Cluster 1 contained predominantly LT-HSCs. As expected, expression levels of protein markers used as the basis for several of these reporter mice, Hoxb5, Fgd5, and Ctnnal1, were highest within Cluster 1 (Nestorowa et al., 2016).

In this thesis, I have focused on the use of the $Fgd5^{ZsGreen+/ZsGreen+}$ mouse. The Fgd5 protein possesses Guanine Exchange Factor (GEF) activity, and has been implicated in the VEGF activation pathway via its interactions with Cdc42. Gazit et al., developed the targeted knock-in/ knock-out $Fgd5^{ZsGreen+ZsGreen/+}$ mouse model, and validated its near exclusivity to cell populations expressing key HSC markers: LSK $CD48^{-}$ $CD150^{+}$. Further tests revealed that cells labelled with the Fgd5 reporter contain all functional HSC activity within the sample. Additionally, even when used as a singular marker within BM samples, the Fgd5 positive cells identified, resembled enriched functional HSC populations, and were capable of successfully reconstituting lethally irradiated mice in several repeated transplantation assays (Gazit et al., 2014).

1.3.5 Single cell approaches (qPCR and RNA-seq)

Although HSC heterogeneity was first observed in functional assays, typically HSC transplantations, the molecular mechanisms driving these differences typically eluded scientists. In order to best dissect the mechanisms that drive fate choice at the single cell level, the development of assays at single cell resolution was required. Stemming in part from the historic inability to isolate individual HSCs, and to differentiate between separate HSC subtypes, the development of novel reporter strategies and surface marker combinations to pull out the functional HSC compartment has unlocked the potential to use single cell approaches to study this rare cell type (Jassinskaja et al., 2023). The first analysis of gene expression within HSCs at the single cell level was performed in 1990, and set the scene for a plethora of single cell HSC qPCR analyses (Brady et al., 1990). Importantly, whilst also identifying heterogeneity within the HSC pools tested, these single cell assays identified a state of lineage priming within the HSC compartment, hinted at by low levels of expression of key lineage-specific genes within the HSC fraction (Mansson et al., 2007, Adolfsson et al., 2005, Laurenti and Gottgens, 2018).

Some of the earliest single cell high-resolution qPCR studies performed on primary HSPC populations utilised microfluidic technology and identified several gene expression signatures within this population (Ramos et al., 2006). This further strengthened the theory that several separate populations with unique molecular and translational signatures exist within this broader LT-HSC phenotype, previously assumed to be a homogenous population (Glozbach et al., 2011)

In line with previous single cell studies, Moignard et al., noted significant heterogeneity within nearly 600 individual freshly isolated primary BM HSPC in terms of their expression of 18 well studied haematopoietic transcription factors, and again noted that subpopulations within this fraction exist in distinct transcriptional states (Moignard et al., 2013). This study also identified a cross-regulatory network of three key proteins: *Gfi1, Gfi1b,* and *Gata2,* which was then functionally validated in cell lines and in *in vivo* transgenic mice studies. This triad was found to be associated with the inhibition of *Gfi1/Gfi1b* antagonism by *Gata2*, in turn regulating HSPC entry into the myelo-lymphoid lineage (Moignard et al., 2003, Wilson et al., 2010). Additionally, single cell qPCR of haematopoietic populations has enabled the analysis and quantification of miRNAs within single haematopoietic cells, and has been used to profile the miRNA landscape coupling haematopoietic differentiation, in the process identifying tightly-regulated miRNA networks underpinning the function of the HSPC pool (Petriv et al., 2010). These studies highlight the invaluable capacity of single cell

transcriptomic studies to unpick the regulatory networks governing HSC behaviour. Importantly, these transcriptomic networks have been shown to be stably maintained and/or oscillate around a fixed mean value, therefore underpinning the maintenance of a HSPC state (Schutte et al., 2016).

The development of single cell RNA sequencing (scRNA-seq), which is not dependent on a targeted gene strategy, or the need for bulk populations, enabled previously unobtainable resolutions in gene expression analysis of thousands of quantifiable genes per cell and has proved to be a hugely important and popular assay in the field. Initially published by Wilson et al in 2015, scRNA-seq was combined with transplantation assays to enable collection of paired molecular and functional data and the establishment of the MolO score to identify functional HSCs via expression of several key genes (previously discussed in section 1.2.7 of this thesis). Following this study, additional work utilising a scRNA-seq data set of 1600 phenotypic HSCs, and several subsets of early progenitors, identified significant transcriptional changes associated with the earliest stages of HSC differentiation were noted in genes associated with altering cell cycle status and metabolism (Dahlin et al., 2018. Nestorowa et al., 2016).

Alongside identifying several fundamental genes and regulatory networks governing HSC fate, self-renewal capacity and multilineage potential, single cell approaches have enabled the refinement of the haematopoietic hierarchical model into a continuum of differentiation matched with incremental changes in the transcriptome of the cells (Laurenti and Gottgens, 2018). In line with developing the hierarchy, a study utilising multiplexed qPCR of 280 surface proteins over 1,500 individual cells, followed by computational progression analysis, identified novel progenitor populations with unique transcriptomic profiles, which could be efficiently isolated through the use of surface markers (Guo et al., 2013, Che and Bode, 2022, Triana et al., 2021). These studies also provided some of the first evidence for the existence of megakaryocyte lineage commitment within the primitive HSPC pool (Psaila et al., 2016).

1.3.6 Bulk assays for HSCs

Alongside single cell approaches, bulk assay techniques such as Chip-seq, proteomic, and phosphoproteomic analyses have become invaluable in unpicking the regulatory mechanisms underpinning HSC biology. These approaches enable the deduction of gene function in the population of interest within fractions isolated based on their phenotype.

1.3.6.1 Proteomics and phosphoproteomics

Arguably, studying protein composition is the most powerful approach for analysing cell types in varying conditions and cellular states. Proteins represent the principal functional component within cells, and through the use of proteomics it is possible to identify, quantify, and characterise the proteins present in bulk populations or single cells of interest (Jassinskaja and Hansson., 2022).

In a pioneering proteomic study by Cabezas-Wallscheid et al., integrated analysis of proteomic, transcriptomic and epigenetic datasets revealed a generally high degree of equivalence between the transcriptome and the proteome (Cabezas- Wallscheid et al., 2014). The strength of proteomics, beyond avoiding the potential 3' end capture bias in transcriptomic approaches (Shi et al., 2021), lies in the fact that the proteome reflects a greater biological complexity than the transcriptome. Proteomic techniques are capable of considering the impact of post-translational modification on genetic transcripts, which influences not only protein folding, but also factors including cellular localisation and protein activation.

However, a limitation of proteomic analysis is the generally substantial cell counts required to perform these assays – traditionally >100,000 cells per condition. This presents a particular challenge when studying rare cell populations such as primary HSPCs, which until recently have been incredibly difficult to expand *in vitro*, and to which challenges still remain, in particular with the expansion of human HSCs. However, the advent of novel methodologies is consistently lowering the cell requirement. Such approaches include tandem mass tag (TMT) labelling (Hernandez-Valladares et al., 2020). However, despite the reduced cell input required for this approach, TMT strategies typically identify lower numbers of proteins than traditional proteomic assays (Dou et al., 2019). Alternatively, nanodroplet processing is a recently developed technique used to facilitate analysis of low-input samples. In these protocols, the entirety of the sample processing and preparation occurs in a single pot in order to reduce sample loss – an important consideration when dealing with samples that are already low in cell number before preparation begins (Zhu et al., 2018, Liang et al., 2021). Similar strategies that work to reduce sample loss are in-StageTip (Kulak et al., 2014) and single-pot, solid-phase-enhanced (SP3) methods (Hughes et al., 2018).

In attempts to perform single cell proteomic analysis, low throughput approaches such as mass spectrometry Time of Flight (CyTOF) are becoming increasingly used, which have been shown to generate proteomics data at the single cell level (Tracey et al., 2021,

Orecchioni et al., 2017). A pioneering study by Knapp et al. used CyTOF to measure the levels of more than 40 markers on single cells from various populations of human cord blood cells pre- and post- growth factor stimulation. These proteins included a selection of activated cell signalling proteins, transcription factors, and cell cycle regulators. Through these experiments, Knapp et al., identified varying pathway-specific responses to stimulation from differing growth factors within enriched human cord blood LT-HSC ($CD49f^{+}$) fractions. Trends noted included an activation of STAT5 following IL-3 exposure, and AKT and MAPK activation following stimulation by SCF or fms like tyrosine kinase 3 (Flt3) (Knapp et al., 2017). More recently, studies have utilised single cell CyTOF to identify key differences linked to gender and ageing within HSC populations (Mohamad et al., 2023). Despite the benefits associated with the low-throughput and high-dimensional protein analysis of CyTOF, this technique relies on antibody panels and a known set of targets to generate their proteomic outputs, reducing its ability to identify novel proteins. Furthermore, considerable variation in CyTOF data between experiments is commonly noted, possibly due to differences in antibody master mix composition and, as a result, several layers of standardisation and normalisation are essential to generate a definitive proteomic dataset (Fernandez-Zapata et al., 2020). Overall, despite developments in sample preparation and the discovery of new mass spectrometry amplification techniques such as isobaric labelling (Specht et al., 2021), only a small number of proteomic studies have been performed on primary HSC populations (Klimmeck et al., 2012, Cabezas-Hallschied et al., 2014, Jassinskaja et al., 2017, Jassinskaja et al., 2021, Zaro et al., 2020). The earliest of these studies required cell inputs of 400,000-1,000,000 (Klimmeck et al., 2012), however more recent studies have successfully reduced this requirement to 50,000 mouse HSCs, and 25,000 human HSPCs (Amon et al., 2019, Zaro et al., 2020).

Phosphoproteomics is a branch of proteomics used to identify solely proteins containing a post-translational phosphate group. As a consequence, phosphoproteomics is primed to decipher and quantify the activity of several kinase regulated signalling pathways within cell samples at one time (Gerritsen and White, 2022). This technique holds incredible potential for studying HSCs as several well studied signalling networks have been linked to HSC self-renewal, differentiation, and metabolic rewiring, and phosphorylation is the governing post-translational modification in these HSPC signalling pathways. However, much like traditional proteomics, HSC numbers remain a limiting factor and therefore the vast majority of phosphoproteomic studies to date have been performed on cell lines or whole tissues (Hallal et al., 2017). Although a handful of studies have performed phosphoproteomic profiling on the HSPC population directly, ~200,000 cells are still necessary to achieve appropriately quantifiable results (Wang et al., 2016).

Overall, despite advances in both low cell number proteomics and phosphoproteomics, the HSC proteome remains relatively poorly understood with refinement of proteomics protocols an ongoing process, leaving many exciting discoveries still to be made.

1.3.6.2 ChIP-Seq and ATAC-Seq in haematopoietic research

Alongside the proteome and transcriptome, it is important to also consider the epigenetic landscape and the state of chromatin accessibility in the cell in order to gather a refined understanding of the molecular mechanisms governing HSCs. With the well studied association of ageing with an altered epigenetic state, it seems highly likely that the epigenetic landscape influences and regulates HSC ageing and accompanying loss of function, and therefore also the development of haematological disease and malignancy (Itokawa et al., 2022). Using chromatin immunoprecipitation sequencing (ChIP-Seq) on stringently purified HSC populations, scientists have been able to identify key regulatory chromatin marks within this population which differ between young (4 months) and old (24 months) mouse HSCs. These regulatory marks include activating H3K4me3 marks (tri-methylation of lysine 4 of histone H3) which increase 6.3% in old HSCs, and repressive H3K27me3 marks (tri-methylation of lysine 27 on histone H3) which increase at the Flt3-Ligand (Flt3L) locus with age, impeding its expression (Sun et al., 2014). Additionally, ChIP-Seq analysis has highlighted epigenetic differences within several HSC subsets – contributing to overarching HSC heterogeneity (Yu et al., 2017).

Unlike ChIP-Seq, which identifies specific interactions between proteins and DNA, ATAC-Seq (Assay for transposable-accessible chromatin with sequencing) acts genome-wide, identifying areas of open chromatin available to be transcribed. In turn, ATAC-Seq can generate a thorough list of transcription factors, enhancers and promotor regions which affect gene expression and ultimately the function of HSCs. ATAC-Seq has highlighted significant differences in chromatin accessibility specifically within the HSC fraction between young and old cells, whilst differences in chromatin accessibility became smaller within increasingly differentiated populations (Itokawa et al., 2022).

The use of genome wide DNA methylation analysis has brought to light several phenomena within HSCs and MPPs that accompany the early stages of haematopoietic differentiation. Whilst similar global levels of methylation existed between all fractions, more than 15,000 differentially methylated regions (DMRs) could be identified between HSC and MPP fractions. It was observed that the number of DMRs increased significantly within

increasingly differentiated populations. For example the HSC versus the most primitive MPP1 populations had 1121 DMRs, mostly associated with a generalised loss of methylation, whilst between MPP2-MPP3/4 1874 DMRs were identified, and an overall increase in global methylation was discerned (Cabezas-Wallscheid et al., 2014).

Taken together, these experiments highlight the great contribution of epigenetic data to furthering our understanding of HSC biology, and demonstrate how important it is to consider the epigenome alongside the transcriptome and proteome to gain a thorough understanding of the systems at play.

1.4 The in vitro expansion of HSCs

Haematopoietic stem cell (HSC) self-renewal is a process that is essential for the development and homeostasis of the blood system. Self-renewal expansion divisions, which create two equally multipotent daughter HSCs from a single parent HSC, underpin the growth of the blood forming system. This property can be harnessed to create large numbers of HSCs for a wide range of cell and gene therapies, but the same process is also a driver of the abnormal expansion of HSCs in diseases such as cancer. This section will detail the importance of the *in vitro* expansion of HSCs, key protocols for the culturing of human and mouse HSCs, the foundational biology which underpins the development of these strategies, and the significant challenges still affecting this field.

1.4.1 Importance of in vitro HSC expansion

This is an exciting time for studying HSCs, with new protocols for expanding mouse HSCs *in vitro* (Wilkinson et al., 2019) being translated to human HSCs (Sakurai et al., 2023) and the molecular drivers of haematological malignancies being mapped to an unprecedented level. This ability to produce large numbers of HSCs has opened the door to a wide range of experimental assays previously considered impossible to perform on HSCs owing to the scarcity of this cell type. Moreover, experiments that have required herculean efforts and hundreds to thousands of mice can now be performed using only dozens (Bain et al., 2022, Bode et al., 2021).

On the clinical front, HSC transplantation (HSCT) is an ever evolving field, and remains one of the sole curative therapies for a range of acquired and inherited haematological diseases and malignancies. With two approaches possible for HSCT: autologous (using the patient's own HSCs) or the more common allogeneic (using healthy donor cells from a human leukocyte antigen (HLA) matched donor), it is well known that in both instances, the dose of

cells given to the patient correlates directly with likelihood of transplant success (Remberger et al., 2020).The minimum cell dose considered safe for patients (i.e. provides a high degree of certainty that the transplanted material will successfully repopulate) is 3-4x 10^6 $CD34^+$ cells/ kg of body weight, which is often larger than can be obtained, especially from autologous sources where $CD34^+$ numbers may fluctuate with the patients' disease burden (Karpova et al., 2019).

Furthermore, in the case of allogeneic HSCT, only 50% of patients are able to find a perfectly HLA matched donor "10/10 match", whilst a further 20-30% rely on a 9/10 matched donor sample. 20-30% of patients therefore do not find a suitably HLA matched donor, furthering the appeal and necessity of refining autologous approaches (Tiercy, 2016). This highlights the massive clinical benefit that HSC *in vitro* expansion holds. The capacity to take donor cells, expand them *in vitro* whilst maintaining their functional potential, and possibly even combining the expansion period with gene therapy protocols before transplanting the expanded, genetically corrected cells back into the patient, would be ground-breaking. Targeting HSCs for gene therapy is an exciting prospect; as the apex of the haematopoietic hierarchy, a genetically corrected HSC could provide an entire corrected haematopoietic system, at all stages of haematopoietic differentiation. Such approaches have been noted most recently for monogenic diseases such as leukodystrophies and sickle cell disease (Spencer-Chapman and Cull 2023, Fumagalli et al., 2022), and experimental approaches combining CRISPR genetic correction with selective expansion of successfully modified clones (Becker et al., 2023) have highlighted the strength of single cell HSC expansion protocols when combined with gene therapy. Despite this potential, in several studies it has been noted that HSC function in terms of self-renewal capacity is lost over the course of the *in vitro* expansion period, as well as variable levels of culture associated differentiation – both of which are significant limitations in terms of ultimate long-term transplantation success (Bastani et al., 2023). However, more recently developed HSC expansion strategies have been generated which aim to mitigate this functional loss, and will be discussed in detail in the following section of this thesis.

Furthermore, the ability to generate vats of mature blood cells *in vitro* is also of clinical interest, in order to meet the increasing demands for functional mature cells for blood transfusions, which often end up being long term, frequently repeated, therapies for patients over several years (de Swart et al., 2020). To date, several cell types have been generated *in vitro*, including T- cells (Seet et al., 2017), neutrophils (Dick et al., 2008), megakaryocytes and platelets (Masuda et al., 2013, van Wilgenburg et al., 2013). Whilst current strategies are exciting proof of concepts which set the stage for future development, they have yet to

generate the vast yields required to meet demands of patients. Improving HSC expansion, providing an increased starting material used to derive these mature cells *in vitro*, would no doubt scale up these approaches and would increase bulk numbers achieved from these protocols.

Several key strategies have been developed for the *in vitro* expansion of both mouse and human HSCs, in order to address these key scientific, and clinical, challenges and demands. These will be discussed in the following section of this thesis.

1.4.2 Key protocols for the in vitro expansion of mouse HSCs

The current gold standard of mouse HSC expansion was developed in 2019, where expansion of up to 899-fold increases in functional HSC numbers can be achieved over 28 days (Wilkinson et al., 2019). Although these cultures are reductionist and intentionally synthetic, in order to avoid batch variability in reagents such as foetal bovine serum (FBS), they are grounded on the information gained over the last decades on SCF and TPO concentrations during the FL expansion phase. In PVA cultures (in contrast to adult BM where much higher doses are utilised), low SCF (10ng/mL) is combined with high TPO (100 ng/mL) to achieve the best expansion results (Figure 1.3, Wilkinson et al., 2019, Bowie et al., 2007). However, despite this breakthrough, we still lack robust markers for functional HSCs post-culture, and HSCs still remain the minority of cells present at the end of the 28 day period.

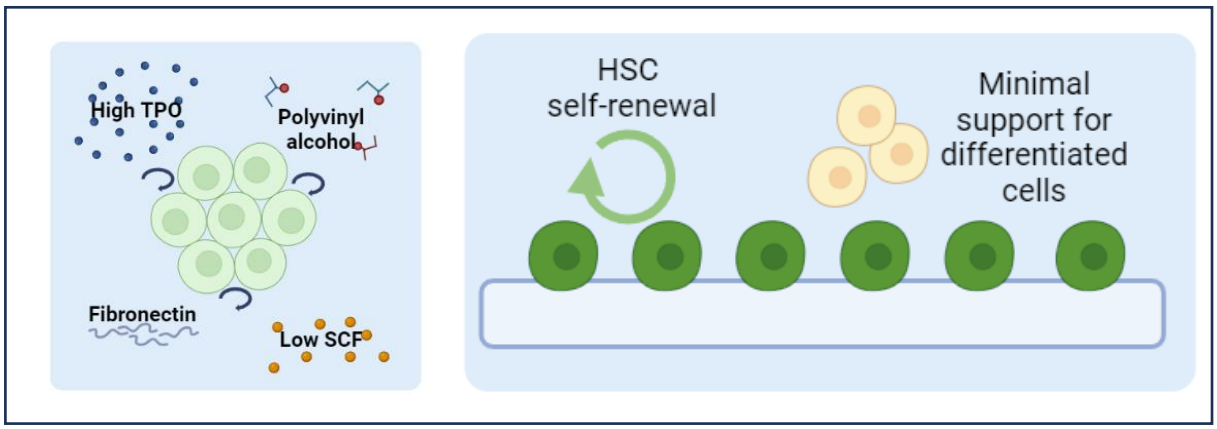

Figure 1.3 **Graphic adapted from Wilkinson et al., 2019 depicting PVA HSC expansion cultures**. Here, a PVA based media supplemented with low SCF (10 ng/mL) and high TPO (100 ng/mL) is used to achieve the best expansion results (Wilkinson et al., 2019, Bowie et al., 2007). Made in BioRender.

Interestingly, studies using this polyvinyl alcohol (PVA)-based protocol show that expansion of the phenotypic HSC compartment occurs largely independently of total cell proliferation in the culture and, as a result, overall cell number is a poor surrogate for HSC expansion (Wilkinson et al., 2019, Che et al., 2022). This is in accordance with previous studies showing that cytokine conditions stimulating rapid proliferation and higher cell numbers often do not yield the most functional HSCs (Audet et al., 1998). Prior to the Wilkinson et al. study, the best expansion attempts with haematopoietic cytokines only achieved HSC maintenance *in vitro* for a week or two at most (Yamazaki and Nakauchi, 2014), suggesting that cytokines alone are limited in their capacity to maintain long-term self-renewal. As a result, numerous other strategies, such as transgene expression, soluble factors and supportive co-cultures, were developed in attempt to expand HSCs *ex vivo* (Sekulovic et al., 2011, Ohta et al., 2007).

1.4.3 Key protocols for the in vitro expansion of human HSCs

Efforts to expand human HSCs, on the other hand, have historically not been so successful. Expansion of human HSCs *in vitro* has proved significantly more challenging than that of mouse, with only modest increases in the number of transplantable HSCs being achieved. Several studies involving cytokines alone achieved a 3-fold increase in HSC number after 10 days using serum free media supplemented with various combinations of IL-6, IL-3, IL-11, Flt-3 ligand, Granulocyte Colony-Stimulating Factor (G-CSF), and SCF (Miller and Eaves., 1997, Bhatia et al., 1997). More recently, groups have succeeded in gaining 3- to 20- fold increases in $CD34^+$ cell numbers using PVA-based media after 7 (Wilkinson et al., 2019), or 14 (Sudo et al., 2021) days. This modest expansion prompted a number of groups to then explore the addition of small molecules to the media such as StemRegenin1(SR1) (Boitano et al., 2010) and UM171 (Fares et al., 2014), both of which substantially improved the traditionally limited levels of human HSC *in vitro* expansion. UM171 elicits its effects on human HSCs via the activation of CULLIN3 ubiquitin ligase and subsequent polyubiquitylation and degradation of the LSD1-CoREST epigenetic regulating complex. This ensures the maintenance of H3K4me2 and H3K27ac marks, which are typically lost rapidly in human HSC during *in vitro* culture (Fares et al., 2014). SR1 antagonises the aryl hydrocarbon receptor and selectively promotes the expansion of human $CD34^+$ cells 12- to 17-fold, whilst also inhibiting proliferation of the $CD34^-$ population (Boitano et al., 2010). Collectively, however, the limited number of long-term serially transplantable HSCs and their purity in expansion cultures remain major obstacles for the field.

Most recently, a breakthrough by Sakurai et al., 2023, has established a chemically defined culture system that enables long-term expansion of human HSCs *in vitro,* reaching approximately 75-fold expansion of total cells and 55-fold expansion of $CD34^+$ cells over 30 days. Here, the key cytokines SCF and TPO have been replaced by the chemical agonists 740Y-P and Butyzamide respectively. The addition of UM171 (or UM729, a structurally similar molecule with very similar effects on HSC expansion *in vitro*) to the expansion culture medium further improves this culture system and allows expansion of cord blood (CB) HSCs that are able to be serially transplanted. However, single cell expansion cultures are still not yet feasible with this approach – largely in part to the lack of markers able to identify HSC populations to high levels of purity (Anjos-Afonso et al., 2022). Despite this constraint, this protocol remains a major discovery in the field and will mitigate many of the previous limitations of working with human cells, such as the limited number of long-term serially transplantable human HSCs generated post-culture and their historically low purity in expansion cultures. This brings us one step closer to allowing scientists to generate clinically useful sources of expanded HSCs.

1.4.4 Using foetal liver HSCs as a guide for in vitro HSC expansion

Although HSCs are first produced during early embryonic development, the key stage and location where they undergo maximal expansion is in the foetal liver, making this tissue a rich source of data for deciphering the molecules driving HSC self-renewal. Another equally interesting developmental stage occurs post-birth, several weeks after HSCs have migrated to the bone marrow, when HSCs undergo a developmental switch and adopt a more dormant state (Bowie et al., 2007, Copley et al., 2013, Kim et al., 2007). Characterising these transition points during development is key, both for understanding the evolution of haematological malignancies and for developing novel protocols to promote HSC expansion (Lewis et al., 2021). Differences in the intrinsic gene regulatory networks and extrinsic cues that regulate FL and adult HSCs ensure that the demands of each ontological stage are met. For FL HSCs, this involves the rapid expansion and establishment of the haematopoietic system, whereas in the adult it is HSC regulation and homeostasis. In particular, in the FL between embryonic day (E) 12.5-15.5, HSC self-renewal is prolific and HSCs are maximally expanding (Bowie et al., 2007). Therefore, understanding the molecular mechanisms that regulate HSC self-renewal at this time point is key to exploit their enormous potential. Through utilising knowledge about regulatory pathways and external biophysical niche signals at play during this key developmental stage, discussed in detail previously in Section 1.2.3 of this thesis, we can aim to recapitulate this environment *in vitro* and refine HSC expansion.

Recent developments in HSC expansion protocols, especially a seminal study by Wilkinson et al., 2019, highlighted the importance of a combination of SCF and TPO supplementation being especially efficient in encouraging *in vitro* HSC expansion. This correlation between SCF and TPO being the key cytokines forming the basis for *in vitro* expansion of adult HSCs, and their importance in development as discussed in Section 1.2.3, is significant and further justifies the need to look towards development for likely targets to improve expansion further.

1.4.5 Key cytokines and proteins for the in vitro expansion of HSCs

Experimentally, cytokines have many advantages for use in HSC expansion and have been combined in a wide range of multi-factorial screening studies. Their ease of use, the reversibility of their effects by removal, and the lack of permanent DNA manipulations make cytokines very attractive for stimulating HSC self-renewal. An early study optimised and assessed the effects of four key cytokines linked to HSC *in vitro* expansion (TPO, FLT3 ligand, SCF and IL-11), performing an extensive two-level factorial analysis, testing every possible factor combination at two different concentrations (Audet et al., 2002). SCF and IL11 were identified as the most potent stimulators of *in vitro* HSC expansion. Based on this and a study by Miller and Eaves,1997, it was concluded that TPO offers no beneficial effect to adult HSC expansion and this was later extended to FL HSCs (Bowie et al., 2007a,b). However, a number of other groups have offered a different perspective, suggesting that TPO is crucial for HSC *in vitro* self-renewal (Nakauchi et al., 2001, Kimura et al., 1998, Solar et al., 1998, Wilkinson et al., 2020, Chou and Lodish, 2010). Explanations for these differences could include the effects of differing base medium and various supplements. Regardless, a large number and variety of cytokine conditions have been optimised over the years, largely still focused on TPO, SCF and gp130 (IL6ST) stimulants (e.g. IL-6, IL-11).

1.4.5.1 SCF and c-Kit

SCF, also known as steel factor, is encoded by the *Sl* gene, and is a growth factor capable of binding to and inducing the downstream signalling of its cognate receptor c-Kit. SCF and its receptor c-Kit are influential both in development and in adult haematopoiesis, where they play key roles in controlling HSC numbers (Metcalf., 2008, McCulloch et al., 1965) and the microenvironmental regulation of HSCs (McCulloch et al., 1964). Mutations in either SCF or c-Kit have been widely associated with haematopoietic defects in mice. For example, mutations occurring within the c-Kit kinase domain result in decreased CFU formation, and therefore reduced HSC function (Kent et al., 2008b). On the other hand, mutations in SCF

impact the supportive BM niche, which is essential for the maintenance of the HSC population, and the CFU forming capacity of HSCs (McCulloch et al., 1965). Interestingly, although FL HSCs are strongly dependent on c-Kit activation, they require much less SCF than adult HSCs despite similar levels of c-Kit expressed on the surface (Bowie et al., 2007b).

SCF has been shown to induce proliferation of HSCs and progenitors in both mouse and human cells, either when acting alone or coupled alongside synergistic cytokines such as FLT3, IL-6, IL-3, and TPO (Ogawa et al., 1997). In these instances it is possible to achieve 14 days of functional HSC expansion, where repopulation capacity is maintained. Additional analysis using individual HSCs has highlighted the ability of SCF to enhance functional HSC self-renewal, and revealed that individual HSCs cultured in SCF supplemented media, compared to a 30-fold lower dose of SCF, present with significantly increased repopulation capacity in a transplantation setting (Kent et al., 2008a). Interestingly, a study utilising KIT negative-regulator SPRED1 (sprout-related EVH1 domain-containing protein 1), found that mice models deficient in SPRED1 (and therefore without the consequent KIT inhibition), presented with increased HSC self-renewal (Tadokoro et al., 2018). A further study blocked SCF-c-Kit signalling via inhibition of lipid raft clustering. As a result of this inhibition, HSCs remained as single cells in a state of hibernation for 5-10 days. This suggests that whilst SCF is essential for HSC cell-cycle entry and subsequent *in vitro* expansion, it may not be fundamental for the maintenance of stemness within this population (Yamazaki et al., 2006).

1.4.5.2 TPO and MPL

Thrombopoietin (TPO) is a secreted protein primarily produced in the liver and contains two key domains: an MPL-binding N-terminal, and a C-terminal glycan domain. Interestingly, TPO also has 2 binding domains with significantly different binding affinities. As a result, TPO binds to MPL sequentially in a two-step assembly model, binding first via the high-affinity Site 1 to the first MPL monomer, before relying on low-affinity Site 2 binding to induce dimerisation of the MPL receptor via interaction with a second MPL monomer. Intriguingly, serum levels of TPO are generally 1000-fold lower than the binding constant of high-affinity Site 1, implying that the vast majority of MPL molecules are unbound at any given time (Cornish et al., 2020). As a result of MPL dimerisation, an array of downstream signalling is induced, acting via JAK-STAT, CREB, AKT and ERK pathways (Tsutsumi et al., 2023).

MPL is a group 1 cytokine receptor, consisting of an extracellular TPO-binding domain and a cytosolic domain enabling intracellular protein interaction and downstream signalling,

connected via a helical transmembrane domain. Lacking kinase activity itself, MPL instead relies on binding to Janus kinase (JAK) proteins, mainly JAK2, in order to initiate its downstream signalling cascade (Drachman et al., 1999). As a result of this dependency, mutations in JAK2 are capable of inducing constitutive activation of MPL downstream signalling (Figure 1.4, Wilmes et al., 2020). As demonstrated in cell lines, surface levels of MPL are dependent on the extent of available TPO. This can be utilised in an experimental setting via the removal of TPO from the culture medium before assay initiation which induces a large upregulation of surface MPL expression, providing a starting point for internalisation assays. Importantly, utilising cycloheximide treatment to block de novo protein synthesis in the cells before resupplying TPO still results in a rapid reemergence of MPL on the cells surface. This implies a reservoir of MPL is retained intracellularly, ready for transport to the membrane (Dahlen et al., 2003).

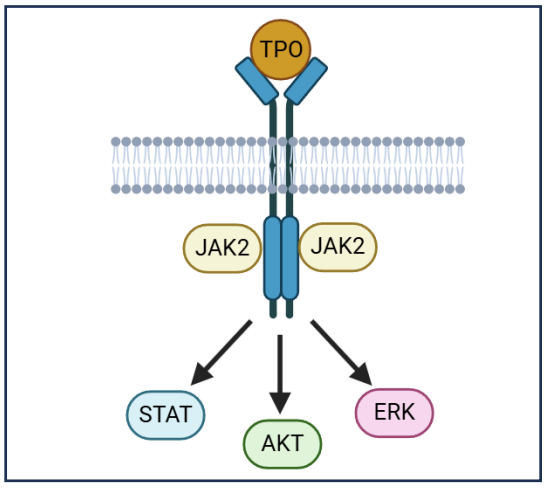

Figure 1.4 **Schematic outlining downstream signalling induced by the MPL receptor following TPO binding.** Image created in BioRender.

TPO and MPL are crucial haematopoietic regulators, modulating megakaryocyte differentiation, platelet production, and platelet homeostasis (Hitchcock et al., 2021). Generally, the concentration of TPO in the plasma is inversely correlated with platelet counts. The TPO receptor, MPL, is predominantly expressed on platelets and megakaryocytes, but is also present on HSCs from the earliest developmental timepoints (Petit-Cocault et al., 2007). TPO plays an important role in regulating HSC self-renewal and is essential for HSC maintenance (Audet et al., 2002), where knock out studies show that TPO-null mice have decreased numbers of repopulating HSCs (Solar et al., 1998) and that genetic deletion of MPL, the TPO receptor, reduces HSC self-renewal potential (de Graaf and Metcalf., 2011). Additionally, genetic perturbation of Lnk, a negative regulator of TPO

signalling whose expression increases with age, increases HSC-self-renewal (Seita et al., 2007). Lnk acts through negatively regulating JAK2, a receptor tyrosine kinase downstream of many different cytokines, including TPO, IL-6 and IL-11 (Gery et al., 2009). A single Lnk-deficient HSC can expand approximately 3000-fold after transplantation (Ema et al., 2005). Notably, TPO and MPL are dispensable for FL HSC survival and expansion (Qian et al., 2007). Furthermore, in humans, the importance of TPO in HSC regulation is highlighted in patients with loss-of-function mutations in MPL who present with congenital amegakaryocytic thrombocytopenia and eventually develop BM failure (Ballmaier et al., 2003).

Several groups have published that TPO is crucial for HSC *in vitro* self-renewal and many groups continue to use the combination of TPO alongside SCF (Solar et al., 1998, De Graaf and Metcalf., 2011). In conclusion, alongside TPO's vital roles in megakaryopoiesis and platelet homeostasis, it is also an important regulator of HSC function, self-renewal, and *in vitro* expansion.

1.4.6 Biophysical and mechanical approaches to refine HSC expansion

The mechanical properties of the HSC niche also appear to be crucial for both the maintenance and regulation of established foetal and adult HSC populations, for haematopoietic commitment and development, and for the initial generation of HSCs via EHT. Given the important role played by the HSC niche, it is conceivable that the historic lack of success in HSC *ex vivo* expansion is at least in part due to the inability of liquid cultures or even stromal co-cultures to satisfy the three-dimensional and mechanical aspects of the HSC niche. Consequently, bioengineering approaches that allow us to both understand the biological importance of, and more accurately imitate, the HSC niche *in vitro* are highly relevant and hold great potential. This is an ongoing challenge, facilitated through the engineering of artificial 3D niches supplemented with extracellular matrix (ECM) proteins and functionalised hydrogels (Bai et al., 2019). In order to mimic the niche accurately, matrix stiffness, ligand type and spatial distribution are important factors that must be considered. Stiffness of the niche has already been linked to HSC morphology, mobility and cell adhesion, and ligand type has a significant impact on the lineage biases of HSCs (Li et al., 2021).

Recently, optical scaffolds made of 3D nanofibers have been demonstrated to permit the culture of cells on structures that maintain high porosity for cell migration and nutrient transport and that are perhaps more realistic models of HSC growth *in vitro*. Nanofibers may be biological (collagen/fibrin/tropoelastin) or synthetic polycaprolactone (PCL), polyethylene

terephthalate (PET), polyurethane (PU), ceramics, a hybrid of both, and/or functionalised with molecules such as CXCL12 to improve HSC culture (Li et al., 2021). Ceramic electrospun nanofibers are particularly exciting and relevant to the study of HSCs, having been shown to mimic a number of bone properties (Esfahani et al., 2017). The diameter of these nanofibers as well as their density and pore size influence the behaviour of cells that are cultured upon them. One example used umbilical cord HSCs, showing that HSCs expand 178- to 194-fold in these 3D cultures compared with 50-fold when using traditional 2D plates (Chua et al., 2006), and another study achieved ~550-fold increases in $CD34^+$ cell numbers (Das et al., 2009). Moreover, murine embryonic stem cells have been shown to have increased survival, proliferation and phenotypic HSC-specific differentiation when cultured in 3D artificial niches (Dehdilani et al., 2016). Finally, MS-5 stromal cells have been used to produce extracellular matrices *in vitro*, which can then act as scaffolds for culturing $CD34^+$ human cord blood cells (Tiwari et al., 2013) and it was shown that the acellular scaffolds increase phenotypic HSCs and CFUs by 80-fold.

Microfluidic devices can also be used to manipulate and control liquids in small volumes (of 10^{-9} to 10^{-18} litres) using channels that are tens of microns in diameter. These are proving to be useful platforms, especially for mimicking cardiovascular forces, such as shear stress, and can also be scaled up for use in bioreactors (Islam et al., 2017; Whitesides, 2006). The future application of such microfluidic approaches in the context of HSC expansion could also provide exciting results. Larger-scale experiments, potentially in combination with hydrogels and/or mechanical stresses, are also now possible and could be used to identify the key pathways that govern HSC expansion and translate these findings to human HSC biology. Fed-batch systems, which provide an automated and continuous supply of fresh media to the cultures, are already being applied with novel small molecules such as UM171 and SR1 (Fares et al., 2014, Boitano et al., 2010) to achieve improved levels of expansion. Combining such promising avenues will undoubtedly lead to success in future clinical-scale human HSC expansion.

1.5 Diseases of the haematopoietic system

As discussed throughout this thesis, the existence of a tightly regulated balance between self-renewal and differentiation within the haematopoietic system is fundamental. Loss of this regulation results in the development of various haematopoietic diseases originating from the HSC population, and if this dysregulation is maintained, can develop into blood cancers (Fabre et al., 2022).

Leukaemia is an example of a heterogeneous group of haematological malignancies, and is the most common cancer in paediatric patients (Metayer et al., 2016). In leukaemias, an increase in HSC self-renewal is coupled by a block in differentiation, resulting in the production of abnormal, and non-functional blast cells (Sell, 2005). Based on the speed of disease onset, as determined by proliferation rates (chronic or acute), and the affected cell type, it is possible to subdivide leukaemias into several subtypes. The vast majority of leukaemias fall into one of the four most common subtypes: acute myeloid leukaemia (AML), chronic myeloid leukaemia (CML), acute lymphoid leukaemia (ALL), and chronic lymphoid leukaemia (CLL) (Khoury et al., 2022). Several predisposing genetic risk factors are associated with leukaemic development, including Shwachman-Diamond syndrome (Myers et al., 2020), Bloom syndrome (Cunniff et al., 2017), Fanconi anaemia (Alter, 2014), and germline mutations in key driver genes such as RUNX1 (Simon et al., 2020). However it is also important to consider that leukaemias often develop spontaneously through the acquisition of random mutations (Derks and van Boxtel, 2023).

Alongside leukaemias, myeloproliferative neoplasms (MPNs) are prevalent haematological diseases and present with several overlapping driver mutations with AML. As a result, patients experience an over-proliferation and expansion of cells of specifically the myeloid lineage, with the potential for leukaemic transformation (Nangalia et al., 2017). The genetic foundations and subtypes of MPNs will be discussed in greater detail in the following section of this thesis.

1.5.1 Myeloproliferative neoplasms

Myeloproliferative neoplasms (MPNs) are clonal haematopoietic disorders, which result in an overproduction of various differentiated haematopoietic cells (Nangalia et al., 2017). There are 3 main diseases that fall underneath the umbrella of MPNs, polycythaemia vera (PV), essential thrombocythemia (ET), and myelofibrosis (MF), linked through their predisposition to both thrombotic complications, and leukaemic transformation (Greenfield et al., 2021). MPNs are frequently classified by their driving mutation, and are split initially into either positive or negative for presence of the mutant fusion protein *BCR-ABL1,* originating from a Philadelphia chromosomal translocation (Tefferi et al., 2015). The negative *BCR-ABL1* MPNs can then be further subdivided based on mutually exclusive JAK2, calreticulin (CALR), and MPL mutations (Tefferi et al., 2015). See Table 2 for relative frequencies of these mutations in MPN types. Of note, the single point mutation $JAK2^{V617F}$, which results in a constitutively active protein and aberrant JAK-STAT signalling (Dusa et al., 2010), is widely prevalent in MPNs and has been linked to 95% of PV cases, and 60% of ET and MF cases.

	Polycythaemia Vera	Essential Thrombocythemia	Primary Myelofibrosis
JAK2	95%	60%	60%
CALR	0%	20%	25%
MPL	0%	3%	7%

Table 1.2 **Frequency of MPN driver mutations.** Relative frequencies of the 3 key driver mutations JAK2, CALR, and MPL within MPN patients. Tefferi et al., 2015

JAK2 is known to be associated with the cytoplasmic fractions of receptors for key haematopoietic cytokines, including TPO, a key component of HSC expansion cultures. The impact of the JAK^{V617F} mutation, which results in a constitutively active JAK2 molecule is thought to incur a survival advantage for the mutant HSC, thereby promoting the myeloproliferative phenotype (Gou et al., 2022). Further genetic aberrations that perturb JAK-STAT signalling are mutations of MPL itself. These mutations induce conformational changes to the MPL receptor that mimic TPO binding, therefore bringing cytoplasmic JAK2 molecules into close enough proximity to induce the downstream JAK-STAT pathway (Nangalia et al., 2017). CALR mutations are noted in the majority of JAK or MPL unmutated patients with ET or MF. These mutations present as either insertions or deletions in the terminal exon of the gene, and result in a +1 base pair shift in the reading frame for this endoplasmic reticulum chaperone protein (How et al., 2019). The mutated CALR again activates JAK/STAT signalling through pathogenically binding to, and activating, the thrombopoietin receptor MPL (Merlinsky et al., 2019).

The last 15 years have seen significant improvements in our ability to understand the molecular basis of these diseases, enabling generation of novel targeted treatments, including JAK inhibitors such as Ruxolitinib (Greenfield et al., 2018). However, despite our ever increasing understanding, allogeneic stem cell transplantation remains the only potentially curative treatment (Shah et al., 2021). MPNs provide an excellent model for investigating haematological malignancies at the earliest stages of disease development, before the malignant transformation occurs. Additionally, the chronic nature of MPNs enables long-term follow-up of patients, and a tracking of patient outcomes. Furthermore, the prevalence of mutations in MPNs affecting the TPO receptor, and downstream TPO signalling (Tsutsumi et al., 2023), make MPNs an especially relevant disease to study in the context of TPO-reliant expansion culture platforms.

2. Aims of this thesis

Despite the vast progress made in the field of *in vitro* HSC expansion, and pioneering protocols for the expansion of mouse (Wilkinson et al., 2019) and human HSCs (Sakurai et al., 2023) being published in the last 5 years, these protocols continue to require refinement. In particular, HSCs remain the minority of cells at the end of the culture period, and we lack markers and reporter systems which enable isolation of expanded HSCs to 100% purity. Therefore, the first aim of this thesis is to identify novel reporter strategies for functional HSCs following *in vitro* culture.

The second aim of this thesis is to adapt and apply HSC expansion systems to sample types that have historically been challenging to expand significantly *in vitro*. Specifically, this thesis aimed to achieve significant *in vitro* expansion of healthy human peripheral blood samples, and human myeloproliferative neoplasm patient samples. Firstly, the ability to expand patient samples *in vitro* would facilitate large scale omics approaches to be performed on these rare cells, which would enable researchers to unpick the molecular mechanisms governing the differences between the healthy and disease states. Secondly, in the case of HSC transplantation assays, cell dose provided to the recipient directly correlates to likelihood of transplant success, and therefore expanding HSCs *in vitro* prior to transplantation would be clinically valuable.

Finally, the third aim of this thesis is to investigate the underlying mechanisms of HSC expansion cultures, in particular the mechanism of action of the key cytokine TPO in expansion protocols. This thesis aimed to uncover functional differences between TPO and alternative TPO mimetics in order to further refine expansion strategies.

3. Materials and methods

3.1. Mice

Mice were maintained in conditions governed by the Home Office PPL as guided by ASPA (Animals Scientific Procedures Act, 1986) and passed through the local AWERB. Mice were kept in individually ventilated cages (IVCs) in specified pathogen free conditions and were provided with continuous bedding, food and water. Mice were culled by exposure to an increasing concentration of CO2 and then confirmational cervical dislocation was performed. Cells were isolated from the bone marrow of the tibia, femur and hips of both hind legs, the sternum, and the spine by crushing the bone in 2% Foetal Bovine Serum (FBS; Sigma or STEMCELL Technologies (SCT)) in PBS (Phosphate-buffered saline, Sigma). Samples were filtered through 20-micron sterile filters before further processing. $Fgd5^{ZsGreen\cdot ZsGeenr/+}$ knock in/knock out mice were purchased from Jackson Laboratories and wild-type (WT) mice were either $Fgd5^{+/+}$ litter mates or C57BL/6. All transplantation recipients were $C57BL/6^{W41/W41}$-Ly5.1 (W41). W41 mice have a missense mutation in the Kit locus. As a result, these mice present with half the numbers of HSCs compared to WT and therefore do not require a full lethal dose of irradiation before undergoing transplantation, instead requiring a lower sub-lethal dose of 3.6Gy.

3.2. Red Blood cell lysis

Red cell lysis was performed using Ammonium chloride (NH4Cl, SCT, Cat.No. 07800). The cells were pelleted by spinning at 300 x g for 5 minutes (min). Then, the supernatant was removed and the pellet resuspended in 3mL PBS 2%FBS. 5mL of NH4Cl was added and cells were incubated for 5 min on ice. After a short vortex to ensure the pellet was fully resuspended, cells were again incubated for another 5 min on ice. The cells were washed with 12mL of PBS 2%FBS (spun down at 300 x g for 5 min, supernatant removed) and then in preparation for lineage depletion, cells were resuspended in 500µL PBS 2%FBS and transferred to a polypropylene test tube.

3.3. Lineage depletion

The EasySep Mouse Hematopoietic Progenitor Cell Isolation Kit (SCT, Cat.No. 19856) was used to enrich haematopoietic stem and progenitor cells (HSPC). The 500µL of cell suspension was incubated with 10 µL of EasySep Mouse Hematopoietic Progenitor Cell (HSPC) Isolation cocktail for 15 min on ice. 20 µL of EasySep Streptavidin RapidSpheres (SCT, Cat.No. 19860) was added for an additional 15 min incubation on ice. 2mL of PBS 2%FCS was added to dilute the sample, and the tube was placed in the EasySep Magnet (SCT, Cat.No. 18000) for a 3 min incubation at room temperature (RT). Whilst still in the

magnet, the supernatant was carefully poured out into a new tube and the magnetic step was repeated another time.

3.4. Isolation of primary HSCs from bone marrow using FACS

The enriched cell populations were stained for ESLAM markers ($CD48^{-}CD150^{+}EPCR^{+}CD45^{+}$), which are able to identify cells with HSC activity across development (Benz et al., 2012). As a live-dead stain, a 1:1000 dilution of 7-Aminoactinomycin D (7-AAD) (ThermoFisher Scientific, Cat.No. A1310) was used. The samples were then sorted on a Beckman Coulter MoFlo Astrios. E-SLAM cells were isolated using CD45 BV421 (Clone 30-F1,1 BD Biosciences (BD)), EPCR PE (Clone RMEPCR1560, SCT), CD150 PE-Cy7 (Clone TC15-12F12.2, Biolegend), CD48 APC (Clone HM48-1, Biolegend), Sca-1 BV605 (Clone D7, Biolegend) and 7-AAD. The following filter sets were used: 585/29 (for PE), 670/30 (for APC), 460/50 (for BV421), 670/30 (for 7AAD) and 610/20 (for BV605). 1 ESLAM cell was sorted into the inner 60 wells of a fibronectin coated 96-well plate, each well already containing 200µL of HSC expansion media (described below). In all experiments, the ESLAM gating strategy was used to sort HSCs (Figure 3.1). Although Sca-1 gating is also included in the panel, it is not used to sort on but instead included for reference and retrospective analysis.

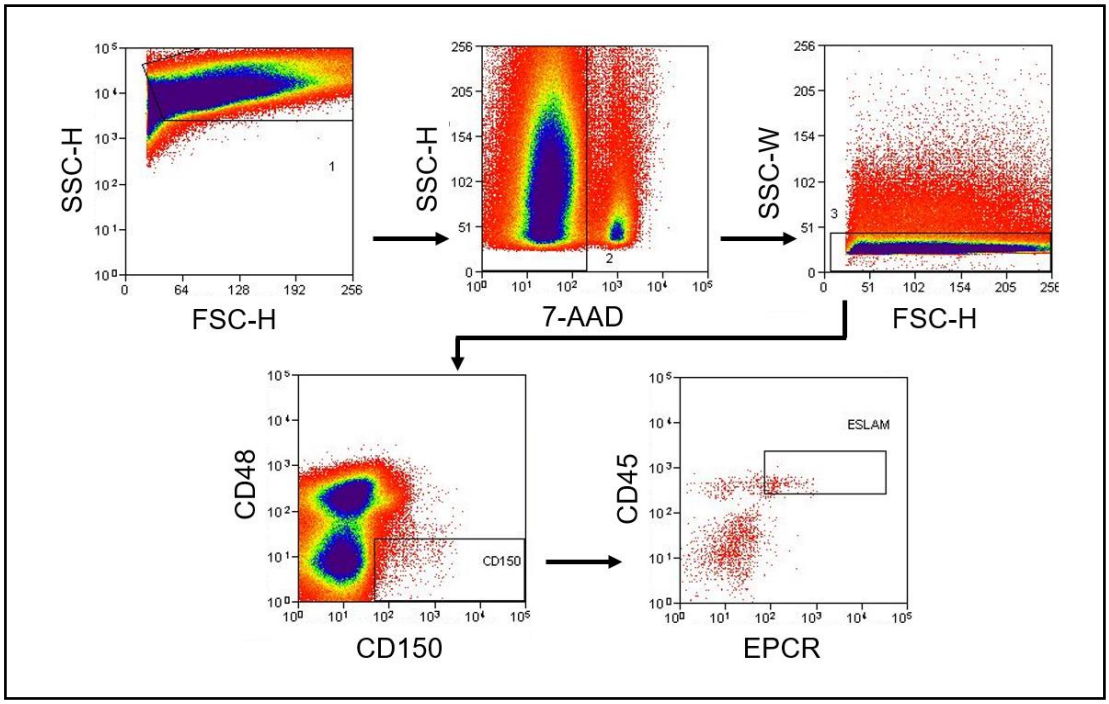

Figure 3.1 **ESLAM Gating strategy for mouse HSCs**. Here, the ESLAM ($CD48^{-}$ $CD150^{+}$ $EPCR^{+}$ $CD45^{+}$) gating strategy is used to isolate fresh HSC populations from mice bone marrow For retrospective analysis and to further validate the ESLAM isolation strategy, HSC markers Sca-1, c-Kit, and Fgd5 are included.

3.5. 28 day PVA based expansion of murine HSCs

Single sorted HSCs were cultured at 37ºC with 5% CO_2 on fibronectin coated 96 well plates in 200µL of Ham's F12 nutrient mix (ThermoFisher Scientific, Cat.No. 11765054) supplemented with 1% Insulin-Transferrin-Selenium-Ethanolamine (ITSX, Gibco, Cat.No. 51500056), 10 mM 4-(2-hydroxyethyl)-1-piperazineethanesulfonic acid (HEPES, Gibco, Cat.No. 15630080), 1% Penicillin/Streptomycin/L-Glutamate (P/S/G, Gibco, Cat.No. 10378016), 100 ng/mL truncated mouse TPO (Peprotech, Cat.No. 315-14), 10 ng/mL mouse SCF (Peprotech, Cat.No. 250-03) and 0.1% PVA (Sigma-Aldrich, Cat.No. 341584). In specified experiments, full length mouse TPO, expressed and purified by Peak Proteins was utilised in place of standard, truncated TPO. Complete medium changes were initiated at day 5/7 and then took place every 2-3 days for the remainder of the 28 day long culture.

3.6. 10 day expansion of mouse HSCs in StemSpan cultures

Single sorted ESLAM cells were cultured at 37ºC with 5% CO_2 on 96-well U-bottom plates (Corning, Cat.No. 3799) in 200µL/well serum free StemSpan media. This consists of an SFEM base media (SCT, Cat.No. 09655) supplemented with 1% Penicillin-Streptomycin (PenStrep) (Sigma-Aldrich, Cat.No. P4333), 1% L-Glut (Sigma-Aldrich, Cat.No. G7513), 0.2% beta-mercaptoethanol (Sigma-Aldrich, Cat.No. 444203), 300ng/mL mouse SCF (SCT, Cat.No. 78064), and 20ng/mL human IL-11 (SCT, Cat.No. 78025.2). These cultures were left undisturbed, with no media changes, for the entire 10 days of culture.

3.7. Flow cytometric analysis of mouse expansion cultures

Clonal populations, derived from initial single ESLAM cells, were stained with EPCR PE (Clone RMEPCR1560, SCT), Sca-1 BV605 (Clone E13-161.7, Biolegend), Mac1 PE-Cy7 (Clone M1/70, Biolegend), Gr1 PE-Cy7 (Clone RB6-8C5, Biolegend), c-Kit APC-Cy7 (Clone 2B8, Biolegend), CD45 BV421 (CLONE HI30, Biolegend), ESAM APC (Clone 1G8, Biolegend) and 7-AAD (ThermoFisher Scientific, Cat.No. A1310). A defined number of Precision count beads (BioLegend, Cat. No. 424902) were also added to each well and allowed each sample to be back calculated and the proportion of the sample that was run through the cytometer to be deduced. On specified occasions, CD321 FITC (Clone OV-5B8, Biolegend) was added to the panel.

Flow cytometry was performed on a CytoflexLX 375 (Beckman Coulter) or a CytoflexLX 355 (Beckman Coulter) and all data were analysed using FlowJo v10 (Treestar, Ashland, OR, USA). To determine success of single cell clones, the percentage of cells in the clonal population being ELSKs ($EPCR^+Lin^-Sca1^+cKit^+$), representative of functional HSCs (Che et

al., 2022), was calculated (Figure 3.2). Alongside using ELSK alone, Fgd5^{+}ELSK cells (combining the Fgd5 reporter, with the ELSK marker combination (FELSK)) can also be used as a surrogate readout for functional HSC content, as well as EELSK (ESAM^{+}ELSK) following the discovery of ESAM as a reporter for functional HSCs post-expansion.

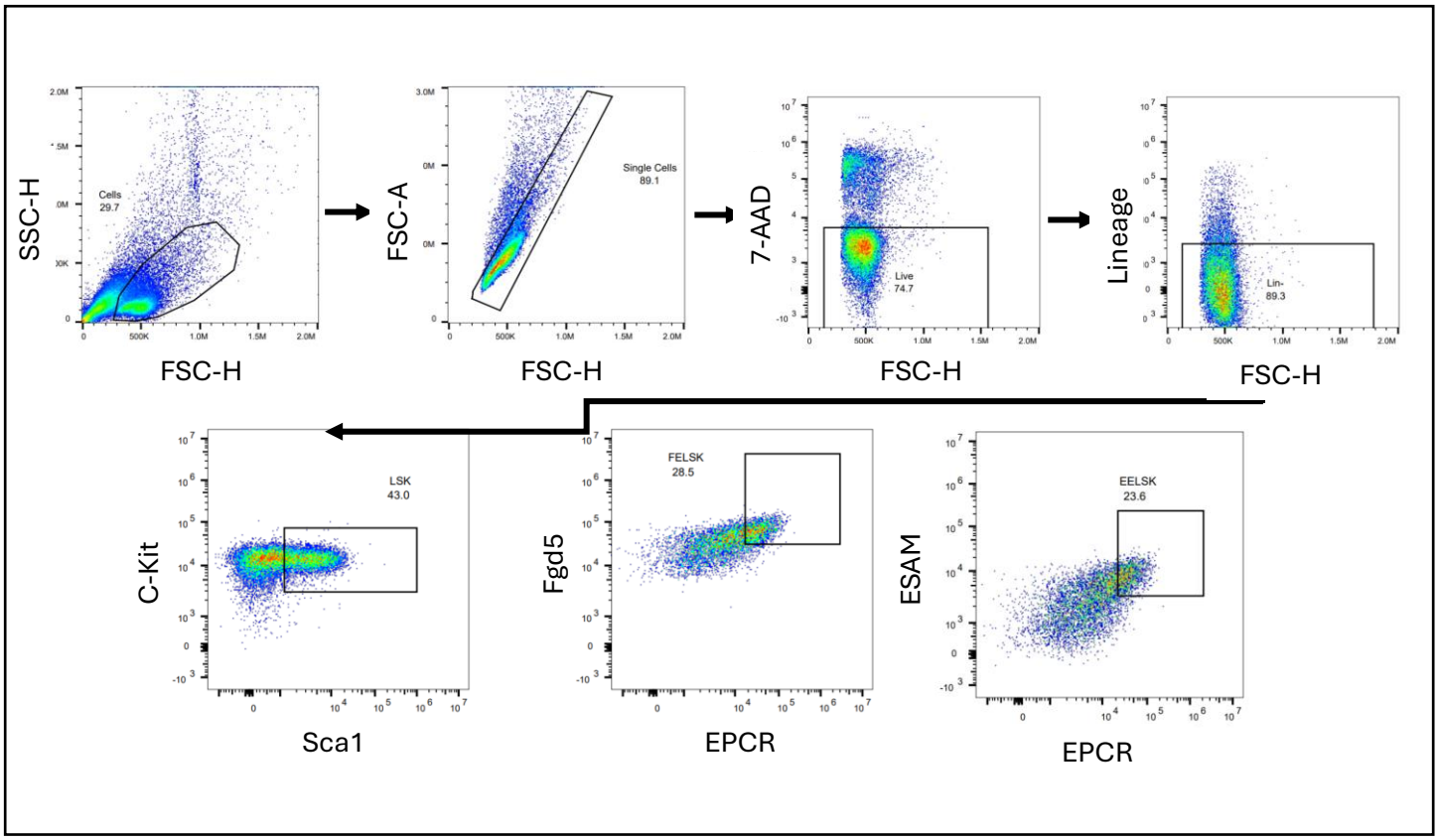

Figure 3.2 **Gating strategy for ELSK/EELSK/FELSK to determine mouse culture success.** EPCR^{+}Lin^{-}Sca1^{+}cKit^{+} (with the optional additions of Fgd5^{+} and ESAM^{+}) are all viable strategies to determine the success of HSC expansion cultures and provide a readout for functional HSCs. The cells were gated initially to remove debris, then sequential gates were set for single cells, Sca1^{+}cKit^{+} and Lineage^{-} to isolate the LSK fraction. Finally, the addition of an EPCR^{+} / Fgd5^{+}EPCR^{+} / ESAM^{+}EPCR^{+} gate identifies the ELSK/ FELSK/EELSK population respectively.

3.8. Bone marrow transplantation assay

Recipient W41 mice were sub-lethally irradiated with a single dose of total body irradiation (1 dose of 3.6Gy). Transplantations were performed via intravenous tail vein injection of 200µL cell suspension using a 29G insulin syringe. Peripheral blood samples were taken as described below at week 4, 8, 12, 16, 20, and 24 week time points. Repopulation is defined as having > 1% donor chimerism and > 1% contribution to the GM (Granulocyte-Macrophage) population at 16 weeks.

3.9. Peripheral blood analysis

Peripheral blood samples were taken from the tail vein at timepoints specified above using EDTA coated microvette tubes (Sarstedt, Cat.No. 20.1288). Red cell lysis using NH_4Cl (SCT, Cat.No. 07800) was performed and samples were then analysed for repopulation levels as previously published (Wilson et al, 2015; Kent et al, 2016). Cells were stained with a cocktail of lineage markers using Ly6g BV421 (Clone 1A8), B220 APC (Clone RA3-6B2), CD3e PE (Clone 17A2), CD11b PE-Cy7 (Clone M1/70), CD45.1 AF700 (Clone A20), and CD45.2 APC-Cy7 (Clone 104). All antibodies were obtained from Biolegend. Flow cytometry was performed on these samples using the CytoflexLX 355 (Beckman Coulter) and this data was analysed using FlowJo v10 (Treestar, Ashland, OR, USA).

3.10. StemBond Hydrogel Fabrication

96-well CELLview plates (Cat.No. 655891, GREINER) were activated to enable StemBond binding. Plates were treated inside a Henniker HPT-200 plasma system before functionalisation with a 5% Bind Silane solution (Cat.No. 17-1330-01. GE healthcare). Plates were then washed with 100% ethanol. Hydrogel solutions were prepared as shown in Table 3.1 before transferring to CELLview plates. Following polymerisation of hydrogel solutions in the wells, gels were rinsed twice in methanol, followed by PBS (Sigma Aldrich), and pH 6.1 MES buffer rinses. Gels were then activated with an EDAC/NHS solution (Cat. No. 1769-25G and 130672-5G, Sigma Aldrich) before washing with a chilled 60% methanol in PBS solution followed by washing with a 50nM pH8.5 HEPES buffer (Cat.No. 15630080, Gibco). The gels were then blocked with an Ethanolamine solution (Cat.No. sc-203042, ChemCruz) in HEPES buffer at room temperature for 30 minutes before rinsing the gels with pH 7.5 HEPES buffer and PBS in order to balance the pH. Gel plates were then sorted at 4℃ until use.

Acylamide (40%)	Bisacrylamide (2%)	Acrylamido hexanoic acid (2M)	H2O	Tetramethylethylenediamine	Ammonium persulphate (10%)
210 µL	163.2 µL	120 µL	2461.8 µL	15 µL	30 µL

Table 3.1 **Volumes to make 3mL of hydrogel solution**

3.11. Human HSC sample selection and preparation for in vitro culture

Frozen human cord blood samples were provided by Anthony Nolan. These samples were previously enriched for CD34 expression and had been verified to expand in StemSpan conditions before being frozen down. Successful expansion in StemSpan conditions consists

of a 10-fold increase in total nucleated cell numbers and a 5-fold increase in $CD34^+$ cell numbers over the course of *in vitro* culture. Patient peripheral blood samples used were obtained from Cambridge and had in the majority of cases been previously pre-enriched for $CD34^+$ cells.

Following sample selection, frozen CD34 enriched blood samples (either cord or patient) were warmed in a 37 degrees Celsius (°C) water bath until 80% thawed. At this point, 1mL of PBS 2%FCS (FCS, Sigma, PBS, Sigma) was added into the sample tube and the sample was mixed gently until thoroughly thawed. The samples were then transferred to a 15mL Falcon tube, containing 10mL PBS 2%FCS and spun at 300 x g for 10 minutes into a pellet before the supernatant was gently removed. The pellet was resuspended in 1mL of 3a media, and then counted on a haemocytometer using Trypan Blue (ThermoFisher Scientific, Cat.No. T10282**)** in a 1:1 dilution. Following cell counting, an appropriate volume of sample, containing the required number of cells, was loaded into the wells of a 96-well CELLBIND plate (Corning, Cat. No. 3337), prefilled with 3a expansion media as described below.

3.12. Magnetic Cell Separation (MACS) enrichment of human mononuclear cell (MNC) samples

Samples are thawed, transferred to a Falcon, centrifuged and supernatant removed as described above. This protocol uses the Miltenyi CD34 MicroBead Kit, Human (Cat. No. 130-046-703). The cell pellet is then resuspended in 300µL of buffer (for up to 10^8 cells), and then 100µL FcR Blocking Reagent and 100µL CD34 Microbeads are added. These are then mixed well and left for 30 minutes at 4°C to incubate. After this, cells are washed by adding 10mL of buffer and spinning the samples at 300g for 10 minutes before completely removing the supernatant. The pellet is then resuspended in 500µL of buffer ready for magnetic separation. The LS column is then placed in the magnetic field of the MACS Separator and is prepared by rinsing with 3mL of buffer. The cell suspension is then added to the column and the flow through (which will contain the unlabelled cells) is collected. The column is then washed 3 times, each with 3mL of buffer – again, all flow through will be collected. The LS column is then removed from the separator and placed onto a collection tube. The column is then loaded with 5mL buffer and a plunger is used to elute the magnetically labelled cells out of the column and into the collection tube.

3.13. Fluorescence activated cell sorting (FACS) of human $CD34^+$ $MPL^{+/-}$ fractions

In order to isolate $CD34^+$ fractions in smaller samples without using MACs enrichment, which would result in a large degree of cell loss, FACS was utilised. Human samples were thawed

as described above, and gently transferred into 10mL PBS 2%FCS in a 15mL falcon. The samples are then spun at 300 x g for 10 minutes and then the supernatant removed using a pipette. The pellets are then resuspended in 120µL PBS 2%FCS and transferred to a FACS tube. 20µL of each sample is then taken for unstained and live-dead controls. The remaining single stains utilise BD CompBeads (BD Biosciences, Cat. No. 552843) rather than cells. To the remaining 100µL, samples are stained with CD34 APC (Clone 581, BD Biosciences), CD38 FITC (Clone HB7, Biolegend), MPL PE (Clone REA250, Miltenyi) and 7-AAD Invitrogen, Cat.No, S7020). Sorted samples were sorted either directly into a 96-well plate pre-filled with 3a expansion media, or into pre-filled Eppendorfs. Samples were sorted on a BD FACSDiscoverer S8 Cell Sorter with BD CellView Image Technology which allowed concurrent sorting and imaging of the cells, enabling visualisation of MPL expression on the sorted cells' surface.

3.14. 3a culture system for in vitro expansion of human HSCs

Culture of human cord or peripheral blood CD34 enriched cells was performed in 96-well CELLBIND plates (Corning, Cat.No. 3337) in a media consisting of IMDM (Gibco, Cat.No. 11504556) supplemented with 1x P/S/G (100x Gibco, Cat. No. 10378016), 1x ITSX (100x Gibco, Cat. No. 51500056), 0.01% Soluplus (BASF, Cat.No. 50477909), 1µM UM729 (SCT, Cat. No. 72332), 5µM 740Y-P (MedChemExpress, Cat. No. HY-P0175) and 0.1µM Butyzamide (Med Chem Express, Cat.No. HY-148748). A schematic outlining this protocol is shown in Figure 3.3. Where specified, the cultures are supplemented with 10ng/mL or 15ng/mL Flt3L (Peprotech, Cat.No. AF-300-19) and 100 µM MTG (monothioglycerol Sigma, Cat.No. M1753).

In certain experiments, Butyzamide is replaced by Romiplostim (Hull University Teaching Hospital)/ Eltrombopag (ATP Bio) /Lusutrombopag (Cambridge Biosciences, Cat.No. 26533) or human TPO (SCT, Cat.No. 78210.1) – concentrations shown below in Table 3.2. Following initial seeding, complete media changes were carried out every 2-3 days for the entirety of the culture period (typically 14-28 days).

Molecule	Low concentration	Mid concentration	High concentration
Eltrombopag	0.14µg/mL	1.4µg/mL	2.8µg/mL
Romiplostim	10ng/mL	100ng/mL	500ng/mL
Lusutrombopag	10nM/mL	100nM/mL	500nM/mL
Human TPO	10ng/mL	100ng/mL	500ng/mL

Table 3.2 **Concentrations of butyzamide replacement molecules tested**. A range of concentrations were tested for each molecule to find an optimum working dose.

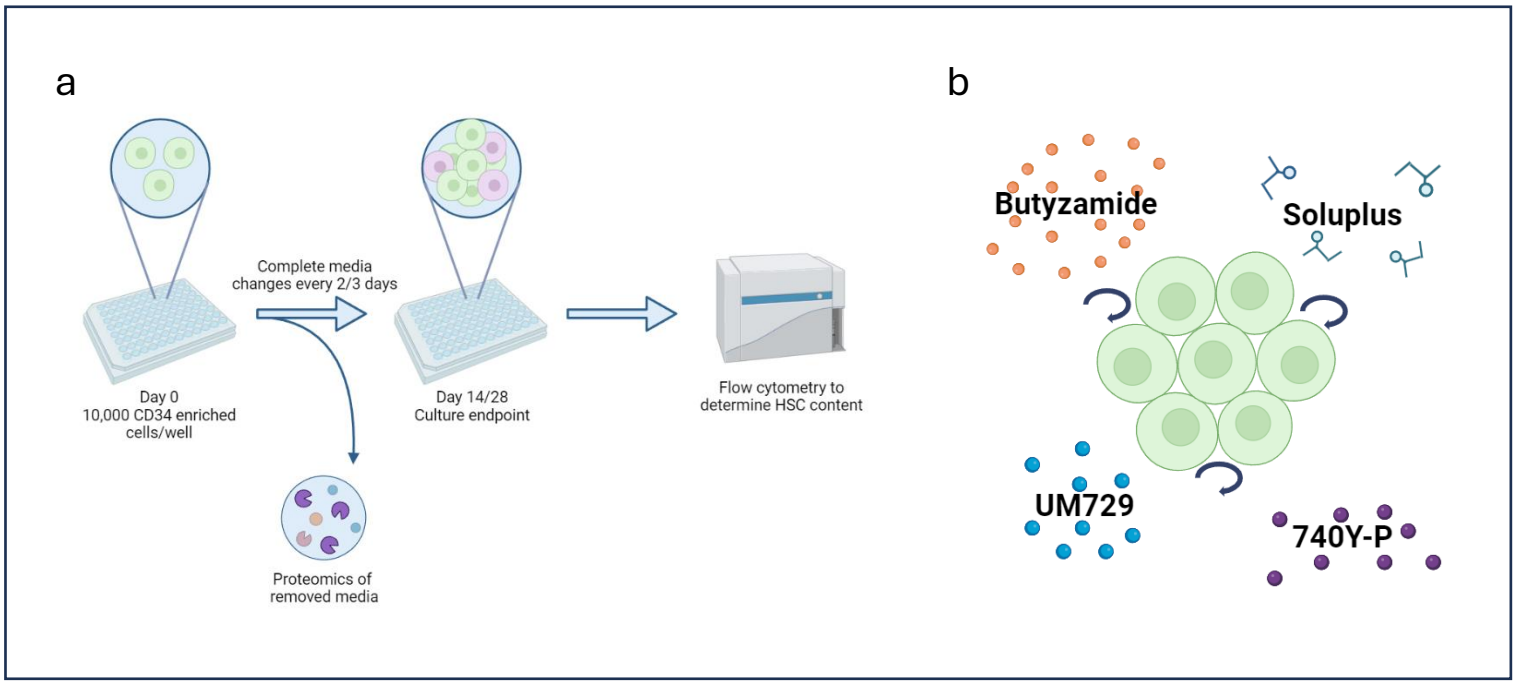

Figure 3.3 **Schematic depicting 3a expansion protocol**. a) Mononuclear cells from human cord or peripheral blood samples are first enriched for CD34 expression, either using FACS of MACS enrichment. 10,000 $CD34^+$ cells are then loaded per well into 200µL of 3a expansion media. Media changes begin on day 3 and continue every 2-3 days through until the end of culture where they are analysed by flow cytometry. b) Schematic showing 3a media composition. Butyzamide and 740Y-P functionally replace TPO and SCF respectively. UM729 is well studied in regards to promoting HSC expansion so is added as the final and third “A” aka activator. Made in BioRender.

3.15. StemSpan culture system for in vitro expansion of human HSCs

Human cord blood samples were prepared as described above and, following counting, were loaded 10,000 cells/well into a 96-well CELLBIND plate (Corning, Cat.No. 3337). Each well containing 200µL of StemSpan media. This is comprised of a StemSpan base media (Stem Cell Technologies, Cat.No 09655) supplemented with SCF (final concentration 150ng/mL, SCT, Cat.No. 78062), TPO (final concentration 20ng/mL, SCT, Cat.No. 78210.1), and Flt3L (final concentration 150ng/mL, Peprotech, Cat.No. AF-300-19). Over the course of a 14 day expansion, media changes are undertaken on days 3, 7 and 11.

3.16. Flow cytometric analysis of expanded human HSCs

Following expansion in 3a media, cell populations were split in half, to allow 2 antibody panels to be used per sample – an HSC panel, and a progenitor panel. The HSC panel consisted of CD34 APC (Clone 581, BD), CD45RA BV421/APCeFluor780 (Clone HI100, Biolegend), CD90 BV605/PE (Clone 5E10, BD), EPCR PE/BV421 (Clone RCR-252, BD), and Sytox Green (ThermoFisher Scientific, Cat. No. S7020) or 7AAD (Invitrogen, Cat. No, S7020) as a live dead stain. Fluorophores vary between experiments due to the addition of further antibodies to the panel, but clones remain consistent. The progenitor panel contained CD34 PerCP-Cy5.5 (Clone 8G12, BD), CD45RA BV421 (Clone HI100, Biolegend) CD135 BV605 (Clone BV10A4H2, ThermoFisher Scientific), CD41 BV711 (Clone HIP8, BD) and Sytox green (Invitrogen, Cat. No, S7020). A fixed number of Precision Count Beads (BioLegend, Cat. No. 424902) was added to each sample, allowing back-calculation of the proportion of the sample that was run through the cytometer.

Flow cytometry was performed on the CytoflexLX 355 (Beckman Coulter), and data was analysed on FlowJo (Treestar, Ashland, OR, USA). In order to determine the success of human HSC expansion, the percentage of cells in each well expressing the marker combination $CD34^{+}EPCR^{+}CD90^{+}CD45RA^{-}$ was calculated (Figure 3.4)

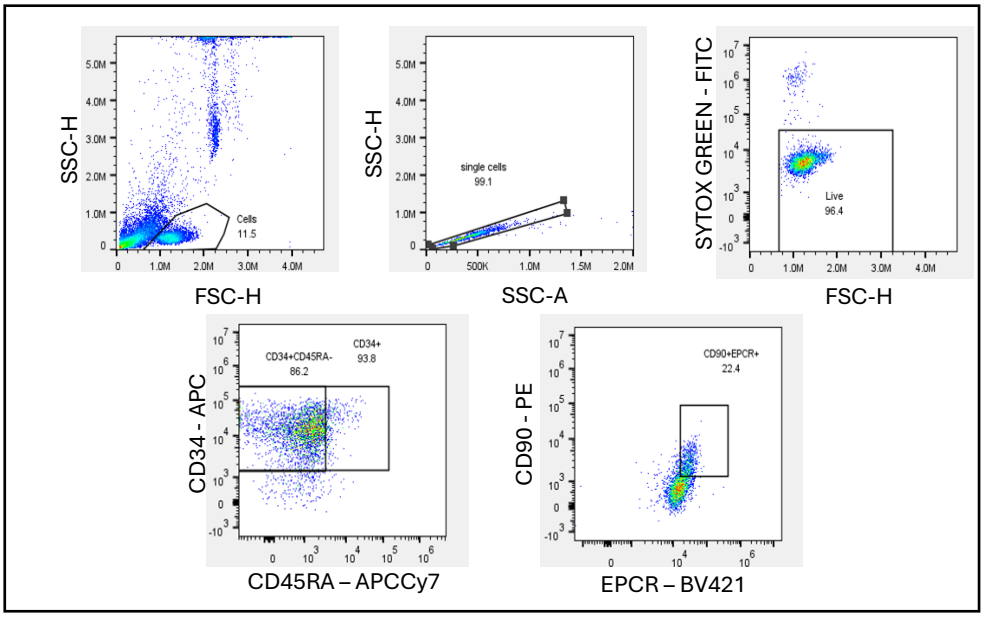

Figure 3.4 **Gating strategy for phenotypic HSC identification post-expansion.** Representative gating strategy for human cord blood enriched cells, post-expansion in 3a medium using $CD34^{+}CD45RA^{-}CD90^{+}EPCR^{+}$ as a readout for phenotypic HSCs. This panel was used to determine success of 3a expansion cultures via determining phenotypic HSC content of each culture.

3.17. MPL quantification

Following completion of flow cytometric analysis of samples, an additional well containing BD Quantibrite Phycoerythrin (PE) beads (BDBiosciences, Cat.No. 340495) is run to enable quantification of PE molecules per cell. Quantibrite beads contain a mix of 4 populations of beads conjugated with 4 known levels of PE molecules per bead. Once the Quantibrite bead samples has been run, subsequent analysis on FlowJo quantifies the mean fluorescent intensity (MFI) of PE within each of the 4 peaks, enabling the generation of a standard curve plotting Log MFI against the Log of the number of PE molecules per cell/bead (Example peak gating and standard curve shown below in Figure 3.5). Once the standard curve has been generated, the Log MFI of varying populations of interest can be plotted and the number of surface PE molecules can be deduced.

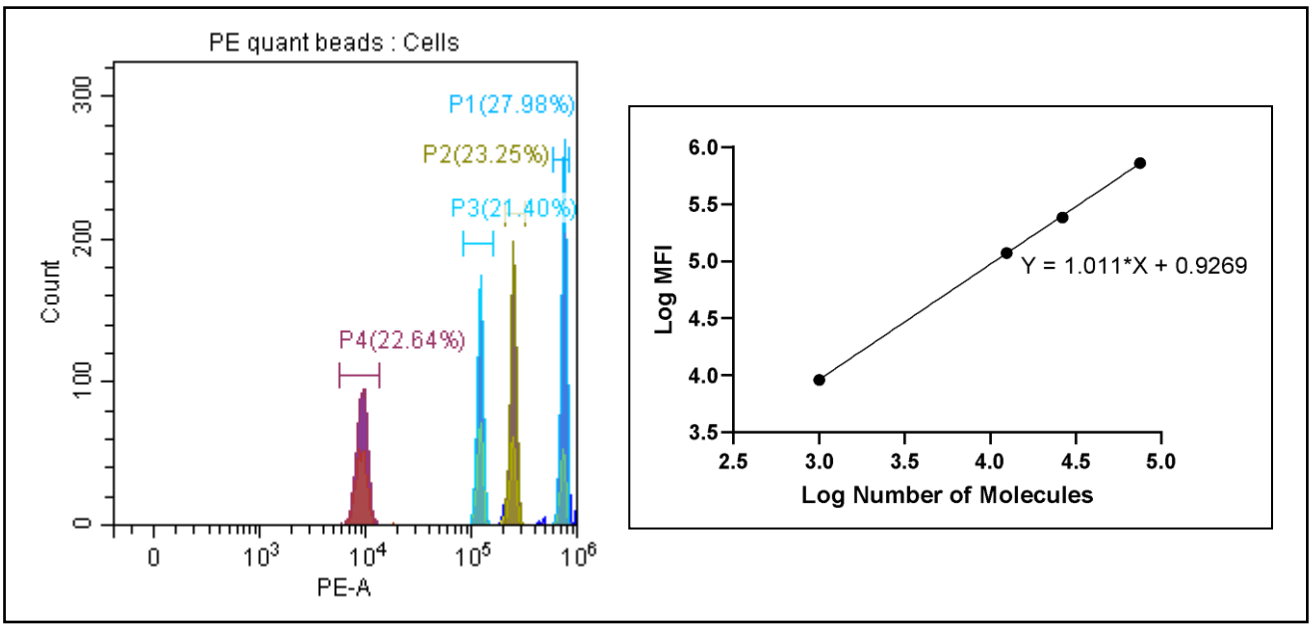

Figure 3.5 **Example gating for PE Quantibrite beads, and representative standard curve.** Through plotting Log MFI of each population, against the log of the known number of PE surface molecules, it is possible to generate a standard curve to which populations with an unknown number of PE molecules can be plotted to allow surface PE quantification.

3.18. Sorting of cells for low cell number proteomics

Human peripheral blood samples from 2 healthy donors, and 2 myelofibrosis patients, were removed from liquid nitrogen storage, and were thawed 80% in a 37°C water bath. The samples were then equilibrated in the storage tube with 200µL PBS 2%FCS (FCS, Sigma-Aldrich) in PBS (Sigma-Aldrich). before tipping into a falcon containing 13mL sterile PBS 2% FCS. The samples were then spun at 300g for 10 minutes at 4°C. The supernatant is then removed, and the cell pellet resuspended in 120µL sterile PBS 2%FCS with 20µL taken for single stains. The remaining 100µL is stained for 30 minutes with 3µL of each antibody – CD34 APC (Clone 581, BD Biosciences), CD38 FITC (Clone HB7, Biolegend), MPL PE (Clone REA250, Miltenyi), before being washed, resuspended in PBS 2% FCS with a 1:1000 dilution of 7AAD (Invitrogen, Cat.No, S7020), and taken to a BD FACSDiscoverer S8 for FACS. The cells were sorted into a LoBind V-bottom 96-well plate (Eppendorf, Cat.No. 0030603303), with 1,10,20, 50 100 or 200 cells per well for each condition and were passed to the proteomics team for processing.

3.19. Urea Lysis of UT7 Cell Line

UT7 cells were cultured in RPMI 1640 (ThermoFisher Scientific, Cat.No, 11875093) supplemented with 10% FCS, 2mM glutamine (Sigma-Aldrich, Cat.No. G7513) and 1x Pen Strep (Sigma-Aldrich, Cat.No. P4333) and were then harvested by centrifugation at 130 x g for 5 minutes at room temperature. The supernatant was then gently removed, and the cells resuspended in PBS as a wash. The sample was centrifuged again at 130 x g for 5 minutes, and the PBS supernatant carefully removed. A 5:1 ratio of room temperature Urea Lysis Buffer (20 mM HEPES pH 8.0, 9 M urea, 1 mM sodium orthovanadate, 2.5 mM sodium pyrophosphate, 1mM β-glycerophosphate) to cell pellet was used to resuspend the pellet. At this step, it is essential that samples are kept at room temperature. Using a microtip sonicator, the lysate was sonicated at 15 W for 3 bursts of 15 seconds. The sample is cooled on ice between each burst for 1 minute. Once sonicated, the sample is centrifuged at 20,000g for 15 minutes at room temperature, and the supernatant, now containing the proteins from the sample, is transferred into a LoBind tube.

3.20. BCA Assay for protein concentration determination

The BCA assay utilised the Pierce BCA Protein Assay Kit (ThermoFisher Scientific, Cat.No. 23225) and is performed in a 96-well plate. Standards had been made up previously, and had been frozen ready to be reused. These standards contained 0, 125, 250, 500, 1000, and 2000µg/mL protein. The assay reagent is made through combining Reagent A and B provided in the kit – 5µL of reagent B in 245µL of reagent A. This can be scaled up if more is required. For each sample, 5µL of sample was loaded into a well, and 95µL of assay reagents was added on top. Samples were diluted to various concentrations with PBS, and then 5µL of the diluted mixture was taken to add to the wells. In addition, 5µL of each standard was added to individual control wells. After the wells had been loaded with sample and assay reagent, the plate is incubated at 37°C for 30 minutes in the tissue culture incubator. After 30 minutes, the plate was taken to a plate reader and using the SoftMax Pro 5.3, the plate was read to determine opacity. Excel was used to determine protein concentration using a standard curve generated from the standards, and the required UT7 cell count for phosphoproteomics was calculated.

3.21. Trypsin digest for proteomics

To each sample, a 1/27.5 volume of DTT reducing solution (19.25mg/mL dithiothreitol in water) is added, and the sample incubated at 55°C for 30 minutes. Once incubation is complete, the samples are cooled at 4°C for 10 minutes before a 1/10 volume of IAM alkylating solution is added to each sample (19mg/mL iodoacetamide in water) and samples

are incubated in the dark at room temperature for 15 minutes. Following incubation, the samples are diluted to a 2M urea concentration (representing a 4-fold dilution from the starting material) with 50nM ammonium bicarbonate. Then a 1:50 (protease:protein, m;m) dilution of trypsin is added to each sample, and is left to incubate at 37°C overnight. The sample is then ready for a desalting step, or to proceed directly to phosphopeptide enrichment.

3.22. C18 column for desalting

This protocol utilises Pierce C18 tips (ThermoFisher Scientific, Cat. No. 87782). Initially, following trypsin digestion, the sample is adjusted to 0.1-1% trifluoroacetic acid (TFA) using 2.5%TFA. The pipette is then set to 10µL, and the C18 tip is loaded onto the pipette tightly. 10µL of 50% acetonitrile (ACN) in water is then aspirated and discarded to wet the tip, this step is repeated once. The tip is then equilibrated by aspirating and discarding 10µL 0.1% TFA twice. 10µL of sample is then aspirated into the C18 tip and then dispensed. Repeat this cycle 3-10 times for maximal sample uptake. The tip is then rinsed by aspirating and dispensing 10µL 0.1%TFA/5% ACN twice. The sample is then eluted slowly via aspiration of 2-10µL of 0.1% formic acid in 50-95% ACN. The sample can then be dispensed into a vial / tube / plate as desired.

3.23. Graphite spin columns for desalting

Firstly, the graphite spin column (ThermoFisher Scientific, Cat. No. 88302) is prepared by removal of the top and bottom cap, before placing into a 1.5mL collection tube and centrifugation at 2000 x g for 1 minute to remove the storage buffer. 100µL of 1M NH_4OH is then added to each column, and the columns are spun at 2000g for 1 minute and the flow-through is discarded, this step is repeated once. The graphite is then activated by the addition of 100µL acetonitrile, before centrifugation at 2000 x g for 1 minute and discarding of flow-through. Finally, to complete column preparation, 100µL of 1% TFA is added to each column before centrifugation at 2000 x g for 1 minute, repeat this step once and discard flow-through. The column is now transferred to a new collection tube and is ready for sample loading. The samples are loaded on top of the resin bed of each column, and allowed to bind for 10 minutes with periodic vortex mixing. Columns are then spun at 1000 x g for 3 minutes, and flow-through discarded. The column is then passed to a new collection tube, and is washed by the addition of 200µL of 1% TFA and centrifuging for 2000 x g for 1 minute. The flow through is then discarded, and this wash step is repeated once. Once washed, the column is transferred to a new collection tube, and 100µL 0.1% formic acid in 50% ACN is added to elute the sample.

3.24. Titanium dioxide phosphopeptide enrichment

Titanium dioxide enrichment beads (MagReSyn® TiO2, ReSyn Biosciences, MR-TID002), are first required to be equilibrated via agitation on a thermomixer at 1100 rpm to ensure an even suspension in storage buffer. Following this, the required volume of enrichment beads (Table 3.3) is transferred to a LoBind 1.5mL Eppendorf (Eppendorf, Cat.No 0030108051), before placing the tube into a magnetic separator to clear the microparticles. At this stage the supernatant, in this instance the storage solution, is able to be removed and discarded. The Eppendorfs can now be removed from the magnetic separator, and 200µL loading buffer is added for 1 minute to equilibrate the beads. The samples are then placed back onto the magnetic separator to allow removal of the loading buffer. The addition and removal of loading buffer is repeated twice to fully equilibrate the beads.

Peptide amount (µg)	Bead Volume (µL)	Bead Amount (µg)
</= 50	20	0.5
100	40	1
200	80	2
500	200	5
1000	400	10

Table 3.3 **Recommended MagReSyn TiO2 beads relative to peptide starting material**

Next, the peptide samples are prepared before phosphopeptide enrichment. Following trypsin digestion, or desalting protocol if necessary, samples are diluted 1:2 (v;v) with 2M glycolic acid in 80% acetonitrile (ACN) and 10% trifluoroacetic acid (TFA) to give a final volume of 200µL. At this stage, the pH of each sample is checked to ensure each is acidic. Once acidity is confirmed, samples are centrifuged at 10,000g for 5 minutes at 4°C to remove any remaining insoluble material. The supernatant, containing the peptides of each sample, is then transferred onto the equilibrated enrichment beads, and is mixed for 20 minutes at 1100 rpm. Once mixed, the Eppendorfs (now containing beads and the peptide samples), are placed onto the magnetic separator, allowing the microparticles to clear, and the supernatant, containing the unbound peptides, can be removed. At this stage 100µL 1M glycolic acid in 80% acetonitrile (ACN) and 5% TFA is added to each sample, and samples are mixed on the thermomixer for 2 minutes at 1100 rpm. Samples are then loaded onto the

magnetic separator and the supernatant is removed. The samples are then resuspended in 100µL Wash Buffer 1 (80% ACN, 1% TFA), mixed for 2 minutes on the thermomixer at 1100 rpm, and supernatant again removed using the magnetic separator. This process is then repeated with 100µL Wash Buffer 2 (10% ACN, 0.2% TFA). Now washed, the samples are eluted from the beads by adding 13.33µL elution buffer to each sample, and mixing for 10 minutes on the thermomixer at 1100 rpm. Once mixed, the magnetic separator is used to clear the microparticles, allowing efficient removal of the supernatant, this time containing the released phosphopeptides which can be transferred to a new LoBind tube (Eppendorf, Cat. No. 0030108051). This step is repeated 2 more times, to ensure complete removal of all phosphopeptides. Once complete, 3% v;v LC-MS grade formic acid is added to each sample to acidify, and pH is confirmed. The sample is now ready for EvoTip loading.

3.25. EvoTip Loading

Before loading, samples are spun at 10,000 x g in order to remove debris, and the supernatant is removed and pellet made up to 20µL in 0.1% TFA. If the sample volume is greater than 20µL, it should be loaded in 20µL increments. Once the corresponding amount of EvoTips (EvoSep, Cat No. EV2011) (one per sample) are acquired and placed into a tip box rack over an empty tip box “dry box”, 20µL of Solvent B (0.1% formic acid in ACN) is added to each tip before centrifugation at 800 x g for 60 seconds, and the disposal of flow through. Isopropyl alcohol (IPA) is then transferred into the appropriate number of wells in a tip adaptor rack, and the tips are placed into the tip adaptor rack wells to soak for 20 seconds, until the tips become translucent. EvoTips are then removed and placed back into the “dry box” and 20µL of Solvent A is loaded into each tip (0.1% formic acid in H_2O). Tips are centrifuged at 800 x g for 60 seconds, and flow through is discarded. Samples are then loaded into the tips, 20µL per tip, as close to the filter as possible, and the tips are spun at 800 x g for 60 seconds. This step can be repeated if several 20µL volumes of sample are required to be loaded per tip. 50µL of Solvent A is then transferred to each tip, and the tips are spun for 800 x g for 60 seconds as a washing step. Once complete, place the tips into a “wet box” containing enough Solvent A to submerge the tips entirely. Remove from the “wet box” and repeat this wash step twice, soaking in the “wet box” between each wash, for a total of 3 washes. Once the wash steps have been performed, 100µL Solvent A is added per tip, and the tips are placed back into the “wet box”, ready to be transferred onto the Bruker TimsTOF HT Mass Spectrometer.

3.26. UT7 cell preparation and MPL internalisation assay

UT7 cells, either WT of JAK2^{V617F} mutated, were spun down at 300 x g for 5 minutes, and washed 3 times with 10mL PBS in order to remove any TPO in which they had been cultured. Once washed, the cells were then resuspended in 1mL RPMI (ThermoFisher Scientific, Cat.No, 11875093) 10% FCS without TPO. The cells were then counted to ensure sufficient cell counts and were incubated overnight to induce maximal surface expression of MPL, the TPO receptor. The following day, cells were resuspended thoroughly, counted on a haemocytometer, and were diluted in RPMI 2% FCS (R2) to allow 10,000 cells to be loaded per well of a 96-well V-bottom plate in a volume of 25µL. 2 plates of WT and 2 plates of JAK2^{V617F} UT7 cells were made up, one of each for MPL internalisation assays, and one for phosphoflow assays (discussed later in Methods). Once loaded into plates, 30µL of R2 was added to control wells, and 30µL of TPO/ TPO mimetics were added to their respective wells – either at varying concentrations,(0.01, 0.1, 1, 10, 100nM) or for varying times (5, 15, 30, 60 minutes at 10nM). Following an incubation period at 37°C for 30 minutes for the concentration series, or variable for the time course, the cells were fixed on ice through adding 15µL of 16% PFA to achieve an ~4% PFA final concentration. The samples were then incubated for 15 minutes at room temperature on a plate shaker set to 550 rpm. Once mixed, the samples are spun at 400 x g for 5 minutes, the supernatant removed, and then the pellets washed with 200µL PBS. For plates designated for phosphoflow analysis, the supernatant is removed, the remaining pellet is resuspended in 200µL methanol and the plates are stored at -80 until required. For plates that are not being frozen down at this point, following washing, the cell pellet is resuspended in 30µL of a 1:10 dilution human TruStain FcX (Biolegend, Cat.No. 422301), and incubated for 15 minutes at 4°C. Whilst the cells are blocking, the MPL antibody Mastermix is prepared, using a 1:100 dilution of CD110 (MPL) PE (Miltenyi, Clone REA250, Cat.No. 130-123-984) in FACS buffer (PBS, pH 7.4, supplemented with 1% (w/v) bovine serum albumin (BSA) and 0.05% (v/v) sodium azide). Once blocking is complete, 70µL FACS buffer is added to each well, and the samples are spun at 400 x g for 5 minutes. The pellet is then resuspended in 30µL antibody Mastermix, or 30µL FACS buffer for the control wells, and the cells are incubated for 1 hour in the dark at room temperature on a shaker set to 550 rpm. After incubation, each well is resuspended in 100µL FACS buffer and is centrifuged for 500g for 5 minutes at 4°C. After centrifugation, the supernatant is removed, and cells are washed with 150µL FACS buffer before being resuspended in a final volume of 80µL of FACS buffer, ready for analysis on a Cytoflex LX.

3.27. Cellular barcoding and phosphoflow assay

Plates containing WT and JAK2^{V617F} UT7 cells treated with MPL agonists at varying time courses, and concentrations, were prepared and frozen down as described in Methods section 3.26. Firstly, the cells are removed from the -80°C freezer and left to thaw at room temperature. Working dye stocks are then thawed, ready for preparation of a master barcode plate. In order to create a barcoding plate, PacBlue (ThermoFisher Scientific, Cat.No.P10163) and DyLight 800 NHS Ester (ThermoFisher Scientific, Cat.No.46421) stocks of 100µg/mL are created in 1.5mL Eppendorfs (Eppendorf, Cat.No 0030123328). In separate 1.5mL Eppendorfs, a series of dilutions are made of both dyes in DMSO (Sigma-Aldrich, Cat.No.D5879). (50, 25, 12.5, 6.25, 3.13, 1.6, 0.8 µg/mL, and a DMSO only control). In a 4x4 grid of a V-bottom 96-well plate, differing combinations of the DMSO only, 0.8 µg/mL, 6.25 µg/mL, and 50 µg/mL dye stocks (Figure 3.6) are combined in in a 1:1 ratio (50µL of each dye) to allow the generation of 16 separate barcodes. The barcodes are then transferred from a 4x4 grid, to 2 columns of 8 to enable easier pipetting, and this barcoding plate can be frozen at -20°C for future use.

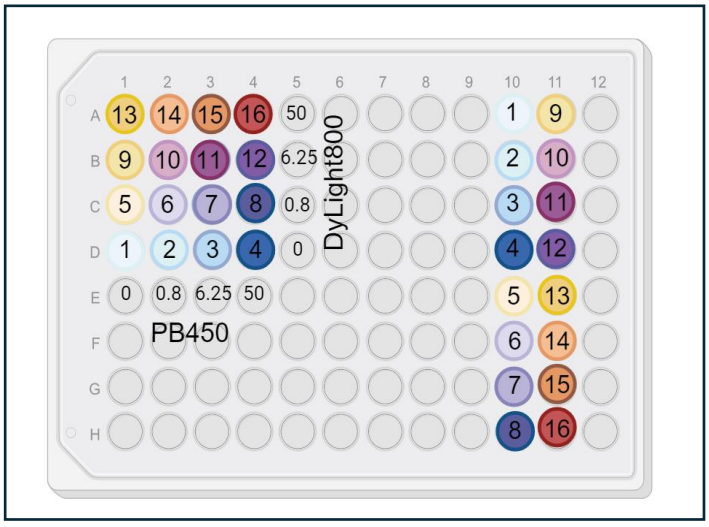

Figure 3.6 **Plate layout for master barcoding plate.** Made in BioRender.

Once the cells are thawed, 60µL cold FACS buffer (PBS, pH 7.4, supplemented with 1% (w/v) bovine serum albumin (BSA) and 0.05% (v/v) sodium azide) is added to each well and the plates are spun at 400 x g for 5 minutes at 4°C. The plates can then be flicked to remove the supernatant, before washing with 200µL cold PBS to remove any residual methanol. With the cells and barcoding plates now ready, 4µL of barcode dye mix is added to each well, and thoroughly resuspended. As each column in the cell plate represents a timepoint, it is vital to ensure that the same barcode is used for each well of the same column, and that each column utilises an individual barcode. Add 200µL cold PBS to each well to balance the

pH. Once the barcode has been added, the cells are incubated for 40 minutes in the dark, at 4°C, on a plate shaker set to 500 rpm. Once incubation is complete, spin down the wells for 5 minutes at 400g, remove the supernatant and wash the pellet with 200µL of cold FACS buffer. The wash step is repeated two more times for a total of three washes. When washing is complete, each row of cells is resuspended in 50µL FACS buffer, and is pooled into a 1.5mL Eppendorf (each row representing a range of timepoints or concentrations of the same agonist). Once pooled, centrifuge the Eppendorfs for 5 minutes at 400 x g to pellet the cells, before removing the supernatant. The cells are then blocked via resuspension of each pellet with 40µL FACS buffer and 10µL Human TruStain FcX (Biolegend, 422302), and incubation at 4°C for 15 minutes. Whilst the blocking step is being performed, the 9 antibody mastermixes are prepared (1:100 dilution of each antibody in FACS buffer, enough for 50µL/well). Antibody combinations are shown below in Table 3.4.

Column	AF48/FITC	AF647/APC
1	pSTAT1 (S727) Clone A15158B, Biolegend	pSTAT3 (S727) Clone A16089B, Biolegend
2	pSTAT3 (Y705) Clone 13A3-1, Biolegend	pSTAT1 (Y701) Clone A17012A, Biolegend
3	pERK (T202/Y204) Clone 20A, BC Phosflow	pMEK1 (S298) Clone A16117B, Biolegend
4		pAKT (S473) Clone M89-61, BC Phosflow
5	pCREB (S133) Clone 87G3, Cell Signalling Technology	pAKT (T388) Clone D25E6, Cell Signalling Technology
6	**PE** mTOR (pS2448) Clone O21-404, BD Phosflow	pSTAT5 (Y694) Clone 47, BD Phosflow
7	pJAK2 Clone E132, Abcam	IRF-1 Clone D5E4, Cell Signalling Technology
8		mTOR Clone 7C10, Cell Signalling Technology
9	Unstained	Unstained

Table 3.4 **Antibody combinations used for phosphoflow** Each column of plate will contain an individual combination of antibodies against two phosphoproteins. Due to the previous barcoding steps of the protocol, each well therefore allows relative quantification of two phosphoproteins on UT7 cells from 5 conditions.

Following the blocking incubation step, the samples are spun at 400 x g for 5 minutes before removal of supernatant and the resuspension of cell pellets in 50µL antibody Mastermix. The cells are incubated for 1 hour at room temperature in the dark, on a shaker set to 550 rpm.

Following incubation, the cells are diluted in 150µL FACS buffer, and the samples are spun at 400 x g for 5 minutes, before the supernatant is removed. The samples are washed once with 200µL cold FACS buffer, before being resuspended in 100µL FACS buffer ready for flow cytometric analysis on a CytoflexLX.

3.28. Picowell and microfluidic fabrication

Before use, BF33 glass substrates are subject to Piranha treatment (3:1 sulfuric acid and 30% hydrogen peroxide), and plasma treatment before undergoing a lamination process to layer an SUEX film onto the surface of the glass. To allow smooth lamination, the substrate and SUEX film were layered between larger polyethylene terephthalate (PET) sheets. The laminator is set to 47°C, and the sample is slowly fed through. Following lamination, the surface PET layer is removed from the SUEX film and using a Kloe Dilase 650, a predesigned Picowell array of total area 1x5mm is patterned into the SUEX layer. No neutral density (ND) filter is used, and velocity is set to 30mm/s, with a beam energy set to 80% of the maximum. Once the exposure step is complete, the BF33 and SUEX substrate is baked for 30 minutes at 85-90°C and then allowed to cool slowly over at least 3 hours (overnight is preferable). Following the post-exposure bake, EC (Ethylene carbonate) solvent is used to develop the chip and remove the non-crosslinked areas (i.e. the areas that were not exposed to UV illumination). Following the development, the chip is then washed in IPA (isopropyl alcohol) and hard-baked at 180°C for 10 minutes.

To prepare for PDMS moulding, the master, which acts as a mould for the PDMS, is cleaned in acetone, IPA, and then deionised water, before using a nitrogen (N2) gun to remove any dust. To prepare the PDMS, using a plastic cup cut down in size to reduce waste, silicone and hardener are mixed in a 7:1 ratio (21mL silicone, 3mL hardener). This is then mixed thoroughly until a uniform cloudy appearance is achieved, before placing it inside a desiccator for 30 minutes to remove any bubbles. The master is then placed inside a petri dish and the PDMS mix is poured gently over. This is then placed back in the desiccator for an additional 30 minutes. Following desiccation, the petri dish containing the PDMS and master is placed in the oven at 65°C overnight. Once baking is complete, a scalpel is used to cut around the edge of the petri dish, and the PDMS and master are removed. The PDMS is then carefully peeled away from the Master, and then cut down to size, leaving at least half a centimetre around the channel. Using a 3mm biopsy punch, holes are punched through the PDMS into the channel, acting as inlets and outlets. The PDMS channel is then washed with deionised water, and the Picowell substrate washed with deionised water and IPA. Both components are then placed into the plasma asher with the surface that will be in

contact with the other component upwards. The setup on the asher is for 2 minutes, at 40 W power and 5 sscm O2. As soon as this plasma treatment is complete, align and bond the samples using the alignment tool and bake at 65°C overnight. The structure achieved at the end of this process is shown in the diagram below (Figure 3.7).

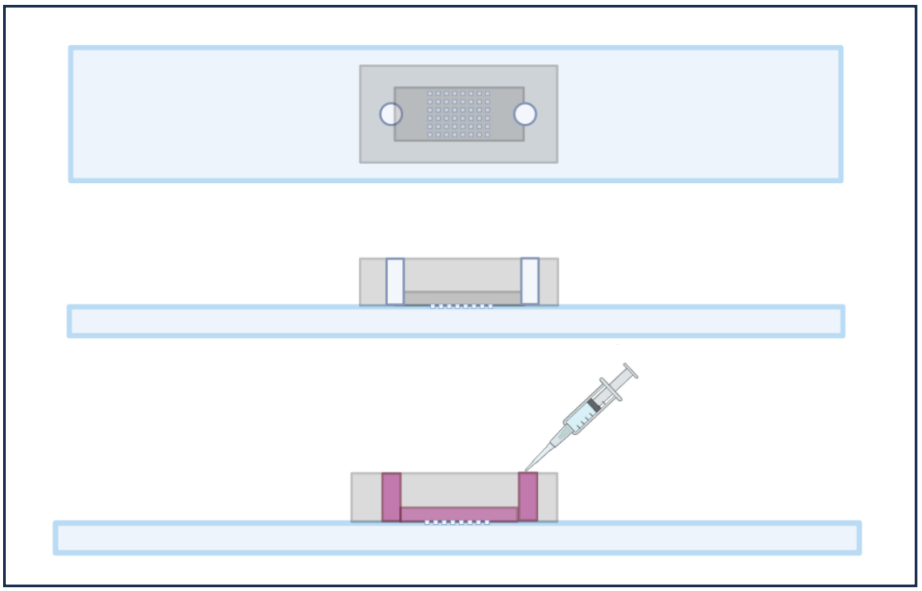

Figure 3.7 **Diagram depicting Picowell design**. Representative diagrams of the Picowell channel engraved on an SUEX/BF33 substrate with PDMS microfluidic channel layered on top. Made in BioRender

3.29. Picowell experiments utilising the Fgd5 system, and loading of ESLAM cells onto chip

Fgd5 mice were culled as described above, and samples underwent red blood cell lysis and lineage depletion. The remaining enriched cell population was stained for LSK markers (Lin^- $Sca1^+cKit^+$) using the following antibodies: Sca-1 BV605 (Clone D7, Biolegend), c-Kit APC-Cy7 (Clone 2B8, Biolegend), Gr1 PE-Cy7 (Clone RB6-8C5, Biolegend), Mac1 PE-Cy7 (Clone M1/70, Biolegend), and a 1:1000 dilution of 7-AAD (ThermoFisher Scientific) to act as a live-dead stain. From the samples, 5000 live $Fgd5^+$ LSK cells were sorted into a sterile 1.5mL Eppendorf containing 500µL of PVA based expansion media on a MoFlo Astrios (Beckman Coulter). Following completion of the sort, the Eppendorf was centrifuged at 300 x g for 5 minutes, before resuspension in 1 or 2 µL of PVA media. This volume was mixed thoroughly and then pipetted gently onto the Picowell chip using a P2 pipette. The Picowell chip was placed into an Ibidi µ-Dish (Ibidi, Cat. No. 81156) and damp filter paper was placed around the inside rim of the dish to limit evaporation. Samples were imaged on LSM980 MP over 24 hours, with images being taken every 15 minutes.

Following the development and addition of a microfluidic channel to the Picowell chip, we were able to refine loading strategies for SLAM ($CD150^+CD48^-Lin^-$) cells. For this, frozen wild type mouse bone marrow samples were thawed in a water bath and then gently poured into a 15mL Falcon tube containing 10mL PBS 2% FCS. 1 mL of additional PBS 2% FCS was then used to wash out the collection tube, before being added to the Falcon tube. Cells were then spun at 300 x g for 5 minutes before removing the supernatant by tipping out and then dabbing onto blue roll to remove any excess media collecting at the lip of the Falcon. The sample was then resuspended in 100µL PBS 2% FCS for antibody staining with the following panel: CD150 BV605 (BD Biosciences, Cat.No. 567309, Clone RUO, CD48 APC (Biolegend, Cat.No. 336713, Clone BJ40), Mac1 PE-Cy7 (Biolegend, Cat.No. 101215, Clone M1/70), Gr1 PECy7 (Biolegend, Cat.No. 108415, Clone RB6-8C5), and a 1:1000 dilution of 7-AAD. The samples were then sorted on a Cytoflex SRT for the live $CD150^+CD48^-Lin^-$ fraction, collecting 2000 cells into a 1.5mL Eppendorf containing 300µL of StemSpan media for the expansion of murine cells. Following the sort, the sample was spun at 300 x g for 5 minutes, the supernatant removed with a pipette, and the pellet resuspended in 10µL StemSpan media. To load into the microfluidic channel, a 2mL syringe was attached to a 20µL pipette tip with the wide base of the tip cut off at the first engraved ring to allow them to fit. The 10µL cell mix was taken up by the syringe into the tip, before gently pushing the tip into the microfluidic inlet (as shown in Figure 3.7) and slowly filling the channel.

3.30. Statistical analysis

All ANOVAs, t-tests and Pearson's correlation statistics were calculated, and graphs were plotted on GraphPad Prism 10.0.2. FragPipe Analyst was used for proteomic analysis.

3.30.1. R studio analysis for PCA and dendrogram plot generation

The following code was used to generate PCA plots from phosphoflow data on RStudio, running R version 4.2.0.

```
> data<-read.csv("file.csv",1)
> pca=prcomp(data,center= TRUE,scale.= TRUE)
> plot(pca$rotation,type="p",pch=1,col=c(1,1,1,1,2,2,2,3,3,3,3,4,4,4,4,5,5,5,5),cex=2,lwd=3)
>legend("topright",c("Butyzamide","Eltrombopag","Media","Romiplostim","TPO"),pch=1,col=c(1,2,3,4,5))
> plot(hclust(dist(t(data),method="euclidean"),method="average"))
```

4. Novel markers for functional expanded mouse haematopoietic stem cells (HSCs) and an investigation into the expansion of ESLAM cells in vitro.

Developing novel and improved culture systems to expand the rare HSC population *in vitro* is a constantly evolving field. Recently, a key paper outlined a new gold-standard protocol for the expansion of functional HSCs *in vitro*, enabling unprecedented increases in mouse HSC number (up to 899-fold) over the course of a 28 day long culture (Wilkinson et al., 2019). However despite this breakthrough, we remain hindered by the fact that HSCs still remain the minority of cells in the culture at the end of the expansion, and we lack robust markers to pull out this population with complete purity.

A widely used approach to the identification of mouse HSCs is the utilisation of the *Fgd5*$^{ZsGreen•ZsGreen/+}$ reporter mouse (Gazit et al., 2014), which facilitates single colour identification of the HSC fraction. However, despite its wide use, the Fgd5 reporter system remains limited by its lack of specificity, marking several haematopoietic populations (Che and Bode et al., 2022). Furthermore, the need for all desired mouse models to be crossed onto the *Fgd5*$^{ZsGreen•ZsGreen/+}$ background in order for this reporter strategy to be used is costly and time consuming, therefore limiting the applicability of this approach. Frequently, the *Fgd5*$^{ZsGreen•ZsGreen/+}$ reporter strategy is combined with the ELSK (EPCR^{+} Lin^{-} Sca1^{+}cKit^{+}) panel for a more accurate reading of the functional HSC content of a well post-expansion as verified by transplantation assays, however these populations still remain contaminated with non-HSCs (Che and Bode., 2022). Therefore, in this chapter I set out to identify novel markers for *in vitro* expanded HSCs, in order to enhance our ability to specifically isolate functional HSC populations post-culture

4.1. Surface marker ESAM can replace reporter gene Fgd5 as a marker for functional in vitro expanded HSCs

Initially, we aimed to replace the use of the *Fgd5*$^{ZsGreen•ZsGreen/+}$ reporter mouse with a more easily accessible surface protein in order to circumnavigate the issues associated with the use of the Fgd5 reporter strategy. When selecting candidates for potential replacement of the *Fgd5*$^{ZsGreen•ZsGreen/+}$ reporter mouse, we initially looked towards RepopSig, a gene set previously generated by the Kent Lab, which can identify the HSC population within several different tissues, at different developmental timepoints, and in both mice and human samples (Che and Bode., 2022). Importantly, this RepopSig was shown to highly correlate with the functional HSC content of expanded clones.

As a starting point, several expansion screens were performed to further functionally validate these RepopSig targets, with a particular focus on surface proteins which have commercially available antibodies against them. In each of the following experiments, expansion cultures were initiated with single ESLAM cells sorted via FACS into fibronectin coated 96-well plates containing 200uL of PVA expansion media (as described in sections 3.4 and 3.5 of this thesis). Following 28 days of *in vitro* expansion (Wilkinson et al., 2019), flow cytometric analysis was utilised to determine the percentage of live cells, and total number of cells, that expressed the marker combination ELSK ($EPCR^{+}Lin^{-}Sca1^{+}cKit^{+}$). This reporter strategy was used as a measure of the HSC content of clones, as previous studies in the Kent Lab have demonstrated that clones containing >20% ELSK cells contain functional HSCs and can be successfully transplanted, meaning they are capable of repopulating the haematopoietic system of a sub-lethally irradiated mouse (Che and Bode., 2022). In addition to ELSK content, Fgd5 expression and expression of various candidate markers were also included in the final day 28 flow cytometric analysis panels (Figure 4.1).

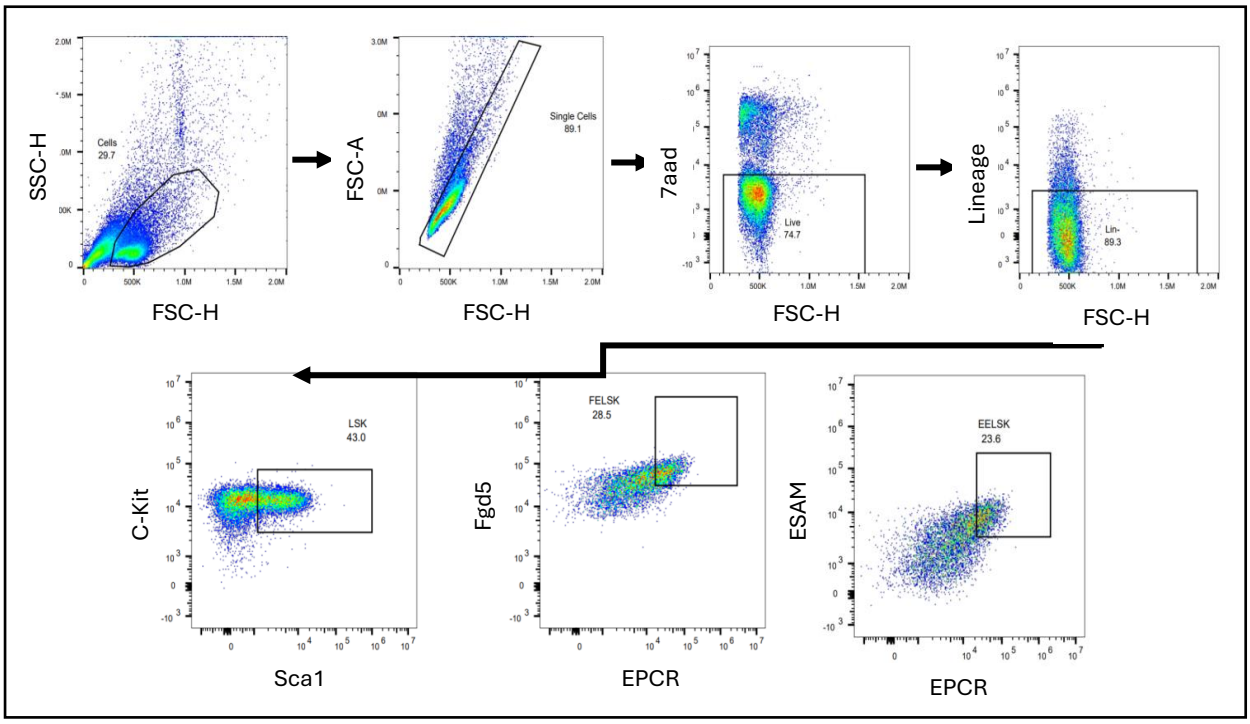

Figure 4.1 **Representative FELSK and EELSK gating strategy**. Used for analysis of expansion cultures either at the endpoint (day 28), or on days 14/21. Following gating for the cell, single cell, and live cell compartments, sequential lineage negative and $cKit^{+}Sca1^{+}$ gates were set to identify the LSK population. Within the LSK population, setting gates of either $Fgd5^{+}EPCR^{+}$ or $ESAM^{+}EPCR^{+}$ allowed separation of the FELSK or the EELSK fractions accordingly.

These expansion screens revealed that Endothelial cell-Selective Adhesion Molecule (ESAM) showed promise at being able to replace the use of the *Fgd5*$^{ZsGreen•ZsGreen/+}$ reporter mouse at marking expanded *in vitro* HSCs (Figure 4.2).

The strong correlations observed between ESAM and both *Fgd5* expression and %ELSK within post-expansion clones strongly suggest that ESAM can function successfully as a marker for expanded HSCs, and reveal that ESAM marks the same HSC-rich populations as the frequently used *Fgd5*$^{ZsGreen•ZsGreen/}$ reporter (Figure 4.2a). Importantly, the correlations between FELSK (*Fgd5*$^{+}$ELSK^{+}*)* and EELSK (ESAM^{+}ELSK^{+}*),* and ELSK and EELSK, are highly significant (Figure 4.2b, Pearson's correlation R value=0.967, p value = <0.00001, Figure 4.2c, Pearson's correlation R^2 value **=** 0.9350, p value = <0.0001), suggesting that ESAM can fully replace Fgd5 as a marker for the functional HSC compartment.

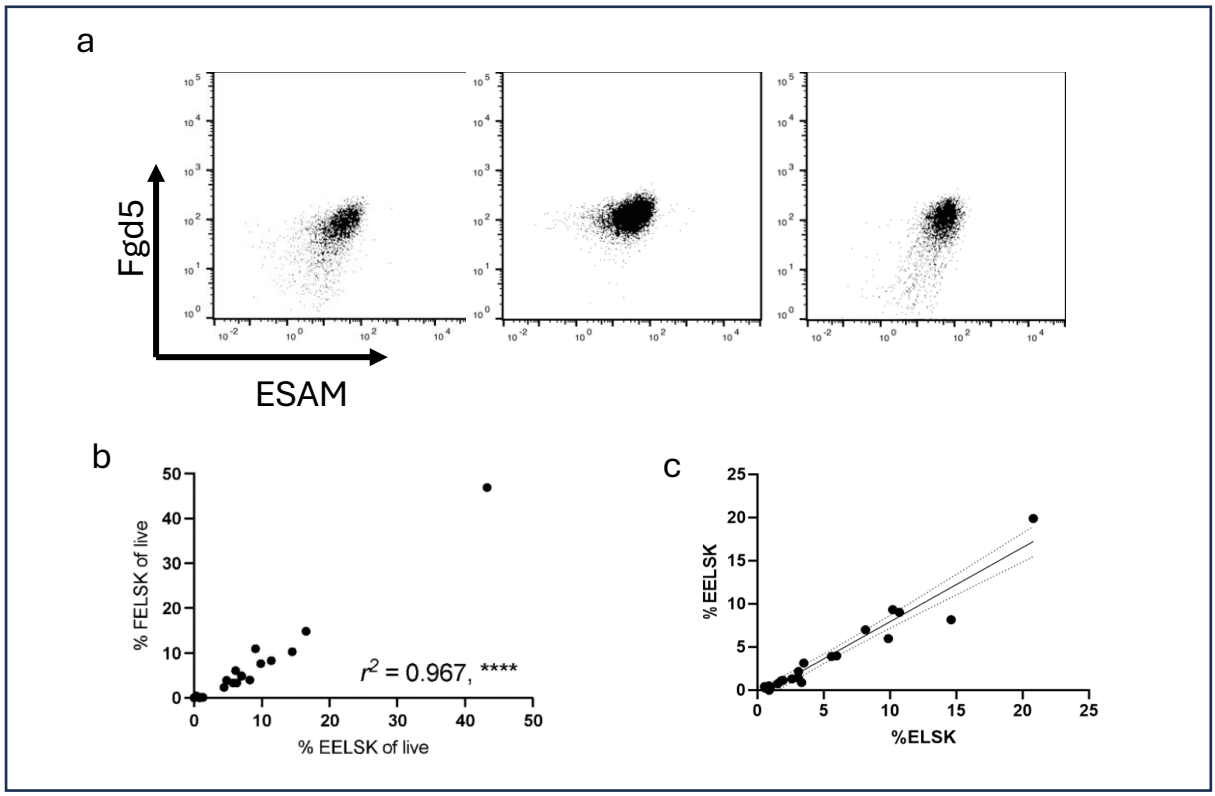

Figure 4.2 **ESAM can replace Fgd5 as a reporter for functional in vitro expanded HSCs.** a) Correlation between expression of ESAM, and the fluorescent reporter Fgd5. This data was collected on day 28 and all cultures were started with a single ESLAM cell. Each plot represents an individual culture, and each point on the graph represents a cell. Each of these plots had previously been gated on single, live, cells. b) Plotting % of cells FELSK against % of cells EELSK reveals a significant positive correlation. This data was collected on day 28 and all cultures were started with a single ESLAM cell. Pearson's correlation R^2 value=0.967, p value = <0.00001 c) Correlation between ELSK content of a clone, and %EELSK. Pearson's correlation R^2 value = 0.9350, p value = <0.0001

4.2. In vivo validation of the ESAM reporter; EELSK provides a specific readout for functional expanded HSCs, and outperforms using ELSK alone.

Despite the efficacy and practicality of the PVA culture system as a screening platform to test new potential reporters, HSC transplantation experiments are still required as the gold-standard for determining the presence of functional HSCs.

Therefore, in order to functionally validate the use of ESAM as a reporter for *in vitro* expanded HSCs, a transplantation experiment into sub-lethally irradiated W41 mice was utilised. As is standard for PVA expansion cultures, single mouse ESLAM cells were sorted into individual wells of a 96-well plate and were expanded for 28 days in PVA based media (Wilkinson et al., 2019). On day 28, each well was mixed thoroughly in order to resuspend the cell population, and 10% of each well's volume was taken for analysis. As described in Methods, the cell samples were stained and analysed via flow cytometry to determine their ELSK and EELSK content and following this, 15 wells were selected for transplantation based on presenting a range of ELSK and EELSK percentages. The entirety of each well was then transplanted into a separate sub-lethally irradiated W41 mouse as described in Methods section 3.8 of this thesis. Due to the missense mutation present in the Kit locus of W41 mice, the accompanying reduced HSC count (approximately half of WT), facilitated the use of a lower, sub-lethal dose of irradiation.

In order to determine the success of transplantation, and therefore the importance of ESAM as a reporter for functional *in vitro* expanded HSCs, peripheral blood analysis was performed at 4, 8, 12, 16, and 24 weeks post-transplantation to ascertain total chimerism, as well as chimerism within the Granulocyte-Macrophage (GM), T-cell and B-cell fractions (Methods section 3.9). A schematic outlining this protocol is shown in Figure 4.3a, and a representative gating strategy is shown below in Figure 4.3b-e. Generally in the field, success in transplantation is defined as > 1% donor chimerism and > 1% donor contribution to the GM fraction at the 16 week point.

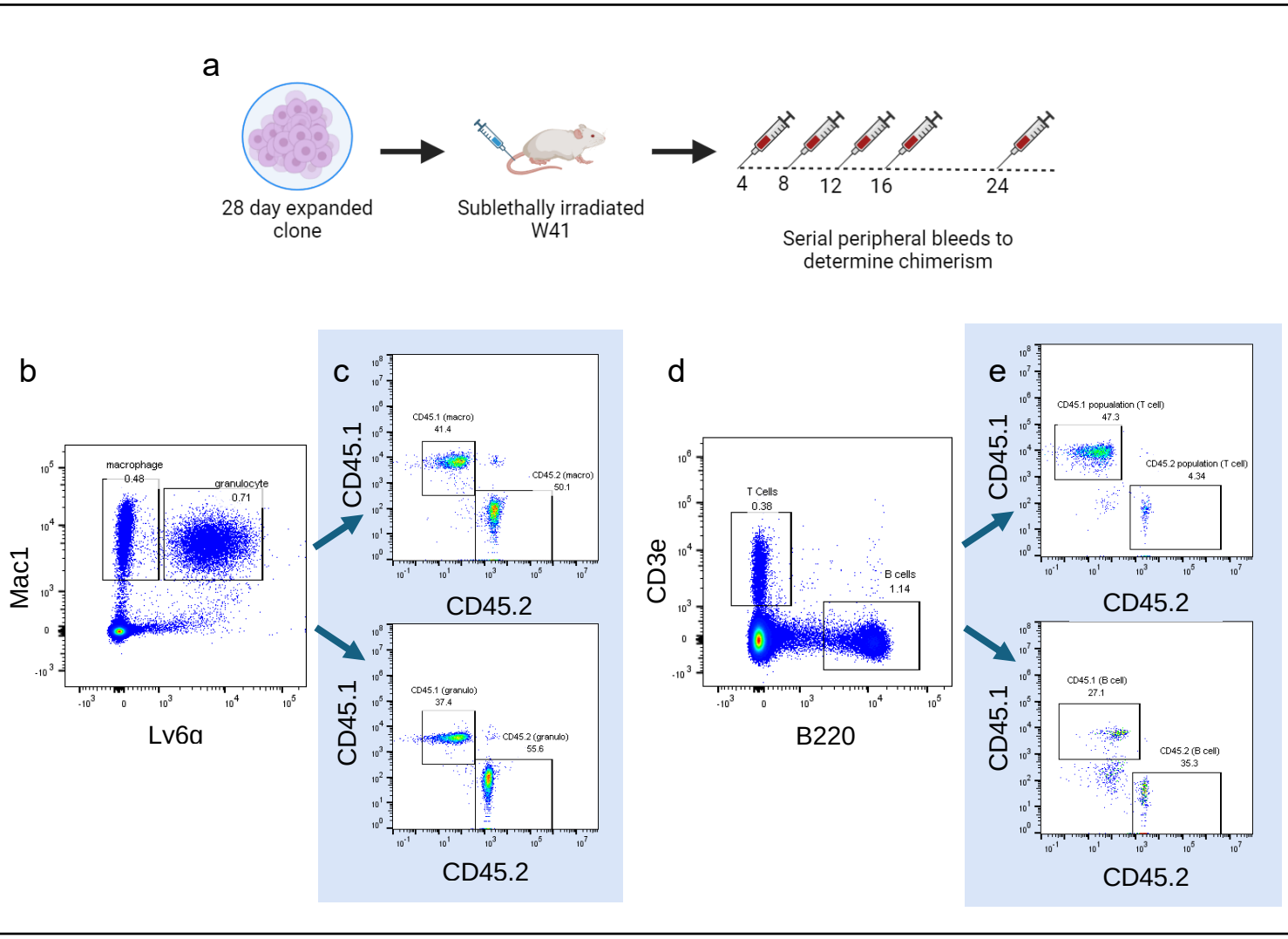

Figure 4.3 **Gating strategy to determine peripheral blood chimerism post transplant**. a) Schematic outlining process of transplantation. Cells are cultured *in vitro* for 28 days, before transplantation of the entire wells contents into a sub-lethally irradiated W41. Peripheral blood bleeds to determine success of transplant in terms of mature cell chimerism are taken at several timepoints. b)*Representative* gating strategy for isolating the granulocyte and macrophage populations from peripheral blood taken post-transplant. c) Within the gates set in 4.3a, CD45.1 and CD45.2 gates are set as shown. $CD45.1^{+}$ cells are the donors own cells, whilst the $CD45.2^{+}$ population represents cells derived from the transplanted cells. d) Gating strategy for isolating T and B cell fractions from peripheral blood post transplant. e) Within the T and B cell gates, CD45.1 versus CD45.2 plots reveal extent of chimerism within each fraction. Schematic created in BioRender

Data gathered from peripheral blood analysis following transplantation reveal a highly significant positive correlation between the percentage of live cells in a clonal population expressing the EELSK marker combination on the day of transplantation, and the success of transplantation as determined by total and GM chimerism at week 24 (Figure 4.4). It is important to note that the inclusion of ESAM in addition to the ELSK reporter strategy improves the correlation with peripheral blood chimerism following transplant, and so is a valuable addition to this panel, further refining our ability to isolate functional HSCs to a

higher purity post-expansion. Furthermore, despite the 20% ELSK threshold historically used to guarantee a clones ability to repopulate a mouse in a transplantation setting (Che and Bode, 2022), several clones within the 5-20% ELSK range at the point of transplantation are also able to generate significant levels of chimerism. Regarding %EELSK, it in fact appears that clones >10% EELSK at point of transplantation are nearly always capable of contributing significantly to chimerism (both total and GM) up to the 24 week timepoint (Figure 4.4, 4.5).

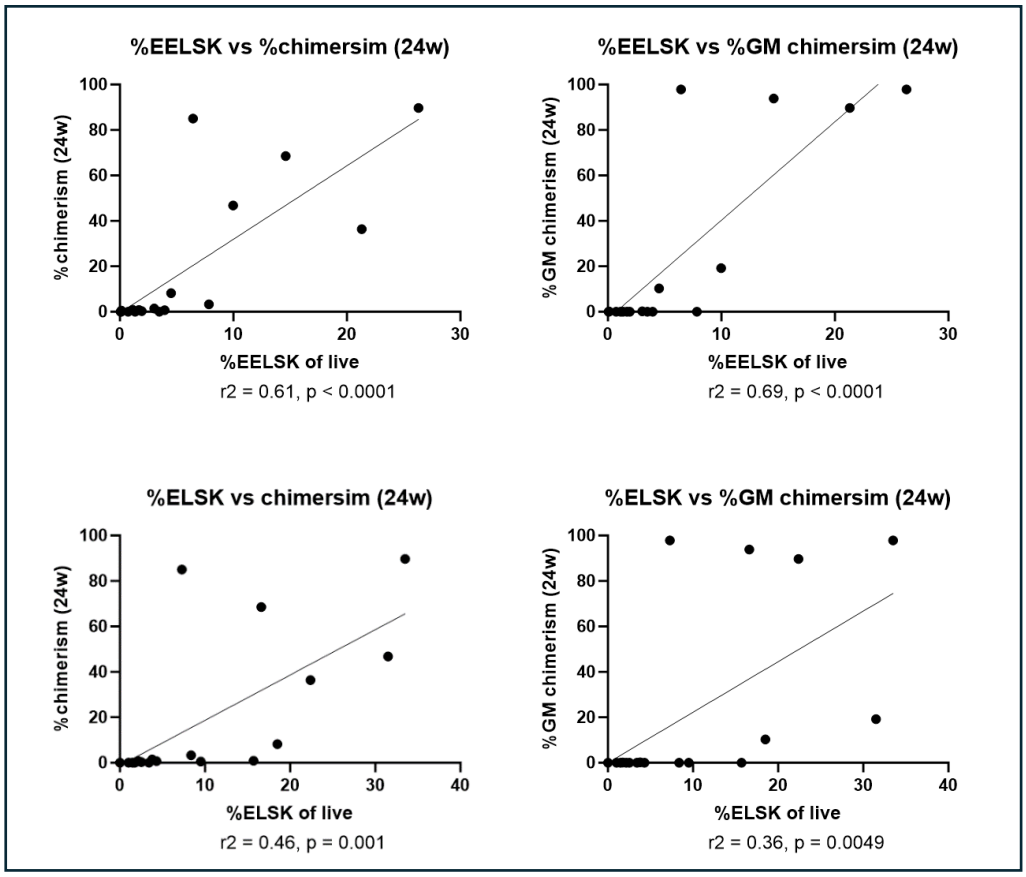

Figure 4.4 **HSC transplantation validates ESAM as a reporter for functional HSCs.** Peripheral blood analysis from the week 12 timepoints following transplantation of 28 day expanded clones. For each timepoint both granulocyte-monocyte (GM) and total chimerism were determined and are plotted against both ELSK and EELSK percentages, as determined by pre-transplantation day 27 flow cytometry.

Ahead of this 15 mouse transplantation experiment, a smaller preliminary transplant was performed, which although containing fewer mice and generally showing lower chimerism, aligns well with the larger transplant, again showing a strong positive correlation between ESAM expression at point of transplant, and total and GM chimerism at the week 24 timepoint (Figure 4.5). Together with the larger transplant, and alongside the flow cytometric

data, ESAM appears to act as an efficient marker for functional expanded *in vitro* mouse HSCs. It would therefore make an advantageous addition to the ELSK panel when aiming to determine the HSC content of a clone, and its functional potential.

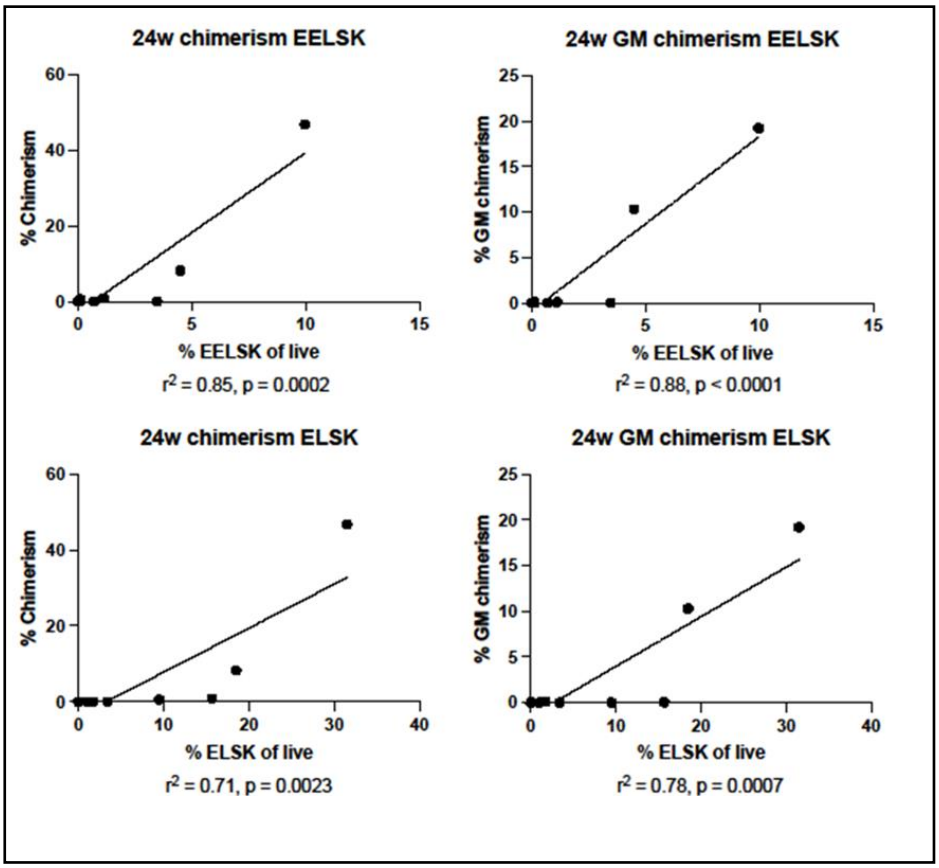

Figure 4.5 **Preliminary ESAM HSC transplantation**. Peripheral blood analysis from week 24 following transplantation of expanded single-cell PVA cultures. GM and total chimerism were measured as a readout for functional HSC content. and the correlations between chimerism and ELSK / EELSK content of the transplanted well are plotted.

However, despite ESAM's capacity to serve as a robust marker for functional HSCs post-expansion, it does lack one valuable ability: being able to act as a predictive marker for culture success. In order to test this, 10% of the contents of single-cell initiated wells was taken on day 14 for flow cytometric analysis in order to determine the %ESAM$^+$ and %EELSK of each well. We then continued these cultures to the day 28 time point, and performed flow cytometric analysis to determine %ELSK of each well. Through plotting each of the day 14 parameters for the well, against the well's final %ELSK at day 28, it is possible to identify day 14 markers which correlate with ultimate culture success. Interestingly, neither of these tested markers correlated significantly with %ELSK at day 28 (Figure 4.6). These results encouraged us to pursue testing additional markers, to find those which would fit this criteria.

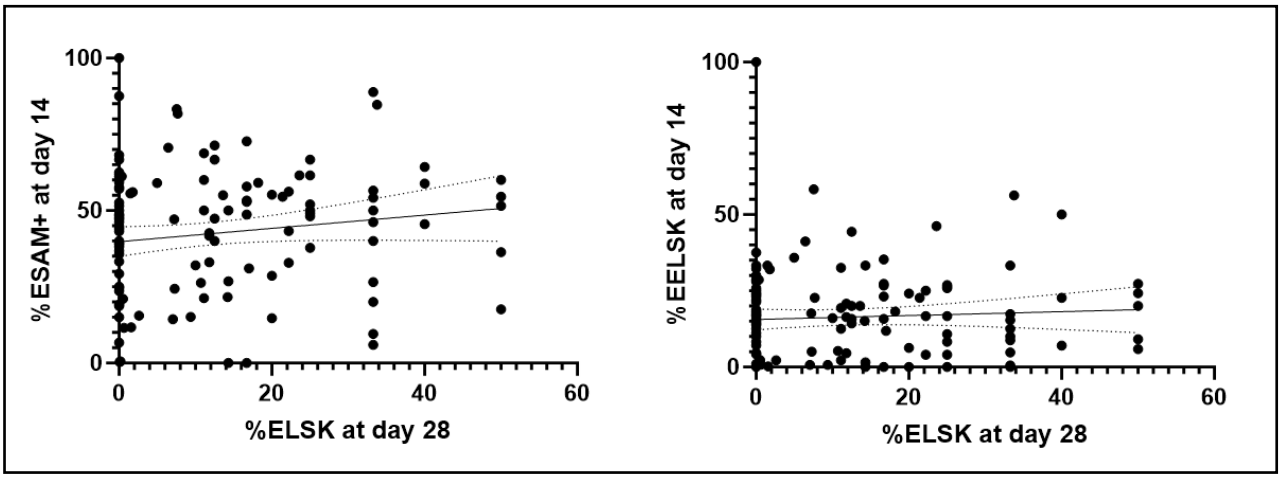

Figure 4.6 **ESAM lacks predictive capacity at day 14**. Data shown is taken from day 14 and day 28 analysis of single-ESLAM initiated clones. Neither ESAM nor EELSK at day 14 correlate with final day 28 %ELSK so both reporter strategies lack predictive capacity. %Fgd5+ and %FELSK were also measured at day 14, but again neither correlated with day 28 %ELSK – data not shown.

4.3. Testing of CD321 as a marker for expanded HSCs

Although ESAM had been identified as a robust reporter strategy for functional HSCs, we continued the process of searching for additional markers to further refine our ability to pull HSCs out of culture at the highest purity possible. CD321 was identified as a promising reporter for the presence of functional HSCs post-expansion through proteomic analysis. Proteomic analysis performed on day 28 expanded clones by Dr. Maria Jassinskaja in the Kent Lab, found a strong correlation between the ELSK content of a clone, and levels of CD321. CD321 is a surface protein localised to tight junctions and has been previously studied in relation to its role in neutrophil infiltration and resultant inflammation, as well as tumour angiogenesis in endothelial cells, and its expression on leukocytes (Fukuhara et al, 2017).

I therefore tested this marker using flow cytometric analysis post-expansion. In order to do this, single ESLAM cells were sorted via FACS and cultured using PVA conditions for 28 days, with 10% removed for analysis at weeks 2 and 3, before being analysed for the final time via flow cytometry on day 28. The final panel for analysis included not only the standard ELSK panel, but also CD321 and ESAM. The data reveals an increase in the Mean Fluorescent Intensity (MFI) of CD321 within populations that become increasingly more specific for HSCs (Figure 4.7 a). It is important to note that this trend is maintained across

the 2, 3 and 4 week timepoints (Figure 4.7a). Additionally, the percentage of cells that were $CD321^+$, or $CD321^+$ LSKs correlated significantly with increased %ELSK at the final day 28 timepoint, showing that CD321 has the potential to act as an efficient reporter for the functional HSC compartment (Figure 4.7 b,c).

When further analysing the data collected from wells over the course of expansion. it is possible to track the percentage of cells in the well expressing CD321, or the marker combinations ELSK and EELSK. Figure 4.7d presents data generated from an average of 60 single-cell initiated cultures over the course of expansion and what is observed is a general decrease in expression of all 3 of these marker combinations from day 14 to day 21, with a slight, but statistically insignificant, uptick by the day 28 timepoint. It is interesting that they all coincide, which supports the concept of a correlation between these three fractions – all marking the same population, just to varying specificity. This data is supported by independent experiments, tracking both the %ELSK and $\%ESAM^+$ of single cell initiated cultures over the expansion period, both of which show a gradual decline in expression of these markers over time. (Figure 4.7e,f).

This data again highlights the benefit of identifying predictive markers which can be analysed at earlier time points (e.g. day 14) and have the capacity to predict the final outcome of the culture at day 28, and identify cultures which will collapse (in terms of %ELSK).

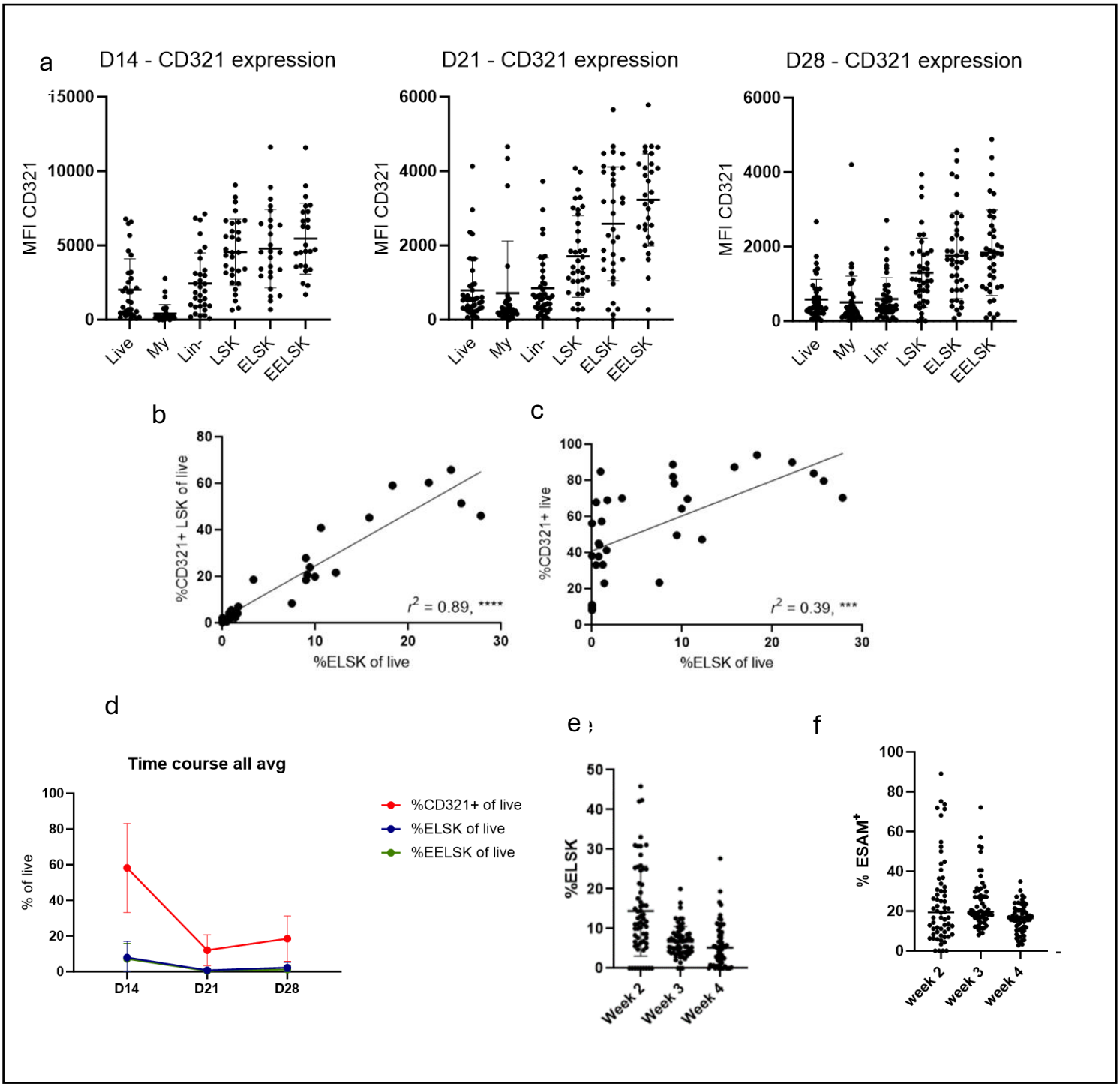

Figure 4.7 **CD321 is a marker of functional in vitro expanded HSCs**. All data collected via flow cytometry on day 28 of PVA expansion. a) Mean Fluorescence Intensity of CD321 plotted with each dot representing a well, for several cell fractions, with HSC frequency within the fraction increasing from left to right. b) Percentage of cells in the well falling within the CD321$^+$ LSK fraction plotted against the %ELSK of the well (simple linear regression, r^2 = 0.89. c) Percentage of cells CD321$^+$ plotted against %ELSK in each well (simple linear regression, r^2= 0.39). d) Tracking of %CD321$^+$, %ELSK, and %EELSK over time. e) %ELSK over the course of culture f) %ESAM$^+$ over 28 days of culture.

4.4. SiglecF as a potential marker of expansion cultures "going bad".

The eosinophil marker SiglecF was identified as an additional promising target due to its presence on a list of genes identified by proteomic analysis found to anti-correlate with RepopSig expression, and so was expected to be a negative marker of functional HSC content. In order to determine if this is the case, single ESLAM cells were expanded over 28 days in standard PVA expansion conditions, and were analysed via flow cytometry on day 28 for expression of SiglecF, as well as ELSK content of the clone.

Interestingly, SiglecF expression generally increased with %ELSK up to ~25% ELSK, however the very best clones presented with significantly lower SiglecF expression (Figure 4.8a). In this regard, SiglecF appears to subdivide the >20% ELSK populations, with low SiglecF expression marking the earliest, most primitive HSC clones with the highest %ELSK (Figure 4.8a). Through taking the top 3 %ELSK clones, it was found that the vast majority of the ELSK cells present were in fact negative for SiglecF, revealing that SiglecF is expressed on, and is marking, a separate population - perhaps the very first "non-HSC" progeny created by LT-HSCs (Figure 4.8b). If further validated, SiglecF has potential to be included alongside existing reporter strategies such ELSK and EELSK to further refine them.

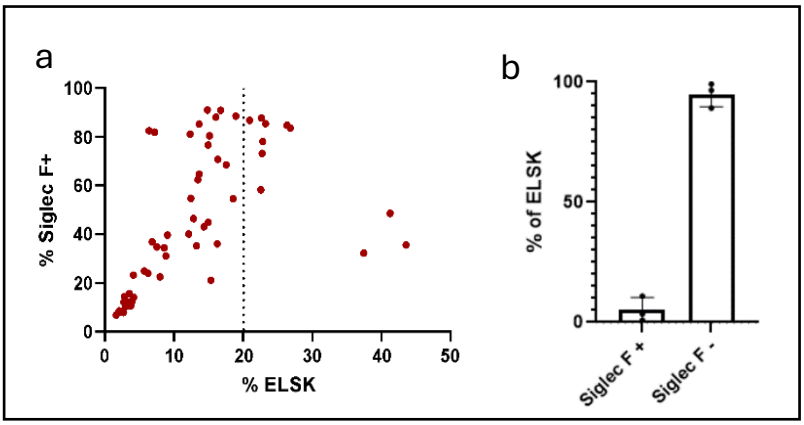

Figure 4.8 **SiglecF marks a non-ELSK fraction, and correlates with culture success**. a) SiglecF expression measured by flow cytometry plotted against %ELSK. Data taken from 60 wells on day 28 of 28-day expansion protocol, cultures initiated with single ESLAM HSC. Cultures falling above the dotted threshold at 20% ELSK contain functional HSCs and are able to be transplanted (Che and Bode, 2022). b) Taking the top 3 clones in 4.8a, this graph shows the percent of ELSK cells in the well that are either positive or negative for co-expression of SiglecF

Additional flow cytometric analysis was performed on clones <20% ELSK, where functional HSC content cannot be guaranteed, but is sometimes present. This analysis revealed a pattern linking the ELSK content of a clone to differences in relative expression of EPCR and SiglecF within the LSK fraction, with relative SiglecF expression generally increasing as %ELSK fell (Figure 4.9)

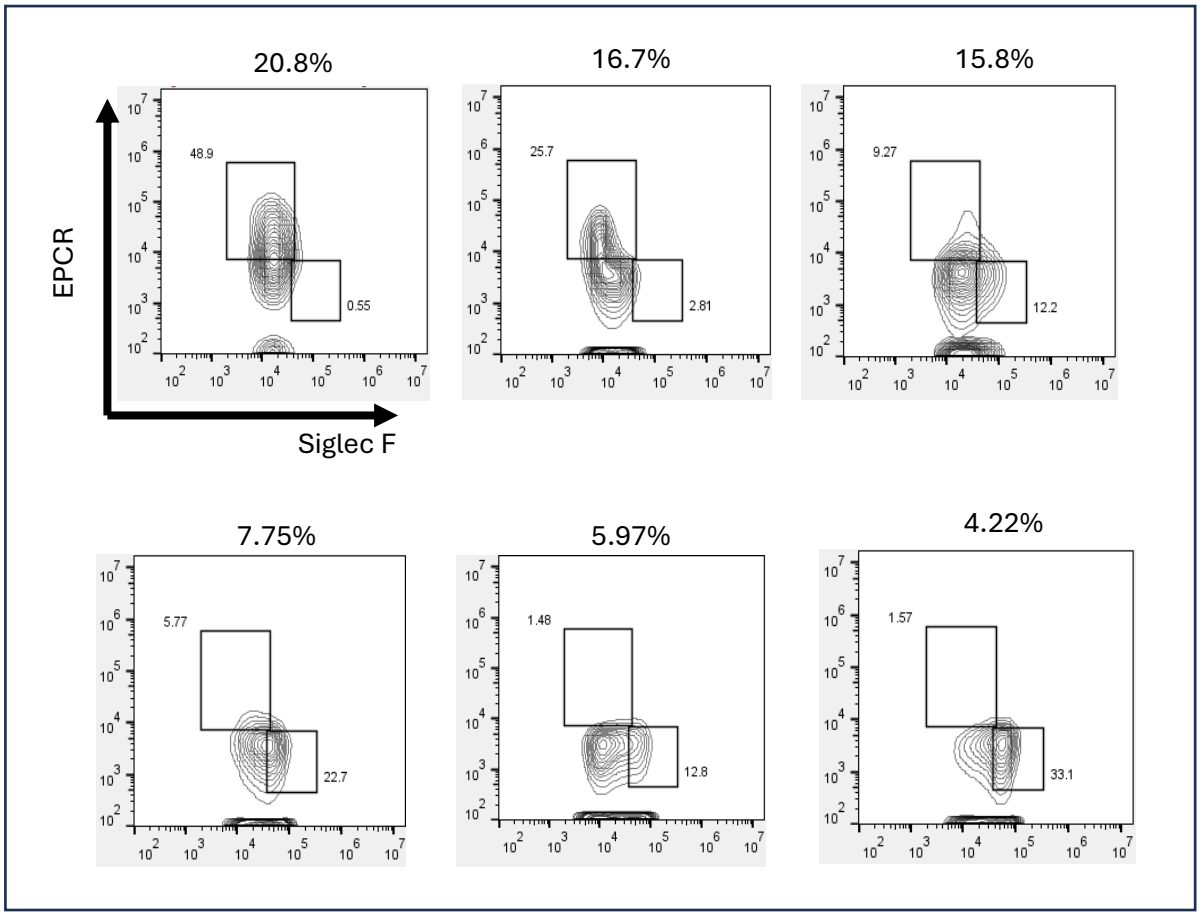

Figure 4.9 **SiglecF versus EPCR expression within the LSK fraction.** Siglec F expression plotted against EPCR expression within a predefined LSK population. Percentage shown above each plots shown the %ELSK of the well. Top Left box marks the $EPCR^{+}SiglecF^{-}$ fraction, and the Bottom Right gate marks the $EPCR^{mid/low}SiglecF^{+}$ population. A trend is visible between % ELSK of the clone, and the relative expression of EPCR and SiglecF.

Further flow cytometric analysis was performed which followed single cell-initiated clones over the course of the 28 day expansion period to determine changes in SiglecF expression over time. On day 14, 10% of each well was taken for analysis, and the remaining 90% remained in culture until day 28 for final day flow cytometry to determine %ELSK and analyse the percentage of SiglecF positive cells.

This data revealed a potential predictive capacity of SiglecF, where SiglecF expression at day 14 anti-correlates with clonal success at day 28 (Figure 4.10), and supports its place on a gene set list found to anticorrelate with RepopSig expression, and therefore the presence of functional HSCs.

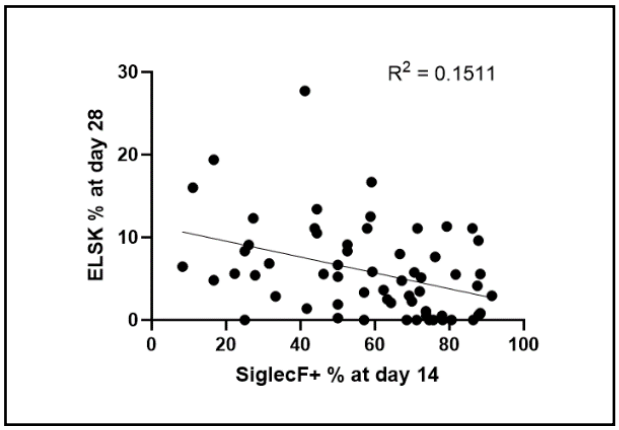

Figure 4.10 **SiglecF may be a predict day 28 culture outcome at the day 14 timepoint**, Percentage of SiglecF+ cells at day 4 correlated with %ELSK at day 28. Pearson's correlation, R^2 = 0.1511

Given that we suspect SiglecF expression may indicate the first stages of differentiation occurring in a clone, it led us to believe that we may be able to distinguish between clones of similar %ELSK which would have different functional output, and even to identify clones below 20% ELSK that may repopulate.

4.5. Functional validation of SiglecF using HSC transplantation

In order to functionally determine the role of SiglecF, and the potential benefit of including it alongside the ELSK reporter strategy, single ESLAM HSCs were sorted into individual wells on a 96-well plate and were expanded over 28 days using PVA based HSC expansion conditions (Wilkinson et al., 2019). On day 27, 10% of each clone was taken for flow cytometric analysis to determine %ELSK and %SiglecF$^+$. Following this, 6 wells with ELSK >10% were selected for transplantation on day 28, based on the percentage of live cells expressing SiglecF in the well at day 27: 2 samples having high SiglecF expression (46.3%, 41.7%), 2 samples having mid SiglecF expression (14.5%, 16.2%,), and 2 samples having low SiglecF expression (0% and 9%). Each sample was transplanted into a separate W41 mouse as previously described in Methods, and peripheral blood analysis at weeks 4, 8, and 16 was performed.

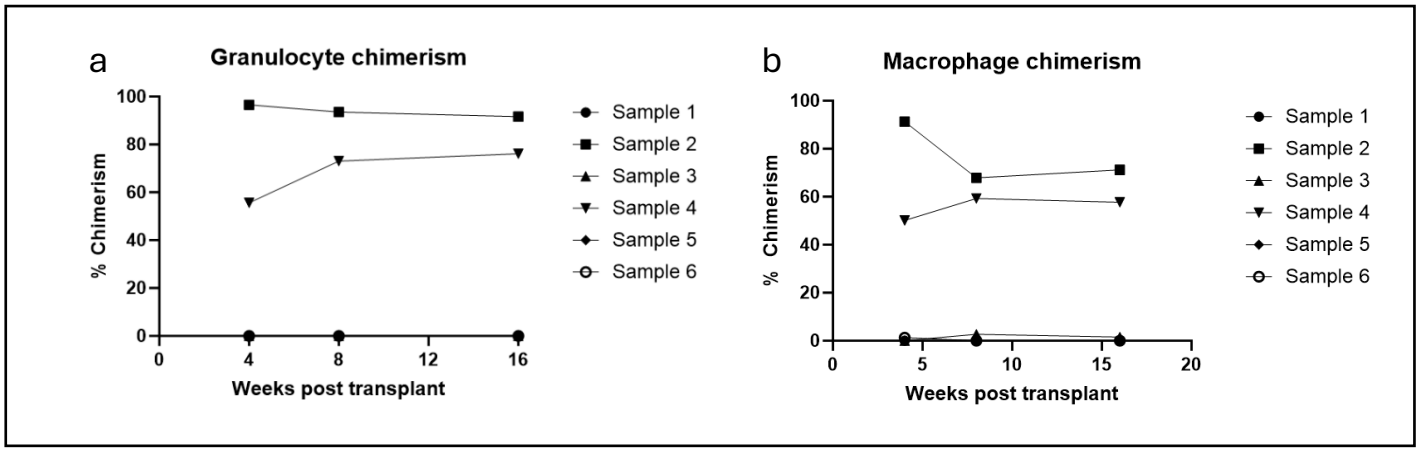

Figure 4.11 **SiglecF expression within clone does not correlate with chimerism following transplantation**. Wells were selected for transplantation based on the percentage of live cells expression SiglecF at day 27. a) Contribution of donor cells (CD45.2) to the granulocyte population at 4, 8, and 16 weeks post-transplant. b) Contribution of donor cells (CD45.2) to the macrophage population at 4, 8, and 16 weeks post-transplant.

In this transplantation experiment, only 2 samples were contributing more than the >1% significance threshold to the granulocyte and macrophage populations by the week 16 timepoint. (Figure 4.11 a,b accordingly). These samples, when analysed pre-transplant, had mid and high SiglecF levels accordingly. Despite the initially promising flow cytometry data regarding SiglecF's potential as a reporter for expanded HSCs, the transplantation experiment, which despite working in the sense of generating successful chimeras, revealed that SiglecF content of a clone does not correlate with the presence of functional HSCs post culture (Figure 4.11). Despite this, SiglecF remains a promising marker, particularly in regard to its capacity to predict day 28 culture success at the week 2 timepoint.

4.6. Novel split-culture approach when expanding HSCs

Despite the reliability of this expansion culture system, when initiating PVA expansion cultures with single ESLAM cells, we are potentially exposed to an array of variation, due to cell to cell heterogeneity, which is often addressed by initiating bulk cultures of 50 starting cells. It is therefore hard to conclude whether differences in response to stimuli or culture conditions are due to the applied pressures, or due to differences in the starting material. Therefore, as a lab we looked at new ways to mitigate this and improve the reliability of our analysis.

In these experiments, as is standard, expansion cultures were initiated with single sorted ESLAM cells in the inner 60 wells of a fibronectin-coated 96 well plate. Media changes were initiated on day 7 and continued every 2-3 days for the remainder of the culture period. On

day 14, each well on the plate was split into 4 equal parts, resulting in the formation of 4 new plates, and media changes were continued until the day 28 time point (Figure 4.12 a).

Firstly, it was vital to determine that wells split from an original source performed similarly to each other after an additional 2 weeks in culture. In order to do this, flow cytometric analysis was performed on the final day of culture (day 28) which revealed that the 4 wells sharing a common origin well all had similar %ELSK.

In order to further validate this split-culture technique, a transplantation experiment was performed which would allow functional verification of HSCs present in the culture, and would allow us to compare functional capacity between the splits. Data taken from this transplantation reveal that each split produces 4 wells with similar functional potential (Figure 4.12 b). This functional potential is defined by total percentage donor chimerism, meaning the percentage of peripheral blood cells present at the 16 week time point that arise from the transplanted cells. As each of the 4 resultant cultures derive from the same original cell, it allows us to treat the newly formed plates with activators/inhibitors etc. and can be sure that the changes we see are a result of the effects of the molecule added, and not a result of variations in the original ESLAM cells that initiate the cultures.

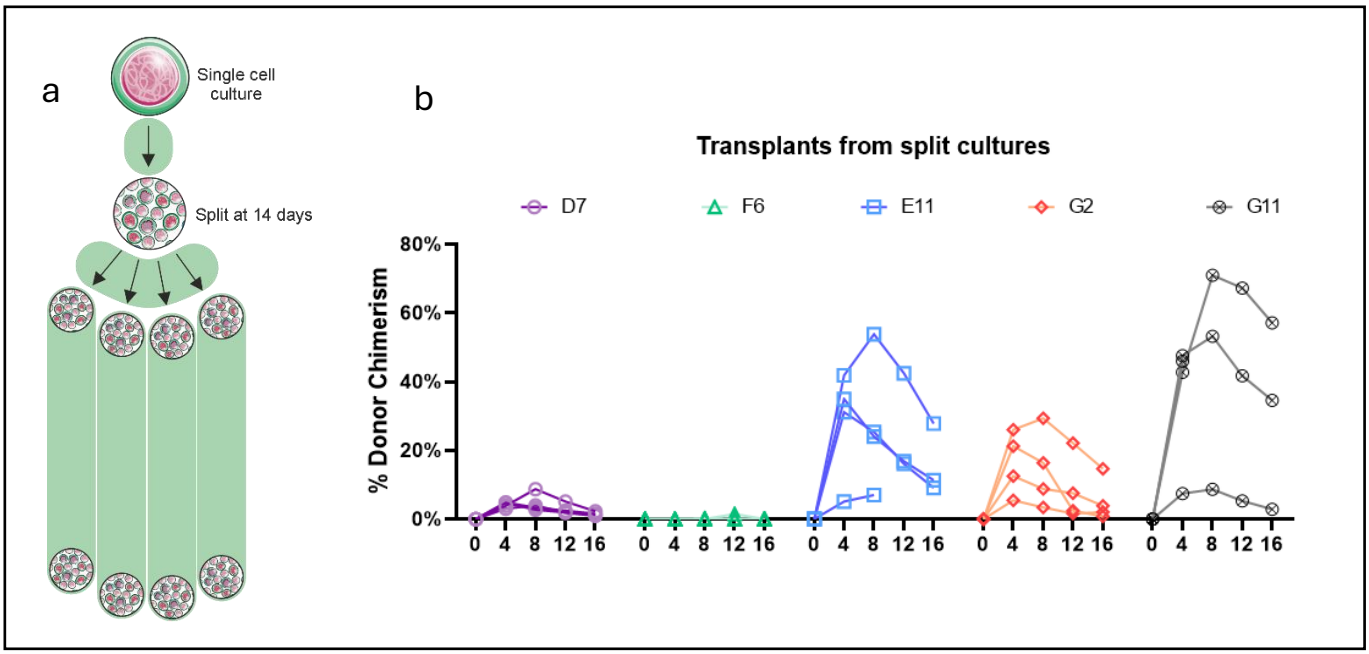

Figure 4.12 **Transplantation validation of the split culture technique**. a) Schematic of day 14 split culture technique. Created by Juan Rubio-Lara. b) Transplant data showing % Donor chimerism post-transplant of split cultures reveal all 4 parts have similar functional output and so validates this method. Each colour represents the original starting well, and the 4 lines of each colour represent the 4 wells produced post-split

4.7. PVA cultures as a screening platform

The ability to compare conditions directly, without concern regarding differences relating to the starting cellular material, unlocked the vast molecule screening capacity of the PVA expansion cultures. Since the validation of this method via transplantation, many molecules thought to impact HSCs have been screened using this system in order to determine their effect on *in vitro* HSC expansion. Several examples are shown below (Figure 4.13).

We first compared the addition of several concentrations of recombinant Vascular endothelial growth factor (VEGF) (to activate VEGF signalling) or a neutralising VEGF antibody to the PVA media, in order to elucidate any potential effect (Figure 4.13 a). Over the course of culture, no significant impact on HSC expansion was noted. Furthermore, the effects of the addition of Follistatin-like 1 (Fstl1) to the PVA media was tested (4.13 b). This is an additional protein identified from the RepopSig and has been identified by other groups as a regulator of murine HSC repopulation (Holmfeldt et al., 2016). Despite this, in this PVA expansion system, it appears to have a negligible effect on the outcome of the culture. Another screen performed was the replacement of PVA (polyvinyl alcohol) in the media with PVP (polyvinyl pyrrolidone), an alternative polymer which may be superior in this system, especially as the role of PVA in this culture model is not fully understood, however no significant differences were identified (4.13c).

Although none of these results showed significance, they highlight just how efficiently this split culture method can be used to screen a huge range of molecules quickly, easily, and, combined with the functionally validated ELSK reporter strategy, without the need to transplant into mice to determine functional HSC content. For context, considering just these three screens, if each well was to be functionally validated via transplantation, this would have required the use of 180 mice.

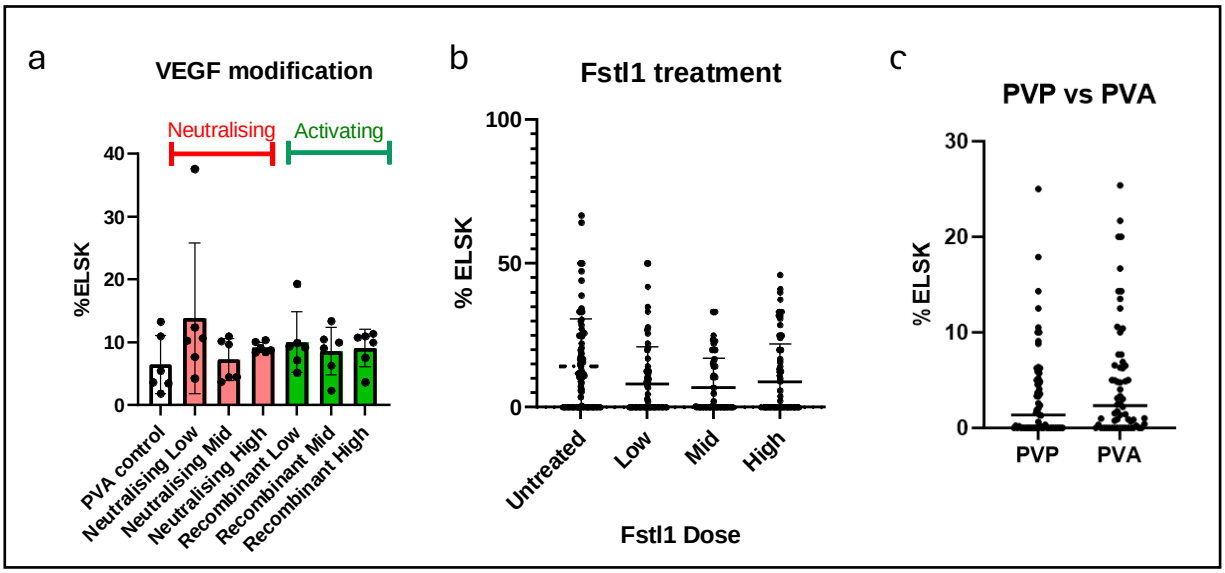

Figure 4.13 **PVA cultures as a screening platform**. Data gathered from day 28 flow cytometric analysis of 60 single-cell initiated PVA expansion cultures utilised as a screening platform for testing the efficiency of new molecules on in vitro HSC expansion. No significant differences were noted. a) Various concentrations of recombinant VEGF and Neutralising VEGF antibody were tested. Recombinant Low: 0.02µg/mL, Mid: 0.2µg/mL, High: 1µg/mL Neut. Low: 0.1µg/mL, Mid: 1µg/mL, High: 5µg/mL. b) Fstl1 treatment was also compared at concentrations of 50ng/mL (low), 200ng/mL (mid), and 500ng/mL (high). c) Both PVA and PVP were tested at 1mg/mL. Further screens completed using the split culture approach but no significant differences and data not shown: Addition of tricarboxylic acid (TCA) to PVA media, and changes in CD244 expression following this, TGFB3 supplementation to media, and Etomoxin treatment.

4.8. PVA expansion cultures become cytokine self-sustaining by day 14

The PVA expansion system is notorious for the volume of cytokines required to maintain these cultures. These cytokines are costly reagents and may deter labs from taking up this methodology. We therefore aimed to determine if it was possible to lower or even remove the cytokines in the media after 14 days of the cultures establishing themselves. To test this, single ESLAM cells were sorted via FACS and then expanded for 14 days, before each well was split into 4 equal parts as described in Section 4.6, in turn generating 4 new plates. Therefore, it is possible to compare directly between conditions, being sure that differences in culture success are due to cytokine differences, not intrinsic differences in the starting material.

One plate was maintained for the remaining 14 days of culture with PVA expansion media supplemented with the standard SCF and TPO (Wilkinson et al., 2019), whilst others had either SCF, TPO, or both, removed. Interestingly, the cytokine removal cultures were able to survive for the remainder of the 28 day culture, whilst maintaining and also expanding the

functional HSC pool. Cultures where TPO alone, and both TPO and SCF were removed, had ELSK percentages at day 21 (Figure 4.14a) and 28 (Figure 4.14b) comparable to control media. Interestingly, SCF removal media outperformed control media – with 8 compared to 2 cultures passing the significant 20% ELSK threshold at day 28 (Figure 4.14 b). This suggests the cultures become cytokine self-sustaining at the week 2 timepoint, and may even imply that the SCF we traditionally continue to supply past the 14 day time point may be excessive.

Moreover, there seem to be several key patterns in the response of cultures to different cytokine combinations. When cultures originating from the same clone are matched, and linked between different conditions based on either common origin, it is possible to see that the clones that have the highest %ELSK for each condition are not all from the same origin well. In fact, we see that clones from the same clonal origin exhibit differential levels of expansion by day 28 in the presence of different cytokines (Figure 4.14c).

In Figure 4.14d, a few key trends are pulled out from this large dataset. The red population represents clones that perform significantly better in the presence of the traditional TPO and SCF combination than any other condition. Whereas the blue and green clones have notably higher %ELSK by day 28 in TPO or SCF removal cultures respectively. Further analysis of these clones at day 14, before initiating the cytokine removal phase of the culture, would help decipher the molecular differences between these heterogeneous populations. If we could identify key markers that would predict a clone favouring a certain media condition, it would allow us to provide personalised media to individual wells, enabling maximal expansion and HSC counts.

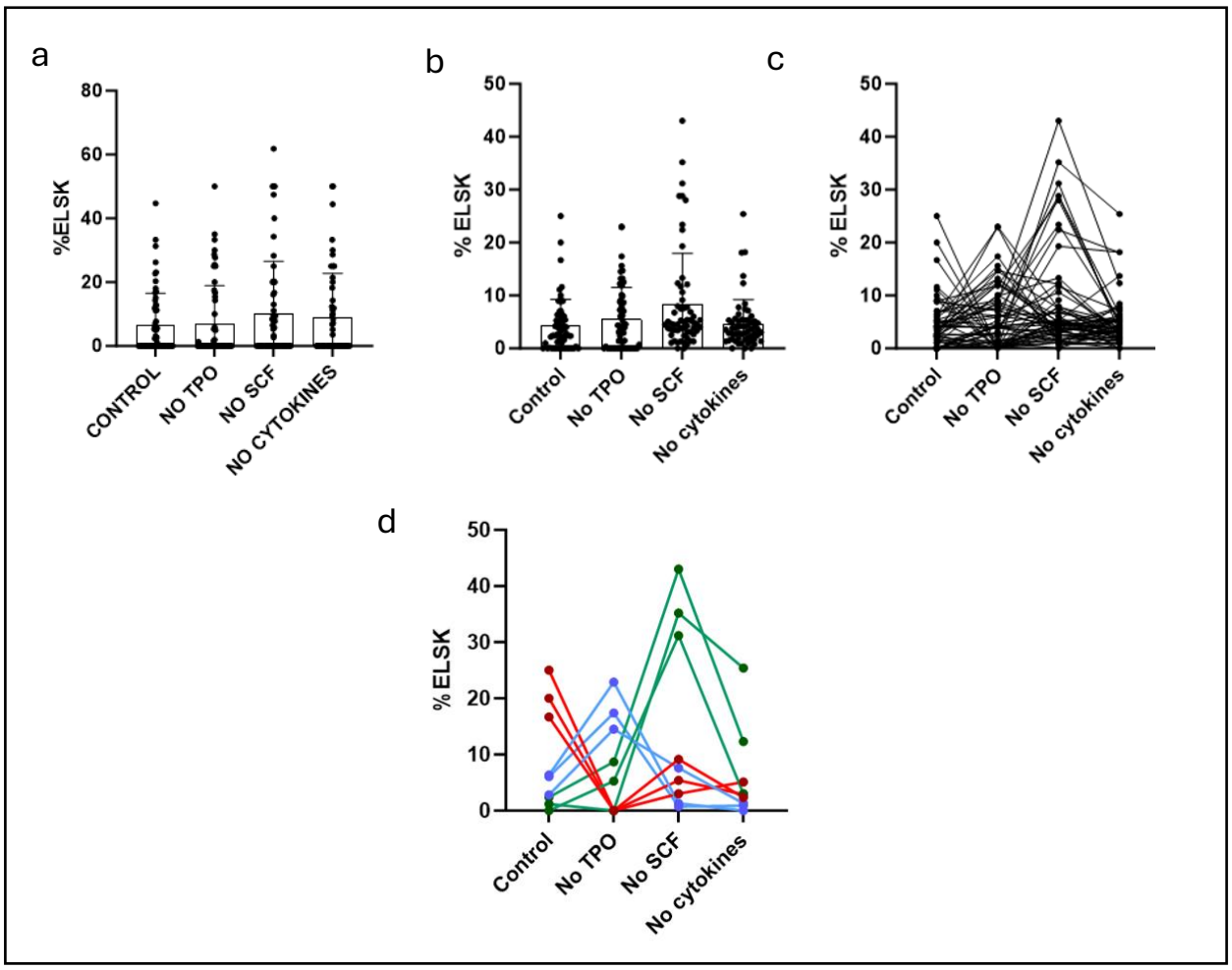

Figure 4.14 **PVA cultures become cytokine self-sustaining by day 14**. Data taken on Day 21 (a) and 28 (b) of expansion cultures initiated with single ESLAM cells, having previously been split into 4 equal parts on day 14. %ELSK of clone is used as a readout of functional HSC content. 60 wells of 4 conditions were tested – control expansion media, removal of TPO, removal of SCF, removal of both SCF+TPO. Control, TPO removed, and No cytokines conditions had similar HSC outputs at weeks 3 and 4. Error bars show standard deviation. (a,b), however removing SCF from the media post day 14 improved functional HSC output of the culture, most notably at week 4(b). c) Linking individual wells (on day 28 analysis data), based on original well allows confirmation that differences in ELSK output are related to cytokine conditions, rather than the culture initiating cell. d) Key patterns in differing response to cytokine availability between wells originating from a common clone. Each of the colours represents a pattern in cytokine response, and includes 3 examples of matches clones following this trend.

4.9. Differences in HSC expansion between truncated versus full length TPO supplemented PVA cultures

Following on from our cytokine removal studies, we aimed to more thoroughly research the impact of the specific cytokines used for this system – in particular the protocols use of truncated (TR) TPO, which contains just the erythropoietin-like binding domain, rather than the full length (FL) wildtype version. We aimed to determine if the addition of a protein more representative of what stem cells will encounter *in vivo* would impact the levels of HSC expansion that could be achieved.

In order to test the effect of adding full length TPO versus TR TPO on HSC expansion and self-renewal divisions, we ran a series of 28 day single-cell initiated PVA cultures in either the presence of FL or TR TPO. Molar concentrations were maintained the same across conditions in order to mitigate differences resulting from protein size.

These clones were then analysed on day 28 by flow cytometry to determine the counts and percentages of several cell fractions present in the well, with an increasing specificity for the HSC fraction as additional markers are added. We observed an increase in the counts of all fractions (Live cells, lineage negative, LSK, ELSK, and EELSK) in truncated TPO compared to full length. However, in terms of percentages of live cells, this was negligible. (Figure 4.15) This is an intriguing result, as both proteins have identical binding site regions, and should be inducing similar downstream signalling, yet significant differences in HSC expansion, in terms of total number of HSCs by day 28, show there must be an underlying benefit to the truncated variant.

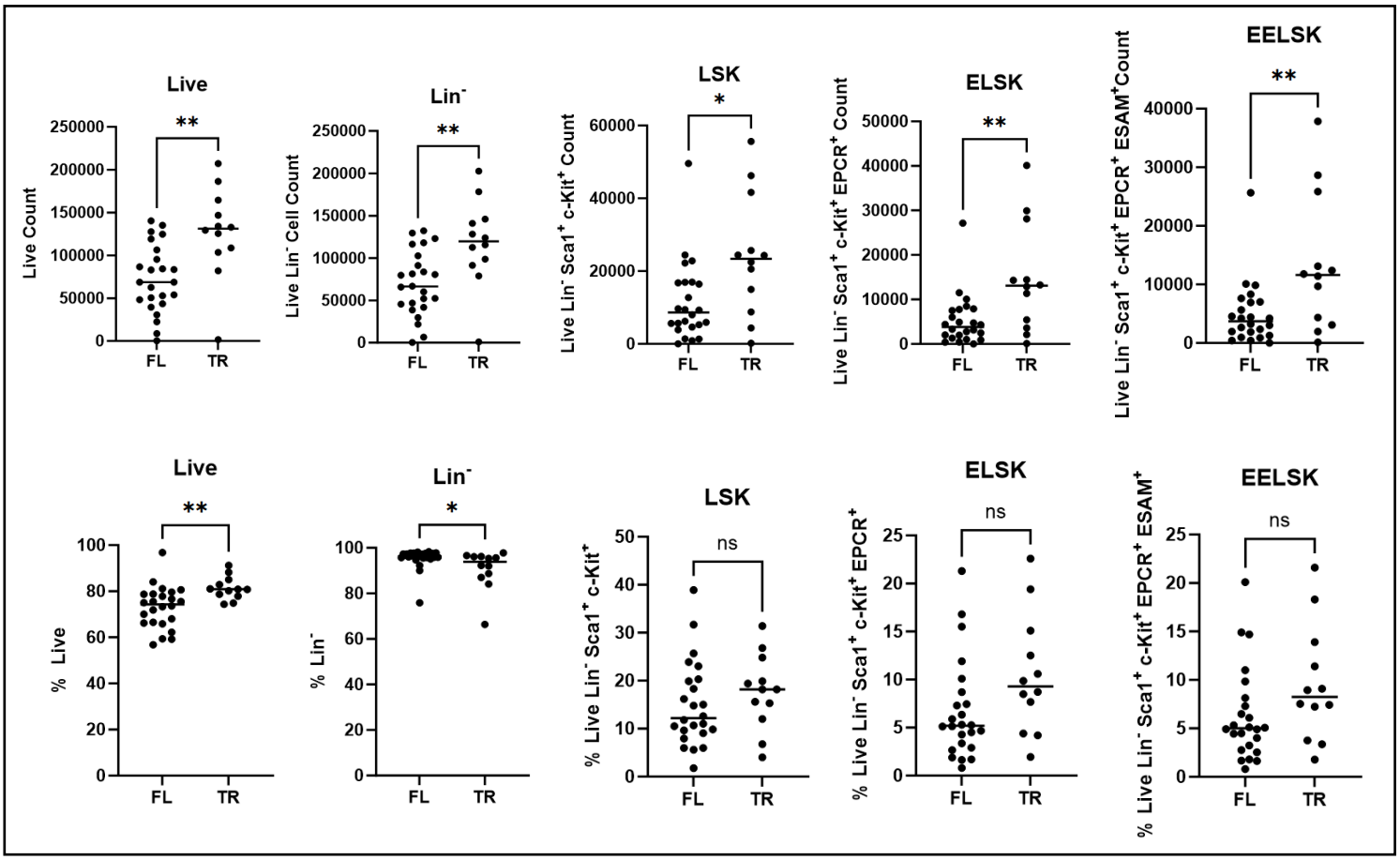

Figure 4.15 **Differences in HSC expansion as a result of full length (FL) versus truncated (TR) TPO use in PVA media**. Day 28 flow cytometric analysis shows increases in counts of all fractions measured when Control (truncated) TPO is compared to full length wildtype TPO. However, the differences we see as a percentage of total live cells are negligible. Fractions become increasingly specific for HSCs from left to right (least specific = Live, most specific = EELSK). Unpaired T-tests were used to compare between conditions. ns = p>0.05, * =p ≤ 0.05, ** =p ≤ 0.01, *** =p ≤ 0.001, **** =p ≤ 0.0001. Line represents mean.

4.10. Sorting ESLAM cells based on MPL expression impacts mouse culture outcomes.

Since delving into the importance of cytokines in expansion cultures, and the differing responses of clones to alternative combinations of SCF and TPO, we found that this was an interesting area to study and is valuable to pursue further. To further investigate cytokine responses *in vitro*, we turned our attention to MPL (CD110) – the receptor for TPO, which is present on HSCs (Tsutsumi et al., 2023). Single-cell initiated PVA cultures were established with individual ESLAM cells gated additionally on MPL expression (Figure, 4.16). MPL is a simple addition to the panel, and it is interesting to note that MPL expression subdivides the ESLAM fraction into two discernible populations, with approximately 70% of ESLAM cells positive for MPL in the majority of instances (Figure 4.16)

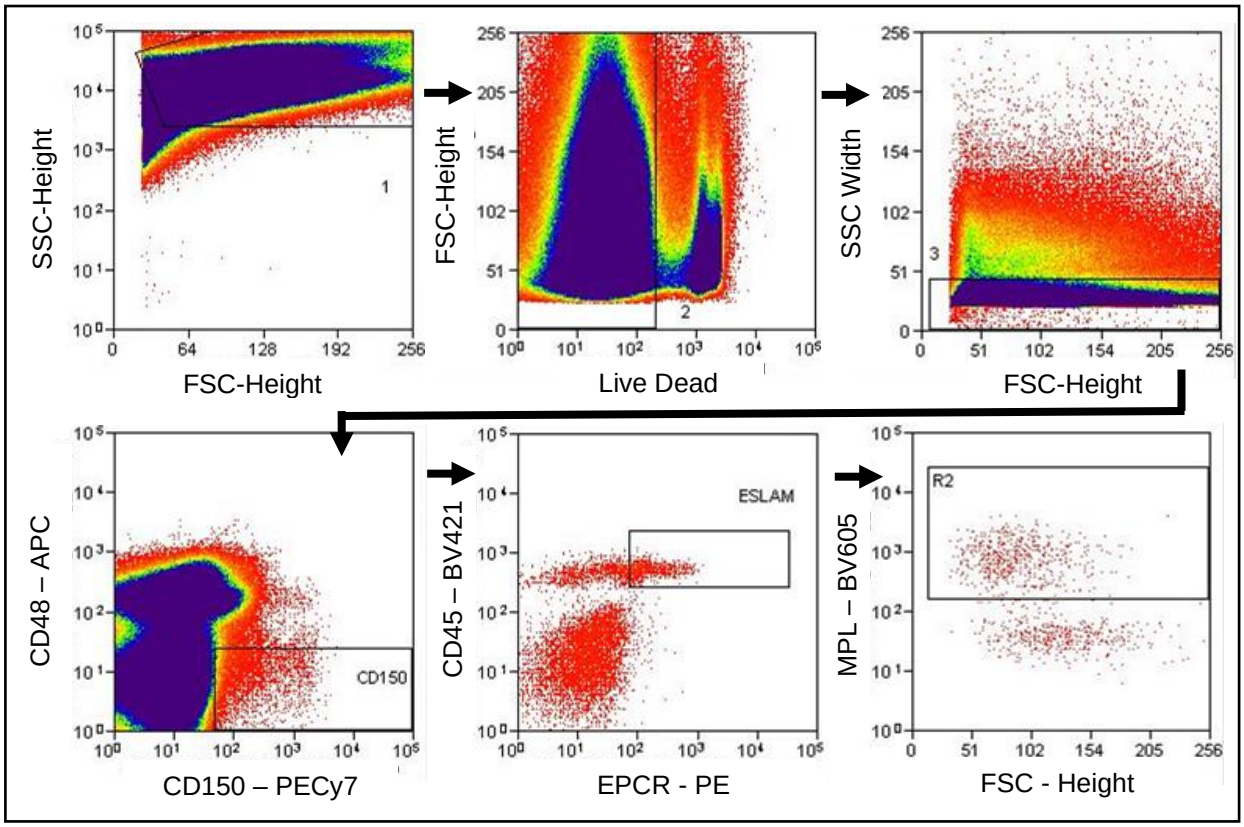

Figure 4.16 **Gating strategy for MPL$^+$ ESLAM cells**. Fresh mouse bone marrow cells underwent red blood cell lysis, lineage depletion, and antibody staining before being sorted via FACS on a MoFlo Astrios. Representative gating is shown here. Going from top left to bottom right the gates are set in the following order: Cells, Live cells, Single cells, CD150$^+$CD48$^-$, CD45$^+$EPCR$^+$, and finally MPL$^+$. The MPL$^-$ positive population is also clearly visible in this final plot.

PVA cultures were then maintained in standard expansion media for the remaining 28 days of culture before flow cytometric analysis on the final day to determine live, lineage negative, LSK, ELSK, and EELSK counts and percentages of live cells. These fractions become increasingly more specific for the HSC population as additional markers are added, and so are an efficient way of determining in which pool of cells any differences we note are occurring in. Data shown in Figure 4.17 is generated from the pooling of 3 independent repeats (180 wells). In the mouse system, it appears that ESLAM cells negative for surface MPL at the point of culture initiation result in clonal populations with higher counts of all fractions tested, including ELSK and EELSK. This trend is carried through in terms of the percentage of live cells each of these fractions make up, however there is no significant difference with respect to %ELSK. This data, although requiring transplantation validation to guarantee the presence of functional HSCs, and to see if this varies between the MPL$^+$ and

MPL$^-$ initiated cultures, raises the possibility of MPL being a valuable marker to add to the ESLAM panel when setting up PVA expansion cultures in order to improve culture outcomes.

This data (Figure 4.17), coupled with the cytokine removal culture data suggesting certain clones favour certain cytokine combinations, indicates the importance of MPL, the TPO receptor, which will be a continued focus of the experiments throughout this thesis.

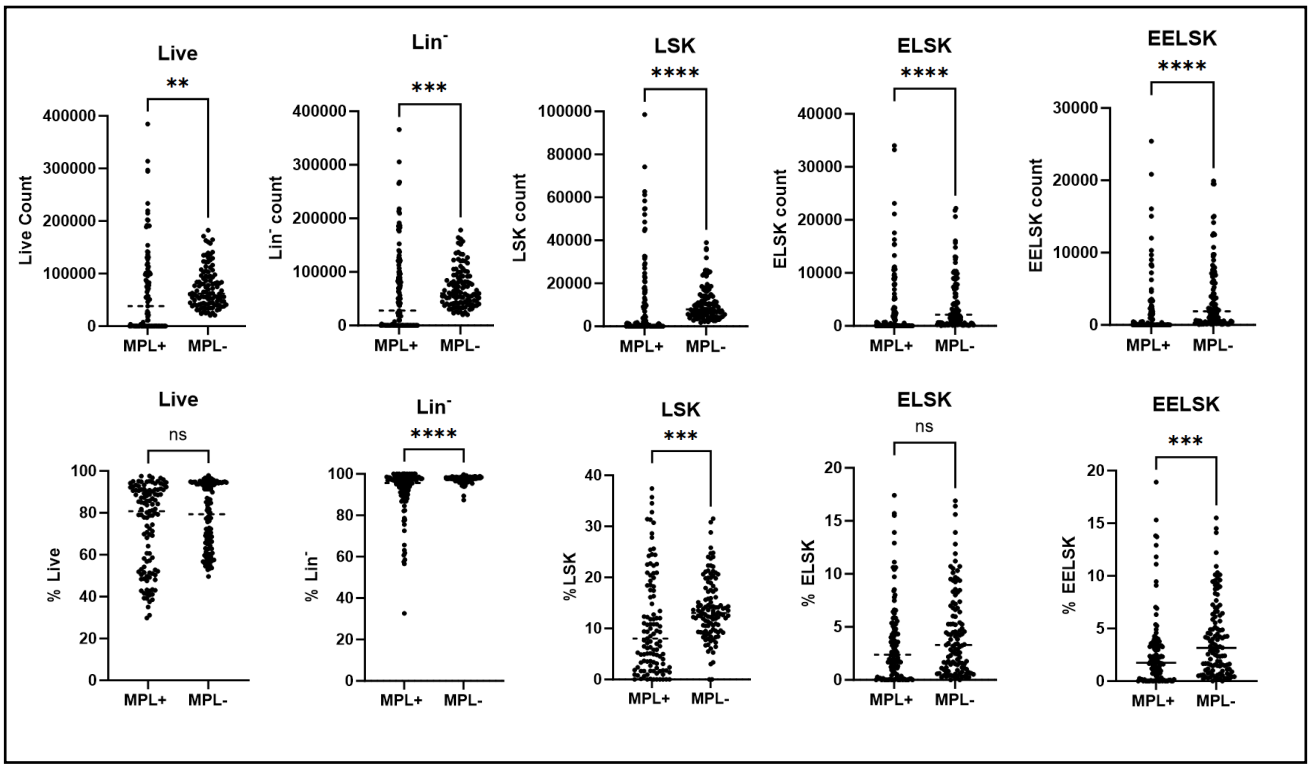

Figure 4.17 **ESLAM cells sorted on MPL expression perform differently in culture**. Day 28 flow cytometric analysis of clones started with either MPL$^+$ or MPL$^-$ ESLAM cells. This data is 3 independent experiments, pooled. Fractions become increasingly specific for HSCs from left to right (least specific = Live, most specific = EELSK). Unpaired T-tests were used to compare between conditions. ns = $p>0.05$, * =$p \leq 0.05$, ** =$p \leq 0.01$, *** =$p \leq 0.001$, **** =$p \leq 0.0001$. Line represents mean.

4.11. Development of a novel Picowell on-chip culturing system for HSCs

Until this point, PVA expansion cultures have been performed using 96-well plates to contain our cells, however this does have limitations, especially when studying the early divisions of single HSCs *in vitro*, and limits our ability to track the early stage kinetics of this model. In 96-well plates, single HSCs are hard to locate, will often move around the well which makes time-lapse microscopy challenging, and if initiating cultures with single cells, it is challenging

to determine which daughter cells arise from which parent, unless cell division is caught occurring directly.
In order to mitigate this and study these early cell divisions, a collaboration with the Photonics department at the University of York has enabled us to develop a novel Picowell chip system which will hold single cells in individual wells on a slide-sized chip which can easily be imaged.

Initially, experiments began with a simple fabrication and chip design, utilising a layer of engraved SUEX and BF33 substrate, to which cells were directly loaded onto the surface via pipetting (fabricated and loaded as described in Methods section 3.28). These first Picowell experiments revealed that sorted Fgd5^{+}LSK cells are able to be successfully loaded onto the chip, and could be imaged via time lapse microscopy for 24 hours whilst remaining viable throughout (Figure 4.18a). Importantly, it was possible to visualise the expression of the green Fgd5 reporter using the LSM980 MP (Figure 4.18b,c), which is encouraging in regards to the applicability of this system to study symmetric vs asymmetric divisions utilising this reporter. However, this experiment did highlight the need to refine the loading strategy in order to achieve an ideal density of 1 cell per well.

Once satisfied that the substrate did not detrimentally affect the cell's survival in the time frames we are interested in, the Picowell chip design was further developed to include a microfluidic channel on top of the Picowell array which would aid loading of cells, and limit evaporation of media, further improving cell viability. The protocol is outlined in Section 3.28 of this thesis, and Figure 4.19 contains a flow chart depicting the key steps of the fabrication process. A schematic of the finalised design, containing both the engraved Picowell array and the microfluidic channel is shown in Figure 4.20, alongside images of the developed chip.

We have since completed several rounds of loading SLAM cells into the device and, after some refinement, have found an ideal loading density of 2000 cells in 10µL. Following on from the process of developing the Picowell chip, which is now standardised and easy to perform, this device can now be utilised more widely by our lab to delve into the early cell division kinetics of individual cells in mouse expansion cultures. A key advantage of this Picowell system is the flexibility of the well array design, with changes in well dimensions and number easily implementable, which unlocks the possibility to use this chip for alternative cell types, including primary human samples, as desired.

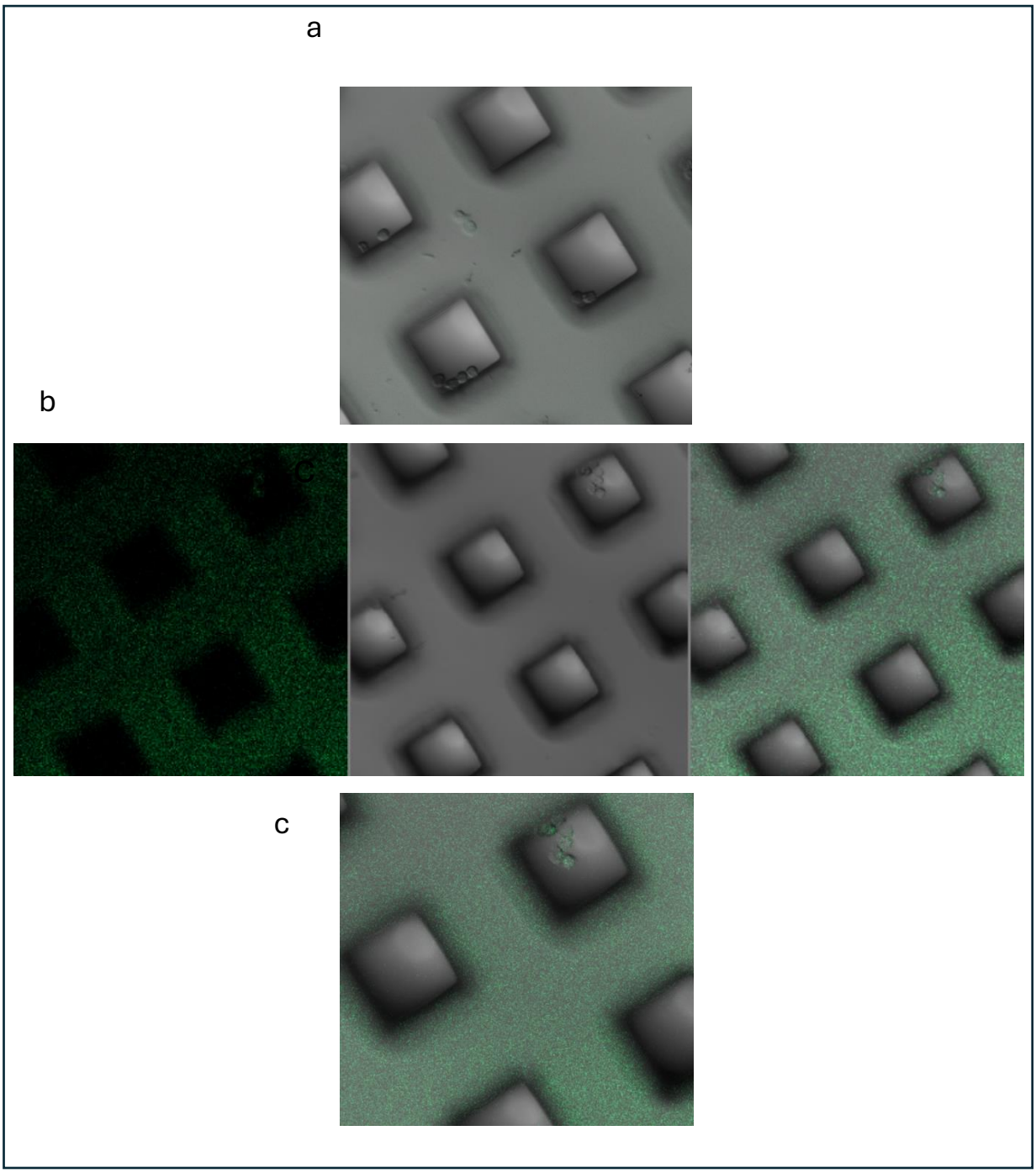

Figure 4.18 **Fgd5+ELSK cells imaged on a Picowell chip**. a) LSK cells loaded onto a Picowell chip, imaged on a LSM980 at 20x. b+c) LSK cells imaged at 20k on a Picowell chip, using both brightfield and fluorescence microscopy. This highlights the visible green fluorescence of the Fgd5 reporter, but also the green autofluorescence of the SUEX.

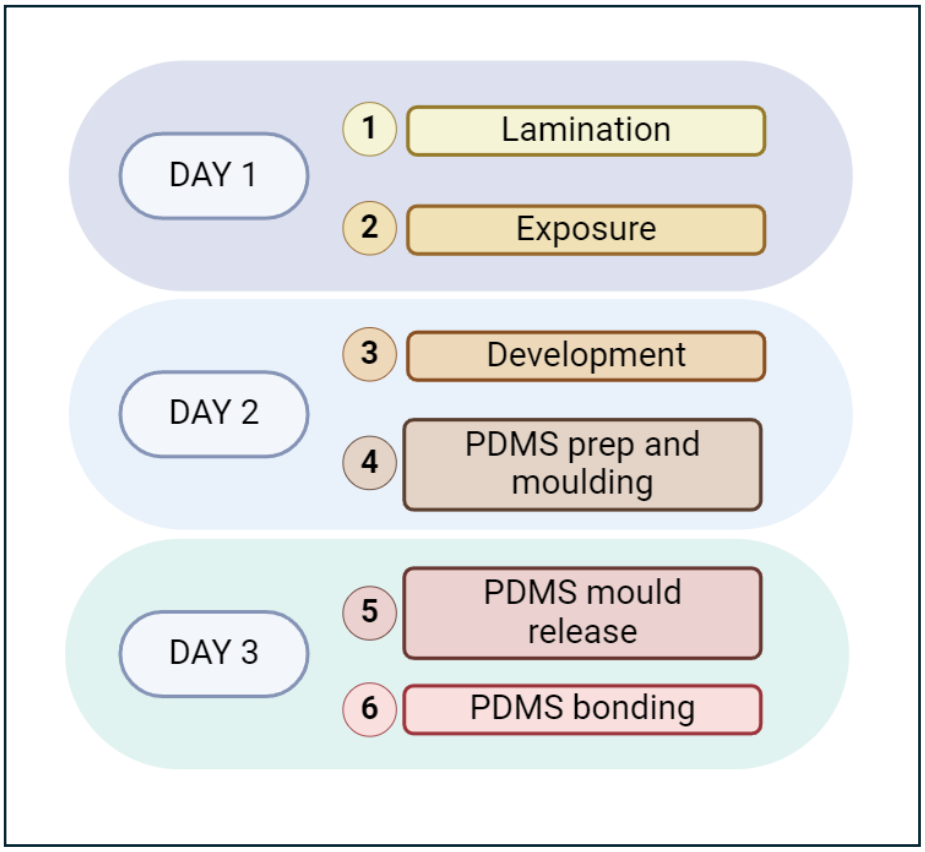

Figure 4.19 **Fabrication process of the finalised Picowell chip design.** A full protocol is included in methods section 3.29. Step 1, Lamination, involves the process of layering an SUEX film onto the BF33 glass substrate. Following this, using a Kloe Dilase 650, exposure to a laser patterns the desired Picowell array into the SUEX layer. The chip is then baked overnight ahead of development with Ethylene Carbonate, a solvent used to remove the non-crosslinked areas (areas left untouched by the laser). The chips are then washed with isopropyl alcohol, and hard baked, ready for storage until the PDMS channel will be added. The 2 components of the PDMS are mixed well then poured over a “Master” chip for moulding, before desiccation to remove bubbles, and an overnight bake. The following day, the PDMS is removed from the Master mould and inlet and outlet holes are created with a 1mM biopsy punch. Following exposure of the bonding sites of the PDMS and SUEX to oxygen radicals in the plasma asher, the two components are now ready for alignment and attachment.

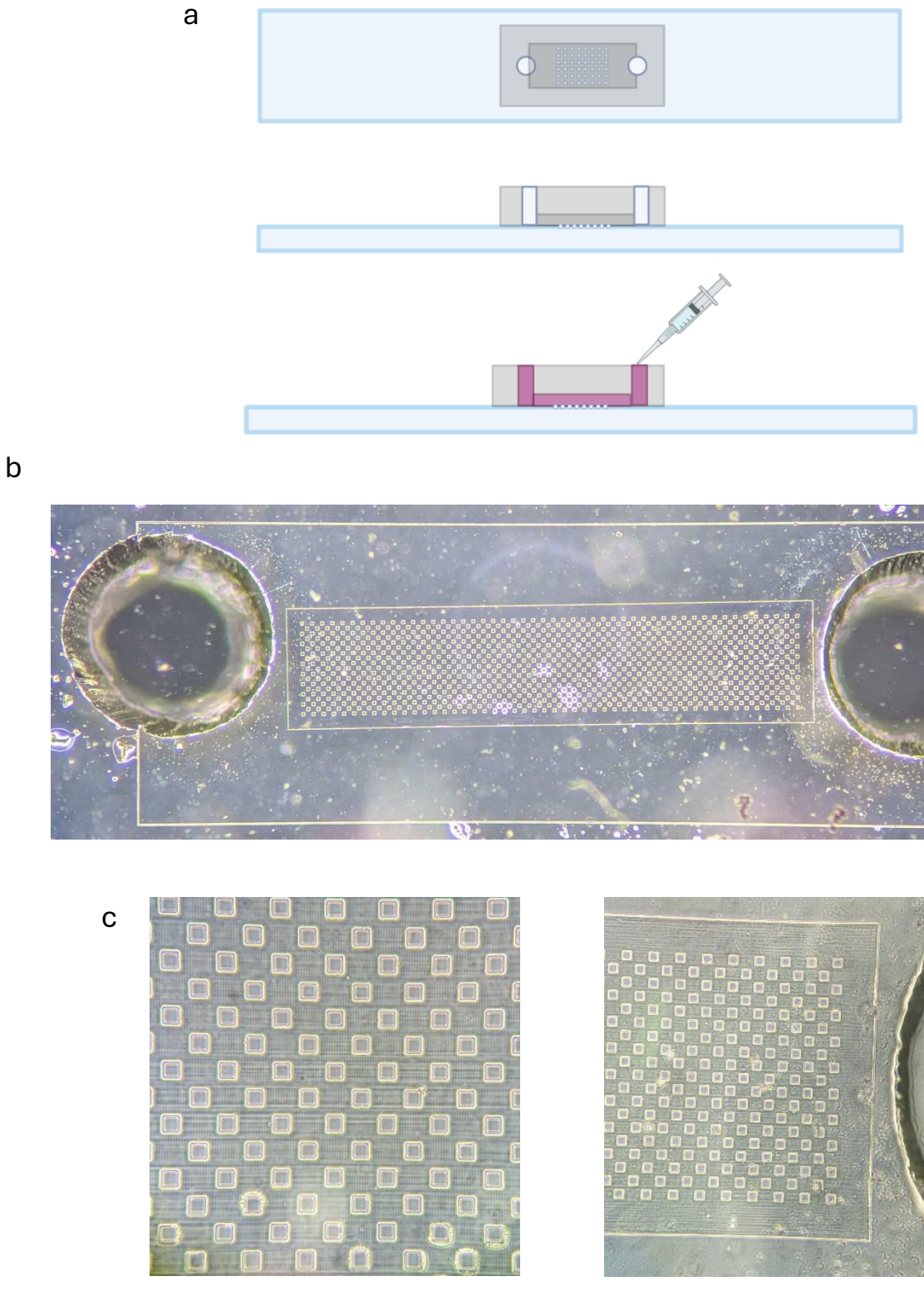

Figure 4.20 **Picowell schematic and images**. a) Representative diagrams of the Picowell channel engraved on an SUEX/BF33 substrate with PDMS microfluidic channel layered on top. b) 10x image of Picowell chip with microfluidic channel. Inlet, outlet, Picowell array, and microfluidic channel are visible. c) 20x and 40x images highlighting detail of Picowell array wells. Schematic created in BioRender.

4.12. Chapter summary

In conclusion for this chapter, we have identified ESAM as a robust marker for functional *in vitro* expanded HSCs, which can replace the use for the *Fgd5*$^{ZsGreen•ZsGreen/+}$ reporter mouse. Initially based on flow cytometric analysis on the final day of culture, this has since been further functionally validated by several HSC transplantation experiments which link the increasing presence of ESAM^{+}ELSK cells at the point of transplantation, with increasing HSC functionality and chimerism post-transplant. Furthermore, we have identified CD321 as a promising HSC reporter, which needs to be further validated by transplantation, but from flow cytometric analysis seems likely to be a valuable addition. We then continued to be guided by proteomic data sets, identifying SiglecF as a potentially interesting marker. Despite the lack of correlation we see between SiglecF and HSC function in a transplantation setting, it does appear to have the capacity to be a valuable asset for predicting day 28 culture success at day 14.

Following the development of a functionally validated split culture approach, this chapter has highlighted the capacity of mouse PVA expansion cultures as a screen for testing novel molecules for their effect on HSC expansion and self-renewal. Combined with the established ELSK and EELSK reporter strategies, this is a significant development in the field, allowing rapid testing of many conditions *in vitro* without the need for expensive and time-consuming HSC transplantation experiments. Instead it is possible to rely on a refined and reproducible flow cytometry panel in order to analyse clones and determine functional HSC content at the end of culture.

Regarding further refinement of the mouse expansion protocol, studies into cytokine removal conditions have shown that these cultures become cytokine self-sustaining by the week 2 timepoint, and in fact seem to out-perform standard conditions following the removal of SCF. As well as improving the percentage of ELSK by the end of expansion, this approach significantly reduces the costs associated with this protocol – increasing the accessibility of this technique. Furthermore, additional analysis into this data reveals several key patterns within the dataset, which show that clones, although all initiated by single ESLAM cells, favour different media compositions post-day 14, which opens up the possibility of personalised media to maximise culture success.

This chapter then continued this investigation into the roles of cytokines in expansion cultures further, comparing the differences in culture outcome between clones supplemented with full length and truncated TPO. A significant improvement in cultures was noted in those

treated with truncated TPO compared to full length, an interesting topic for further structural analysis. The role of TPO in these cultures was becoming increasingly interesting as identified the stark differences TPO could make to culture success, and so single-cell cultures were initiated with MPL^+ and MPL^- ESLAM cells. Significantly improved counts and percentages of HSCs were observed at the end of culture in MPL^- ESLAM initiated clones.

Finally this chapter details the development of a novel Picowell chip system for culturing HSCs *in vitro*. This process began with a simplified design, validating the biocompatibility of the materials with our cells of choice and confirming cells maintain viability when on-chip. From there, we developed a more sophisticated design, containing a microfluidic channel to aid loading and limit evaporation. Now the fabrication of this chip has been standardised, it opens the doors for easy modification to test alternative cell types, such as primary human cells.

5. Human HSC expansion systems

Maintaining and expanding human HSCs *in vitro* has been a long standing challenge in the field of experimental haematology, and has proven to be significantly more difficult to achieve than for mouse. Previous gold-standard approaches for the culture of human HSCs *in vitro* have typically achieved just 3 to 20-fold increases in HSC number over the course of culture (Wilkinson et al., 2019, Sudo et al., 2021). Historically, these systems have involved human HSCs being cultured in serum free media, supplemented with various combinations of key cytokines – including Stem Cell Factor (SCF), Granulocyte–Colony Stimulating Factor (G-CSF), Interleukin-6 (IL-6), Interleukin-3 (IL-3) and Fms-like tyrosine kinase 3 ligand (Flt3L) (Miller et al., 1997, Bhatia et al., 1997). More recently, groups have experimented with the addition of small molecules to these media formulations, which have improved the levels of expansion that can be achieved to up to 17-fold, but still result in comparably small increases compared to mouse (Fares et al., 2014, Boitano et al., 2010). However, a recent paper published by our Japanese collaborators details a groundbreaking expansion protocol, the 3a expansion system, which enables long term expansion of up to 55-fold expansion of CD34+ cells over the course of a 14 day culture. With early access to this protocol from our collaborators, we aimed to establish this system and test its capacity for expanding rarer patient peripheral blood samples.

Expanding human samples *in vitro* has many benefits, firstly the ability to unlock a range of experimental assays, previously impossible to perform on human HSCs due to the scarcity of the cell type. These include proteomic and transcriptomic analyses, enabling us to unpick key mechanisms driving self-renewal and proliferation in these cells. Furthermore, the *in vitro* expansion of specifically peripheral blood samples from both healthy and patient donors is incredibly valuable. These samples tend to be more readily available and clinically relevant than cord bloods, yet have historically lacked robust expansion strategies. Developing systems which would allow the expansion of patient HSCs *in vitro* has the potential for circumnavigating the need for xenograft models in order to increase the cell numbers from these samples, whilst also providing methods for efficient screening of novel molecules on these rare cells. Additionally, in the context of HSC transplantation, often the sole curative therapy for blood disorders, it has been well studied that the cell dose given to the patient correlates directly with treatment success (Remberger et al., 2020). Therefore the capacity to expand cells *in vitro* from a wide range of sources, particularly those more easily accessible such as peripheral blood, is highly valuable.

5.1. Direct comparison of the 3a expansion protocol against the current gold standard for in vitro HSC expansion

Initially, it was important to test this newly developed 3a expansion protocol to the previous gold-standard of StemSpan expansion cultures (protocol in Methods 3.14). In order to test this, the two conditions were compared directly using cord blood samples. We utilised a CD34 enriched cord blood sample which had been counted on a haemocytometer, with trypan blue staining used to remove dead cells from the count, and then loaded 10,000 live cells per well. Importantly, for these cultures, flat-bottom CELLBIND plates are used. These plates have been precoated with a polymer to encourage the attachment of cells to the base of the well, and to protect them from potential removal during media changes. These cells were subject to 14 days of *in vitro* expansion in either Stemspan conditions, or the novel 3a expansion media. On day 14, the samples were stained for CD34 APC, CD45RA APC-eFluoro780, CD90-PE, EPCR-BV421 and Sytox green, as described in Methods section 3.16, and were analysed via flow cytometry to determine their phenotypic HSC content (pHSC: $CD34^+CD45Ra^-CD90^+EPCR^+$). Representative gates are shown in Figure 5.1. The flow cytometric data collected at day 14 show a striking improvement in both phenotypic HSC count, and percentage of phenotypic HSCs in each well under 3a conditions compared to StemSpan conditions (Figure 5.2).

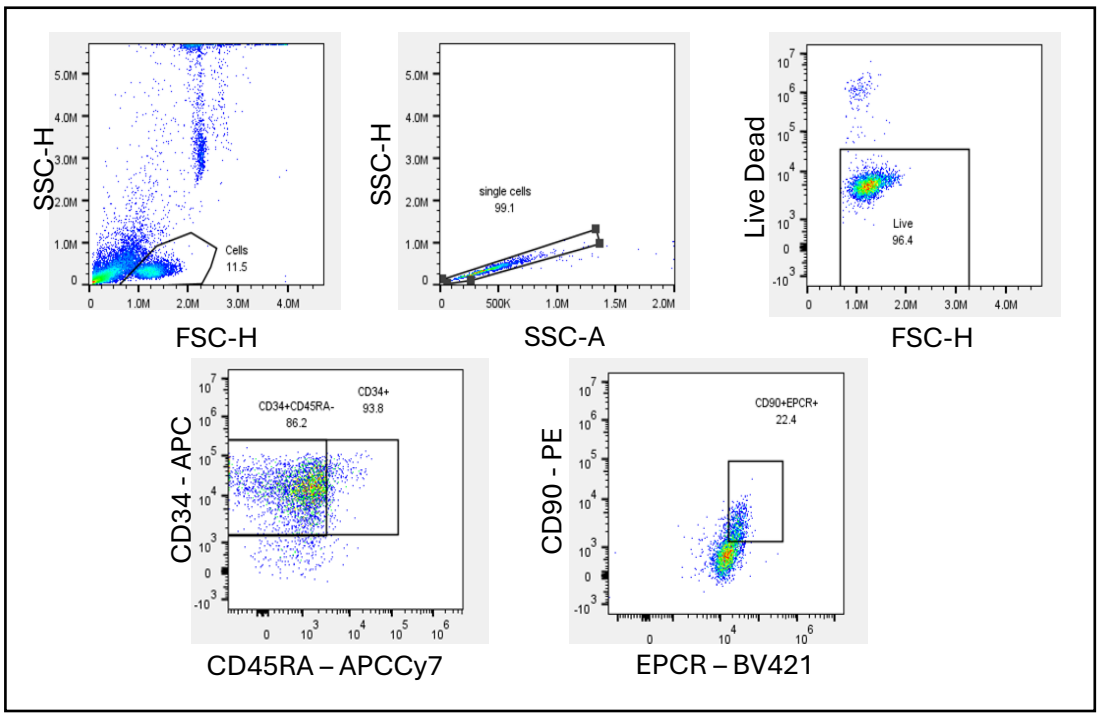

Figure 5.1 **Representative gating strategy for phenotypic human HSCs post-expansion**. An initial cell gate is set, within which sequential gates are set on single cells, live cells, the $CD34^+CD45RA^-$ fraction, finally the $CD90^+EPCR^+$. This final gate, ultimately the live, $CD34^+CD45RA^-EPCR^+CD90^+$ population, is what we would consider to be phenotypic HSCs.

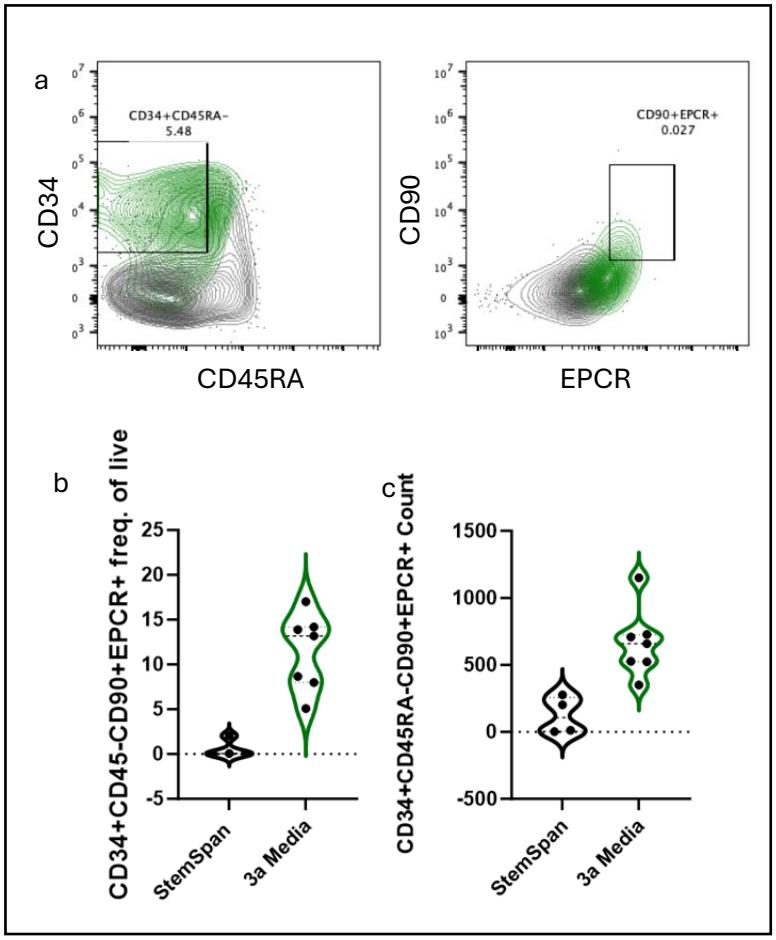

Figure 5.2 **3a conditions outperform the previous gold-standard of StemSpan expansion cultures.** Data comparing extent of in vitro expansion of human $CD34^+$ enriched cord blood samples in 3a conditions versus StemSpan conditions. a) Representative gating strategy for phenotypic HSCs. Previous to these gates, cells, single cells, and live cells (using Sytox green as a live dead stain) were set. The green contours show the gating for 3a expanded cells, whilst the black contours show the gating for StemSpan expanded cell populations. b) Comparison of the percentage of cells in each culture being phenotypic HSCs in Stemspan vs 3a conditions. $P \leq 0.001$ c) Comparison of total phenotypic HSC count in StemSpan vs 3a conditions. $P \leq 0.01$.

5.1.1. Addition of Flt3L to 3a media improves efficiency of human cord blood expansion cultures and enables expansion of $CD34^+$ cells from alternative sources.

In order to further refine our existing 3a culture protocol, with advice from collaborators in the University of Oxford, we tested the effect of adding Fms-like tyrosine kinase 3 ligand (Flt3L) into our expansion media at a concentration of 10ng/mL, with hopes of improving culture efficiency and purity. Flt3L is a key cytokine which has historically been used widely in previous attempts to refine the *in vitro* expansion of human HSCs (Miller et al., 1997, Bhatia et al., 1997, Audet et al., 2002), and so is a logical and evidence-based addition into the expansion media for the 3a system.

Cultures were initiated with 10,000 cord blood $CD34^+$ cells per well, as per the published protocol (Sakurai et al., 2023). The effect of supplementing Flt3L to the media was tested in both traditional 3a expansion cultures where Butyzamide is used as a TPO-receptor mimetic, as well as 3a expansion cultures where Butyzamide had been replaced with TPO itself at a concentration of 100ng/mL. The expanded samples were analysed on day 14 by flow cytometric analysis to quantify counts and percentages of phenotypic HSCs (pHSCs), as determined by the $CD34^+CD45RA^-CD90^+EPCR^+$ fraction (representative gating in Figure 5.1).

As shown in Figure 5.3, it is clear that the addition of Flt3L to human cord blood expansion cultures improves pHSC counts within the day 14 expanded samples, in both standard butyzamide 3a conditions and TPO supplemented media. Flt3L supplementation also significantly improves pHSC percentages at day 14 in TPO supplemented 3a media, and slight increases are also observed in the standard butyzamide 3a media. Since the collection of this data, Flt3L supplementation at 10ng/mL into 3a expansion media has become standard, and has contributed significantly to the robustness of this protocol. Furthermore, increasing the Flt3L dose to 15ng/mL has enabled us to successfully expand harder-to-grow peripheral blood samples from both healthy and diseased donors. Additionally, upon recommendation by collaborators, Monothioglycerol (MTG - 100μM, Sigma, Cat.No. M1753) has also been consistently included in our 3a media composition.

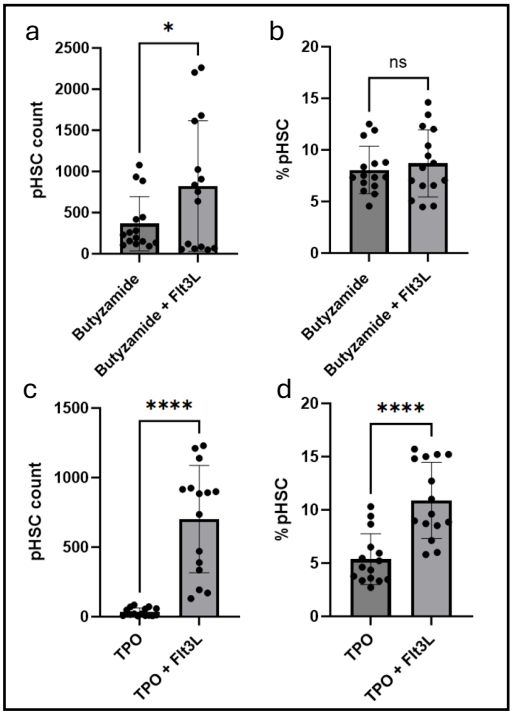

Figure 5.3 **Day 14 flow cytometric analysis of 3a expansion cultures with or without Flt3L supplementation**. Samples were initiated with 10,000 $CD34^+$ cord blood cells per well in a 96-well CELLBIND plate. Here, 3a media containing either standard Butyzamide or TPO, is compared with and without Flt3L supplementation. It is clear that Flt3L supplementation significantly improves HSC yields post-expansion. Differences in day 14 pHSC counts (a) and percentages (b) with Butyzamide, as well as pHSC counts (c) and percentages (d) following a TPO supplemented culture are shown. Unpaired T-tests were used to compare between conditions. ns = $p>0.05$, * =$p \leq 0.05$, **** =$p \leq 0.0001$

5.1.2. Human cord blood HSC expansion may be improved by 2d and 3d gel substrates

An ongoing and recent focus within the HSC expansion field has been on the use of biophysical approaches to refining *in vitro* expansion, as the importance of mechanical regulation on HSCs is coming to light.

Working with collaborators within the Kent Lab who have expertise in the fabrication of biocompatible hydrogels, standard plastic culturing systems, in this case the standard CELLBIND plates utilised for the 3a expansion culture, were compared to 2-dimensional (2d) and 3-dimensional (3d) gels as a substrate for HSC expansion. Cultures were initiated with 10,000 $CD34^+$ cord blood cells, onto either CELLBIND plates, onto a 2d hydrogel, or mixed into a 3d gel, and were then expanded for 14 days in 3a media before flow cytometric analysis on the day 14. Interestingly, we noted a significant increase in the counts and

percentages of phenotypic HSCs achieved at the end of culture when using a 2d gel instead of plastic to culture these samples, however we see this significant difference disappear when 3d gels are used (Figure 5.4). This is an interesting discovery, again highlighting the fundamental importance of the physical environment in HSC self-renewal, and the ability to regulate culture outputs through mechanical stimuli.

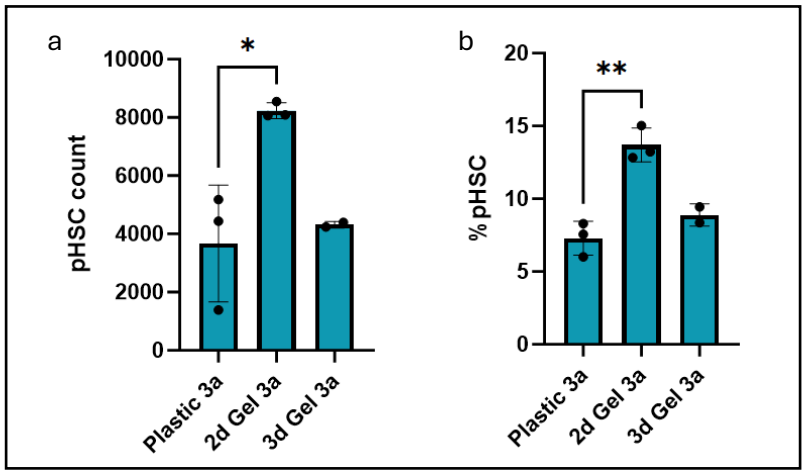

Figure 5.4 **Culturing human HSCs in a 2d gel instead of on plastic improves culture outcomes**. Flow cytometric analysis of day 14 expanded cord blood CD34 enriched cells. Traditional CELLBIND plastic plates were compared with 2D and 3D gels in terms of their ability to expand pHSCs ($CD45^+CD45RA^-EPCR^+CD90^+$). To determine culture success counts (a) and percentages (b) of pHSCs were measured on day 14. Unpaired T-test, * = $p \leq 0.05$, ** =$p \leq 0.01$

5.1.3. FITC Dextran versus Soluplus in 3a expansion cultures

Continuing with our investigation into the mechanical regulation of HSC expansion *in vitro,* we aimed to further experiment with replacing Soluplus in culture. The role of Soluplus in these 3a expansion cultures is not well defined, and microscopy seems a promising tool to elucidate its role, as it will enable us to determine if the molecule is taken up by the cells, or acts as a scaffold in the media, perhaps having roles in presenting other molecules/cytokines to the cells. Whilst there is no labelled Soluplus available for imaging, we turned to a similar molecule, Dextran, which is also known to be a promising functional alternative to PVA (the Soluplus equivalent in mouse cultures), but is also possible to acquire in a FITC labelled form. Before proceeding to microscopy analysis, we aimed to determine if FITC Dextran performs similarly to Soluplus in expansion cultures. As is standard for 3a expansion, we loaded 10,000 $CD34^+$ enriched human cord blood cells per well of a CELLBIND 96-well plate, and cultured the cells for 14 days. The only change being the replacement of Soluplus with the same concentration of FITC Dextran in the media. However, the data collected by day 14 flow cytometric analysis of these cultures reveal that

Dextran stunts the growth of the cultures, reducing both phenotypic HSC (pHSC) and $CD34^+$ counts and percentages of live cells (Figure 5.5). Unfortunately, the impairment of Dextran on the cultures limits our ability to use this molecule for imaging, so alternatives must be found.

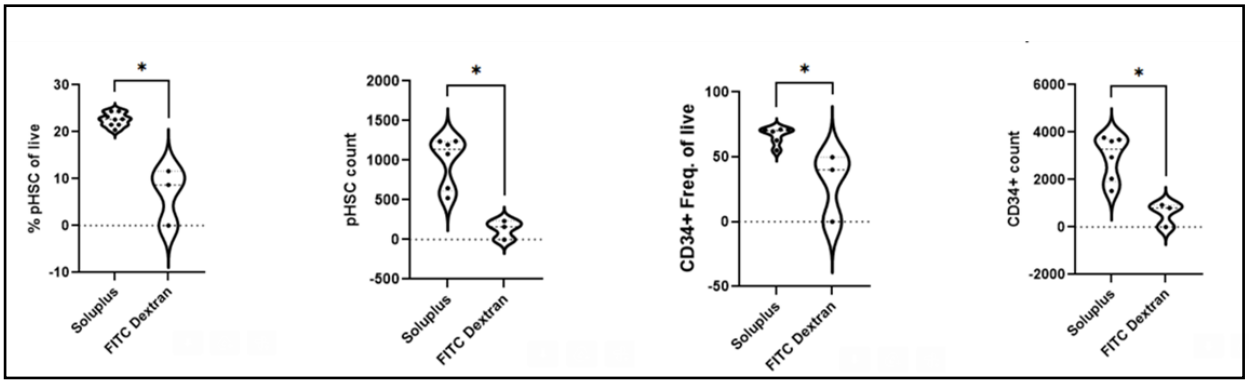

Figure 5.5 **Soluplus provides significantly better culture outcomes than FITC Dextran in 3a media**. Day 14 analysis of 3a expansion cultures. Samples were initiated with 10,000 $CD34^+$ cord blood cells per well in a 96-well CELLBIND plate. This experiment compared the efficiency of traditional 3a media (containing Soluplus) versus 3a media where Soluplus had been replaced with FITC Dextran. As shown above, FITC Dextran cultures presented with lower $CD34^+$ and pHSC counts and percentage of live cells. Unpaired T-Test, $P \leq 0.05$

Further 3a expansion screens were performed to determine if replacing Soluplus with either unlabelled Dextran, or PVP, as tested previously in the mouse expansion culture system (Section 4.7 of this thesis), are able to improve the levels of expansion or culture purity observed over the course of 14 days of 3a culture. Once again, we see that although PVP provides comparable levels of %pHSCs at the end of culture, both Dextran and FITC Dextran resulted in significantly poorer performing clones (Figure 5.6). These notable differences in expansion, as a result of a simple supplementation between similar polymers, are compelling evidence for the importance of mechanical regulation and biophysical influence on the *in vitro* expansion of human HSCs. Whilst already a focus for several groups in the field, this is the one of the initial examples of the impact of mechanobiology within the 3a system.

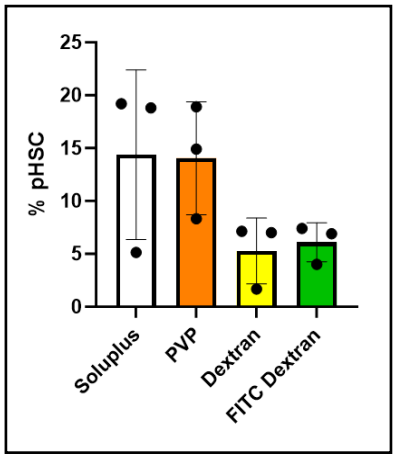

Figure 5.6 **Day 14 analysis of 3a expansion cultures following supplementation with Soluplus alternatives**. Cultures were initiated with 10,000 CD34$^+$ cord blood cells per well. Soluplus and PVP presented comparable levels of %pHSC at the final day time point, whereas Dextran and FITC Dextran had consistently lower levels of %pHSC in each well at the end of 14 days of culture. Error bars show standard deviation.

5.2. Peripheral blood CD34$^+$ cells from myeloproliferative neoplasm patients can be successfully expanded in 3a conditions

Following the successful, and now reliable, expansion of cord blood CD34$^+$ cells in the 3a system, the next steps focused on aiming to apply this protocol to peripheral blood HSCs. The frequency of HSCs in peripheral blood samples is lower than in cord blood, and the CD34$^+$ cells present in these samples typically exhibit lower levels of proliferation in response to cytokines (Hordyjewska et al., 2014). Furthermore, cord blood samples contain higher frequencies of primitive HSCs than peripheral blood samples. Additionally, when dealing with patient samples, especially from diseases with highly variable phenotypes, we often see stark differences in phenotypic HSC (pHSC) counts and percentages between patient peripheral blood samples, and even between samples from the same patient over time. These challenges make the *in vitro* expansion of peripheral blood samples a particular challenge. When culturing healthy peripheral blood samples, it is possible to use mobilised peripheral bloods – in these instances, the donor has been given a stimulus ahead of the sample being taken which will mobilise HSCs from the bone marrow into circulation, which increases the frequencies of CD34$^+$ and pHSCs in the sample, in turn aiding its *in vitro* expansion. However, these samples are rarer and so initially, myeloproliferative neoplasm (MPN) patient samples were used – as these naturally have higher CD34$^+$ and pHSC counts and percentages than peripheral blood samples from healthy controls, and gaining the ability to expand these samples *in vitro* would hold massive clinical benefit.

In the following experiment, peripheral blood samples were collected from MPN patients with JAK2^{V617F} mutations, and had been enriched for CD34^{+} cells before freezing. The JAK2^{V618F} mutation is a very common mutation within MPN patients, present in 95% of PV patients, and ~60% of MF and ET cases (Tefferi et al., 2014). These samples were prepared as described in Methods section 3.11, counted on a haemocytometer, and were then loaded into a 96-well plate at either 10,000, 50,000 or 500,000 CD34^{+} cells/well.

As a first attempt at this experiment, these higher loading densities were tested as the pHSC frequency within the sample, the extent of their *in vitro* survival, and ability to expand in culture is poorly understood. Additionally, there has been no previous work detailing their behaviour in 3a expansion conditions. These cells were expanded for 14 days in 3a conditions supplemented with Flt3L and MTG, and were analysed on day 14 using flow cytometry to determine their phenotypic HSC content (CD34^{+}CD45RA^{-}CD90^{+}EPCR^{+}) (Figure 5.7). The data reveal increasing CD34^{+} and pHSC counts with increasing starting cell number, but a significant decrease in CD34^{+}% and pHSC% of total cells (Figure 5.8). This reveals a decrease in efficiency of larger cultures, perhaps due to some level of contact inhibition or increased concentration of secreted inhibitory molecules in the media due to larger cell number. Alternatively, it is possible that the greater cell numbers exhaust supportive media components within the well, inhibiting further expansion.

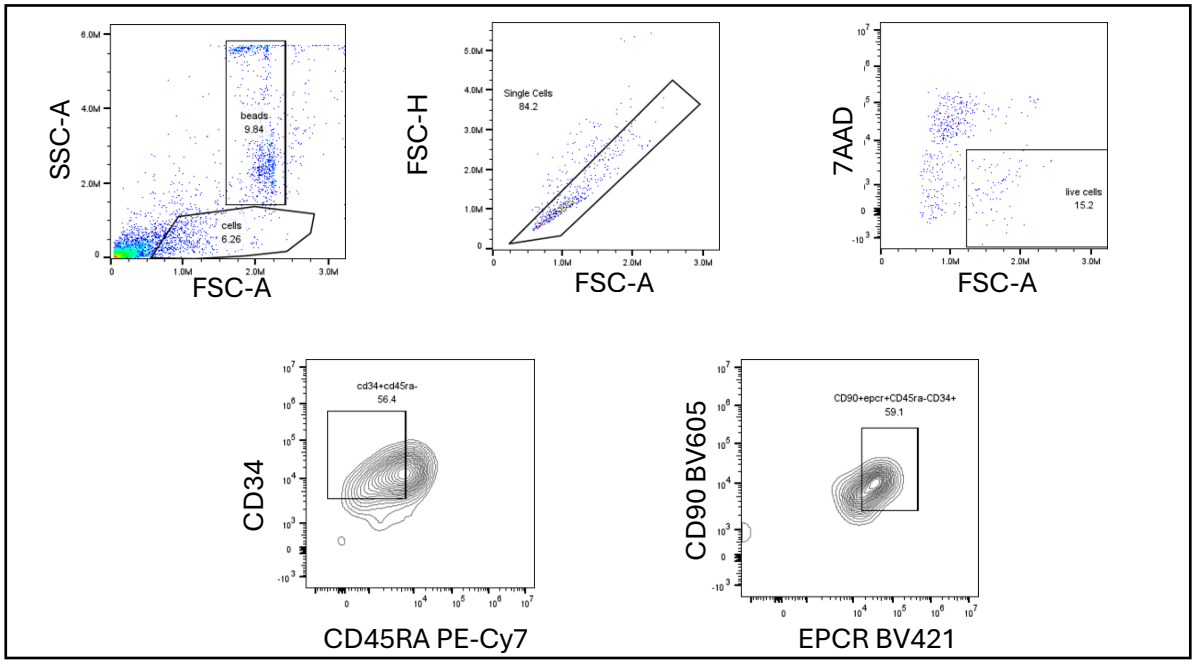

Figure 5.7 **Day 14 gating strategy to identify expanded HSCs from MPN patient peripheral blood samples**. Representative gating strategy used to determine phenotypic HSC (pHSC) content of expanded cultures grown from CD34^{+} cells from the peripheral blood of MPN patients. A specific dose of Precision Count beads added per well allowed back-calculation of pHSC counts

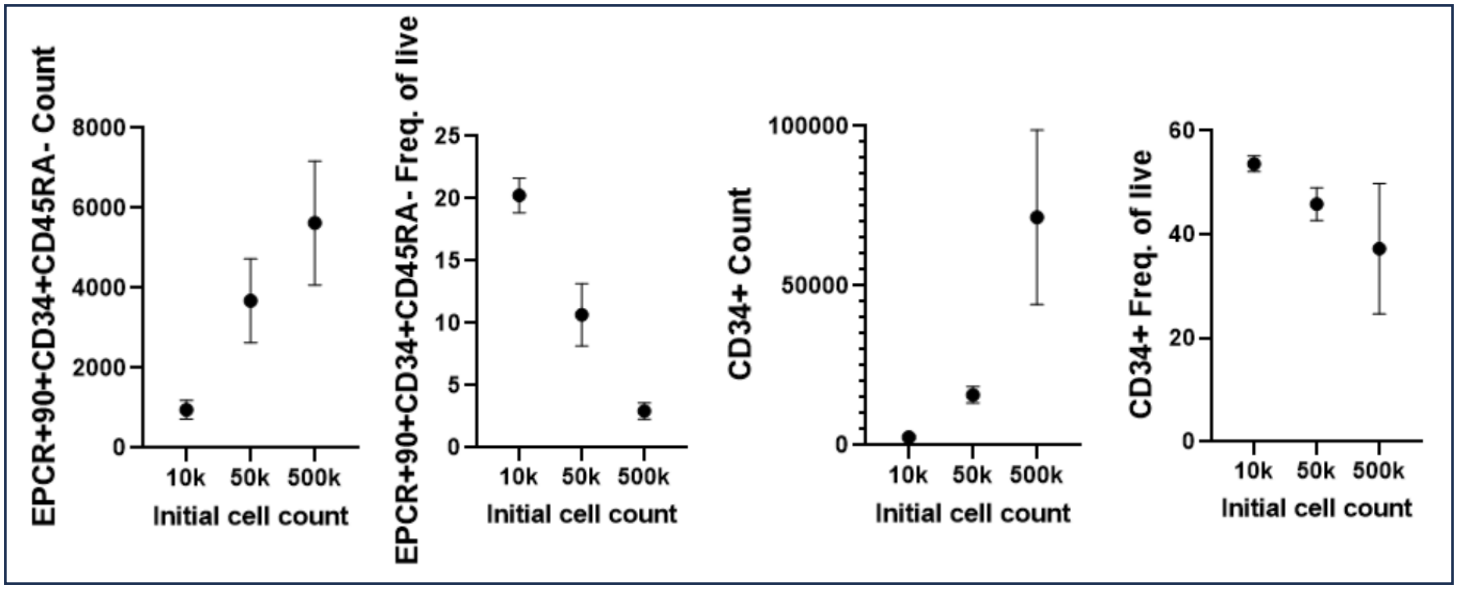

Figure 5.8 **10,000 starting cells per well is the most efficient loading density for human MPN peripheral blood CD34$^+$ cells**. Flow cytometric data generated from human MPN patient CD34$^+$ initiated cultures on day 14 of expansion in 3a media. Data collected from 10x 10k wells, 5x 50k wells, and 5x 500k wells. As shown, CD34$^+$ and phenotypic HSC counts increase in line with increasing starting cell counts. However, despite this, %CD34$^+$ and %pHSC decrease as starting cell count increases. Error bars show standard deviation.

As a result of this data, 10,000 cells per well was maintained as the standard loading density for this new sample type, as this starting material enabled significant levels of HSC expansion, resulting in ~1000 pHSCs from a handful of initiating HSCs, whilst also maintaining cultures of a similar purity to cord blood samples (~20% pHSCs).

Most importantly, this is the first demonstration of the successful expansion of human MPN patient samples in the 3a system, and the greatest *in vitro* expansion of peripheral blood MPN patient samples to date. Increasing the number of stem cells from these patients unlocks the ability to perform assays previously limited by cell number on this rare population, as well as to use these expansion cultures as a screening platform. Together, these will allow us to better understand the mechanisms governing these rare cells, therefore identifying potential therapeutic targets which would have the capacity to limit the self-renewal of these diseased cells.

5.3. Mobilised peripheral blood from healthy donors can be successfully expanded in 3a conditions supplemented with MTG and Flt3L

Following the successful expansion of MPN samples, we then progressed to test the expansion capacity of healthy mobilised peripheral blood samples. For this experiment, bulk

mobilised peripheral blood $CD34^+$ cells from healthy donors were sorted 10,000 cells per well.

This population was then expanded in 3a conditions for 14 days, supplemented with Flt3L at the higher concentration of 15ng/mL and 100 µM MTG. On day 14 the well was stained as described in Methods 3.16 and the gating strategy used to identify the $CD34^+CD45RA^-CD90^+EPCR^+$ fraction, representative of phenotypic HSCs (pHSCs), is shown below in Figure 5.9. Data collected from day 14 show that these samples could be successfully and robustly expanded over the course of a 14 day culture period. Within the initial 10,000 seeded $CD34^+$ cells from a healthy, mobilised peripheral blood sample, typically 2-3 of these cells would be functional HSCs. As shown in Figure 5.10, by day 14 we are seeing significantly higher numbers of pHSCs per well of around 1000, with ~25% of all live cells being pHSCs. This is an similar frequency to the percentages observed in cord blood expanded samples, and is an exciting result, proving for the first time the applicability of the 3a expansion culture system to mobilised peripheral blood samples. Also of note, is that 47% of pHSCs were expressing MPL, the TPO receptor, and that expression of this marker seems to subdivide the pHSC fraction following *in vitro* expansion (Figure 5.10).

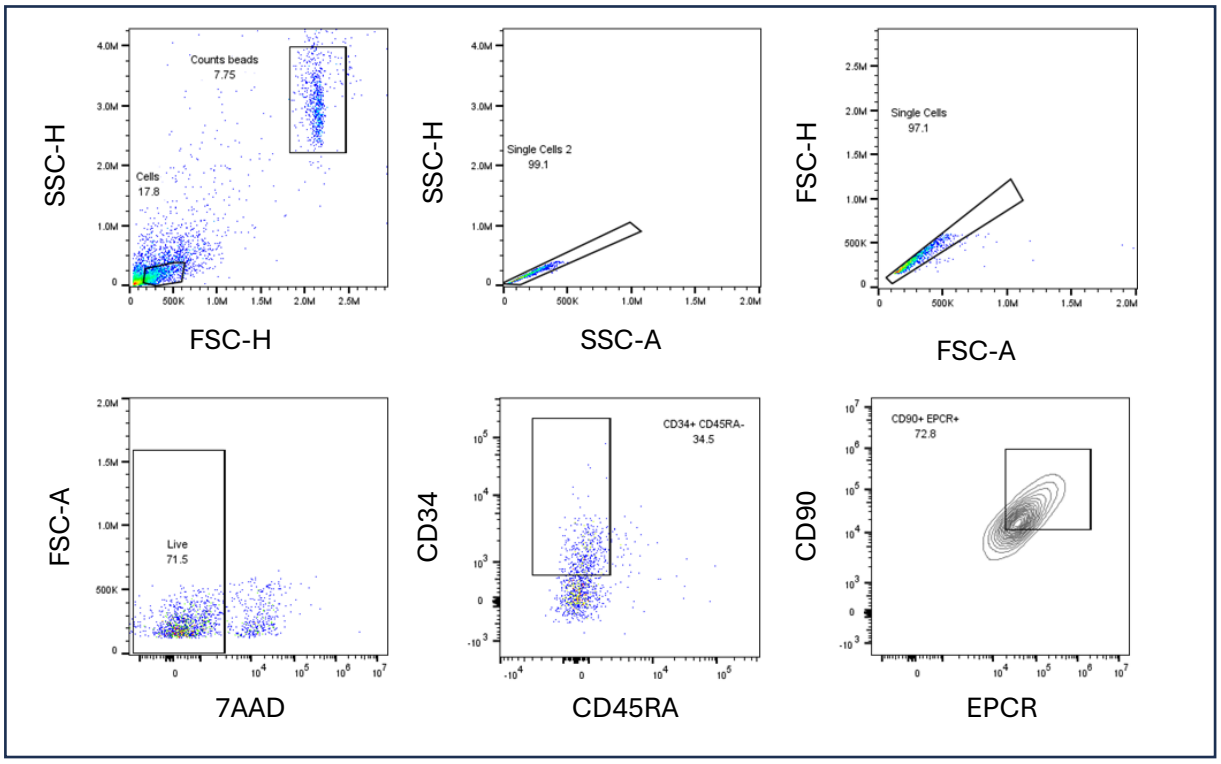

Figure 5.9 **Representative gating strategy for post-expansion human mobilised peripheral blood samples from healthy donors.** Cells are first identified, and then sequential gates are set for single cells (twice), live cells, $CD34^+CD45RA^-$, and then $CD90^+EPCR^+$ fractions.

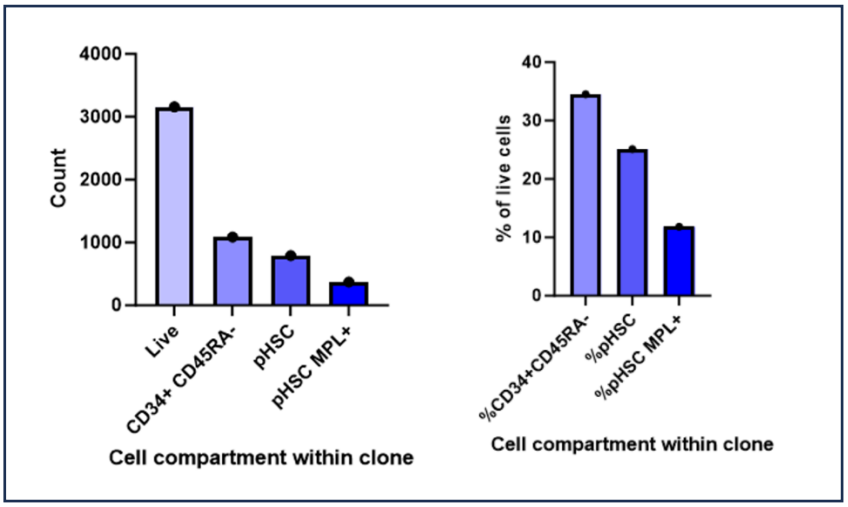

Figure 5.10 **Composition of expanded wells originating from mobilised peripheral blood show that the pHSC fraction can be subdivided based on MPL expression.** Data showing counts and percentages of various cell compartments post-expansion in 3a conditions. Of note, by day 14, pHSCs make up 25.1% of total live cells, with 47% of this fraction also being positive for MPL expression.

5.4. Differences in human MPN versus healthy 3a expanded samples

Following preliminary experiments optimising the loading density of MPN peripheral blood samples in culture, side by side cultures of MPN and healthy samples were run, to note any key differences observed between the two.

The following experiments were initiated with 10,000 $CD34^+$ samples, from either healthy donor or MPN patient peripheral blood samples. Flow cytometric analysis compared 14 day MPN 3a cultures against 14 day healthy 3a cultures (Figure 5.11). We observe a significantly increased number and percentage of $CD34^+$ cells in healthy control cells, however we also note a marked decrease in both the number of pHSCs, and the purity of the culture as determined by %pHSC in these same samples. Conversely, whilst MPN patient samples had a smaller %$CD34^+$ by the final day 14 of culture, the %pHSC was increased. Whilst we cannot draw robust conclusions and comparisons on the basis of just two samples for each condition, it is interesting that in these instances, by the end of culture, the MPN cultures had on average 1 in 2.75 $CD34^+$ cells being phenotypic HSCs, whilst in the healthy sample 1 in 7 $CD34^+$ are classified as phenotypic HSCs. As we expect the MPN samples containing a $JAK2^{V617F}$ mutation to have an HSC survival advantage, it is reassuring to see that these increased counts and percentages of phenotypic HSCs ($CD34^+CD45RA^-CD90^+EPCR^+$) at the end of the culture period agree with this.

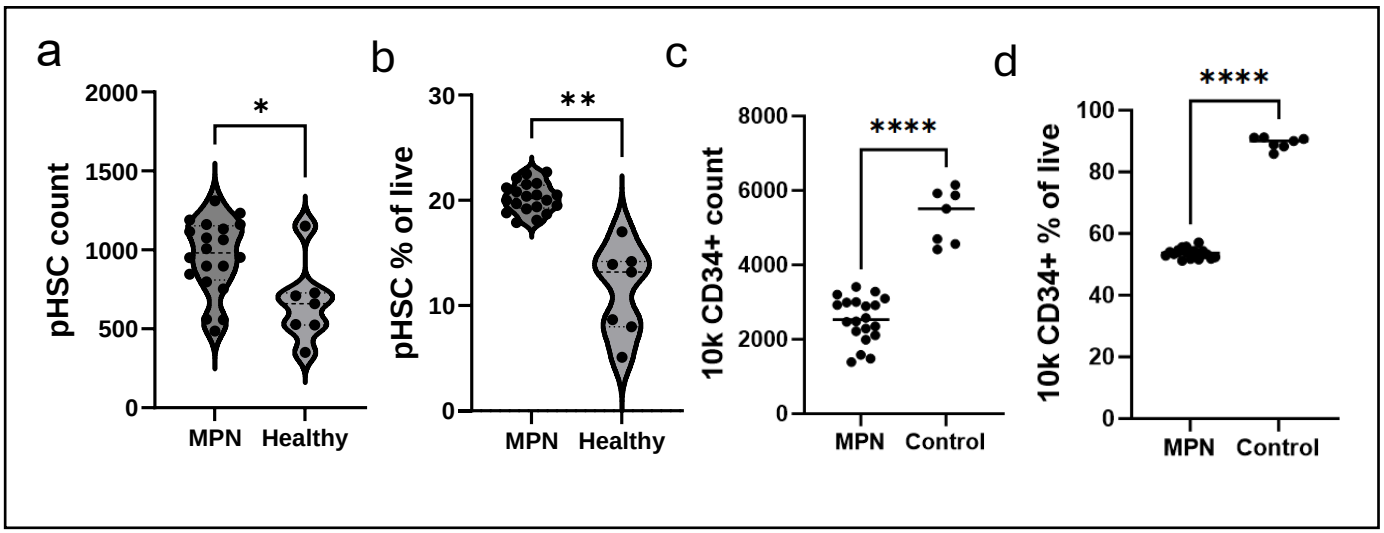

Figure 5.11 **Differences in pHSC and CD34+ counts and percentages are noted between healthy and MPN CD34$^+$ expansion cultures**. Healthy and MPN human CD34$^+$ enriched samples were expanded for 14 days in 3a media and then analysed via flow cytometry for presence of phenotypic HSCs and CD34$^+$ cells. Healthy samples had an increased number and percentage of CD34$^+$ cells, however MPN samples had an increased count and percentage of phenotypic HSCs. Unpaired T-test, * = $p \leq 0.05$, ** =$p \leq 0.01$, **** =$p \leq 0.0001$

5.5. Human mobilised peripheral blood can be successfully sorted on the BD FACSDiscoverer S8 Cell Sorter, allowing concurrent imaging of surface MPL and CD38 expression

Following Chapter 4, and the data gathered involving the fundamental roles of TPO and the TPO receptor MPL in expansion cultures, we had an ongoing interest in the mechanism of these molecules. Therefore, using a S8 FACSDiscoverer sorter with CellView capacity we aimed to see if it was possible to visualise MPL on the surface of individual CD34$^+$ cells from freshly isolated human mobilised and non-mobilised healthy peripheral blood samples, and to sort human samples robustly on this marker. Through combining robust sorting strategies previously tested over the course of this project, with the imaging capacity of this sorter, it was possible to sort the live CD34$^+$ MPL$^{+/-}$ cell fractions from both mobilised and non-mobilised samples from healthy donors with concurrent imaging of the cells (Representative gating shown in Figure 5.12). The samples were thawed and prepared for sorting as described in Methods sections 3.11 and 3.13.

In this experiment, the sorter was calibrated to image every live cell that is recorded – although data intensive, this setup enables visualisation of any cell population present within the sample, and would allow comparisons between fractions to be made. The data collected reveal that the CellView system can easily visualise surface MPL expression (Figure

5.13a,b), alongside simultaneously imaging surface CD38 expression (Figure 5.13b). Unfortunately, our standardised and tested anti-human CD34 antibody uses APC as a fluorophore which is not available for imaging on the S8 FACSDiscoverer. However, with possible panel rearrangements, and the validation of alternative staining panels in the future, the success of this experiment suggests it would be easy to visualise CD34 expression also.

The ability to directly visualise molecules on the surface of cells is a valuable tool. Single cell initiated cultures are an ideal example of this. If culture outcomes, as determined by flow cytometry, could be linked back to an individual cell, and its image, it would be possible to identify correlations between factors such as membrane distribution of certain markers and polarisation of different surface proteins, to culture outcomes. Image analysis to determine these correlations, and possibly machine learning or AI approaches in order to aid this analysis, is a growing area of interest in the field. However, the first step remains collecting these images efficiently through the use of reliable flow panels and sorter technology. This data, showing the clear visualisation of several key proteins, on the surface of a rare and valuable cell population, is a promising starting point to begin unpicking the full potential of this system.

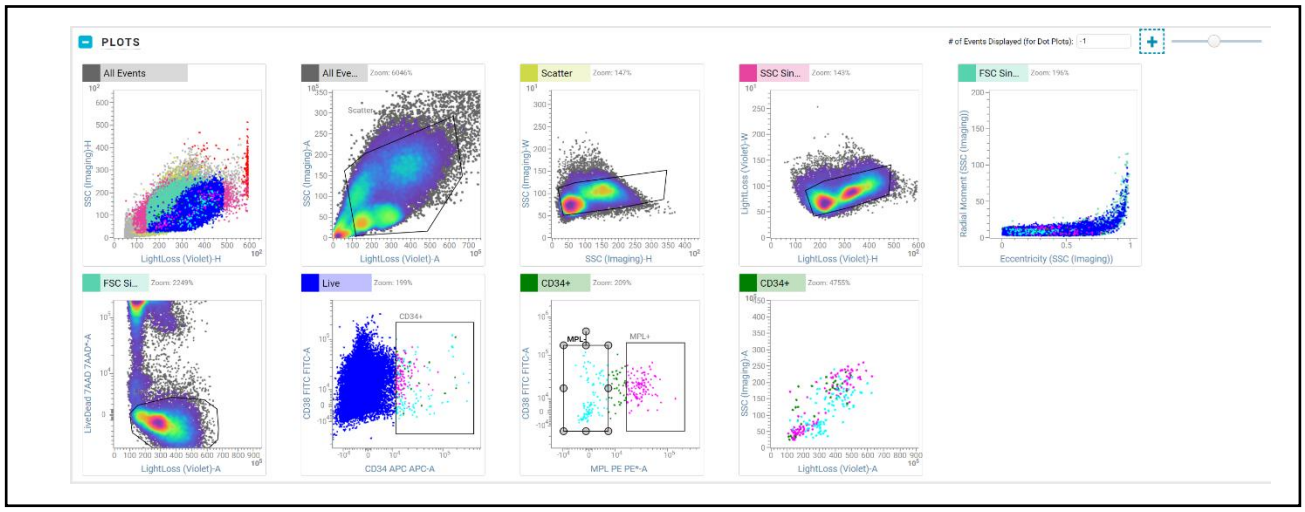

Figure 5.12 **Representative gating strategy for sorting MPL$^{+/-}$ CD34^{+} cells**. Gating strategy used on the BD FACSDiscoverer S8 cell sorter to isolate CD34^{+} MPL$^{+/-}$ fractions from mobilised healthy peripheral blood samples. Following cell gating, single cells are identified through the successive use of two gates (SSC-H vs SSC-W, and then LightLoss-H vs LightLoss-W). A live cell gate is created using 7AAD, and then our fractions of interest are isolated by CD34$^{+,}$ followed finally by MPL$^{+/-}$ gates.

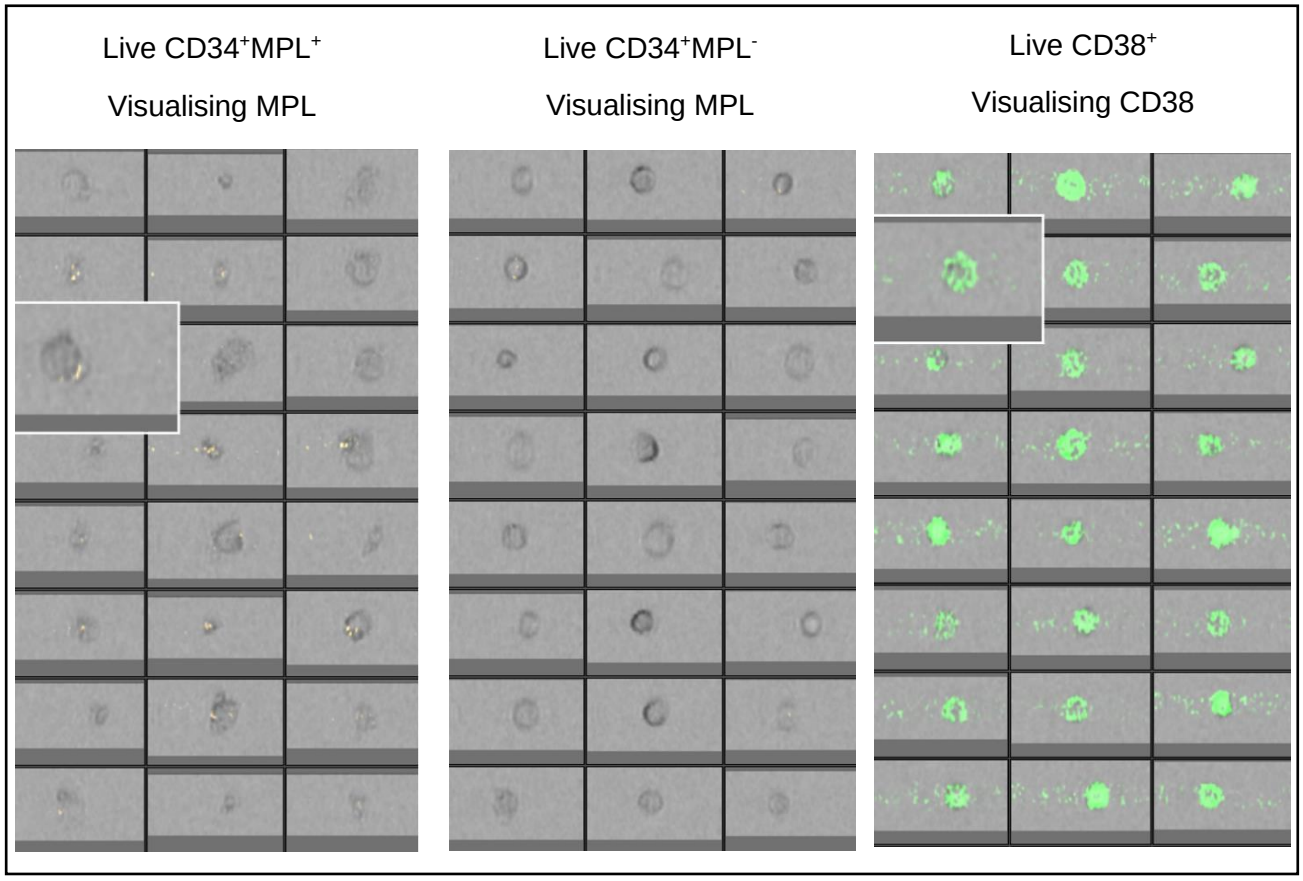

Figure 5.13 **Example images from the CellView technology on the BD FACSDiscoverer**. a) CD34 APC^{+} MPL PE^{+} fraction, with PE fluorescence being visualised. b) CD34^{+} MPL^{-} fraction, again with PE expression visualised. b) CD38 FITC^{+} fraction, with FITC expression being visualised.

Regarding additional data relating to MPL that can be extracted from this initial sort data, as shown in Figure 5.12, it is clear that MPL expression subdivides the CD34^{+} population within healthy mobilised peripheral blood samples, much like it does the ESLAM population in mice. Generally this division is close to 50:50 between the two fractions (Figure 5.14), but with slight variations noted between individuals. It is also important to consider that negligible MPL expression is observed within the CD34^{-} compartment in healthy mobilised samples, and the MPL expression within this fraction is significantly lower than in the CD34^{+} fraction within the same sample (Figure 5.14).

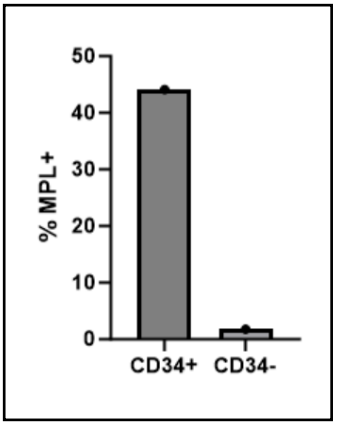

Figure 5.14 **Differences in MPL expression between CD34$^+$ and CD34$^-$ fractions within mobilised peripheral blood samples.** We note a significant decrease in the percentage of MPL positive cells within the CD34$^-$ fraction compared to the CD34$^+$ fraction in freshly isolated peripheral blood samples. Data collected from S8 FACSDiscoverer, gates shown in Figure 5.12.

5.6. MPL expression differences between healthy and MPN patient samples

Following successful sorting of CD34$^+$MPL$^{+/-}$ fractions from mobilised peripheral blood samples we aimed to quantify differences in MPL surface expression between the two populations, to ensure we were in fact sorting the correct populations. In order to do this, Quantibrite PE beads were used (Methods section 3.17). In order to quantify MPL molecules using these beads, they are ran on the cytometer following the samples and contain 4 populations of beads, each with a known number of surface PE molecules. These 4 populations are easily visible on a PE plot (Figure 5.15a), and can be gated on, and MFI recorded. Through plotting MFI of each population versus the number of surface molecules of PE, it is possible to generate a standard curve to plot other populations of interest onto (Figure 5.15b). This allows rapid quantification of the number of surface molecules, in this case marked by a PE antibody.

These data were collected during sorting of peripheral blood samples from both healthy and MPN donors, used to initialise expansion cultures. In these instances, myelofibrosis (MF) patient samples were used – MF being one of the three diseases that fall under the MPN category (Nangalia et al., 2017).

This technique verifies that both CD34$^+$ MPL$^{+/-}$, and live MPL$^{+/-}$ fractions in both healthy and MPN patient sorted samples are in fact correctly high and low for MPL (Figure 5.15 c,d). Also interesting is the significantly greater number of surface MPL molecules observed on the MPL$^+$ fractions from healthy mobilised peripheral blood samples than MF samples. Further analysis performed on the flow cytometric data gathered from these sorts reveal key differences in CD34$^+$ and MPL$^+$ percentages between these samples (Figure 5.15e,f). In

terms of $CD34^+$ percentages within the fresh populations, healthy mobilised samples have a frequency of $CD34^+$ cells averaging around 3.6% of live cells. On the other hand, MF samples have a higher variation in $CD34^+$ composition, which likely correlates with disease burden and severity (Figure 5.15e). This variation is a confounding factor which makes the *in vitro* expansion of these samples particularly challenging, as although patient and treatment information can somewhat predict the CD34 content, this remains highly variable between individuals, and even between the same individual at different time points. Regarding percentage of lives cells positive for MPL, we also note significant differences in fresh peripheral blood samples between healthy donors and MF patients, however these differences are lost when looking within the live $CD34^+$ population (Figure 5.15f).

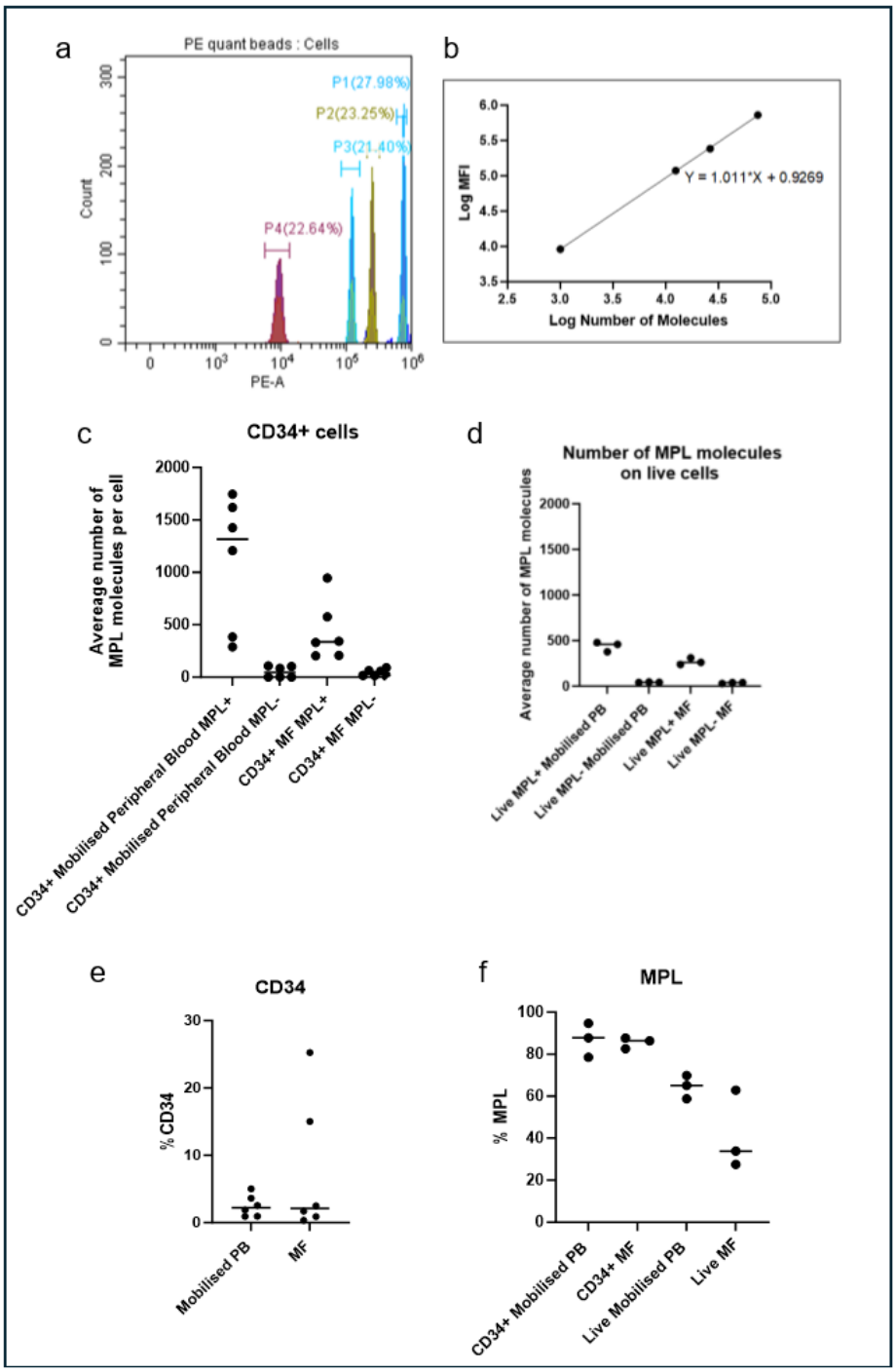

Figure 5.15 **MPL expression levels differ between healthy and MF samples**. a) Representative gating used to identify the 4 peaks, correlating to a known number of molecules of the protein per cell, using BD Quantibrite PE beads (Methods section 3.17). b) Plotting the MFI of each selected peak (a) versus the known number of molecules present on each population allows generation of a standard curve. c) Quantification of the number of MPL molecules on the surface within the $CD34^+$ fraction of several different sample types. d) MPL molecule quantification on the surface on cells within the live cell fraction of several sample types. e) Differences between healthy mobilised PB and MF PB samples in percentage of live cells $CD34^+$ at point of sorting. f) Differences in percentage of live cells MPL^+ between healthy and MF PB samples.

5.7. Success of MPN PB culture is dependent on MPL expression at point of culture initiation

Following the sorting of $CD34^+$ $MPL^{+/-}$ fractions, and the quantification of MPL levels within these populations, further investigations were conducted into the functional relevance of the presence, or lack, of surface MPL on the $CD34^+$ cells used to initiate the cultures. Before the development of the 3a expansion protocol supplemented with Flt3L, experiments such as this would have been impossible to complete – highlighting again the benefit of these protocols to the field of haematology. In order to investigate the role of MPL expression on the *in vitro* expansion of HSCs, and simultaneously further test the expansion capacity of patient samples, MPN patient samples were taken and sorted to isolate the $CD34^+$ fraction, either positive or negative for MPL.

These samples were stained for FACS as described in Methods, and were sorted on the BD FACSAria, using gating shown in Figure 5.16. These samples were then expanded in 3a conditions for 14 days, with flow cytometric analysis on day 7 (10% of well contents) and day 14 (entire contents of well) using BD Quantibrite™ PE Phycoerythrin Fluorescence Quantitation Kit (Cat.No.340495) to quantify surface MPL expression in terms of the number of MPL molecules per cell.

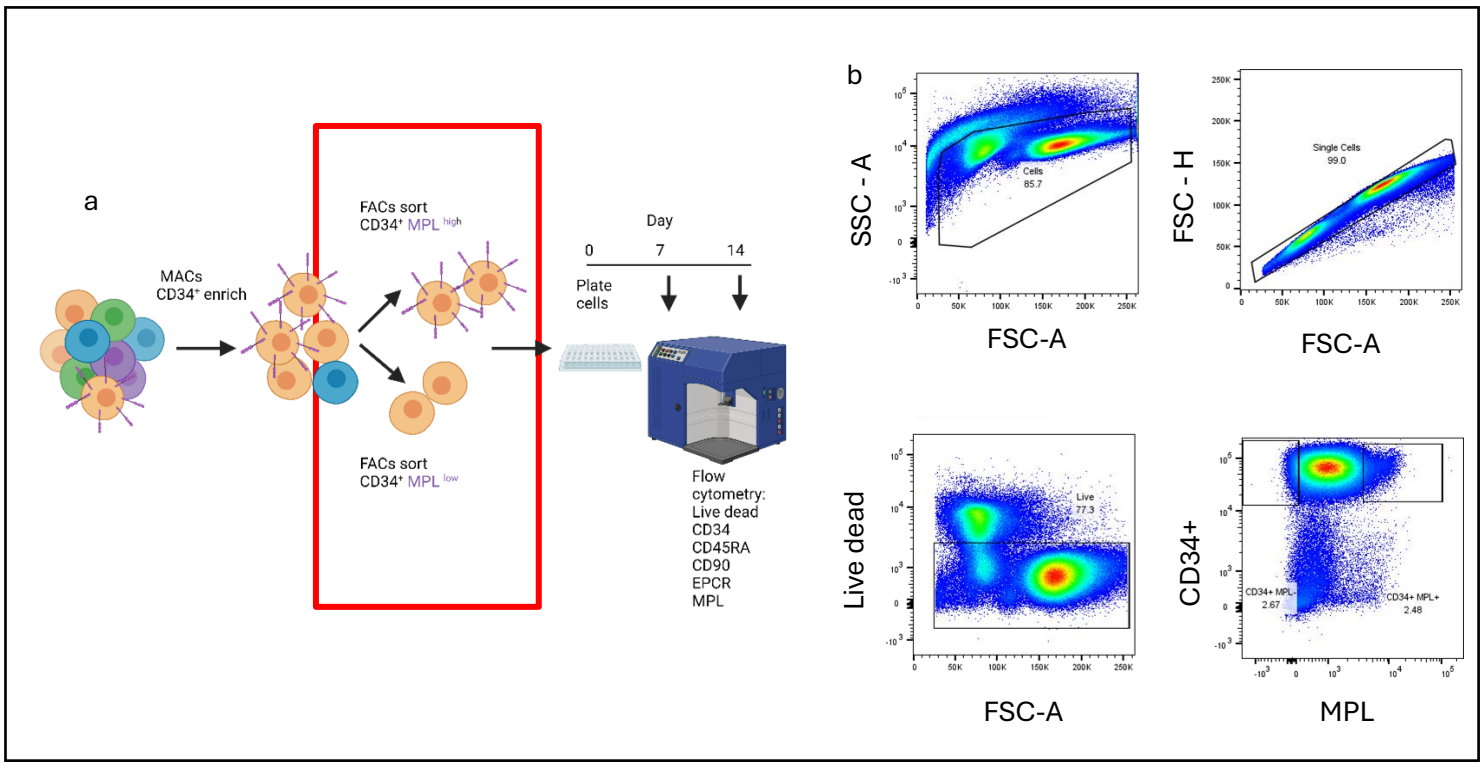

Figure 5.16 **Experimental outline of CD34^{+} MPL$^{+/-}$ 3a expansion culture setup**. a) Schematic depicting experimental protocol. Following CD34 enrichment, MPN patient PB cells were sorted for CD34^{+} MPL$^{+/-}$ fractions. These cells were then plated at a density of 10,000 cells per well in a 96-well CELLBIND plate and cultured for 14 days. 10% of each culture on day 7, and the entire culture at day 14, was taken for flow cytometric analysis to determine phenotypic HSC content. b) Gating strategy for the sort used to isolate CD34^{+} MPL$^{+/-}$ fractions.

As shown in Figure 5.17, by day 7 we see a slight increase in the number of MPL molecules per cell in the initially positive, compared to the initially negative MPL samples within the expanded CD34^{+} population. This difference becomes significant when looking within the pHSC compartment. This difference in expression is further increased by day 14 (Figure 5.18), however this difference is exacerbated due to the initially MPL negative fraction having collapsed in culture by this point (Figure 5.18b) – therefore significantly skewing our data. As a result, we decided to focus on tracking the changes in MPL expression within the MPL positive sorted fraction over time (Figure 5.19), where culture associated upregulations of surface MPL expression are observed. Within the CD34^{+} compartment, despite a consistent upregulation of surface MPL over the culture period, expression levels remain lower than those of expanded pHSCs. pHSC MPL expression is highest by day 7, before marginally dropping off by day 14. Yet despite this, MPL expression within the pHSC compartment remains slightly higher than that of the bulk CD34^{+} fraction for the duration of the culture period.

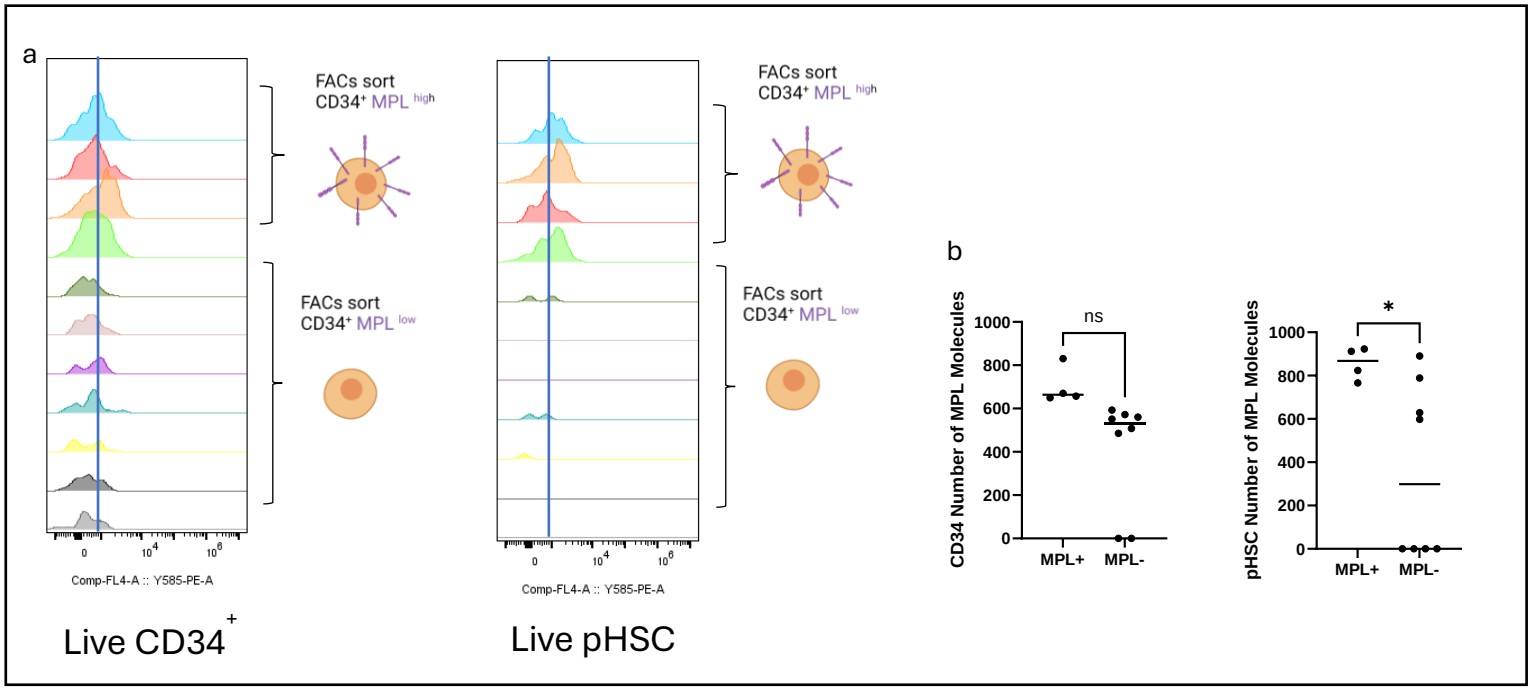

Figure 5.17 **Day 7 surface MPL quantification on expanded MPN patient peripheral blood samples.** a) Each coloured shape on each graph represents MPL surface expression for an individual expanded sample from an individual well when analysed on day 7 of expansion. Comparison of MPL expression levels in the $CD34^+$ and pHSC compartments, between initially MPL^+ and MPL^- sorted fractions. b) Comparison on surface MPL expression between samples initially MPL positive / negative after 7 days. Unpaired T-test ns = $p>0.05$, * = $p \leq 0.05$

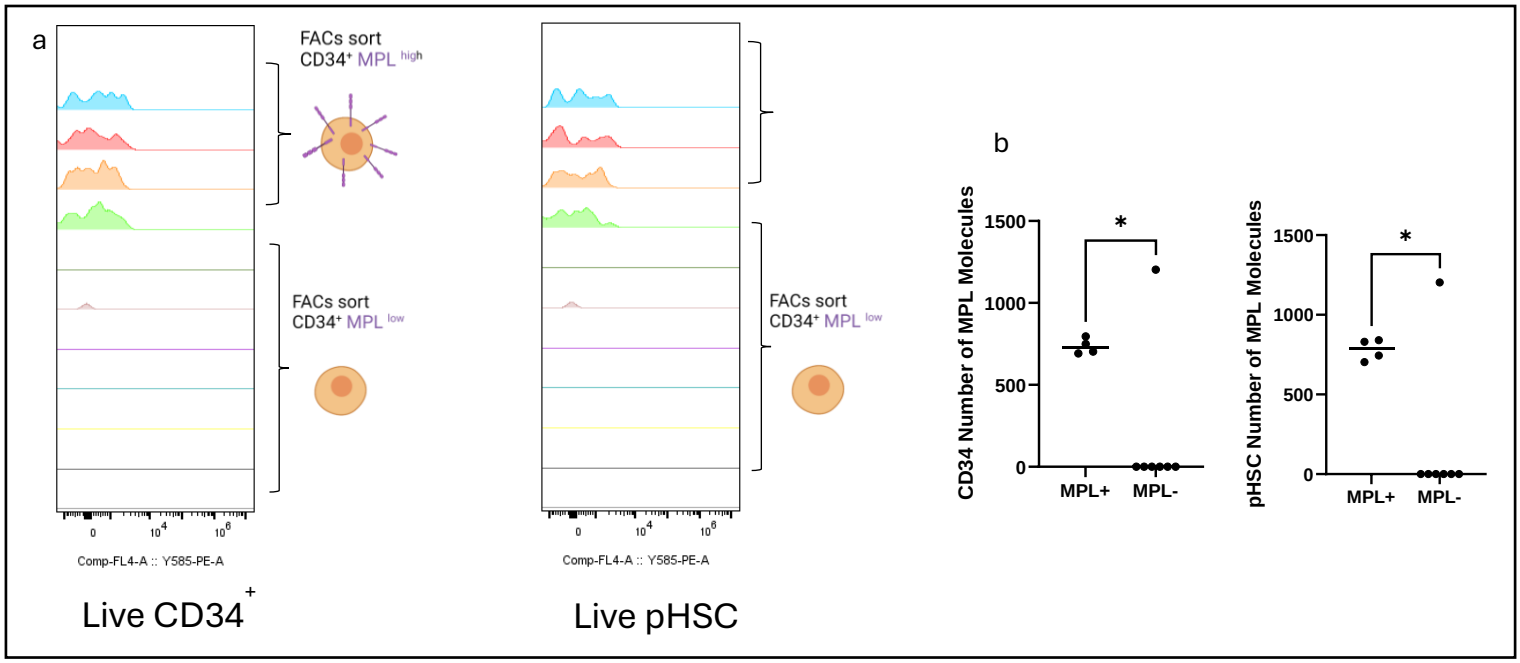

Figure 5.18 **Day 14 surface MPL quantification on expanded MPN patient peripheral blood samples**. a) Each coloured outline represents MPL surface expression for an individual expanded sample on day 14 of expansion. These samples are divided into initially MPL^+ and MPL^- sorted fractions. b) Comparison on surface MPN expression between samples initially MPL positive / negative after 14 days. Unpaired T test, * = $p \leq 0.05$,

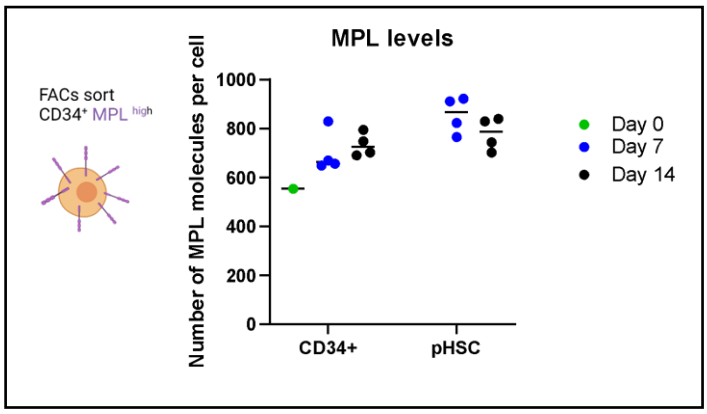

Figure 5.19 **Tracking of surface MPL expression within MPN patient samples over 14 days of in vitro culture in 3a media**. Through combining MPL quantification experiments performed on day 0 when the samples were initially sorted, with quantification performed on day 7 and day 14 of culture, it is possible to track MPL expression changes over time, in this case within the MPL positive sorted fraction.

As previously discussed, the $CD34^{+}MPL^{-}$ sorted fractions performed poorly in culture, with almost all wells entirely collapsing by day 14, whilst the MPL positive fractions expanded well (Figure 5.20). This was determined by flow cytometric analysis at day 14, which revealed significantly higher counts and frequencies of $CD34^{+}$ cells and pHSCs within cultures initiated by MPL positive cells.

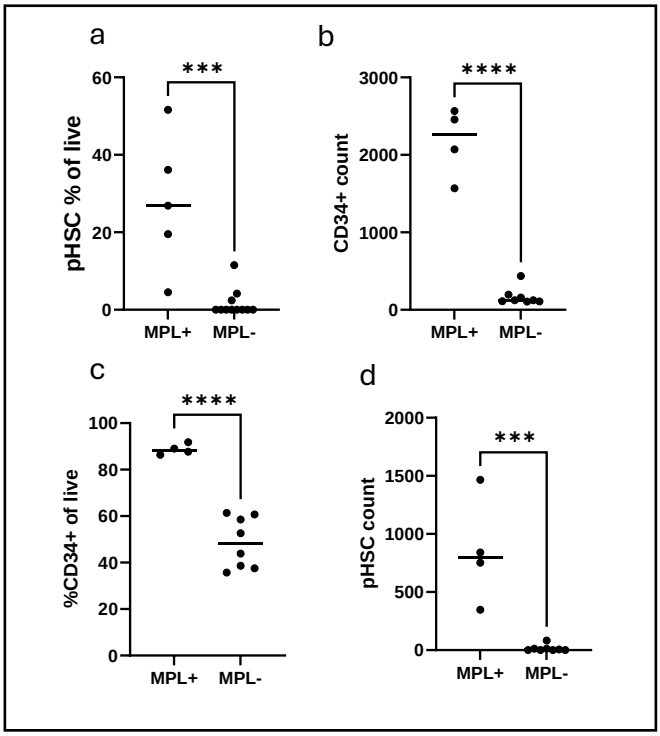

Figure 5.20 **Final Day 14 flow cytometric analysis of expanded non-mobilised peripheral blood $CD34^{+}$ $MPL^{+/-}$ cells from MPN patients**. Data reveals a much higher expansion success rate in MPL^{+} sorted fractions, in terms of both $CD34^{+}$ and pHSC counts and percentages. Unpaired T-test, *** =p ≤ 0.001, **** =p ≤ 0.0001, Line shows mean

These striking differences are especially noteworthy due to the opposite effect observed as a result of the presence of MPL on the starting material in mouse cultures. This data also offers MPL as an example of a potentially useful marker to be combined with sorting strategies to refine the starting material for 3a cultures.

5.8. Chapter summary

In conclusion, in this chapter we established the use of the novel 3a expansion culture system at the University of York, and performed several direct comparisons to the previous gold-standard culturing system, StemSpan. Data gathered highlight the far greater counts and frequencies of phenotypic HSCs achieved at the end point of 3a expansion cultures over StemSpan cultures over 14 days. Further data also highlight the benefits of supplementing 3a expansion media with Flt3L in order to improve pHSC output from cultures, in both TPO or butyzamide containing cultures. This comparison is key as although butyzamide is the standard TPO-receptor agonist utilised in 3a media, TPO is arguably the more clinically relevant molecule, and the focus on TPO and its receptor MPL is continued throughout this thesis.

Following the establishment of this protocol, and refining the setup and maintenance of these cultures to result in reliable outputs when using cord blood samples, a focus was set to look at the role of mechanical regulation as a result of biomechanical stimuli upon the cultures. Two key approaches were used to highlight the importance of the physical environment on the expansion of human HSCs, the first compared culturing human $CD34^+$ cord blood cells in standard plastic CELLBIND plates to the use of 2d or 3d gels as a substrate. Data collected post-expansion reveal that 2d gels provide a significant benefit in terms of counts and frequencies of pHSCs over plastic, whilst 3d gels did not provide any statistically significant improvement. The other biophysical screen performed on these expansion cultures was the replacement of Soluplus in the media with alternative biocompatible polymers: PVP, Dextran, and a labelled FITC Dextran variant. Although PVP did not induce any difference in HSC output post-culture, both unlabelled Dextran, and FITC labelled Dextran resulted in significantly poorer performing clones. Although the specific role of Soluplus is not well understood in these cultures, it is thought it may have a role in presenting cytokines to the expanding cells. Despite the lack of a defined role in the expansion culture system, it is clear that replacing Soluplus with similar polymers results in large downstream effects regarding culture outputs, and is therefore invaluable to the system. Together, these two experiments highlight the dependence of HSCs on their

physical environment to regulate their behaviour and self-renewal, and the potential to further refine expansion by mechanical manipulation of the HSC *in vitro* niche.

Following this, we aimed to refine the 3a expansion system to enable expansion of human HSCs from sources other than cord blood – particularly peripheral blood samples. We managed to achieve the first expansion of MPN patient $CD34^+$ cells *in vitro* with the 3a expansion system, and the greatest expansion of MPN patient samples *in vitro* to date. We then looked towards healthy peripheral blood samples, historically known to be harder to expand due to lower levels of $CD34^+$ cells present in the sample. However, this can be somewhat mitigated through the use of mobilised samples, where stimuli given to the donors before the sample is taken, such as G-CSF, induce the temporary movement of HSCs from the bone marrow into circulation . Using mobilised samples, we were able to expand healthy peripheral blood HSCs *in vitro* in 3a expansion culture conditions.

Having unlocked the capacity to expand both healthy and MPN patient peripheral blood HSCs, we could compare these samples directly to identify differences between the two in expansion conditions. Within MPN samples, higher pHSC counts and percentages were noted, whilst also exhibiting lower $CD34^+$ counts and percentages at the end of the 14 day culture period. This results in a significant difference in the frequencies of HSCs within the $CD34^+$ compartment at the end of culture between healthy and diseased samples, with MPN patient samples having 1 in 2.75 $CD34^+$ cells being pHSCs at the end of culture, compared to 1 in 7 in healthy samples. This reflects the HSC self-renewal advantage observed in these patients, particularly those presenting with a $JAK2^{V617F}$ mutation, which all of the tested patient samples contained.

Investigations then continued into the role of the TPO receptor MPL on the function of human $CD34^+$ cells and HSCs. Firstly, it was necessary to sort the $CD34^+$ $MPL^{+/-}$ fractions, which was achieved using the S8 FACSDiscoverer, allowing concurrent imaging of surface MPL and CD38 on the sorted cells. Furthermore, MPL surface quantification was used to validate that the $MPL^{+/-}$ fractions did in fact present with higher and lower levels of MPL molecules per cell. Data gathered during these sorts reveal that MPL expression subdivides the human $CD34^+$ population, and that the MPL expression is markedly higher in $CD34^+$ than $CD34^-$ fractions.

Additionally, quantification of surface MPL levels on cells between healthy and MPN patient samples reveal key differences in MPL expression between the two. Most interestingly, we

see that MPL surface expression is notably higher on healthy peripheral blood samples, than patient samples – especially within the live, $CD34^+$ fraction.

Finally, utilising newly validated, robust expansion strategies for MPN patient samples, it is possible to perform experiments previously impossible to undertake on this cell type. A fitting example of this forms the final part of this chapter, where 3a expansion culture of patient samples, combined with our ability to robustly sort $CD34^+$ $MPL^{+/-}$ fractions and quantify MPL molecules per cell, allows us to determine the impact of the presence of MPL on $CD34^+$ cells at the point of culture initiation on expansion outcomes. We reveal that $CD34^+$ MPL^+ cells significantly outperform their $CD34^+MPL^-$ counterparts, with the $CD34^+MPL^-$ initated cultures collapsing before reaching the final day 14 timepoint.

Overall, this chapter details the first instances of expansion on this scale for these notoriously hard to culture samples, and identifies key differences in expansion capacity between healthy and MPN patient peripheral blood $CD34^+$ cells. Finally, we demonstrate the benefit of being able to expand these sample types, identifying MPL as a potentially valuable marker to add to the sorting panel used to isolate cells to initiate these 3a cultures, in order to improve efficiency and culture output.

6. An investigation into the role of TPO and TPO mimetics in human 3a expansion cultures

Thrombopoietin (TPO) is a key haematopoietic cytokine widely used in both mouse and human expansion culture systems to encourage HSC self-renewal and survival *in vitro* (Tsutsumi et al., 2023). Knockout models of both TPO and its receptor MPL note a significant impairment of HSC function and generate HSC populations incapable of reconstituting a mouse in a transplantation setting (Kimura et al., 1998). Additionally, mutations in MPL result in decreased numbers of haematopoietic stem and progenitor cells (HSPCs), and are associated with the development of bone marrow failure disorders (de Graaf and Metcalf, 2011, Ballmaier et al., 2003).

TPO, alongside SCF, have become the basis of both human and mouse HSC expansion cultures and the basis of their use is founded on our understanding of the FL stage of development, where HSCs are maximally expanding (Wilkinson et al., 2019). However, in the most recent iteration of human HSC expansion protocols, published by Sakurai et al. in 2023, TPO and SCF are replaced by chemical mimetics in order to achieve a more consistent and animal-free expansion culture system. In the case of TPO, butyzamide is used as an MPL agonist in these conditions, and supports maximal expansion of human HSCs over the course of *in vitro* expansion. This discovery opened the door for us to ask a range of questions about the functional role of TPO in 3a expansion cultures, and allows us to consider more widely what differs in the cells response to TPO versus alternative TPO mimetics. In this chapter, this thesis aimed to decipher the differences in TPO receptor internalisation, and downstream signalling induced by TPO and alternative mimetics. Using a range of techniques ranging from cellular barcoding, to phosphoflow, and phosphoprotomics this chapter identifies key differences which allow a greater understanding of these molecules, and has the potential to aid further refinement of expansion culture systems.

Furthermore, alongside comparing TPO to butyzamide; eltrombopag, lusutrombopag, and romiplostim were also included in these studies, all of which are clinically utilised MPL agonists used to treat thrombocytopenia (Cheng et al., 2012, Bussel et al., 2021, Yoshiji et al., 2023). With clinically minded researchers interested in studying these more clinically-relevant alternatives, verifying the ability of these molecules to support HSC expansion in the 3a system, and unpicking their mechanism of action by quantifying the downstream signalling induced via the TPO receptor following stimulation, this study aimed to broaden the applicability of the 3a expansion system.

6.1. Butyzamide can be replaced by TPO in in vitro cultures

Initial experiments aimed to firstly determine if TPO would support the *in vitro* expansion of human cord blood CD34+ cells, and to directly compare the performance of TPO supplemented 3a cultures to standard butyzamide supplemented 3a cultures.

Human samples were thawed, counted, and loaded 10,000 cells per well as described in Methods section 3.11. Each well contained 200µL of 3a expansion media containing either butyzamide, as was the published MPL-agonist used in this protocol (Sakurai et al., 2023), or a matched concentration of TPO in place of butyzamide. The 3a cultures were maintained for 14 days with media changes every 2-3 days, before being analysed by flow cytometry at day 14 to determine culture success as determined by $CD34^+$ and phenotypic HSC (pHSC – $CD34^+CD45RA^-EPCR^+CD90^+$) counts and percentages. Example gates for post-expansion analysis are shown in Figure 6.1. The flow cytometry data collected on the final day of culture reveal that TPO and butyzamide do perform comparably *in vitro,* with no significant differences between the two conditions in terms of pHSC counts, $CD34^+$ percentages of live cells, and pHSC percentages of live cells. The only significant differences were observed in $CD34^+$ counts, although these were slight (Figure 6.2). This data promisingly reveals the capacity of MPL-agonists other than butyzamide to support the functional expansion of HSCs *in vitro*.

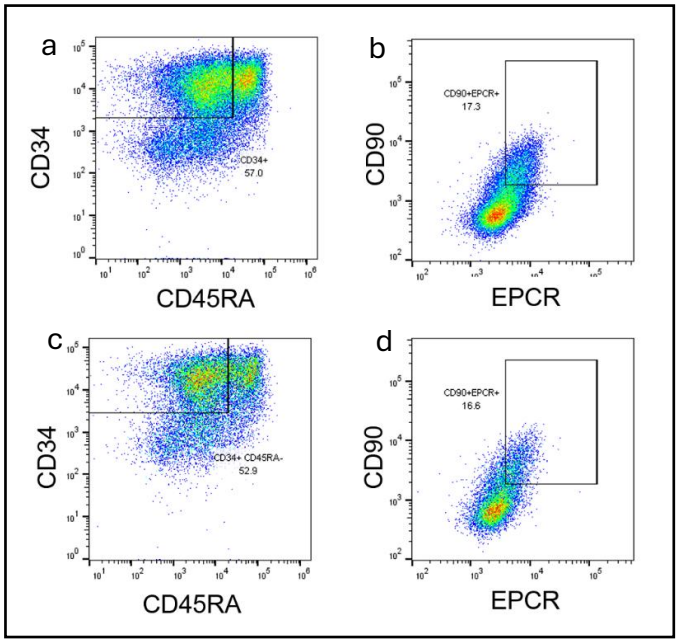

Figure 6.1 **Representative gating for post expansion phenotypic HSCs following either standard 3a or TPO supplemented 3a culture.** Following gating for cells, single cells, and live cells (not shown), sequential gates are set for the CD34+ CD45RA-, and EPCR+ CD90+ fractions to identify the phenotypic HSCs. Conditions compared are standard 3a media supplemented with butyzamide (a,b), and 3a media supplemented with TPO (c,d).

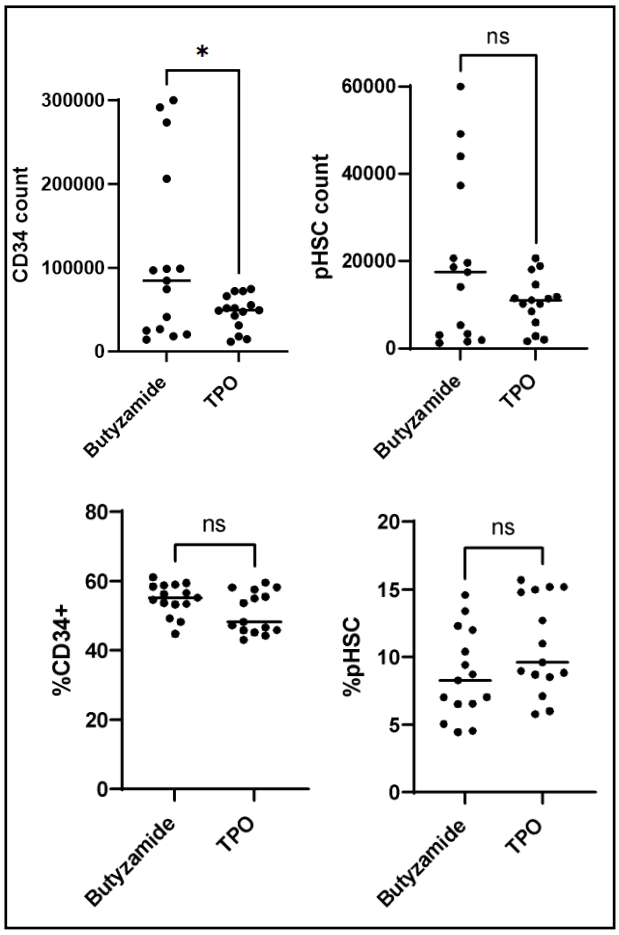

Figure 6.2 **Butyzamide and TPO support human HSC expansion over 14 days in 3a expansion cultures**. Day 14 flow cytometric analysis of 3a expansion cultures, initiated with 10,000 CD34+ cord blood cells. Data shows differences in $CD34^+$ and pHSC content in expanded clones between standard Butyzamide supplemented cultures, and TPO supplemented cultures. Unpaired T-test, ns = $p>0.05$, * = $p \leq 0.05$,

6.2. Butyzamide can be functionally replaced by alternative TPO receptor agonists

In order to further understand and refine the 3a expansion culture system, we then attempted to replace the TPO receptor (MPL) agonist butyzamide with alternative agonists, in order to find a potentially more clinically relevant replacement, and to test the reliance of the cultures on butyzamide specifically. In all of these cultures, the 3a conditions were supplemented with Flt3L (10ng/mL) and MTG (100μM)

We first tested a variety of MPL agonists (eltrombopag, lusutrombopag, romiplostim, and TPO), each at 3 concentrations (concentrations specified in Methods 3.14) to compare expansion performance against traditional 3a cultures. We also included a StemSpan control well, in order to have a comparison to the previous gold-standard protocol for expanding human HSCs. For all cultures, cord blood $CD34^+$ enriched cells were used – these samples

were thawed and seeded 10,000 cells per well of a 96-well CELLBIND plate, and cultured in either 3a conditions or StemSpan conditions for 14 days as shown in Methods sections 3.11 / 3.14 / 3.15. The cultures were then analysed via flow cytometry on day 14 to determine pHSC content, using panels and gating shown in Figure 6.3. The flow cytometric data taken on day 14 reassuringly agrees with previous experiments, showing that StemSpan conditions result in significantly higher total live cell numbers by the end of culture, but vastly lower numbers of pHSCs (Figure 6.4). When analysing pHSC count across the range of tested molecules, a few conditions stand out as having comparable or even improved numbers of HSCs in the cultures after 14 days. These conditions are lusutrombopag Low and Mid concentrations (10nM and 100nM), and TPO Low (10ng/mL). Lusutrombopag is of particular interest and was selected initially for this screen as it is an FDA approved drug, currently used clinically to treat thrombocytopenia, making it a promising butyzamide replacement to scientists more interested in the clinical relevancy of the system**.**

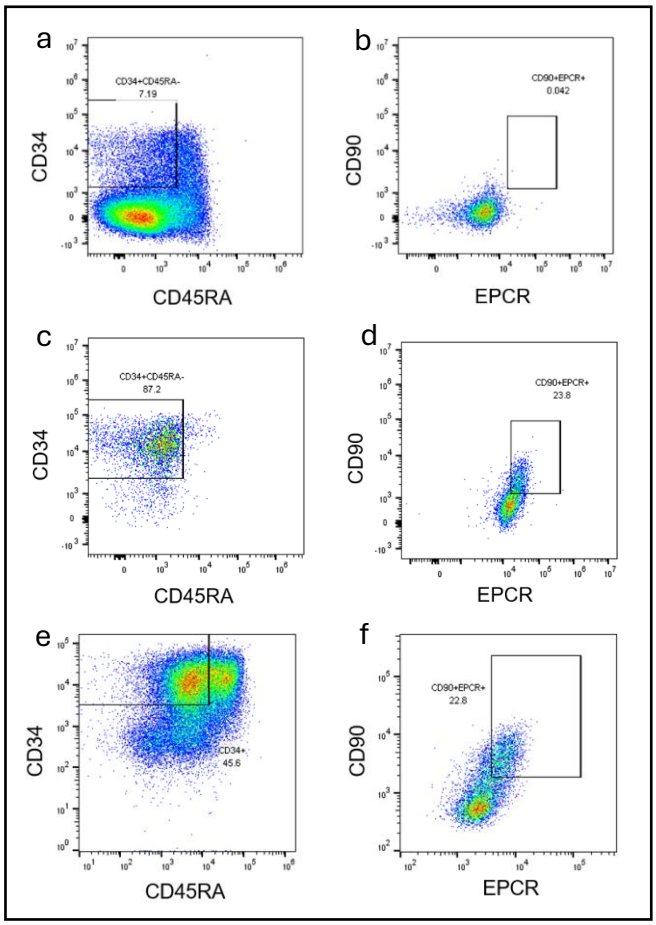

Figure 6.3 **Stemspan, 3a, and Lusutrombopag 3a post-expansion gating for phenotypic HSCs**. Following gating for cells, single cells, and live cells (not shown), sequential gates are set for the CD34+ CD45RA-, and EPCR+ CD90+ fractions to identify the phenotypic HSCs. Conditions compared are StemSpan (a,b), standard 3a media supplemented with butyzamide (c, d), 3a media supplemented with lusutrombopag (e, f)

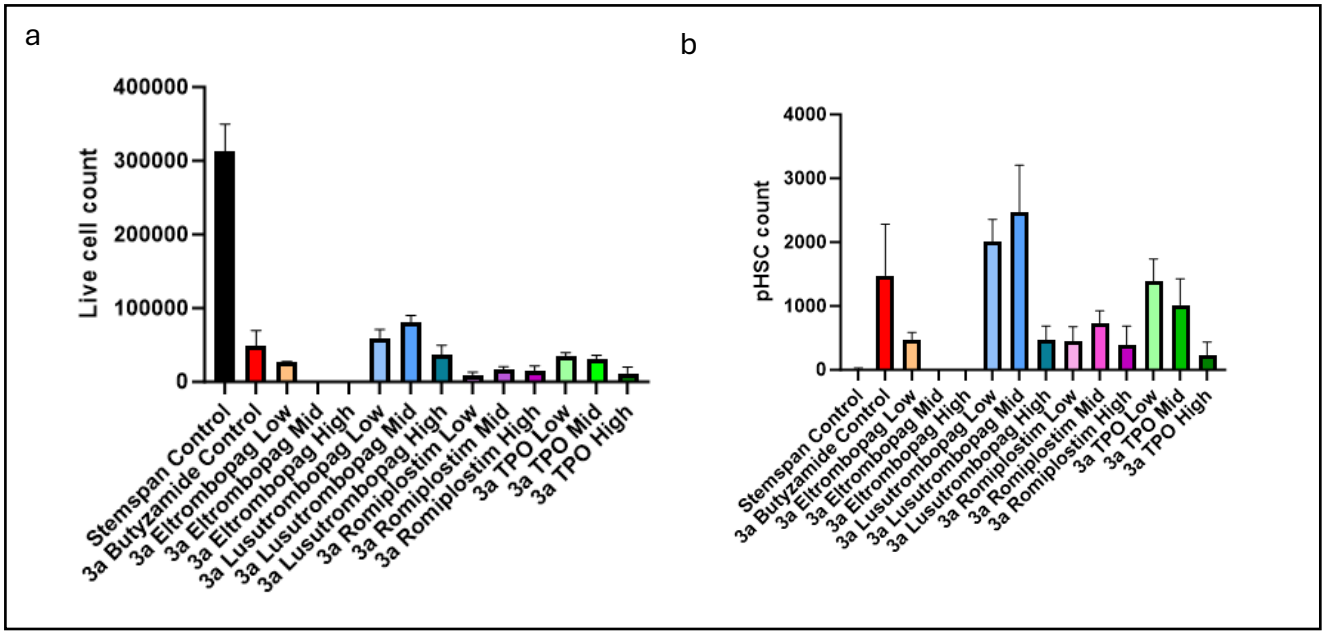

Figure 6.4 **Comparison of live cell and pHSC counts achieved by TPO and TPO mimetics in 3a expansion cultures**. Day 14 flow cytometric analysis of modified 3a expansion cultures and Stemspan cultures. pHSC is defined by $CD34^+$ $CD45RA^-$ $EPCR^+$ $CD90^+$. Error bars show standard deviation.

We additionally can break down the composition of each of these wells, from each condition, considering the percentage of the cells in the well that are $CD34^+CD45RA^-$, and pHSCs ($CD34^+CD45RA^-CD90^+EPCR^+$). Again, it is clear that the conditions of interest (lusutrombopag Low and Mid, and TPO Low) present with similar well content breakdowns to that of the butyzamide control (Figure 6.5). Whilst other conditions also have similar percentage breakdowns to that of butyzamide, the pHSC counts for these conditions (Figure 6.4) are markedly lower. This is important to consider as for omics techniques, and for clinical procedures such as HSC transplantations, transplant efficiency and likelihood of success are directly correlated to HSC number. Importantly, this data again highlights the improvements the 3a conditions have made to the *in vitro* expansion of HSCs compared to the previous gold-standard StemSpan, with StemSpan showing a much lower frequency of pHSCs and $CD34^+CD45RA^-$ cells.

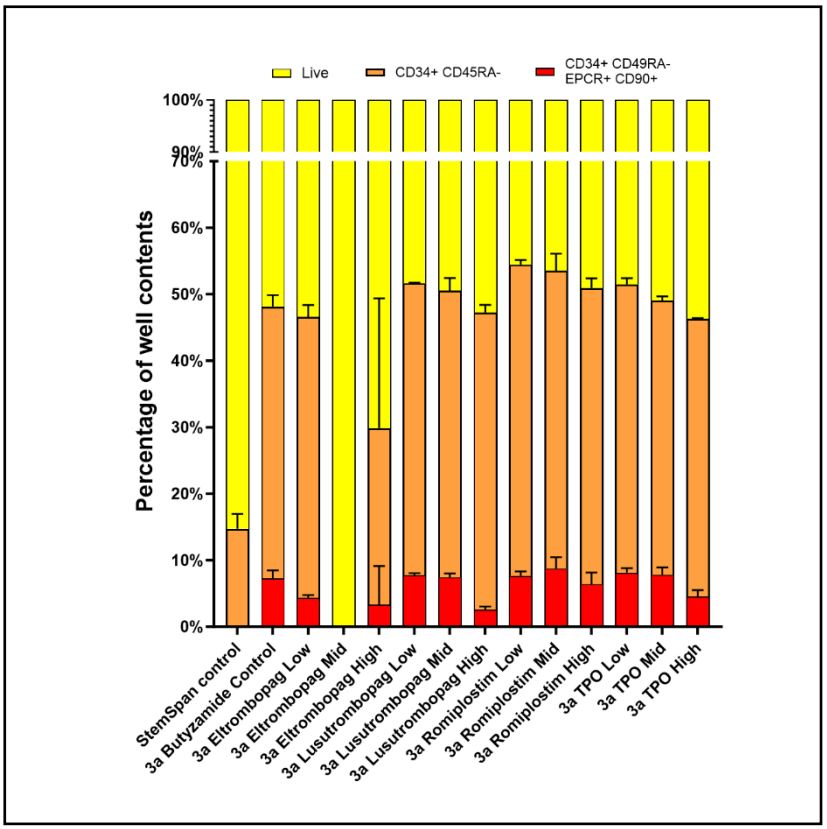

Figure 6.5 **Comparison of well contents following 14 days of 3a expansion using TPO or TPO mimetics**. Flow cytometric analysis performed on day 14 of expansion. Well composition showing percentages of live cells known to be pHSCs ($CD34^+$ $CD45RA^-$ $EPCR^+$ $CD90^+$) and percentage of live cells $CD34^+CD45RA^-$ within the wells. Each column represents the mean of 3 individual wells. Error bars show standard deviation.

Following on from the initial test of these conditions, we repeated this experiment with a focus on the lusutrombopag mid (100nM/mL) and TPO low (10ng/mL) concentrations to firm up the validity of these as alternatives. With the known donor-to-donor variability of human cord samples, it is vital to test any improvement to the 3a culture system with several independent samples. These cultures were also supplemented with Flt3L, theorised to support expansion of human HSCs from sources other than cord blood. The data gathered from a repeat of these conditions with a new donor sample show that butyzamide, TPO, and lusutrombopag are all comparable in the extent of HSC expansion they support *in vitro*, with minimal differences in terms of $CD34^+$ and pHSC counts and percentages post-culture (Figure 6.6). This is reassuring and implies that butyzamide is able to be successfully replaced. In terms of $CD34^+$ cell counts at the end of culture however, we do see lower counts in TPO low media, however as a change in the percentage of live cells, this is minimal. Regarding pHSC counts, again the pHSC count in the TPO Low condition is slightly lower, but again as a percentage of live cells, this is insignificantly different to butyzamide, and is in fact improved compared to the %pHSC of lusutrombopag. An important take away

from this experiment is that both lusutrombopag mid and TPO low concentrations are able to successfully expand human cord blood HSCs *in vitro*, to comparable levels to the gold-standard Butyzamide 3a cultures. Furthermore, this experiment revealed that Flt3L supplementation, when using human cord blood samples, does not provide a significant increase in culture purity or HSC counts by the end of *in vitro* expansion (as compared to results Figure 6.2).

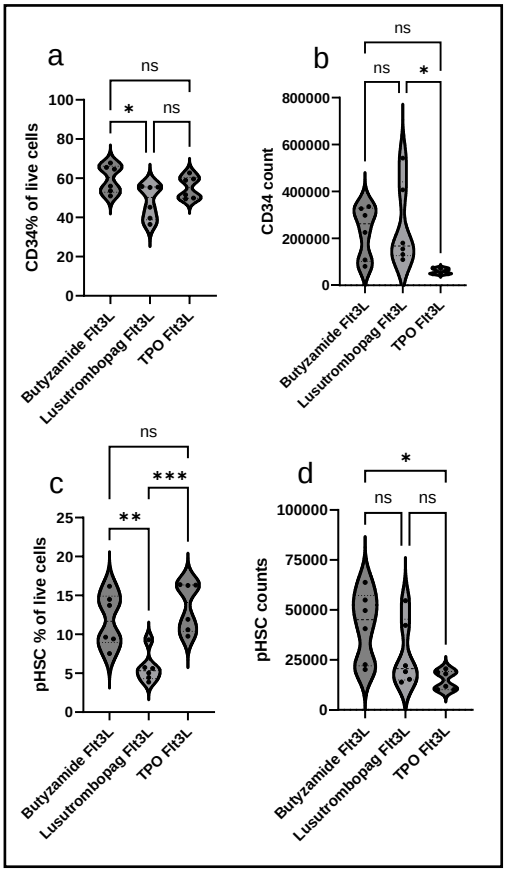

Figure 6.6 **Lusutrombopag, TPO, and Butyzamide can all reliably support human HSC expansion**. Day 14 flow cytometric analysis of 3a expanded human cord blood samples comparing Butyzamide to TPO and Lusutrombopag. Plots show $CD34^{+}$ and pHSC counts and percentages of live cells on day 14. Comparisons were performing using an unpaired T-test, ns = $p>0.05$, * = $p \leq 0.05$, ** =$p \leq 0.01$, *** =$p \leq 0.001$

6.3. MPL internalisation following TPO, and TPO mimetic, stimulation

The ligand-dependent internalisation of MPL is the predominant method of regulating the surface levels of the receptor, and therefore influences the cells' sensitivity to TPO and TPO mimetics (Hitchcock et al., 2021). Tight regulation of this process is therefore essential to prevent uncontrolled cellular proliferation. Predominantly, the process of MPL internalisation

relies on endocytosis of the receptor within clathrin-coated vesicles, and is dependent on adaptor protein 2 (AP2) (Mellman et al., 2000, Hitchcock et al., 2008). Importantly, in the BaF3 cell line, TPO-induced internalisation of MPL correlates with TPO-stimulated cellular proliferation, which implies that internalisation of the receptor-ligand complex is vital to facilitate downstream signalling. Therefore, a key stage of the experimental setup involves starving cells of TPO ahead of treatment, as this induces a significant upregulation of surface MPL, therefore increasing the cells sensitivity to TPO.

Given the importance of MPL internalisation on TPO sensitivity and signalling, internalisation assays were performed on UT7 cells, an acute megakaryoblastic leukaemia cell line, in order to compare induction of receptor internalisation between TPO and a series alternative TPO mimetics (romiplostim, eltrombopag, butyzamide, and lusutrombopag). DMSO, PBS, and RPMI media were used as controls. In this experiment, both WT UT7 cells, and a mutated $JAK2^{V617F}$ UT7 cell line was used. The $JAK2^{V617F}$ UT7 cell line is cultured in TPO free media in order to select for cells expressing the mutated JAK2 variant which enables constitutive activation of this receptor, regardless of TPO binding. The $JAK2^{V617F}$ mutation, as discussed in Section 1.5.1 of this thesis, is a common mutation in MPN patients, present in 95% of PV cases, and 60% of ET and MF patients. Due to the close interactions of JAK2 with MPL, and its influence over downstream signalling, it is interesting, and important, to consider the differences between both WT and $JAK2^{V617F}$ cells' response to TPO stimulation.

As described in Methods Section 3.26, cells were subject to overnight TPO starvation, in RPMI media with 10% FBS, in order to induce maximal surface expression of MPL. The following day, cells were exposed to either varying concentrations of, or for varying times to, TPO and a selection of TPO mimetics. When varying concentrations of agonists were tested, 30 minutes of exposure was used, and for the time course tests, a concentration of 10nM was utilised. To ensure consistency, for every condition tested, 10,000 UT7 cells were used. Following stimulation of either WT or $JAK2^{V617F}$ mutated UT7 cells, the cell populations were fixed before being stained for surface MPL and then ran on a CytoflexLX to determine MPL expression. Subsequent analysis of flow cytometry data enabled quantification of MPL expression relative to maximal for all timepoints and concentrations tested. Figure 6.7 demonstrates the gating strategy used to identify the cell population and an example histogram showing MPL-PE expression within this population.

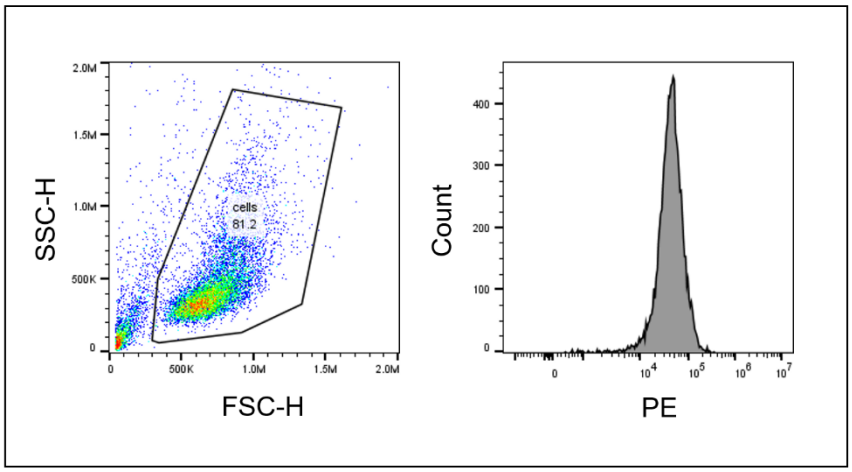

Figure 6.7 **Representative gating strategy used to quantify MPL internalisation.** The antibody against MPL is tagged with a fluorescent PE molecule enabling relative quantification of MPL levels on the surface on UT7 cells. Histogram shows the spread in PE fluorescence values within the gated cell population.

The data reveal that only TPO and Romiplostim are capable of inducing significant levels of MPL internalisation in WT UT7 cells in any condition (Figure 6.8). In time course data, significant internalisation of MPL is induced in WT UT7 cells after just 5 minutes of *in vitro* exposure to TPO and romiplostim. In regards to concentrations necessary to induce internalisation in WT UT7 cells, TPO- and romiplostim-induced internalisation of MPL did not become significant until concentrations of 1nM were reached (Figure 6.8). Beyond this time point, extent of MPL internalisation did continue to increase, but began to plateau by 100nM. Much like WT UT7 cells, in JAK2^{V617F} mutated UT7 cells, over the entire time course tested MPL internalisation was only induced by romiplostim and TPO (Figure 6.9). However, differing to WT, the highest tested concentration of butyzamide (100nM) was able to induce low levels of MPL internalisation, although this remains significantly lower than that of TPO and romiplostim (Figure 6.9).

This is an important discovery, as due to the essential nature of butyzamide in 3a expansion cultures, where without butyzamide present in the media, expansion cultures collapse, it is very surprising that butyzamide does not induce any significant internalisation of the TPO receptor. These differences in receptor internalisation may result from the differing binding sites of romiplostim and TPO, and butyzamide and lusutrombopag. Whilst TPO and romiplostim bind to the N-terminal domain of MPL (Sarson-Lawrence et al., 2024, Broudy and Lin, 2004), both butyzamide and eltrombopag are theorised to bind closer to the juxta/trans-membrane domain of the receptor (Pogozheva et al., 2023, Levy et al., 2020, Lv et al., 2024). A schematic demonstrating these differences is shown in Figure 6.16. As a

result, these alternative binding sites may not induce reliable internalisation of the receptor. However, it is still intriguing that although butyzamide is indispensable for 3a expansion cultures, and so must be inducing a significant level of downstream signalling from MPL, it does not induce significant internalisation in WT or VF (JAK2^{V617F} mutated) cells.

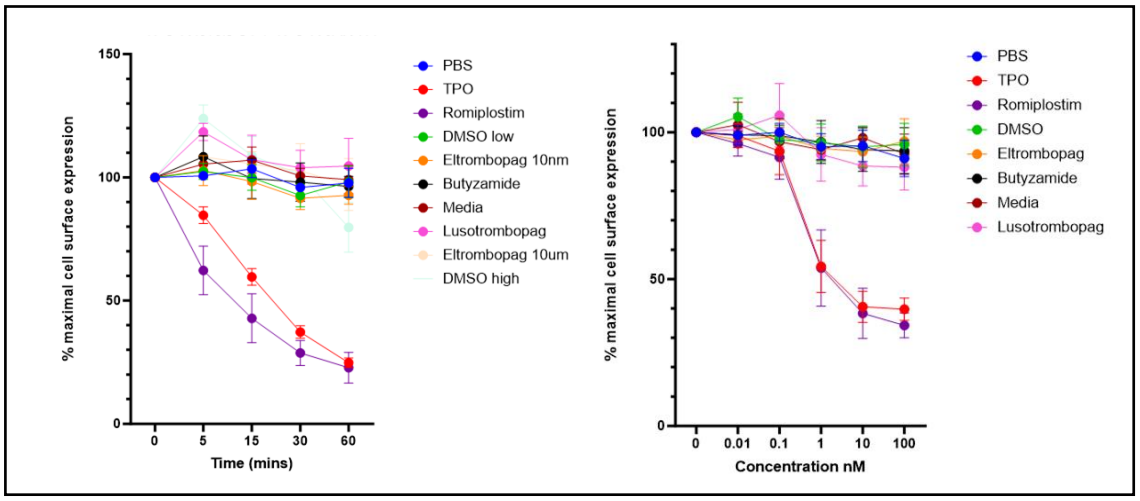

Figure 6.8 **Internalisation assays show that only TPO and Romiplostim induce MPL internalisation in WT TPO cells.** Data showing extent of TPO internalisation relative to maximum surface expression as achieved under TPO starvation (time 0 / concentration 0nM). As shown, only TPO and Romiplostim are capable of inducing significant levels of TPO internalisation. Error bars show standard deviation.

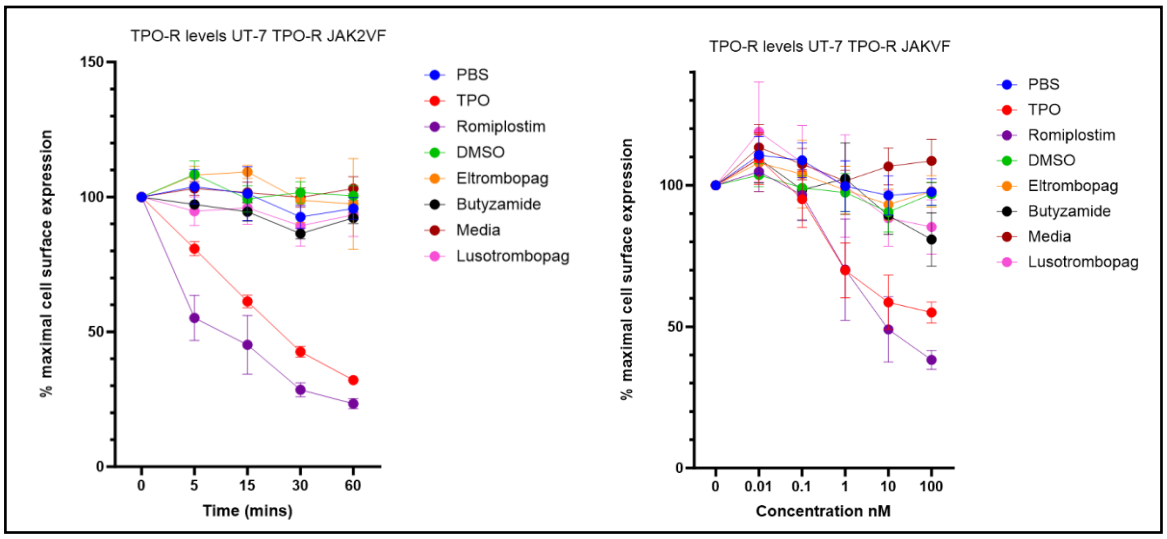

Figure 6.9 **Internalisation assays reveal only TPO and Romiplostim induce MPL significant internalisation on JAK2^{V617F} mutated UT7 cells.** Internalisation shown as relative to maximal surface expression of MPL following overnight TPO starvation. Unlike WT cells, a smaller, but still significant, level of MPL internalisation was induced by butyzamide, but only at high concentrations of 100nM. Error bars show standard deviation

6.4. Fluorescent barcoding and phosphoflow of TPO/TPO mimetic stimulated UT7 cells

Following internalisation assays which identified key differences in MPL internalisation following TPO/TPO mimetic stimulation, the focus shifted towards deciphering differences in downstream signalling induced by these alternative agonists.

To do this, fluorescent barcoding was combined with phosphoflow cytometry to quantify expression of several phosphoproteins in many conditions simultaneously. This efficient protocol enables a large number of conditions to be screened rapidly, within just a few wells of a 96-well plate. The complete protocol is described in Methods Section 3.27, and Figure 6.10 outlines the key steps in this protocol. Briefly, 10,000 WT/JAK2^{V617F} UT7 cells previously treated with varying agonists for varying exposure times, or concentrations, are transferred into a 96-well plate as shown below (Figure 6.10). In this plate, each row represents an agonist, whilst each column represents a timepoint or concentration. For all timepoints, a concentration of 10nM was used (other than for the Eltrombopag high condition, where 10µM was used). Each column was barcoded with a unique dye mix of Dylight 800 and PacBlue to enable separation from the other timepoints/concentrations. Following barcoding staining, each row is pooled for blocking, before being separated out along a row in a new 96-well plate, this time with each column representing an individual pair of antibodies against 2 phosphoproteins, using FITC and APC. As a result, each well contains data on the expression of 2 phosphoproteins within 5 conditions. Following completion of staining, the 96-well plate is run on a Cytoflex LX flow cytometer and gating, as shown in Figure 6.11, enables isolation of the 5 barcoded populations within each well. Once the 5 barcoded populations have been gated, determination of median FITC and APC values within each population enables relative quantification of phosphoproteins present in each sample. Sequential analysis of the flow cytometric data enables generation of data showing relative expression of phosphoproteins relative to time 0 or concentration 0 (untreated), and allows comparison of downstream signalling pathways induced by differing TPO mimetics.

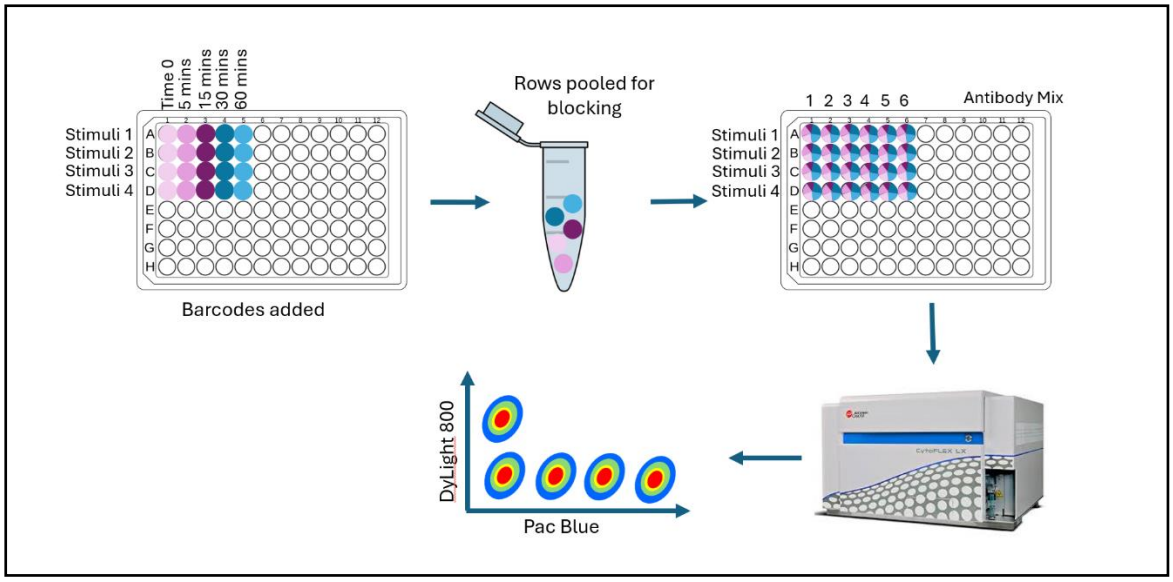

Figure 6.10 **Schematic of fluorescent barcoding and phosphoflow protocol.** Several stimuli are tested simultaneously in a 96 well plate, with each row representing a stimulus, and each column representing a timepoint or concentration. Following barcoding, rows are pooled for blocking, before separating out along a row with each column containing different antibody mixes against different phosphorylated proteins. Once staining is complete, and necessary washed have been performed, the samples are ready to be read on a flow cytometer. Made in BioRender

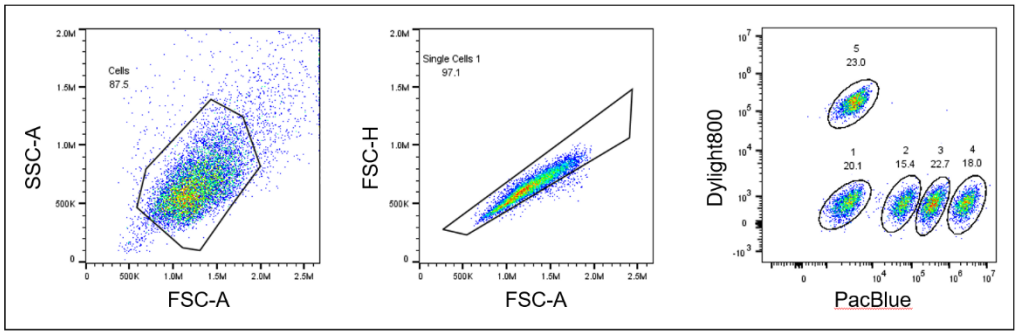

Figure 6.11 **Representative phosphoflow gating strategy.** Initially, cell and single cell gates are set, and then gates are set for the 5 (or 6, not shown) barcoded populations per well. Each of the barcoded populations represents a different concentration, or exposure time, of the MPL agonist. Within each of these gates, median values for FITC and APC allow quantification of 2 phosphoproteins, in 5-6 conditions, per well.

In order to visualise the phosphoflow data, a series of heatmaps were generated, all using the same axis, to enable direct comparison between expression of different phosphoproteins. Each of the following heatmaps represents an individual phosphoprotein, each row represents an MPL agonist, and each column represents a timepoint (Figures 6.12 and 6.13,) or concentration (Figure 6.14 and 6.15). Interestingly, several key differences are noted between agonists in their induction of varying phosphoproteins in both WT and

JAK2^{V617F} UT7 cells. Firstly, in the time course tests, downstream signalling via pSTAT5 Y694 is more significantly induced by TPO and romiplostim treatment, followed by intermediary levels of induction by the higher 10μM concentration of eltrombopag. The lowest levels of induction were by butyzamide, lusutrombopag, and the lower 10nM concentration of eltrombopag in both WT and JAK2 mutated UT7 cells lines (Figure 6.12, Figure 6.13). Similar patterns, where the highest signalling is induced by TPO and romiplostim, are noted in both WT and JAK2^{V617F} UT7 cells in pSTAT3 S727, pERK T202/Y204, pJAK2, and pCREB S133, and are noticeable after just 5 minutes of TPO/romiplostim stimulation. Comparatively, pMEK1 and pAKT levels remain significantly more universal between stimuli, with only slight differences noticeable in WT and JAK2^{V617F} UT7 cells when the heatmap scale is reduced to maximum 3-fold. For all phosphoproteins tested, over all timepoints, the lower of the eltrombopag concentrations tested (the same concentration as the other agonists), induced the lowest levels of downstream signalling via the targets selected.

In terms of concentration screens, where concentrations of 0.01 to 100nM were tested for each agonist or control, similar patterns were noted in the downstream signalling pathways induced by each agonist, but concentrations of 1nM and above were generally required to observe any significant changes. Reassuringly, concentration dependent induction of phosphoprotein signalling was observed in a range of tested agonists. TPO and romiplostim in particular produced strikingly dose dependent responses in UT7 cells in pSTAT3 S727, pCREB S133, and pSTAT5 Y694 pathways (Figure 6.14).

These discoveries are significant as not only do they highlight the ability of alternative MPL agonists to induce individual downstream signalling signatures, but these studies also demonstrate the comparatively large signalling output induced by TPO and romiplostim, both of which, as discussed previously, bind to the MPL N-terminal domain. This data implies that small molecules binding closer to the juxta/trans-membrane domain are less able to induce a robust, and wide ranging downstream signalling cascade from MPL. Figure 6.16 outlines a schematic summarising the differences in downstream signalling induced by TPO and alternative TPO mimetics: romiplostim, butyzamide, and eltrombopag. Key trends include maximal signalling via STAT, AKT and ERK following TPO/romiplostim stimulations, and decreasing levels of JAK, STAT, and ERK downstream signalling observed in butyzamide and eltrombopag treated UT7 cells.

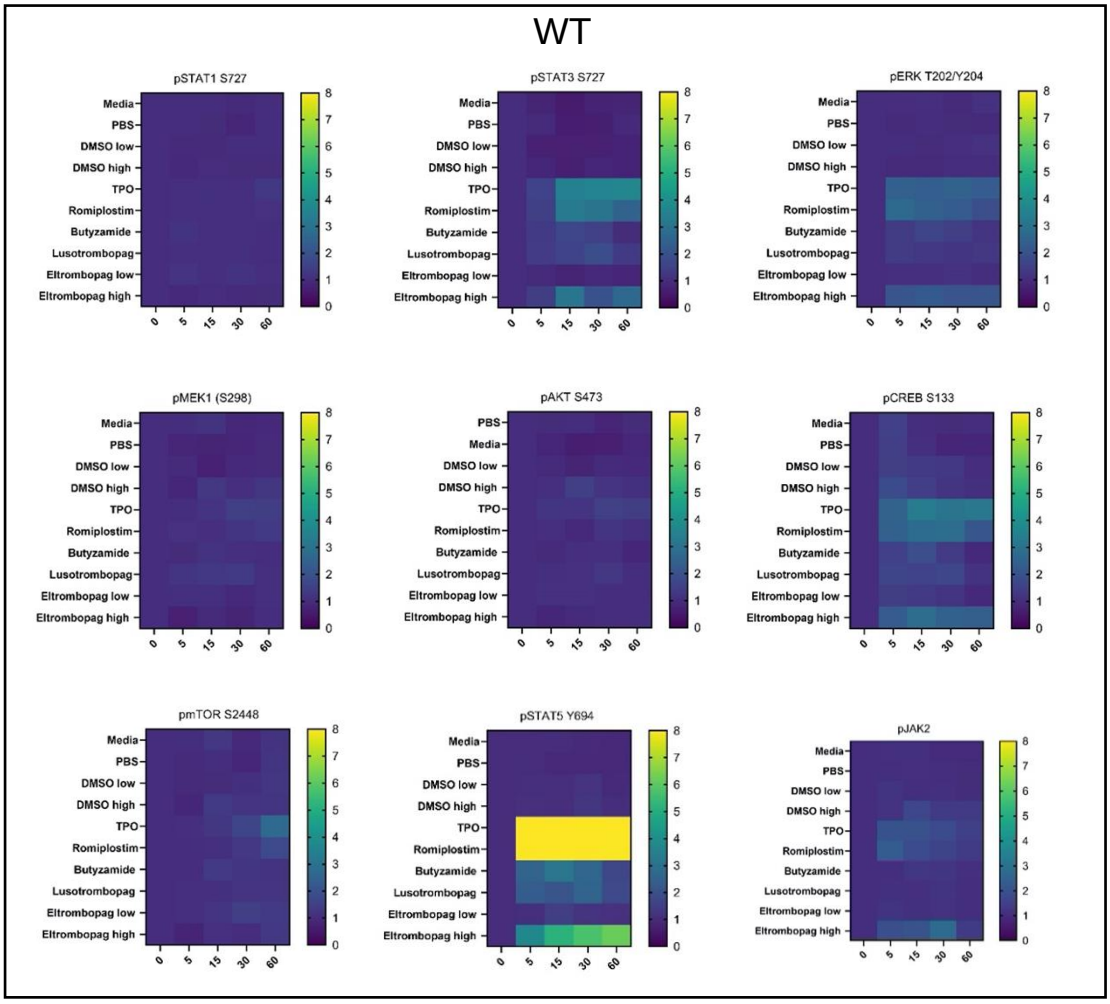

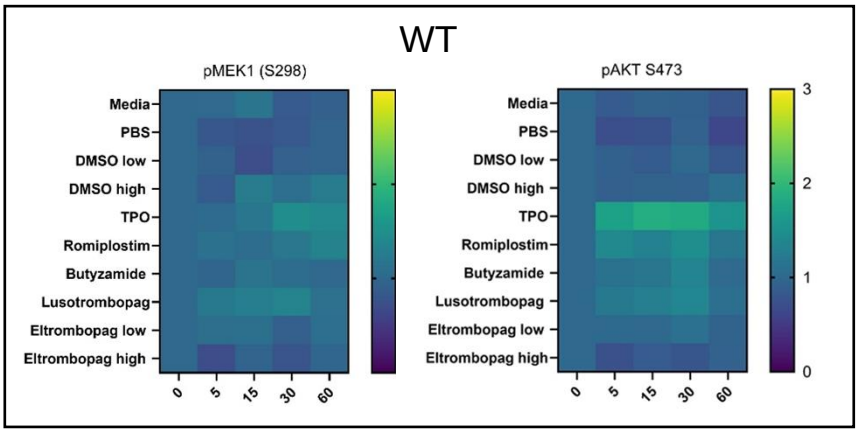

Figure 6.12 **Heatmaps of time course phosphoflow data following TPO/TPO mimetic stimulation in WT UT7 cells.** Each heatmap represents a separate phosphorylated variant of a protein. Within each heatmap, each row represents a different agonist, and each column represents a timepoint (in minutes). The first set of 8 heatmaps use a larger scale, reaching 8-fold change as the maximum in order to allow comparison between a significant range in fold-changes relative to time 0 expression. The second pair of heat maps contain a scale reaching 3-fold at the maximum, of two selected phosphorylated proteins with lower overall changes in order to highlight the differences observed between conditions.

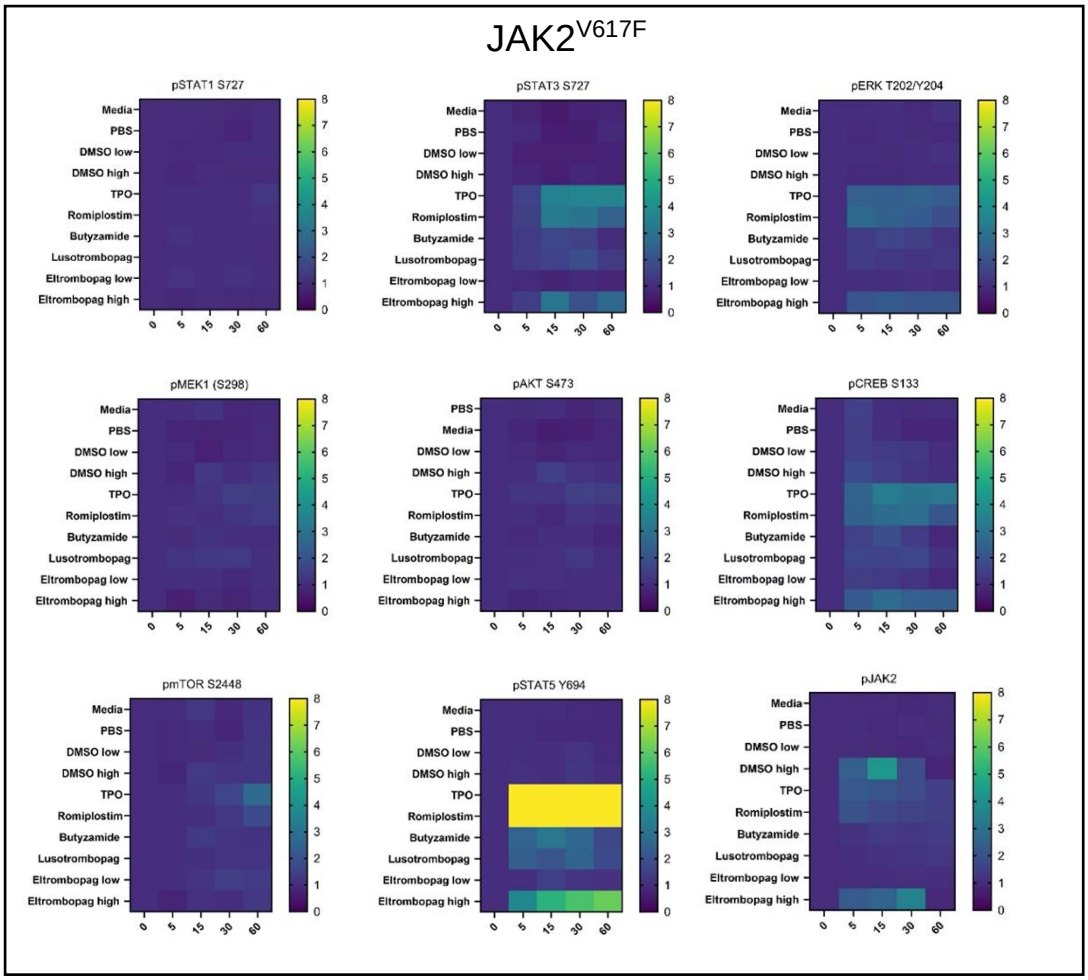

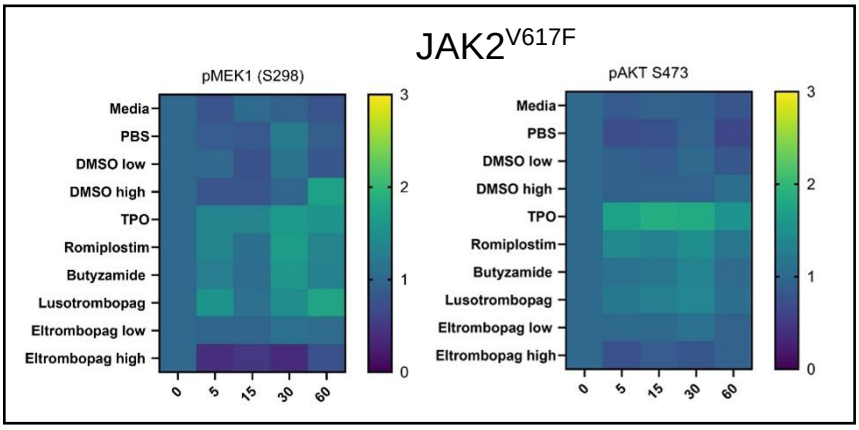

Figure 6.13 **Heatmaps of time course phosphoflow data following TPO/TPO mimetic stimulation in JAK2^{V617F} mutant UT7 cells.** Each heatmap represents a separate phosphorylated variant of a protein. Within each heatmap, each row represents a different agonist, and each column represents a timepoint (in minutes). As in Figure 6.12, the first 8 heatmaps utilise a scale reaching a maximum of 8-fold increase relative to time 0, whilst the second two highlight phosphoproteins with smaller differences, with a scale reaching 3-fold at the maximum.

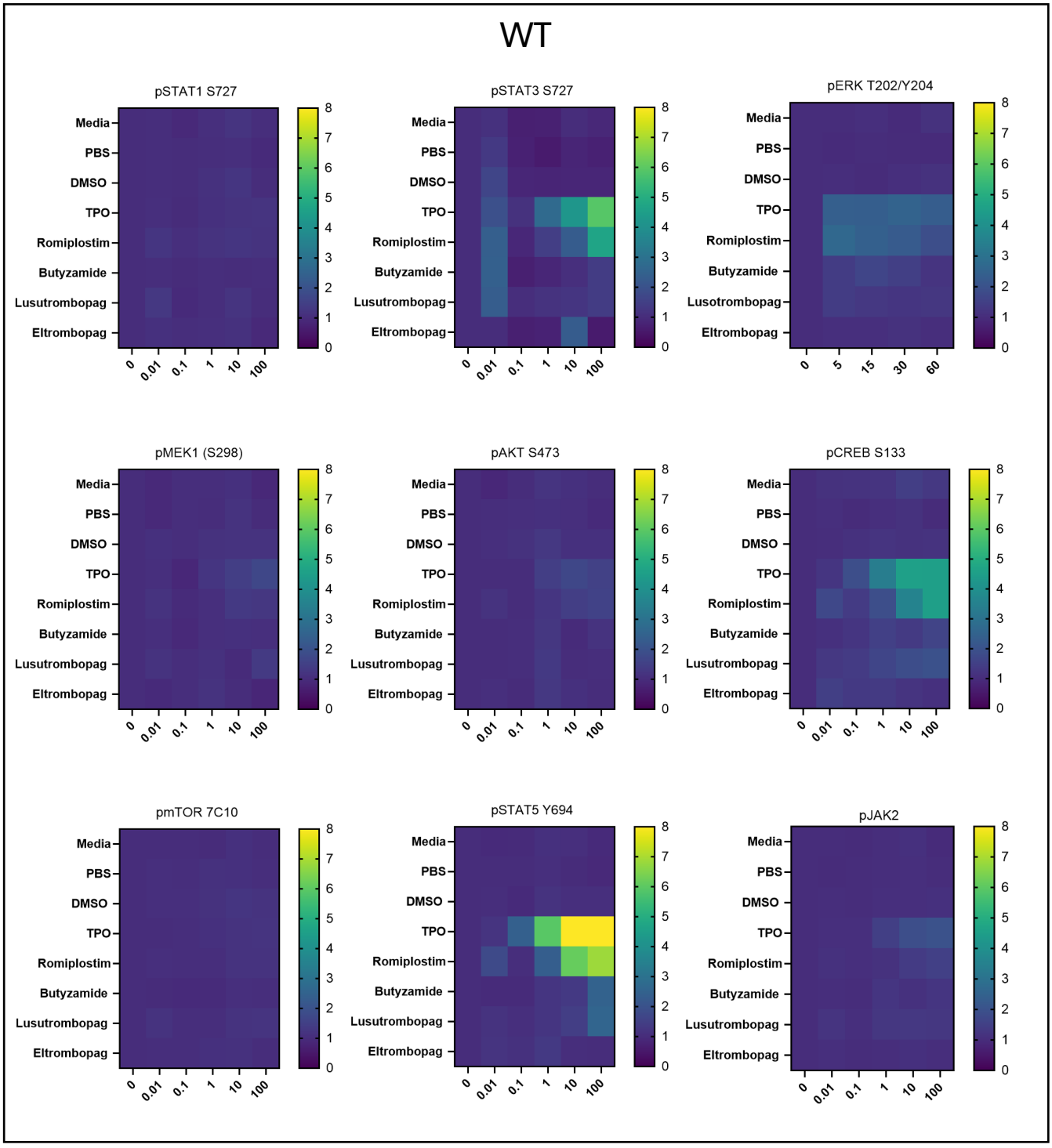

Figure 6.14 **Heatmaps of concentration series phosphoflow data following TPO/TPO mimetic stimulation in WT UT7 cells.** Each heatmap represents a separate phosphorylated variant of a protein. Within each heatmap, each row represents a different agonist, and each column represents a concentration (nM).

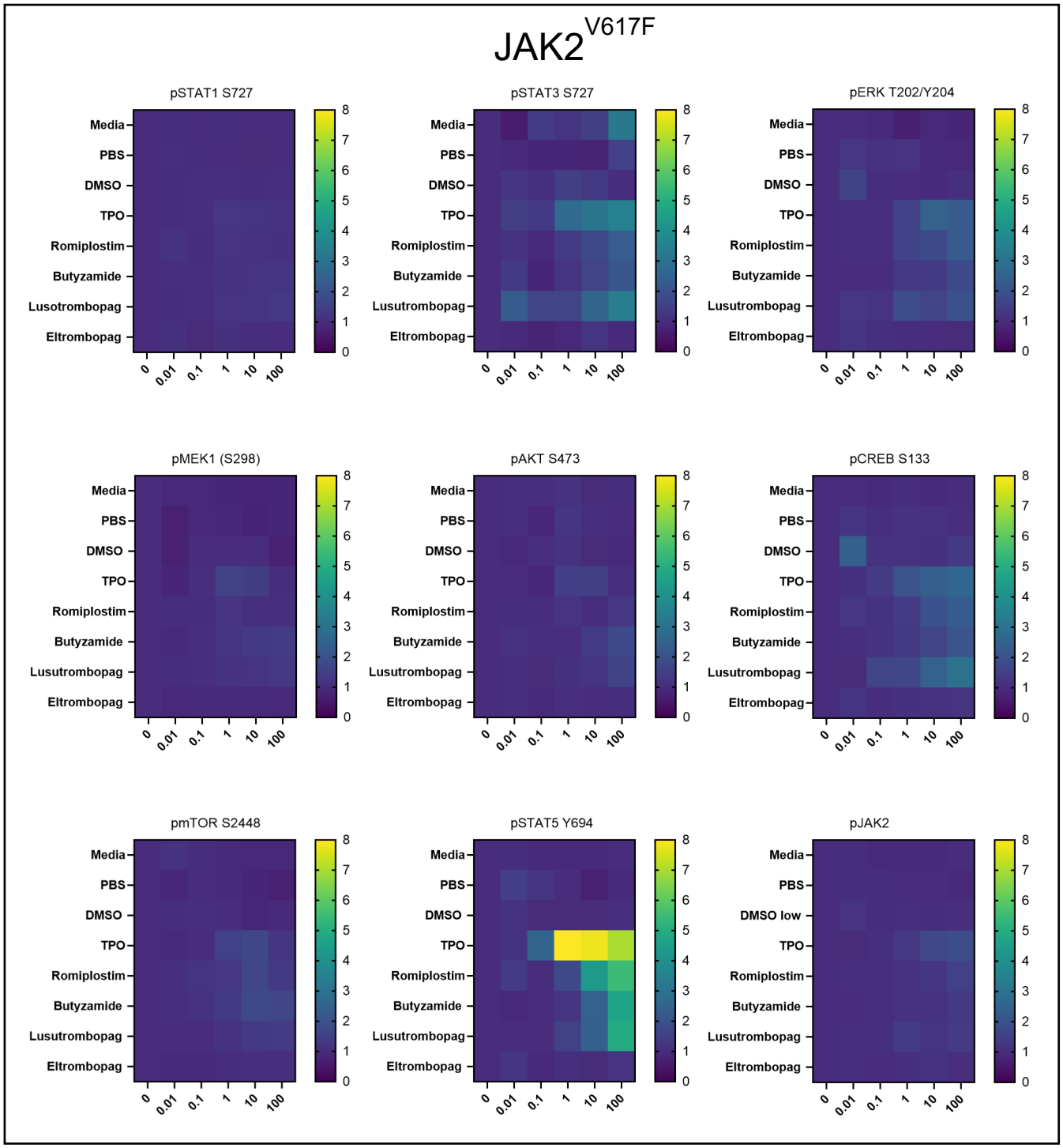

Figure 6.15 **Heatmaps of concentration series phosphoflow data following TPO/TPO mimetic stimulation in JAK2^{V617F} mutant UT7 cells.** Each heatmap represents a separate phosphorylated variant of a protein. Within each heatmap, each row represents a different agonist, and each column represents a concentration (nM).

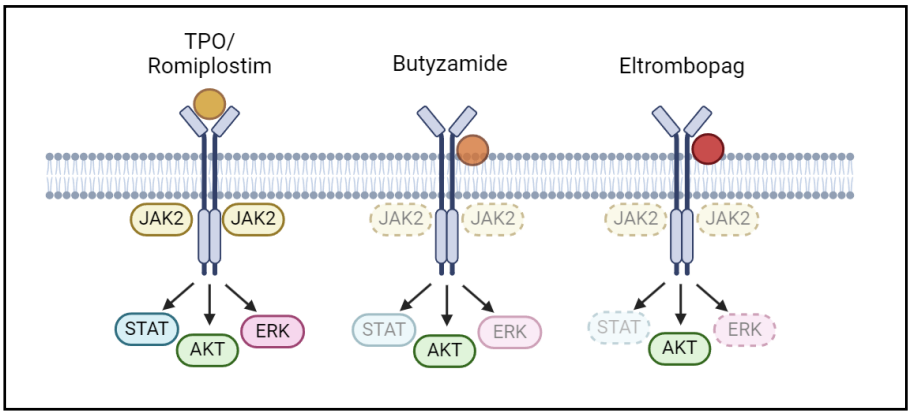

Figure 6.16 **Schematic outlining differences in downstream signalling induced by TPO/TPO mimetics.** This schematic outlines key variations in downstream signalling induced by TPO and TPO mimetics, and highlights the potential in media personalisation, and selecting mimetics best suited for the desired outcome. Darkness of shading, and solid/dashed outline reflect strength of signalling through that phosphoprotein following specified stimulation. Darker colour and complete (not dashed) outline = strongest signalling. Made in BioRender.

The heatmaps shown above in Figures 6.12 – 6.15 are normalised individually, with each heatmap normalised to the control conditions within itself – i.e. time 0 or concentration 0nM. This meant that differences between JAK2^{V617F} mutated cells and WT cells could not easily be inferred. Additional phosphoproteomic data, shown below in Figure 6.17 shows data where VF cells have been normalised to WT control cells and as expected, show a higher level of pSTAT5 phosphorylation and activation downstream of MPL, even in starved (time 0) conditions - a result of the constituent activation of the mutated JAK2 protein. Following TPO stimulation of starved cells for 30 minutes at a concentration of 10nM, a matched concentration to the time course series shown above, pSTAT5 Y694 signalling increased in both WT and VF mutated UT7 cells, but as expected remained higher in the VF pool when compared to their WT counterparts.

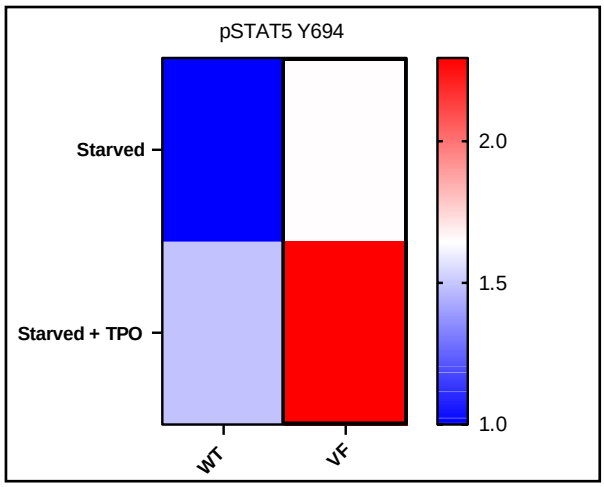

Figure 6.17 **Comparison of pSTAT5 signalling in WT and JAK2^{V617F} mutated UT7 cells with and without TPO stimulation.** Starved cells, meaning TPO had been removed from the cells media overnight before measurements were taken, were compared to cells which had been starved and then treated for 30 minutes with 10nM of TPO.

6.5. Development of a phosphoproteomics protocol for the human UT7 cell line engineered to express MPL

Following phosphoflow analysis of downstream signalling which elucidated some key differences in signalling induced by alternative TPO mimetics, we aimed to perform phosphoproteomic analysis to verify our findings and to more thoroughly investigate the impact of TPO, and TPO mimetics on UT7 cells. However, before these tests could be performed, it was necessary to refine the phosphoproteomic protocol specifically for the UT7 cell line. Furthermore, a series of dilutions of starting material were tested in order to identify the ideal protein quantity required for future tests. Following urea lysis of UT7 cells as described in Methods Section 3.19, BCA assays were performed in order to quantify the amount of protein in the cell lysate (Methods Section 3.20). From this data it was possible to generate a series of dilutions; specifically 1, 5, 20 and 100µg, which then went through an overnight trypsin digestion. In this experiment, following the overnight trypsin digest, 3 approaches were compared for the desalting step of sample preparation: no desalting, C18 tips, and Graphite desalting columns (Methods Sections 3.22, 3.23). Desalting is an important process in proteomics sample preparation, as it removes any unwanted contaminant salts, such as urea used in the initial lysis buffer, of which high concentrations impede mass spectrometry analysis. Additionally, desalting steps concentrate the protein samples of interest. Subsequent sample acidification and phosphopeptide enrichment (Methods 3.24) generate a sample ready to be loaded onto EvoTips, and able to be run on a Bruker TimsTOF HT (Trapped Ion Mobility Spectrometry Time Of Flight, High Throughput) mass spectrometer using the 15 PASEF-DDA (data dependent acquisition, parallel accumulation-serial fragmentation) method.

Following data collection on the mass spectrometer, protein hits were then searched against the entire human proteome using FragPipe. Graphite Spin Column enrichment was highlighted as the superior desalting protocol for UT7 cells, and these tests identified 20µg and above as suitable protein quantities for future proteomic analysis (Figure 6.17). Graphite Spin Columns provided not only high numbers of phosphosites and phosphopeptide identifications, but also generated the highest levels of phosphopeptide enrichment of all three approaches tested. It is likely that the markedly lower phosphoprotein purities and counts generated from the C18 columns, especially at the higher loading densities, result from a maxing out of column capacity. Furthermore, in order to test any biases in the superior graphite column protocol, and to ensure an even spread of proteins from all cellular components is captured in this approach, the entire human proteome was compared to the phosphoproteomic output from the 100µg, graphite column sample (Figure 6.18). Compellingly, a similar distribution in the percentage of total proteins falling within each cellular compartment is observed between the two data sets. Additionally, although the number of proteins is lower in the phosphoproteomic data set, this is to be expected, and again we see a similar relative distribution between all cellular compartments.

In terms of quantity of protein lysate required, from 20µg of protein and higher, significant levels of phosphopeptide and phosphosite IDs were achieved, providing us with a lower limit for protein lysate necessary for a sufficient output. Following the establishment of the refined protocol, and the quantification of protein lysate required for this technique, this experiment opened the doors for a range of future studies utilising this method, as will be discussed in the following section of this thesis.

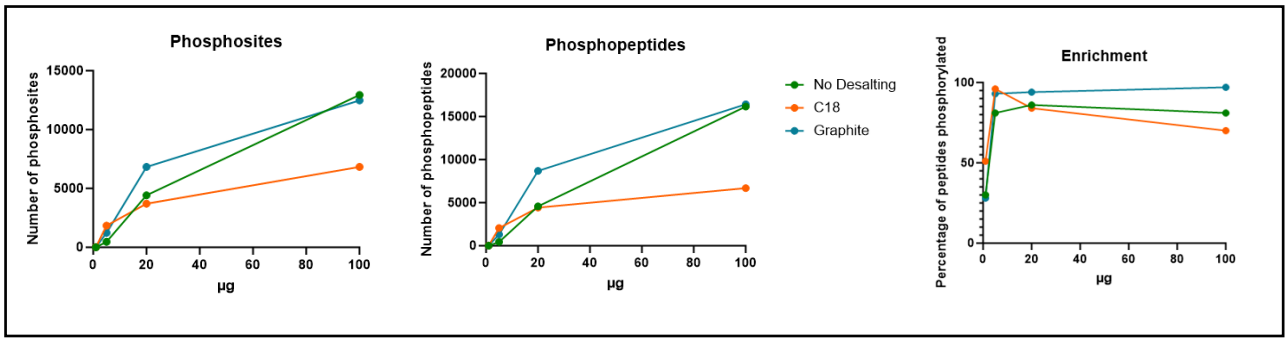

Figure 6.18 **Refining a phosphoproteomics protocol for UT7 cells.** Comparison of desalting protocols to find the best and to determine suitable amount of protein for future experiments. Each condition is compared in terms of numbers of phosphosites and phosphopeptides identified, and total enrichment. Graphite columns provide the greatest number of phosphosites, phosphopeptides, and phosphopeptide enrichment.

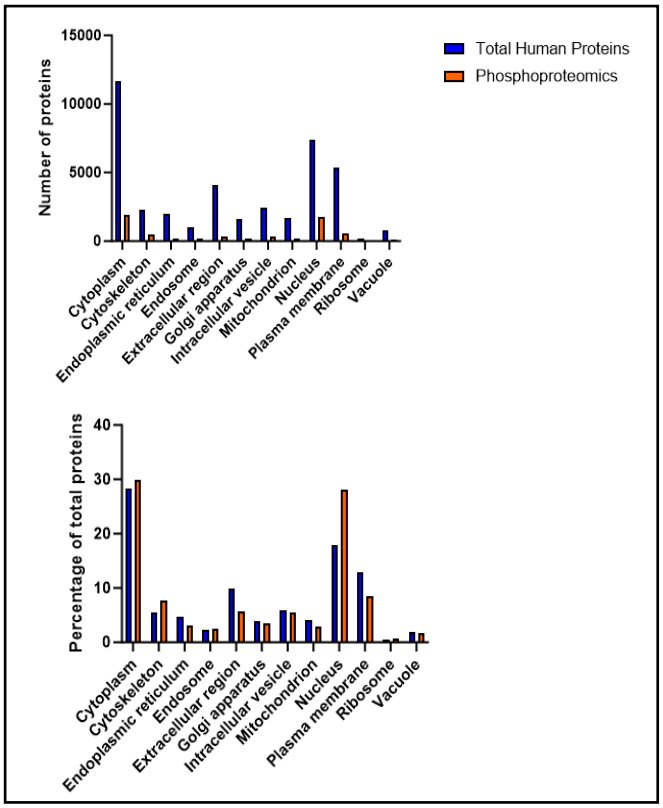

Figure 6.19 **Comparison of the distribution of cellular localisation of proteins identified in phosphoproteomic analysis versus the total human proteome.** 100µg graphite column enriched UT7 cell sample was compared to the total human proteome in order to verify a suitably unbiased capture.

6.6. Phosphoproteomic analysis of TPO mimetic treated UT7 cells identifies key differences

Following the refinement of a phosphoproteomic protocol for UT7 cell lines, sequential experiments were performed to study the effect of TPO and TPO-mimetic stimulation on phosphoprotein expression. 500,000 WT UT7 cells were loaded per well of a 96-well plate and were treated with a range of TPO mimetics for 30 minutes at a 10nM concentration (n=4 for each condition). This cell count would provide approximately 100µg of protein lysate per sample. Following stimulation, the cells were subject to a urea lysis step, and an overnight trypsin digest (Methods Sections 3.19, 3.20, 3.21) before undergoing graphite column desalting and phosphopeptide enrichment (Methods Sections 3.23, 3.24) the following day. The samples were then run on a TimsTOF HT mass spectrometer, acquiring data using a custom PASEF-DDA method. Phosphoprotein hits were then searched using FragPipe for identification and relative quantification using a 1% False Discovery Rate (FDR). Multiple test correction for pair-wise testing used a Local and Tail Area based approach, the most appropriate test for large data sets, in place of the overly stringent Benjamini-Hochberg FDR

calculation. Sample minimum imputation was applied to the data, and a q < .001 significance threshold was set. Following this analysis, 1302 of 25745 phosphoprotein identifications were classified as significant. As shown in Figure 6.19. a high and comparable number of features, in this case identified phosphoproteins, was observed in each sample tested. This confirms the phosphoproteomic protocol performed well, and provides a strong foundation for further analysis and comparison between conditions. Clustering analysis performed on FragPipe, and based on the 1302 significant proteins, showed that the sample groups clustered reliably, according to the stimuli they had been treated with, with significant quantifications between all groups (Figure 6.20). Furthermore, PCA analysis of the significantly differentially expressed proteins confirms sample clustering according to treatment (Figure 6.21a), however of note, the Romiplostim- and TPO-treated samples did overlap slightly. This is interesting and correlates with their similar binding sites on MPL (N-terminal domain), and their ability to induce internalisation of the MPL receptor upon binding, both of which differ from the other agonists. Furthermore, samples treated with eltrombopag, the only agonist unable to support HSC expansion *in vitro,* cluster the furthest from the other groups. This clustering pattern is additionally verified in Figure 6.21b, a cluster dendrogram utilising a Euclidean distance method to determine similarities between samples.

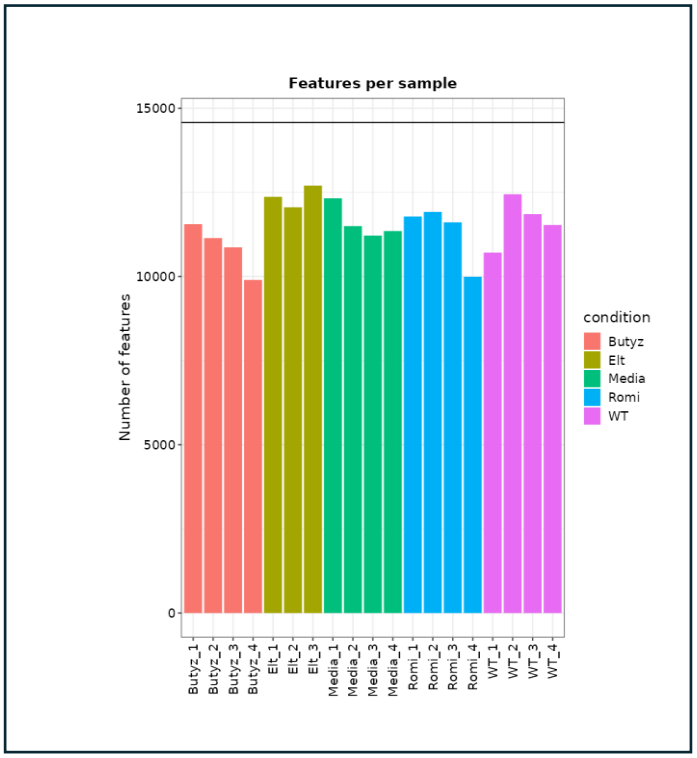

Figure 6.20 **Number of features identified per phosphoproteomics sample.** Each sample presented with a high and comparable number of features identified. WT= WT TPO, Butyz = butyzamide, Elt=Eltrombopag, Media = Control RPMI media, Romi = romiplostim. Image created on FragPipe Analyst.

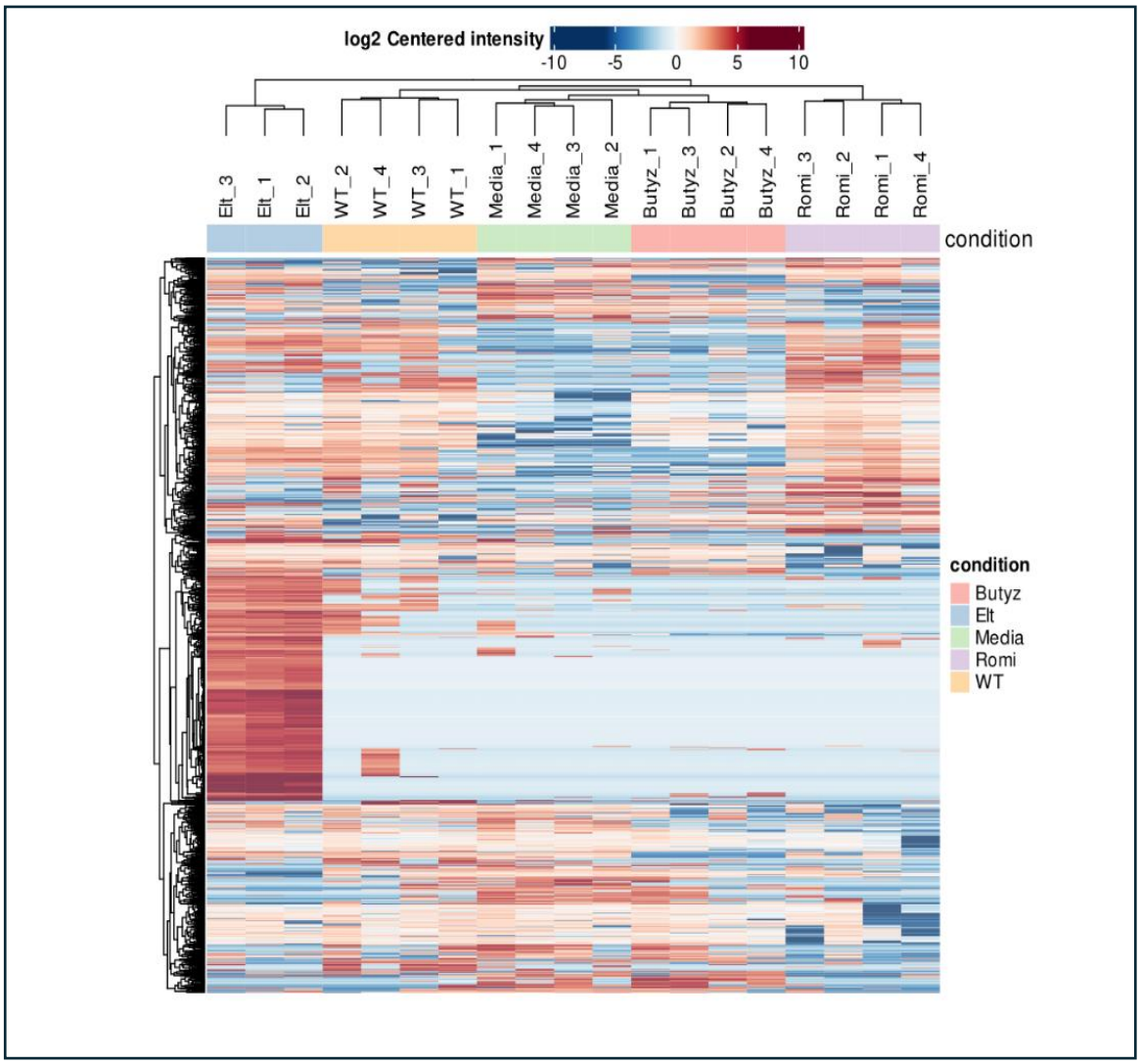

Figure 6.21 **Heatmap clustering of phosphoproteomic samples show reliable grouping based on MPL-agonist.** Generated based on 1302 of 25745 significant features. Minimum percentage of non-missing values in at least one condition set to 75. Adjusted P-Value set to <0.001, with minimum imputation, and using local and tail area-bases FDR correction. WT= WT TPO, Butyz = butyzamide, Elt=Eltrombopag, Media = Control RPMI media, Romi = romiplostim. Image created on FragPipe Analyst.

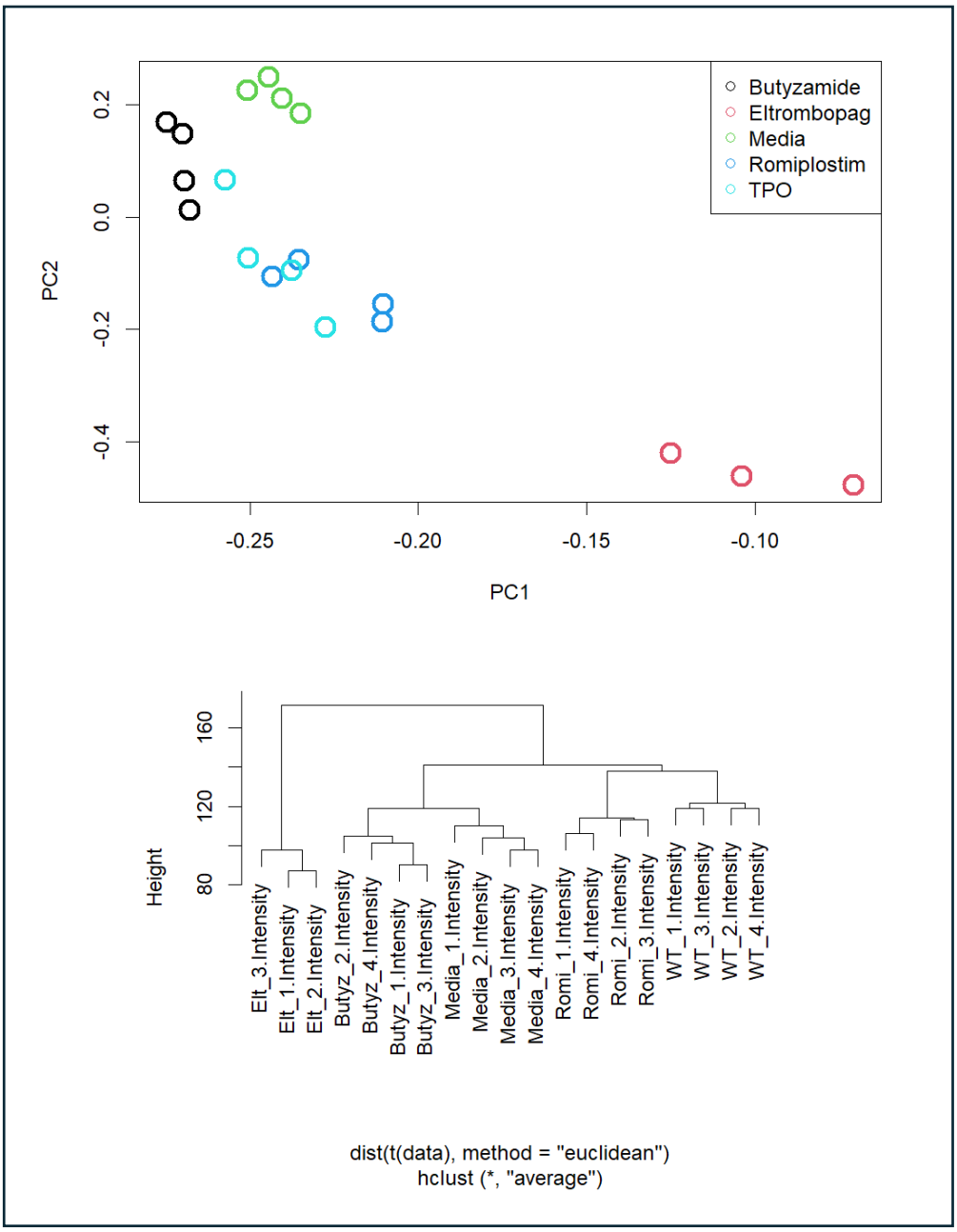

Figure 6.22 **Clustering analysis of phosphoproteomic data.** a) PCA plot of MPL-agonist treated UT7 cells phosphoproteomic data, using prcomp function in R. Code for analysis shown in methods section 3.30.1. Black=Butyzamide, Red = Eltrombopag, Green = Media, Dark blue = Romiplostim, Blue = TPO. b) Dendrogram clustering analysis based on Euclidean distance methods and “average” method – code shown in methods section 3.30.1 Elt = eltrombopag, Butyz = butyzamide, Romi = romiplostim, WT = TPO. Image created on FragPipe Analyst.

Once confirmation of clustering according to stimuli had been robustly confirmed, direct comparisons between stimuli and RPMI media were performed to determine specific upregulation of proteins relative to control. Volcano plots outlining these differences, and quantification of the number of up- and down-regulated proteins is shown in Figures 6.22 and 6.23, with a significance threshold set to p>0.001, and significant fold-change set to 2.

Interestingly, phosphorylated ESAM, identified in Chapter 1 of this thesis as a marker of functional mouse HSCs post-expansion, and previously identified as a potential marker for freshly isolated, primitive human HSCs (Ishibashi et al., 2016), was increased in control (media treated) UT7 cells relative to butyzamide stimulated UT7 cells (Figure 6.22a).

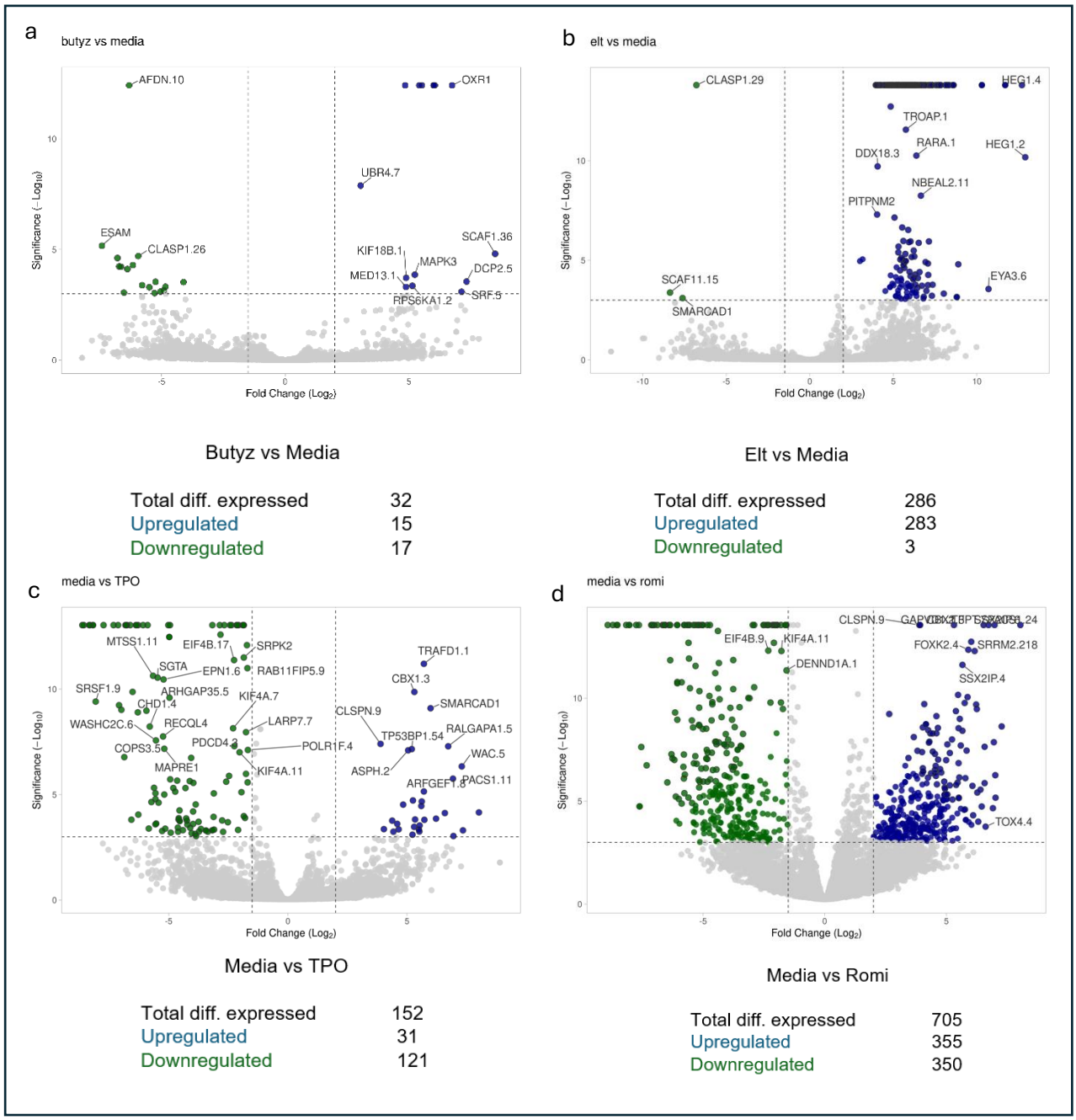

Figure 6.23 **Volcano plots of phosphoproteomic data comparing MPL-agonists to control conditions (Media)**. Significance threshold set to p>0.001, and significant fold-change set to 2. Ranking hits for gene labelling based on Manhattan distance.

Following comparison to control conditions, comparisons between, butyzamide, TPO, and TPO-mimetic treated UT7 cells could be performed (Figure 6.23). As above, the significance threshold is set to p>0.001, and significant fold-change set to 2. Cells were labelled based on the Manhattan distance, a calculation based on the sum of absolute differences between the coordinates of the origin, and the point of interest. ESAM was identified again in this data set, in this instance due to its upregulation in romiplostim treated UT7 cells, when compared to butyzamide treated UT7 cells (Figure 6.23c).

Strikingly, only 1 phosphoprotein was identified in significantly upregulated in butyzamide treated UT7 cells in comparison to eltrombopag-treated – Cytoplasmic linker associated protein 1 (pCLASP1.29), despite butyzamide being the best performing agonist in 3a culture conditions, and the lack of HSC-supporting effects of eltrombopag in culture (Figure 6.23b). CLASP1.29 is also shown to be significantly more highly expressed by the HSC-culture supportive TPO- and romiplostim- treated UT7s in comparison to eltrombopag treated cells (Figure 6.23d,e). A variant CLASP protein, CLASP1.26 was also found to be upregulated in TPO-treated UT7s when compared to butyzamide-treated cells (Figure 6.23a). CLASP1 is a microtubule-associated protein, and is involved to the connection of microtubules to the cellular cortex (Lansbergen et al., 2006). Further studies have shown an interactivity of CLASP1 with the CLIP family of molecules, and support their role of spindle microtubule stabilisation at the kinetochore – therefore having an important role in mitosis (Maiato et al., 2003).

Furthermore, pSTAT5 was identified to be significantly more highly expressed in romiplostim- and TPO-treated UT7 cells when compared to butyzamide-treated UT7 cells (Figure 6.23a,c). This concurs with the previously collected phosphoflow data which reveal higher levels of pSTAT5 induction following romiplostim and TPO stimulation, both of which bind to the N-terminal domain of MPL, unlike the alternative agonists which bind to the juxta-/transmembrane domain.

Overall, this phosphoproteomic dataset identifies key phosphoprotein responses to stimulation by TPO, butyzamide, and alternative TPO-mimetics, aiding our understanding of the mechanism of action of these agonists. Furthermore, it appears to confirm and validate the insights into downstream signalling variation generated from the phosphoflow data.

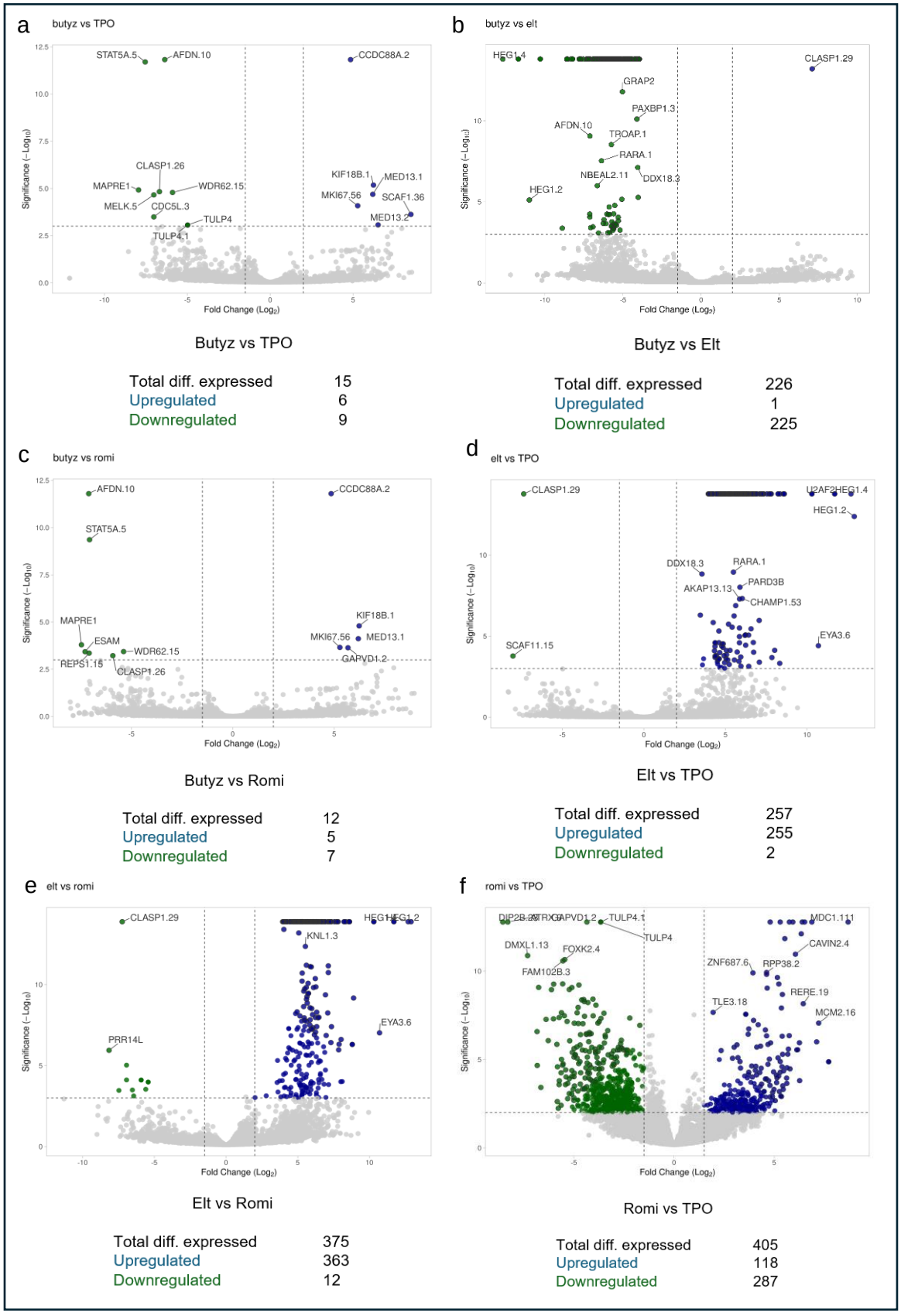

Figure 6.24 **Volcano plots showing differences in phosphoproteins between TPO and Butyzamide stimulated UT7 cells.** Significance threshold set to p>0.001, and fold-change significance set to 2. Ranking hits for gene labelling based on Manhattan distance.

6.7. Low cell number proteomics using primary human CD34$^+$ cells

Despite the important and insightful data gathered from these phosphoproteomic screens – the limitation remains that although UT7 cells provide an accessible and representative model, these cells used will differ in their proteome, albeit slightly, from primary human cells. However, in order to utilise the rare human HSPC populations of interest, it is first necessary to reduce the cellular input required for proteomic screens, and even more so if phosphoproteomic analysis was to be performed on this sparse pool of cells. We therefore aimed firstly to test a range of primary human CD34$^+$ cell counts, specifically 200, 100, 50, 20, 10 and 1 cell(s) per sample in proteomic analysis. In this experiment, peripheral blood samples from 2 healthy donors, and 2 myelofibrosis patients were used. The full method is outlined in Methods Section 3.18. of this thesis but briefly, following removal of these samples from liquid nitrogen storage, they were thawed in a 37°C water bath before being resuspended in PBS 2% FCS. The samples were then centrifuged at 300g for 10 minutes to pellet the cells, before resuspension of the pellet in an antibody master mix containing CD34 APC, CD38 FITC, and MPL PE. Following a 30 minute incubation, washing steps were performed and 7-AAD was added to each sample as a live-dead stain. The BD FACSDiscoverer S8 was used to sort either live CD34$^+$, live CD34$^+$ MPL$^+$, or live CD34$^+$MPL$^-$ cells into wells of a LoBind V-bottom 96-well plate at densities of 1, 10, 20, 50, 100 and 200 cells per well. Once sorted into the plates, samples were subjected to Sodium Deoxycholate (SDC)-induced lysis, before being ran on a Bruker TimsTOF mass spectrometer, with data acquired in PASEF-DIA (parallel accumulation-serial fragmentation, Data Independent Acquisition) mode. Once the samples had been run, protein ID search was performed against previously generated in-house data acquisitions with a 1% false discovery rate (FDR) threshold set at the protein identification level.

Unfortunately, no proteins were able to be identified from any of the 1 or 10 cell samples, however one of the live CD34$^+$ 20 cell samples was able to quantify a small number of proteins. From 50 cells and above, each sample ran was able to generate a larger number of protein identifications (Figure 6.24), however the numbers achieved still remain relatively low. However, this is not necessarily a surprising result, as due to the protective hibernating state of the most primitive HSC populations, they tend to generally present with lower levels of protein synthesis than other haematopoietic cell lines and cell types.

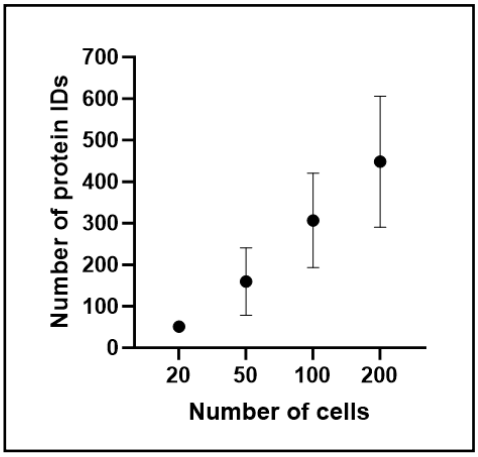

Figure 6.25 **Number of protein IDs achieved from low cell number proteomics**. As is expected, increasing cell counts provide a consistently increasing number of protein IDs per sample. Error bars show standard deviation.

Although any reliable comparison between WT and MF conditions is not possible using this dataset, due to low protein identification counts, it is interesting that, when looking at the 200-cell samples, several significant differences between healthy and diseased $CD34^+$ cells are still observed (Figure 6.25). Reassuringly, of the proteins identified as significantly different within the two populations, several have been identified in previous studies to be associated with haematological diseases. For example, Eukaryotic Translation Termination Factor 1 (ETF1), a polypeptide chain release factor, has been shown to be deregulated in leukaemogenesis (Stoddart et al., 2016), and vital for leukaemic cell survival (Sellar et al., 2022), whilst Cathepsin S (CTSS), a member of the peptidase C1 family, has been published in relation to its inverse relationship with microRNA mir-17 in AML, and correlation with an improved leukaemic prognosis (Cao et al., 2022). Furthermore, the expression of Nicotinamide phosphoribosyltransferase (NAMPT) on the surface of $CD34^+$ cells has recently been identified as a promising novel biological marker for myelofibrosis disease evolution and patient survival, with higher surface levels of NAMPT indicating hyper-myeloproliferative potential of the disease. As a result, increased surface levels of NAMPT are theorised to facilitate malignant transformation (Campanelli et al., 2021). In this study, ETF1, CTSS, and NAMPT were all expressed more highly in the MF patient samples, as opposed to the healthy control samples tested.

This is a promising start, as although variance is high and coverage is low, this preliminary experiment has been a beneficial first step at developing proteomic protocols for primary HSPC populations, and sets the stage for further refinement.

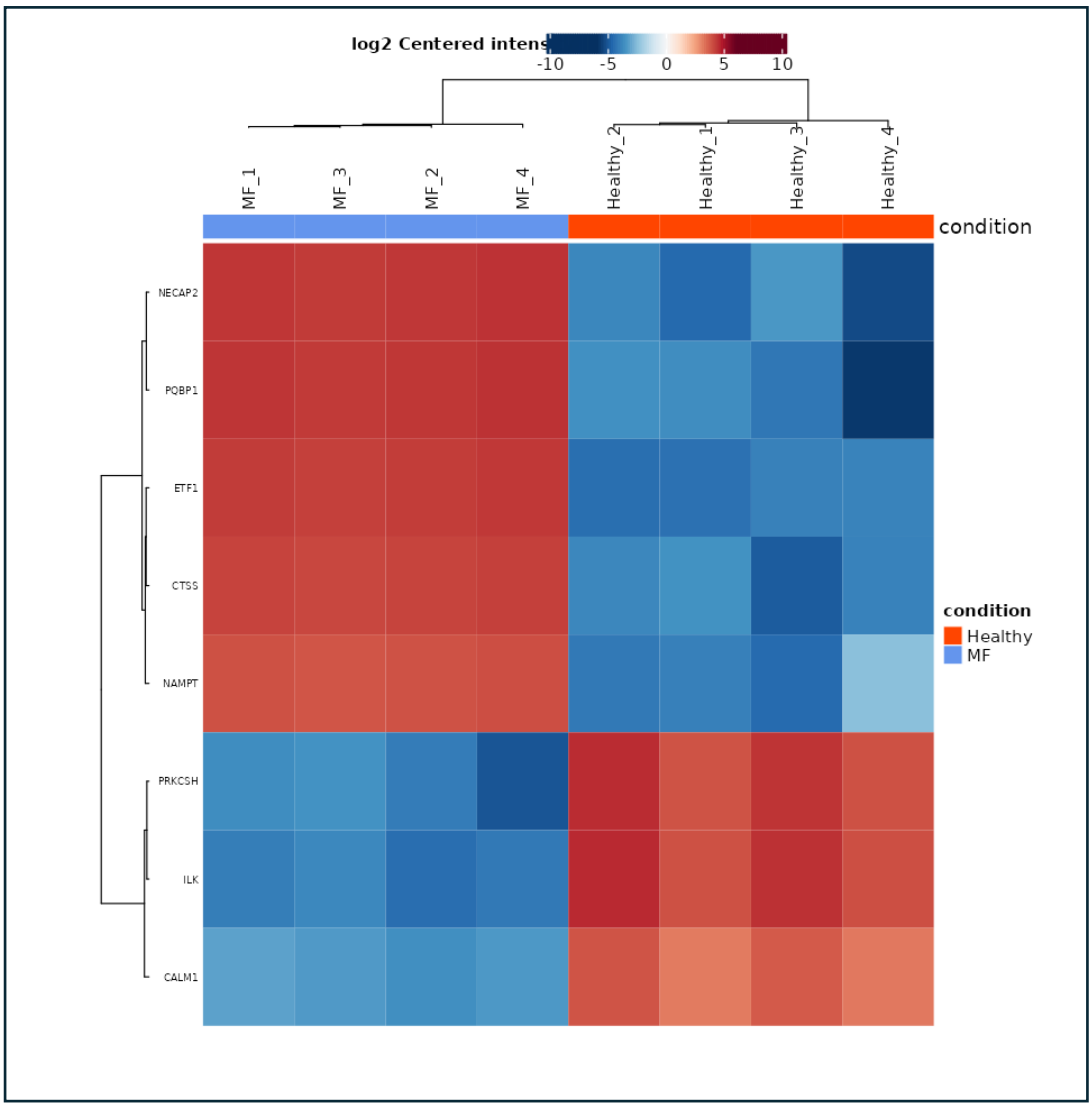

Figure 6.26 **Differentially expressed proteins between myelofibrosis (MF) and healthy 200-cell CD34⁺ peripheral blood samples.** Several key proteins were differentially expressed between the two conditions – including a handful previously linked to haematological diseases. Plot generated in FragPipe Analyst utilising DIA analysis with a p-value cut off of<0.05. No imputation was used and Benjamini Hochberg analysis was used for FDR correction.

6.8. Chapter summary

In conclusion, this chapter initially focused on the functional validation of alternative TPO-mimetics in 3a expansion cultures. Firstly butyzamide, the published MPL-agonist in the 3a expansion system (Sakurai et al., 2023), was shown to be able to be replaced by TPO in the 3a expansion system, and provides comparable culture outcomes. Additional screens testing clinically used TPO-mimetics romiplostim, lusutrombopag, and eltrombopag again revealed

that alternative chemical agonists are also sufficient to support *in vitro* expansion of human HSCs. However, the outcomes of cultures supplemented with these alternative molecules was significantly more variable. Whilst lusutrombopag provided comparable expansion to butyzamide, romiplostim resulted in slightly poorer culture outcomes, and eltrombopag was significantly poorer. However, for scientists with a stronger clinical focus, utilising these FDA approved, and clinically used molecules in the 3a system will appeal regardless of marginally lower expansion levels achieved.

Following the functional validation of these molecules in expansion cultures, further tests were performed to elucidate the differences in mechanism of action of these molecules. Initially, internalisation assays were performed on UT7 cell lines, an acute megakaryoblastic cell line, treated with TPO, butyzamide, and the alternative TPO mimetics. Fascinatingly, only TPO and romiplostim were capable of inducing significant internalisation of MPL.

Following on from internalisation studies, fluorescent barcoding and phosphoflow cytometry were utilised in order to identify differences in the levels of various phosphorylated proteins in UT7 cells treated with a selection of MPL agonists, including TPO and butyzamide. Phosphoflow analysis identified key differences in downstream signalling induced by alternative MPL agonists. However, generally, TPO and romiplostim were identified as agonists which induced a comparatively large downstream signalling output, relative to eltrombopag, lusutrombopag, and butyzamide – specifically in terms of pSTAT3 S727, pERK T202/Y204, pJAK2, and pCREB signalling. As discussed previously, both TPO and romiplostim bind to the MPL N-terminal domain, whilst eltrombopag, lusutrombopag and butyzamide and theorised to bind to the juxta/trans-membrane domain on MPL. As a result, this data implies that small molecules that bind closer to the juxta/trans-membrane domain of MPL are less capable of inducing a robust downstream signalling cascade from MPL.

In order to further investigate the differences in downstream signalling induced by TPO and alternative MPL-agonists, the next experiments aimed to perform phosphoflow analysis on treated UT7 cells. However, this initially required a series of tests to refine a phosphoproteomic protocol for WT and JAK2^{V617F} mutated UT7 cells. Titration of protein lysate starting material, and comparison of various desalting protocols identified graphite spin column desalting, and a starting quantity of at least 20µg protein, to be ideal for future experimentation.

Subsequent phosphoproteomic analysis was then performed on UT7 cells treated with the same selection of MPL-agonists identified, in line with previously phosphoflow data, pSTAT5

as being significantly more highly expressed in romiplostim- and TPO- treated UT7 cells, compared to butyzamide-treated cells. Furthermore, it identified microtubule-associated protein Cytoplasmic linker associated protein 1 (pCLASP1.29) as being present at significantly higher levels in UT7 cells stimulated with HSC expansion supportive agonists (romiplostim, TPO, and butyzamide), compared to UT7 cells treated with eltrombopag, the only agonist of those tested which was unable to support HSC expansion *in vitro*.

However, despite the interesting data generated from phosphoproteomic analysis, the study is hindered by the use of a cell line, UT7, rather than primary human cells. As discussed throughout this thesis, starting cell number is a fundamental limitation of proteomic approaches, as such it is necessary to develop novel, low input, protocols to allow proteomic analysis of these rare cells. To begin this process, we utilised primary human peripheral blood $CD34^+$ cells from healthy controls, and myeloproliferative neoplasm patients. Using FACS, a series of cell loading densities from 200 to 1 cell(s) per well was loaded into a 96-well V-bottom plate, and processed for proteomic analysis on a Bruker TimsTOF mass spectrometer, with data acquired in PASEF-DIA mode. From loading counts of 20 cells and higher, protein IDs were able to be generated from every sample. When the 200 cell samples, both healthy and MF, were compared, several differentially expressed genes were identified – with several of those upregulated in the MF conditions being previously linked to haematological disease, specifically MF, outcomes, and leukaemic stem cell survival.

Overall, this chapter has validated the activity of TPO and several alternative clinically used TPO-mimetics in 3a expansion cultures. Furthermore, internalisation, phosphoproteomic, and phosphoflow studies have identified important differences in MPL internalisation in downstream signalling induced by the alternative mimetics - not only furthering our understanding of the mechanism of action of these drugs, but also allowing personalisation of expansion cultures systems to favour certain pathways.

7. Conclusion and discussion

7.1. Summary and major findings

The first Results chapter of this thesis focused on the identification of novel reporter strategies for *in vitro* expanded mouse HSCs. This aim was fulfilled, with Chapter 4 showing that ESAM was identified as a novel marker for functional expanded HSCs, able to replace the Fgd5 reporter mouse strategy. Functional validation revealed that the EELSK ($ESAM^+EPCR^+Lin^-Sca1^+cKit^+$) content of the well, as a percentage of live cells, correlated strongly to transplantation outcome post-culture, with EELSK notably exhibiting a stronger functional correlation than the previously used ELSK strategy. This chapter also highlighted the capacity of PVA culture systems to act as a screen for novel molecules to determine their effect on HSC expansion, particularly when combined with a split culture approach. Using the split culture method, it was discovered that PVA expansion cultures can survive without cytokine supplementation from day 14 of culture onwards, and are capable of relying on endogenous cytokine production from this point, massively reducing the financial cost of this system. The final part of this chapter focused on the development of a novel Picowell chip platform for the *in vitro* expansion of mouse HSCs, which enables physical isolation of individual cells, and therefore easier quantification of early cell-division dynamics. The addition of a microfluidic channel on top of the Picowell chip design unlocks the possibility of longer term culture on this platform, and opens the doors to assays such as on-chip antibody staining, and visualisation of populations of interest.

The second results chapter of this thesis switched focus towards the expansion of human HSCs, first validating the 3a culture system as a superior expansion protocol for human cord blood HSCs when compared to the previous gold-standard of StemSpan. Further experimentation confirmed the benefit of Flt3L supplementation in 3a expansion culture medium, enabling expansion of HSCs from sources other than cord blood. As a result of this development, the first successful expansion of peripheral blood HSCs from both healthy control donors and MPN patients in 3a conditions was performed, in turn meeting the second aim of this thesis. Several key differences were also identified in the expansion potential of MPN and healthy peripheral blood samples – notably including increased phenotypic HSC counts and percentages in expanded MPN patient samples, coupled with an increased culture purity. As a conclusion to this chapter, MPL, the TPO receptor, was identified as a beneficial marker to add to initial sorting panels to improve HSC culture outcomes. $CD34^+MPL^+$ human cells performed robustly in culture, whilst $CD34^+MPL^-$ initiated cultures collapsed consistently.

The final results chapter, in line with the third aim of this thesis, aimed to investigate in depth the role of TPO in HSC expansion protocols, and to compare the effect of TPO to alternative TPO mimetics. Initially, 3a expansion screens functionally validated TPO, and alternative TPO-mimetics (lusutrombopag, eltrombopag, and romiplostim) as sufficient substitutes for the standard MPL-agonist butyzamide in 3a expansion cultures. Once functionality in culture had been determined, internalisation assays identified TPO and romiplostim as the only agonists capable of inducing MPL internalisation, and fluorescent barcoding and phosphoflow assays identified key differences in downstream signalling induced by these alternative mimetics. Phosphoproteomic analysis of cells treated with these MPL-agonists also identified variations in expression of phosphorylated proteins dependent on the stimuli provided to the cells, and validated observations made in the phosphoflow assays. Finally, at the end of this chapter, the development of a low-cell number proteomic protocol for primary human $CD34^+$ cells is described, which identified several differences in protein expression between healthy and myelofibrosis samples, several of which have been previously linked to myelofibrosis disease outcomes and leukaemic stem cell survival.

In conclusion, this thesis has identified ESAM as a novel reporter strategy for functional, expanded mouse HSCs. Furthermore, it outlines the development of a novel Picowell platform for HSC expansion, capable of physically isolating individual HSCs for imaging and analysis. In terms of the *in vitro* expansion of human HSCs, it validates a Flt3L and MTG supplemented 3a expansion culture system capable of robustly expanding peripheral blood samples from healthy donors and MPN patients for the first time, in turn identifying key differences in the expansion capacity of these samples. Finally, in-depth analysis of butyzamide, TPO, and alternative TPO-mimetics, using internalisation assays, fluorescent barcoding and phosphoflow analysis, and phosphoproteomics provides a deep dive into the roles of MPL-agonists in 3a expansion cultures.

7.2. Future direction for this project

7.2.1. Functional validation of mouse HSC reporter strategies and the cytokine removal culturing system

Whilst ESAM has been demonstrated in this thesis as a novel marker for functional HSCs post-expansion, and when combined with the ELSK strategy provides an improved correlation with transplantation success over ELSK alone, it still does not isolate HSCs to 100% purity. Before the robust roll-out of ESAM as a more widely-used reporter strategy, it would be beneficial to perform serial transplants of post-expansion $ESAM^+$ELSK (EELSK) cells using a limiting dilution assay (LDA) approach in order to more accurately calculate the

functional LT-HSC content of each well. This gold-standard transplantation approach would also be beneficial to apply to post-expansion CD321^{+}ELSK cells, as this marker combination also provides a promising readout for functional HSC content. Following the recent development of the RepopSig, a gene expression signature capable of identifying functional HSCs from multiple cellular states, including post-culture (Che and Bode, 2022), it would be interesting to score the EELSK fractions using qPCR for RepopSig target genes, relative to ELSK and LSK fractions. The RepopSig score is shown to not correlate directly with all MolO signature genes, perhaps highlighting the limited capacity of the MolO score to identify functional expanded HSCs.

The benefits of cytokine removal PVA cultures, where cytokines are removed at day 14 and media changes continue without cytokine supplementation, provide a sound financial benefit and additionally, in the case of specifically SCF removal, appear to actually improve culture outcomes. However, this data is so far based solely on flow cytometric analysis and calculation of ELSK frequency in the well which, despite being functionally validated in the sense that clones >20% ELSK are known to contain functional HSCs (Che and Bode, 2022), lacks the ability to quantify LT-HSC content within each population. Ideally, LDA serial transplantations would again be performed in order to robustly verify this finding, and to quantify HSC content.

7.2.2. Validation of MPL as a marker for fresh HSCs able to robustly expand in vitro

The development of novel isolation strategies for HSCs is an ongoing and evolving challenge in the field and to date the ESLAM isolation strategy is the gold-standard for mouse HSCs, whilst human culture systems typically rely on bulk CD34^{+} cells to initiate cultures. This thesis identified MPL as a promising marker for fresh HSCs that correlates strongly with culture success. In mouse HSCs, MPL^{-}ESLAM cells outperform MPL^{+}ESLAM cells in terms of higher EELSK, ELSK, and LSK outputs at the final timepoint. Interestingly however, it appears the opposite is the case for human PB cells, and the differences appear even more stark, where MPL^{-}CD34+ cells seem completely unable to expand in culture and often collapse entirely before the final time point, whilst MPL^{+}CD34^{+} cells are capable of robust expansion in 3a conditions.

A potential explanation for the poorer expansion performance of the sorted MPL^{+} ESLAM population is the possibility that the MPL antibody induces a transient partial blocking of MPL functionality via its binding, either as a result of disrupting the binding site or impeding receptor dimerisation. However, not all MPL molecules on the surface of every cell would be

bound by an antibody, leaving a residual level of MPL signalling. As a result, MPL^{+} sorted mouse cells may have overall reduced downstream signalling from MPL, which may explain the poorer outcomes given the known roles of MPL signalling in HSC self-renewal and maintenance (Audet et al., 2002). The differences in culture outcomes observed between $MPL^{+/-}$ fractions are smaller in mouse cells than in their human counterparts and could possibly be explained by the eventual internalisation of the blocked receptors and their conjugate antibodies, and the trafficking of newly formed and therefore unblocked MPL molecules to the cell surface, enabling the resumption of signalling. This could result in MPL^{+} cells initially expanding more slowly in culture, before expanding to maximal levels following internalisation of the receptor-antibody complex, and resupply of unaffected MPL molecules to the cell surface. Further studies, particularly focused on sampling expanding populations at varying time points over the course of expansion would be able to determine if this was the case.

Additionally, it is important to consider that the human samples, where the effect of $MPL^{+/-}$ sorting on culture outcomes was analysed, were myelofibrosis patient samples, presenting with mutant $JAK2^{V617F}$. As a result, we should expect some level of constituent activation of JAK2, a fundamental signalling protein downstream of MPL in these samples. Although the differences are stark, and robustly replicated in patients with varying variant allele frequencies, it would still be valuable to repeat these experiments with healthy mobilised peripheral blood samples to verify these differences are still observed.

As the differences in culture performance are dramatic, it would also be beneficial to test any *in vivo* functional discrepancies between the $MPL^{+/-}$ sorted fractions. This could easily be performed, firstly in mouse ESLAM cells, by the FACS sorting of fresh $MPL^{+/-}$ ESLAM cells, and direct transplant into sub-lethally irradiated W41 mice. Through performing peripheral bleeds over 6 months post-transplant, and utilising flow analysis to determine whether cells present in the peripheral blood are from donor/recipient origin, it would be easy to identify differences in repopulation capacity of these two fractions. To test human $CD34^{+}MPL^{+/-}$ performance *in vitro*, similarly structured xenograft assays would need to be performed. Additionally, a simpler *in vitro* CFU / LTC-IC assay for either mouse or human cells, combined with an LDA approach, would enable quantification of HSCs within each fraction. As neither human $CD34^{+}$, or mouse ESLAM identification strategies are able to isolate HSCs to complete purity, there is still the possibility that the $MPL^{+/-}$ fractions vary in their LT-HSC frequency, and this may also contribute to the observed differences in culture performance.

7.2.3. Determining the role of internalisation on MPL downstream signalling

A focus of the final results chapter of this thesis was on the specific and varying roles of TPO, and alternative TPO mimetics in an expansion context. TPO is a key haematopoietic cytokine and has long been used in HSC *in vitro* expansion cultures (Audet et al., 2002, Chou and Lodish, 2010, Wilkinson et al., 2020). In the context of *in vitro* expansion systems, cytokines provide an easy to use agonist for stimulating self-renewal. Coupled by the ability to reverse their effects upon removal, and that cytokines do not induce permanent modifications to DNA, they continue to be widely used in the field. As such, understanding the mechanism of action of these haematopoietic cytokines in the context of *in vitro* expansion systems is fundamental to furthering the field, and improving culture success. Most recently, Sakurai et al., developed a 3a expansion culture protocol for human cord blood HSCs, which replaced the two key cytokines SCF and TPO with chemical mimetics 740Y-P and butyzamide respectively. This thesis focused on deciphering the role of TPO and TPO-mimetics on the TPO receptor, MPL, and the associated downstream signalling induced by these molecules.

In order to begin deciphering any key differences in the mechanism of action of these molecules, internalisation assays were performed to determine the response of MPL to TPO and a range of alternative agonists (butyzamide, used in the 3a expansion culture system, and a selection of clinically used agonists: lusutrombopag, eltrombopag, romiplostim). Interestingly, only TPO and romiplostim, the only two of the selection of agonists that bind to the N-terminal domain of MPL, were capable of inducing robust internalisation. Furthermore, phosphoflow studies show that TPO and romiplostim induce the greatest levels of overall downstream signalling, but also reveal agonists incapable of inducing MPL internalisation did still induce moderate levels of downstream signalling, which shines the light on questioning the importance of internalisation of the receptor on subsequent signalling pathway activation. Additionally, the lack of butyzamide, or any TPO mimetic, in 3a expansion cultures results in the failure and collapse of expanding cells, therefore some level of MPL agonism is essential for HSC survival and expansion *in vitro*, even if the agonist doesn't induce internalisation. Whilst these studies are compelling and phosphoflow studies are backed up by independent phosphoproteomic experiments, these experiments were performed on cell lines, and so repetition of these now established and reliable assays in primary cell lines would be a logical next step forward.

Intriguingly, a study by Irannejad et al., proposed that receptors (in this example, β_2-adrenoceptors, a typical G-protein coupled receptor) are capable of being activated in the

early endosomal membrane, and that this population of internalised receptors actively contribute to the downstream cyclic AMP response (Irannejad et al., 2013). Since then, the role of endocytosed receptors in regulating downstream signalling has been highlighted in both GPCRs and receptor tyrosine kinases (von Zastrow and Sorkin, 2021). This raises the possibility that a certain degree of signalling is induced by all TPO-mimetics, regardless of any internalisation they induce of MPL, whilst the excess expanse of signalling observed downstream in cells treated with TPO and romiplostim results from additional signalling taking place from ligand-bound endocytosed receptors. In the future it would be interesting to validate the existence of downstream signalling induced specifically from internalised MPL, in order to corroborate this theory.

7.2.4. Potential applications of the novel Picowell platform for cell culture

On the engineering side, the fabrication, testing, and application of the novel Picowell chips, will enable real-time imaging of individual HSCs during their initial divisions when expanding *in vitro*. The strength of this chip lies in having several hundred wells in one field of view. As panning between wells is no longer needed, it enables shorter intervals between imaging and therefore increasingly accurate time-scales of the division process, in turn allowing easier analysis of results. Furthermore, the addition of a microfluidic channel to the Picowell design enables the possibility of constant perfusion of new media to the cells, allowing significantly longer culture times, and may enable us to start performing experiments such as intracellular staining on-chip.

With the protocol for Picowell development now established, adaptations of chip characteristics, such as well diameter and depth, are easy to implement, increasing the applicability of this platform to alternative cell types. Furthermore, the total matrix size can easily be scaled up, increasing the number of wells, and therefore the number of cells that can be cultured simultaneously. Additionally, the PDMS microfluidic channel structure which is laid over the Picowell chip can easily be modified, just requiring the construction of novel moulds with the required design, which is a relatively rapid process. Possible adaptations of the microfluidic channel which would be interesting to test would include the creation of 2 or 3 separate channels running in parallel over the Picowell array, with individual inlets and outlets, rather than the current design of the array being encased entirely in one channel. In this instance, each channel could contain, for example, a different media composition, and therefore imaging of the chip would allow concurrent imaging of cells in several conditions simultaneously. Additionally, experimental variability would be dramatically reduced between conditions, allowing direct comparisons in cellular proliferation and survival to be made.

The impact of the biophysical environment is well studied in the context of stem cell biology and the niche (Li et al., 2021) and this Picowell platform is particularly exciting in its potential to provide mechanical stressed to the cells cultured upon it, and therefore better mimic the cells natural microenvironment. Members of the Kent Lab have been using newly developed compression systems which utilise a network of pneumatic valves which lay upon the microfluidic channels and compress the device, and therefore the cells contained in the structure. Data gathered from the Kent Lab have provided exciting observations that compressive stress can influence HSC differentiation capacity, something that would be interesting to pursue further (Personal communication, Dr Rasha Rezk). If this pneumatic compression structure could be combined with the Picowell channel, it could facilitate on-chip immobilisation, compression, and subsequent imaging of individual HSPCs.

Whilst early tests of the Picowell design have used manual loading of cells via a pipette directly into the inlet of the microfluidic channel, the use of a syringe pump to provide a consistent flow would be a valuable addition. Also, as the cells loading onto a Picowell assay are contained in individual wells, they should be held in place which would allow the constant, gradual perfusion of fresh media from a syringe pump through the channel, providing nutrients and removing waste products to facilitate longer term cellular survival on-chip. An outlet tube into a vessel could then allow collection of flow through for further analysis. The possibility of simply reducing outlet size relative to inlet size also provides a promising alternative method to increase on-chip pressure and induce cellular compression.

7.2.5. Improving our understanding of, and functionally validating, the 3a expansion culture system

Historically, until the development of the most recent expansion systems for mouse and human HSCs: PVA culture system (Wilkinson et al., 2019), and 3a expansion cultures (Sakurai et al., 2023) respectively, the ability of scientists to maintain, let alone expand, HSCs *in vitro* was a huge challenge (Kumar et al., 2017). The field has largely relied on media supplemented with various hematopoietic cytokine combinations in order to support HSCs in an *in vitro* environment, however expansion of generally only 2-4 fold of functional HSCs was achieved in both mouse (LSK) and human ($CD34^+$) cells (Sauvageau et al., 2004). One study achieved a 10-fold expansion of human $CD34^+CD38^-$ cells over just 4 days of culture, however this study was hindered by a loss of all functional HSCs, capable of repopulating a mouse in a transplantation setting, by day 9 of the culture period (Bhatia et al., 1997). The more recent use of small molecules, such as UM171 and SR1 further

improved our ability to culture HSCs *in vitro.* Whilst SR1 supplementation into expansion media facilitated expansion of human umbilical cord CD34+ cells by an unprecedented 50-fold (Boitano et al., 2010), UM171 supplementation then proceeded to expanded human HSCs almost 100-fold and improved HSC culture purity 13-fold compared to DMSO treated controls (Fares et al., 2015). Importantly, UM171 is included in the 3a expansion culture system, and so remains a gold standard reagent for enhancing *in vitro* human HSC expansion. Combined with the replacement of key cytokines SCF and TPO with chemical mimetics 740Y-P and butyzamide, this paper achieved 30 days of unprecedented expansion of serially transplantable HSCs (Sakurai et al., 2023). Combined with the chemically defined, and therefore biocompatible, nature of the medium, this groundbreaking paper set the stage for a myriad of studies previously never possible of this cell type - historically limited either by HSC number, or the length of time cells were required to survive in culture.

Following the establishment of the 3a expansion system for human HSCs here at York, and the refinements made to increase expansion reliability for all sample types, the functional validation of 3a expanded HSCs is an important next step. This could come in the form of *in vitro* assays such as CFU or LTC-IC screens which would enable quantification of HSC fractions within the phenotypic HSC pool, currently used as a surrogate readout for functional HSCs in flow cytometric analysis of final day clones. Secondly, utilising xenograft transplantations of final day expanded human samples into immunodeficient mice (NSG/NOG) would enable validation of the presence of functional HSCs post-expansion capable of robust repopulation (Goyama et al., 2015). Additionally, by performing final day flow cytometric analysis for a range of markers of interest on a fraction of each well before transplantation, it would be possible, as this thesis has demonstrated in the mouse system, to correlate expression of certain markers within the pool with functional outcomes in xenograft settings. Analysis of fractions of 3a cultures at various time points over the entire expansion period would also be beneficial and would enable us to track changes in well composition over time as well as identify potentially predictive markers of culture success at earlier time points.

Alongside performing xenograft analysis on *in vitro* expanded populations, xenografts would be useful tools to enable us to refine our culture initiating populations, as when combined with an LDA strategy could quantify HSCs within populations of interest. An example that would nicely follow on from the work of this thesis would be to perform xenografts of primary $CD34^{+}$ $MPL^{+/-}$ fractions, and compare functional HSC content between them, given that we have observed significant differences in their culture performance between these two populations. This would allow us to determine if the stark differences in culture performance

are down to the lack of functional HSCs within the MPL^- pool, or that the HSCs present in that fraction are unable to survive in the *in vitro* culture environment.

Now the 3a system can reliably expand myelofibrosis patient samples, it would be valuable to move on to testing samples from patients with alternative blood disorders – such as ET, PV, and leukaemias. ET and PV samples would likely be more challenging as their peripheral $CD34^+$ counts would be lower than that of MF patients, but with further refinement to the starting material, and refinement to the culture system media components, the starting cell numbers required will hopefully decrease with time. With a plethora of work being done in the CRISPR and gene therapy space currently, the ability to combine these approaches with a selective expansion of successfully corrected cells, in order to achieve greater cell numbers for transplantation, would be transformative.

7.2.6. Further applications of the 3a culture system

Alongside the previously discussed benefits of improved expansion protocols where generating greater HSC numbers *in vitro* unlocks assays historically impossible to execute on this cell type, and improves HSC transplantation outcomes, a focus for the future is the applicability of cell and gene therapies to the HSC population. HSCs present a particularly exciting opportunity as a gene therapy target - due to their position at the apex of the haematopoietic hierarchy, a genetic correction within this pool would provide a haematopoietic system free from the mutation in all lineages (Sagoo and Gaspar, 2021).

Recent developments in the HSC gene therapy space have focused on monogenic diseases such as beta-thalassemia and sickle cell disease (Tucci et al., 2022, Spencer Chapman et al., 2023). Here, HSCs are collected from the patient, genetically edited to correct the mutation *in vitro*, and perfused back into the patient - it is easy to extrapolate the important role combining approaches such as this with gold-standard *in vitro* expansion of the successfully edited population would have in order to improve treatment outcomes. A recent study has successfully demonstrated this, using mouse HSCs genetically edited *in vitro* to correct a single point mutation before screening individual cells for desired and off-target mutations, and then expanding clonal populations from these cells, whilst maintaining their functional LT-HSC potential (Becker et al., 2023). In the future, translation of this work into the human HSCs, and attempts to perform gene therapy on more complex diseases would be ultimate goals, and would be groundbreaking in the fields of gene therapy and personalised medicine.

Furthermore, the lessons learnt from the culturing of HSCs and blood cells *in vitro* can be harnessed to perform directed differentiation of HSCs down specific lineages *in vitro.* This would provide large vats of mature, differentiated cells ready in order to meet ever increasing perfusion demands in the clinic (Bozhilov et al., 2023). For example, platelet transfusions are used to treat bleeding in those with thrombocytopenia and are a lifesaving, and increasingly used, treatment, however rely solely on donor provided cells. Being able to produce megakaryocytes and platelets en masse *in vitro* via directed differentiation from HSCs has therefore been a key focus of the haematology field, with approaches such as 3d culture systems, and culture media consisting of haematopoietic cytokines, human albumin, and small molecule supplements providing the most recent iterations (Yang et al., 2016, Guan et al., 2017). T- cells (Seet et al., 2017) and neutrophils (Dick et al., 2008) have also been able to be generated directly from HSC populations, however there are several lineage differentiation pathways still to define *in vitro*, and importantly increasing the scale of mature cell production.

7.2.7. Low cell number proteomic and phosphoproteomic analysis of primary HPSCs

Proteomics provides arguably the most insightful analysis of cells, and details the biological complexity of a sample far more than transcriptomic approaches which are unable to consider important post translational modifications. Additionally, several studies have identified a discordance between transcript and protein abundance (Liu et al., 2016, Buccitelli and Selbach, 2020), further strengthening the need for proteomic analysis of primary HSPC samples. However, the application of proteomic techniques to primary human HSPC samples still largely eludes us, with only a handful of studies to date attempting proteomic analysis of these populations (Klimmeck et al., 2012, Cabezas-Wallschied et al., 2014, Jassinskaja et al., 2017, Jassinskaja et al., 2021, Zaro et al., 2020). Despite years of development, this field has remained hindered by the typically high cell counts required for these protocols, with even the most recent studies still requiring counts of 50,000 mouse HSCs, and 25,000 human HSCs, and these limitations are compounded by the scarcity of the HSPC population,

In this thesis, an initial attempt at low cell number proteomics on primary human $CD34^+$ cells was performed, with sample sizes of 20 cells and over facilitating identification of a small number of protein hits from both healthy peripheral blood and blood from patients with myelofibrosis. Whilst a handful of significantly differentially expressed proteins were identified in the 200 cell samples between healthy donors and MF patients, variance remains high, and sample coverage remains too low to draw any accurate comparison between

conditions at this point. This thesis also details the phosphoproteomic analysis of UT7 cells (a human acute megakaryoblastic cell line) treated with either TPO, or a range of TPO-mimetics. Following a series of tests to refine desalting protocols and starting quantity, a minimum of 20µg of protein was found to be necessary to ensure a high count of phosphopeptide identifications (~10,000). Whilst the data gathered from this experiment identified key differences in the cells' response to MPL agonism by these alternative mimetics, 20µg is still a large quantity of protein to extract from primary human HSPCs, and would require cell counts of approximately 400,000.

A next logical step towards achieving robust proteomic data from low-input primary HSPC samples would be the testing of the recently published microPhos (µPhos) protocol on this sample type (Oliinyk et al., 2024). Through the limiting of liquid volumes at all steps of the protocol, and the reduction of sample transfer steps, the µPhos technique is able to identify 17,000 phosphosites from a 20µg sample size and 6,200 phosphosites from a 1µg sample, with approximately a 90% enrichment for phosphorylated proteins. With the possibility of just 1µg of protein needed, this would require primary HSPC counts of approximately 20,000 which are much more achievable, especially when combined with expansion protocols to increase sample size. Therefore, the combination of *in vitro* expansion protocols of sample types of interest (i.e. primary human cord blood / peripheral blood/ bone marrow aspirates) that would enable generation of the required cell counts, with subsequent proteomic/ phosphoproteomic analysis appears to be a promising avenue for future research, but remains hindered by the possibility of culture-induced changes to the proteome.

Ideally, the ultimate goal would be to develop robust single-cell proteomic techniques for human HSCs, which would help combat the myriad of issues associated with the known heterogeneity of the HSC pool that impact bulk studies. With a very recent preprint on bioRxiv using single-cell proteomics by Mass Spectrometry (scp-MS) of 2,500 individual human CD34+ cells to produce the first proteomic data set outlining the initial steps of the haematopoietic differentiation (Furtwängler et al., 2024), it appears that we are just entering an exciting stage in the field where these studies, although rare and still with limitations in data depth and variance, are finally coming to fruition. The advent of this technology is hugely important from a clinical perspective, facilitating a greater understanding of healthy and diseased cellular states, and in turn hopefully highlighting opportunities to exploit them to develop novel therapies.

7.2.8. Application of this work to fields outside haematology

Alongside the impact this work will have on the field of haematology, aspects of this project can be applied to other cell systems and related fields. HSCs are some of the most accessible stem cells and so are some of the most well studied and have provided us with an excellent model for studying the fundamental traits of tissue stem cells, the importance of a stem cell niche, the maintenance of genome integrity within stem cell populations, mechanisms governing stem cell self-renewal and differentiation, and the roles of stem cells in ageing and disease (Orkin and Zon, 2009, Beumer and Clevers, 2024). Therefore, the study of HSCs has wider reaching applications than just the haematopoietic system.

In particular, the heterogeneity within the HSC pool, and the model of a hierarchically ordered haematopoietic system with a stem cell population residing at the apex, has provided a strong basis in understanding the organisation of other high-turnover tissues such as the intestinal epithelium (Yousefi et al., 2018). Due to the similarities between these two hierarchies, much can be learnt from the more established haematopoietic field in order to further our understanding of intestinal stem cells, and guide therapeutic development in the intestinal epithelium - for example for colorectal cancers (Hervieu et al., 2021).

Outside of academia, the development of robust culturing systems, combined with functionally validated flow cytometric reporter strategies for HSCs as outlined in this thesis, establishes a useful screening platform. Applications of this system are wide ranging and include providing pharmaceutical companies an easy way to perform large scale screening of novel drug treatments for their effect on HSC self renewal without the costly and time-consuming requirement to transplant into mice in order to validate and quantify HSC content.

7.2.9. Conclusion

This is an exciting time for studying HSCs, with new protocols for expanding mouse HSCs *in vitro* being translated to human HSCs and the molecular drivers of haematological malignancies being mapped to an unprecedented level. This ability to produce large numbers of HSCs has opened the door to a wide range of experimental assays previously considered impossible to perform on HSCs owing to the scarcity of this cell type. Moreover, experiments that have required hundreds to thousands of mice can now be performed using only dozens, a particularly exciting development from a 3Rs perspective (replacement, reduction, and refinement of animals in research). As such, the next decade promises to enable researchers to dissect in detail the molecular mechanisms governing HSC behaviour at the level of the epigenome, transcriptome, proteome and signallome (Bode et al., 2021).

In addition to allowing large scale screens such as proteomics and metabolomics to be undertaken with sufficient cell numbers, improved expansion, particularly of human HSCs, would unlock a huge clinical benefit, with implications in BM rescue, gene therapy and a better understanding of childhood and adult leukaemias. The potential of achieving these highly sought-after clinical applications is closer than ever, due to the development of a new human HSC expansion protocol using a fully defined, synthetic, and clinically compatible media. We have most recently been able to further refine this 3a system to unlock the expansion of CD34 enriched cells from more easily accessible mobilised and non-mobilised peripheral blood samples from healthy donors and patients with MPNs.

8. References

Abramson, S., et al. (1977). "The identification in adult bone marrow of pluripotent and restricted stem cells of the myeloid and lymphoid systems." J Exp Med 145(6): 1567-1579.

Acar, M., et al. (2015). "Deep imaging of bone marrow shows non-dividing stem cells are mainly perisinusoidal." Nature 526(7571): 126.

Adamo, L., et al. (2009). "Biomechanical forces promote embryonic haematopoiesis." Nature 459(7250): 1131-1135.

Adolfsson, J., et al. (2005). "Identification of Flt3+ lympho-myeloid stem cells lacking erythro-megakaryocytic potential a revised road map for adult blood lineage commitment." Cell 121(2): 295-306.

Akashi, K., et al. (2000). "A clonogenic common myeloid progenitor that gives rise to all myeloid lineages." Nature 404(6774): 193-197.

Aksoz, M., et al. (2024). "Hematopoietic stem cell heterogeneity and age-associated platelet bias are evolutionarily conserved." Sci Immunol 9(98): eadk3469.

Allsopp, R. C., et al. (2001). "Telomere shortening accompanies increased cell cycle activity during serial transplantation of hematopoietic stem cells." J Exp Med 193(8): 917-924.

Alter, B. P. (2014). "Fanconi anemia and the development of leukemia." Best Pract Res Clin Haematol 27(3-4): 214-221.

Amon, S., et al. (2019). "Sensitive Quantitative Proteomics of Human Hematopoietic Stem and Progenitor Cells by Data-independent Acquisition Mass Spectrometry." Mol Cell Proteomics 18(7): 1454-1467.

Anjos-Afonso, F., et al. (2022). "Single cell analyses identify a highly regenerative and homogenous human CD34+ hematopoietic stem cell population." Nat Commun 13(1): 2048.

Audet, J., et al. (2001). "Distinct role of gp130 activation in promoting self-renewal divisions by mitogenically stimulated murine hematopoietic stem cells." Proc Natl Acad Sci U S A 98(4): 1757-1762.

Audet, J., et al. (2002). "Common and distinct features of cytokine effects on hematopoietic stem and progenitor cells revealed by dose-response surface analysis." Biotechnol Bioeng 80(4): 393-404.

Avgustinova, A. and S. A. Benitah (2016). "Epigenetic control of adult stem cell function." Nat Rev Mol Cell Biol 17(10): 643-658.

Azzoni, E., et al. (2021). "The onset of circulation triggers a metabolic switch required for endothelial to hematopoietic transition." Cell Rep 37(11): 110103.

Bai, T., et al. (2019). "Expansion of primitive human hematopoietic stem cells by culture in a zwitterionic hydrogel." Nat Med 25(10): 1566-1575.

Bain, F. M., et al. (2022). "Lessons from early life: understanding development to expand stem cells and treat cancers." Development 149(20).

Balazs, A. B., et al. (2006). "Endothelial protein C receptor (CD201) explicitly identifies hematopoietic stem cells in murine bone marrow." Blood **107**(6): 2317-2321.

Ballmaier, M., et al. (2003). "Thrombopoietin is essential for the maintenance of normal haematopoiesis in humans: development of aplastic anemia in patients with congenital amegakaryocytic thrombocytopenia." Ann N Y Acad Sci 996: 17-25.

Basheer, F., et al. (2019). "Contrasting requirements during disease evolution identify EZH2 as a therapeutic target in AML." J Exp Med 216(4): 966-981.

Bastani, S., et al. (2023). "The quest for the holy grail: overcoming challenges in expanding human hematopoietic stem cells for clinical use." Stem Cell Investig 10: 15.

Batsivari, A., et al. (2020). "Dynamic responses of the haematopoietic stem cell niche to diverse stresses." Nat Cell Biol 22(1): 7-17.

Becker, A. J., et al. (1965). "The Effect of Differing Demands for Blood Cell Production on DNA Synthesis by Hemopoietic Colony-Forming Cells of Mice." Blood 26: 296-308.

Becker, H. J., et al. (2023). "Controlling genetic heterogeneity in gene-edited hematopoietic stem cells by single-cell expansion." Cell Stem Cell **30**(7): 987-1000 e1008.

Beerman, I., et al. (2010). "Functionally distinct hematopoietic stem cells modulate hematopoietic lineage potential during aging by a mechanism of clonal expansion." Proc Natl Acad Sci U S A 107(12): 5465-5470.

Belluschi, S., et al. (2018). "Myelo-lymphoid lineage restriction occurs in the human haematopoietic stem cell compartment before lymphoid-primed multipotent progenitors." Nature Communications 9.

Benveniste, P., et al. (2010). "Intermediate-term hematopoietic stem cells with extended but time-limited reconstitution potential." Cell Stem Cell 6(1): 48-58.

Benz, C., et al. (2012). "Hematopoietic stem cell subtypes expand differentially during development and display distinct lymphopoietic programs." Cell Stem Cell 10(3): 273-283.

Beumer, J. and H. Clevers (2024). "Hallmarks of stemness in mammalian tissues." Cell Stem Cell 31(1): 7-24.

Bhatia, M., et al. (1997). "Quantitative analysis reveals expansion of human hematopoietic repopulating cells after short-term ex vivo culture." J Exp Med 186(4): 619-624.

Bigas, A. and L. Espinosa (2012). "Hematopoietic stem cells: to be or Notch to be." Blood 119(14): 3226-3235.

Bode, D., et al. (2021). "Exploiting Single-Cell Tools in Gene and Cell Therapy." Front Immunol 12: 702636

Boiers, C., et al. (2013). "Lymphomyeloid contribution of an immune-restricted progenitor emerging prior to definitive hematopoietic stem cells." Cell Stem Cell 13(5): 535-548.

Boitano, A. E., et al. (2010). "Aryl hydrocarbon receptor antagonists promote the expansion of human hematopoietic stem cells." Science 329(5997): 1345-1348.

Boulais, P. E. and P. S. Frenette (2015). "Making sense of hematopoietic stem cell niches." Blood 125(17): 2621-2629.

Bowie, M. B., et al. (2006). "Hematopoietic stem cells proliferate until after birth and show a reversible phase-specific engraftment defect." J Clin Invest 116(10): 2808-2816.

Bowie, M. B., et al. (2007a). "Identification of a new intrinsically timed developmental checkpoint that reprograms key hematopoietic stem cell properties." Proc Natl Acad Sci U S A 104(14): 5878-5882.

Bowie, M. B., et al. (2007b). "Steel factor responsiveness regulates the high self-renewal phenotype of fetal hematopoietic stem cells." Blood b(11): 5043-5048.

Bozhilov, Y. K., et al. (2023). "In Vitro Human Haematopoietic Stem Cell Expansion and Differentiation." Cells 12(6).

Brady, G et al., (1990). *Representative in Vitro cDNA Amplification From Individual Hemopoietic Cells and Colonies*. *METHODS IN MOLECULAR AND CELLULAR BIOLOGY* 2.

Brennan, P. J., et al. (2013). "Invariant natural killer T cells: an innate activation scheme linked to diverse effector functions." Nat Rev Immunol 13(2): 101-117.

Broudy, V. C. and N. L. Lin (2004). "AMG531 stimulates megakaryopoiesis in vitro by binding to Mpl." Cytokine 25(2): 52-60.

Bryder, D., et al. (2006). "Hematopoietic stem cells: the paradigmatic tissue-specific stem cell." Am J Pathol 169(2): 338-346.

Buccitelli, C. and M. Selbach (2020). "mRNAs, proteins and the emerging principles of gene expression control." Nat Rev Genet 21(10): 630-644.

Buckley, S. M., et al. (2011). "Maintenance of HSC by Wnt5a secreting AGM-derived stromal cell line." Experimental Hematology 39(1): 114-123 e111-115.

Busch, K., et al. (2015). "Fundamental properties of unperturbed haematopoiesis from stem cells in vivo." Nature 518(7540): 542-546.

Bussel, J. B., et al. (2021). "A Review of Romiplostim Mechanism of Action and Clinical Applicability." Drug Des Devel Ther 15: 2243-2268.

Cabezas-Wallscheid, N., et al. (2014). "Identification of regulatory networks in HSCs and their immediate progeny via integrated proteome, transcriptome, and DNA methylome analysis." Cell Stem Cell 15(4): 507-522.

Cabezas-Wallscheid, N., et al. (2017). "Vitamin A-Retinoic Acid Signaling Regulates Hematopoietic Stem Cell Dormancy." Cell 169(5): 807-823 e819.

Camacho, V., et al. (2017). "Regulation of normal and leukemic stem cells through cytokine signaling and the microenvironment." Int J Hematol 105(5): 566-577.

Campanelli, R., et al. (2021). "New Markers of Disease Progression in Myelofibrosis." Cancers (Basel) 13(21).

Cao, Y., et al. (2022). "Overexpression of miR-17 predicts adverse prognosis and disease recurrence for acute myeloid leukemia." Int J Clin Oncol 27(7): 1222-1232.

Carrelha, J., et al. (2024). "Alternative platelet differentiation pathways initiated by nonhierarchically related hematopoietic stem cells." Nat Immunol 25(6): 1007-1019.

Challen, G. A., et al. (2010). "Distinct hematopoietic stem cell subtypes are differentially regulated by TGF-beta1." Cell Stem Cell 6(3): 265-278.

Che, J. L. C and Bode (2022). "Identification and characterization of in vitro expanded hematopoietic stem cells." EMBO Rep 23(10): e55502

Chen, D. W., et al. (2024). "Inflammatory recruitment of healthy hematopoietic stem and progenitor cells in the acute myeloid leukemia niche." Leukemia 38(4): 741-750.

Chen, J. Y., et al. (2016). "Hoxb5 marks long-term haematopoietic stem cells and reveals a homogenous perivascular niche." Nature 530(7589): 223-227.

Chen, M. J., et al. (2009). "Runx1 is required for the endothelial to haematopoietic cell transition but not thereafter." Nature 457(7231): 887-891.

Cheng, G. (2012). "Eltrombopag, a thrombopoietin- receptor agonist in the treatment of adult chronic immune thrombocytopenia: a review of the efficacy and safety profile." Ther Adv Hematol 3(3): 155-164.

Cheng, H., et al. (2020). "New paradigms on hematopoietic stem cell differentiation." Protein Cell 11(1): 34-44.

Cheng, T., et al. (2000). "Hematopoietic stem cell quiescence maintained by p21cip1/waf1." Science 287(5459): 1804-1808.

Cheshier, S. H., et al. (1999). "In vivo proliferation and cell cycle kinetics of long-term self-renewing hematopoietic stem cells." Proc Natl Acad Sci U S A b(6): 3120-3125.

Cho, R. H., et al. (2008). "A new mechanism for the aging of hematopoietic stem cells: aging changes the clonal composition of the stem cell compartment but not individual stem cells." Blood 111(12): 5553-5561.

Chou, S. and H. F. Lodish (2010). "Fetal liver hepatic progenitors are supportive stromal cells for hematopoietic stem cells." Proc Natl Acad Sci U S A 107(17): 7799-7804.

Chua, K. N., et al. (2006). "Surface-aminated electrospun nanofibers enhance adhesion and expansion of human umbilical cord blood hematopoietic stem/progenitor cells." Biomaterials 27(36): 6043-6051.

Christensen, J. L., et al. (2004). "Circulation and chemotaxis of fetal hematopoietic stem cells." PLoS Biol 2(3): E75.

Copley, M. R., et al. (2013). "The Lin28b-let-7-Hmga2 axis determines the higher self-renewal potential of fetal haematopoietic stem cells." Nat Cell Biol 15(8): 916-925

Copley, M. R. and C. J. Eaves (2013). "Developmental changes in hematopoietic stem cell properties." Exp Mol Med 45: e55.

Cornish, N., et al. (2020). "Monoallelic loss-of-function THPO variants cause heritable thrombocytopenia." Blood Adv 4(5): 920-924.

Crisan, M. and E. Dzierzak (2016). "The many faces of hematopoietic stem cell heterogeneity." Development 143(24): 4571-4581.

Crozatier, M. and A. Vincent (2011). "Drosophila: a model for studying genetic and molecular aspects of haematopoiesis and associated leukaemias." Dis Model Mech 4(4): 439-445.

Cunniff, C., et al. (2017). "Bloom's Syndrome: Clinical Spectrum, Molecular Pathogenesis, and Cancer Predisposition." Mol Syndromol 8(1): 4-23.

Dahlen, D. D., et al. (2003). "Internalization of the thrombopoietin receptor is regulated by 2 cytoplasmic motifs." Blood 102(1): 102-108.

Dahlin, J. S., et al. (2018). "A single-cell hematopoietic landscape resolves 8 lineage trajectories and defects in Kit mutant mice." Blood 131(21): e1-e11.

Das, H., et al. (2009). "Ex vivo nanofiber expansion and genetic modification of human cord blood-derived progenitor/stem cells enhances vasculogenesis." Cell Transplant 18(3): 305-318.

de Graaf, C. A. and D. Metcalf (2011). "Thrombopoietin and hematopoietic stem cells." Cell Cycle 10(10): 1582-1589.

de Haan, G. and S. S. Lazare (2018). "Aging of hematopoietic stem cells." Blood 131(5): 479-487.

de Lima, M., et al. (2012). "Cord-blood engraftment with ex vivo mesenchymal-cell coculture." N Engl J Med 367(24): 2305-2315.

Dellorusso, P. V., et al. (2024). "Autophagy counters inflammation-driven glycolytic impairment in aging hematopoietic stem cells." Cell Stem Cell 31(7): 1020-1037 e1029.

Dehdilani, N., et al. (2016). "Improved Survival and Hematopoietic Differentiation of Murine Embryonic Stem Cells on Electrospun Polycaprolactone Nanofiber." Cell J 17(4): 629-638.

Derks, L. L. M. and R. van Boxtel (2023). "Stem cell mutations, associated cancer risk, and consequences for regenerative medicine." Cell Stem Cell 30(11): 1421-1433.

de Pooter, R. F., et al. (2019). "Cutting Edge: Lymphomyeloid-Primed Progenitor Cell Fates Are Controlled by the Transcription Factor Tal1." J Immunol 202(10): 2837-2842.

de Swart, L., et al. (2020). "Impact of red blood cell transfusion dose density on progression-free survival in patients with lower-risk myelodysplastic syndromes." Haematologica 105(3): 632-639.

Dias, S., et al. (2008). "E2A proteins promote development of lymphoid-primed multipotent progenitors." Immunity 29(2): 217-227.

Dick, E. P., et al. (2008). "Ex vivo-expanded bone marrow CD34+ derived neutrophils have limited bactericidal ability." Stem Cells 26(10): 2552-2563.

Dick, J. E., et al. (1985). "Introduction of a selectable gene into primitive stem cells capable of long-term reconstitution of the hemopoietic system of W/Wv mice." Cell 42(1): 71-79.

Ding, L., et al. (2012). "Endothelial and perivascular cells maintain haematopoietic stem cells." Nature 481(7382): 457-462.

Dou, M., et al. (2019). "High-Throughput Single Cell Proteomics Enabled by Multiplex Isobaric Labeling in a Nanodroplet Sample Preparation Platform." Anal Chem 91(20): 13119-13127.

Doulatov, S., et al. (2012). "Hematopoiesis: a human perspective." Cell Stem Cell 10(2): 120-136.

Drachman, J. G., et al. (1999). "Thrombopoietin signal transduction requires functional JAK2, not TYK2." J Biol Chem 274(19): 13480-13484.

Duncan, A. W., et al. (2005). "Integration of Notch and Wnt signaling in hematopoietic stem cell maintenance." Nat Immunol 6(3): 314-322.

Dusa, A., et al. (2010). "JAK2 V617F Constitutive Activation Requires JH2 Residue F595: A Pseudokinase Domain Target for Specific Inhibitors." Plos One 5(6).

Dykstra, B., et al. (2007). "Long-term propagation of distinct hematopoietic differentiation programs in vivo." Cell Stem Cell 1(2): 218-229.

Dykstra, B., et al. (2011). "Clonal analysis reveals multiple functional defects of aged murine hematopoietic stem cells." J Exp Med 208(13): 2691-2703.

Dzierzak, E. (2002). "Hematopoietic stem cells and their precursors: developmental diversity and lineage relationships." Immunol Rev 187: 126-138.

Dzierzak, E. and A. Bigas (2018). "Blood Development: Hematopoietic Stem Cell Dependence and Independence." Cell Stem Cell 22(5): 639-651.

Dzierzak, E. and A. Medvinsky (1995). "Mouse embryonic hematopoiesis." Trends Genet 11(9): 359-366.

Eaves, C. J. (2015). "Hematopoietic stem cells: concepts, definitions, and the new reality." Blood 125(17): 2605-2613.

Eliasson, P. and J. I. Jonsson (2010). "The hematopoietic stem cell niche: low in oxygen but a nice place to be." J Cell Physiol 222(1): 17-22.

Ema, H., et al. (2005). "Quantification of self-renewal capacity in single hematopoietic stem cells from normal and Lnk-deficient mice." Dev Cell 8(6): 907-914.

Ema, H., et al. (2014). "Heterogeneity and hierarchy of hematopoietic stem cells." Exp Hematol 42(2): 74-82 e72.

Ema, H. and H. Nakauchi (2000). "Expansion of hematopoietic stem cells in the developing liver of a mouse embryo." Blood 95(7): 2284-2288.

Esfahani, H., et al. (2017). "Electrospun Ceramic Nanofiber Mats Today: Synthesis, Properties, and Applications." Materials (Basel) 10(11).

Fabre, M. A., et al. (2022). "The longitudinal dynamics and natural history of clonal haematopoiesis." Nature 606(7913): 335-342.

Fares, I., et al. (2014). "Cord blood expansion. Pyrimidoindole derivatives are agonists of human hematopoietic stem cell self-renewal." Science 345(6203): 1509-1512.

Fares, I., et al. (2017). "EPCR expression marks UM171-expanded CD34(+) cord blood stem cells." Blood 129(25): 3344-3351.

Fatima, S., et al. (2012). "Abcg2 Expression Marks Tissue-Specific Stem Cells in Multiple Organs in a Mouse Progeny Tracking Model." Stem Cells 30(2): 210-221.

Ferguson, V. L., et al. (2003). "Bone development and age-related bone loss in male C57BL/6J mice." Bone 33(3): 387-398.

Fernandez-Zapata, C., et al. (2020). "The use and limitations of single-cell mass cytometry for studying human microglia function." Brain Pathol 30(6): 1178-1191.

Fitch, B. A., et al. (2022). "Decreased IL-10 accelerates B-cell leukemia/lymphoma in a mouse model of pediatric lymphoid leukemia." Blood Adv 6(3): 854-865.

Flach, J., et al. (2014). "Replication stress is a potent driver of functional decline in ageing haematopoietic stem cells." Nature 512(7513): 198-202.

Flanagan, J. G., et al. (1991). "Transmembrane form of the kit ligand growth factor is determined by alternative splicing and is missing in the Sld mutant." Cell 64(5): 1025-1035.

Foudi, A., et al. (2009). "Analysis of histone 2B-GFP retention reveals slowly cycling hematopoietic stem cells." Nat Biotechnol 27(1): 84-90.

Frame, J. M., et al. (2016). "Definitive Hematopoiesis in the Yolk Sac Emerges from Wnt-Responsive Hemogenic Endothelium Independently of Circulation and Arterial Identity." Stem Cells 34(2): 431-444.

Fukuhara, T., et al. (2017). "A novel immunotoxin reveals a new role for CD321 in endothelial cells." PLoS One 12(10): e0181502.

Fumagalli, F., et al. (2022). "Lentiviral haematopoietic stem-cell gene therapy for early-onset metachromatic leukodystrophy: long-term results from a non-randomised, open-label, phase 1/2 trial and expanded access." Lancet 399(10322): 372-383.

Furtwängler, B., et al. (2024). "Mapping the human hematopoietic stem and progenitor cell hierarchy through integrated single-cell proteomics and transcriptomics." bioRxiv: 2024.2007.2005.602277.

Ganuza, M., et al. (2022). "Murine foetal liver supports limited detectable expansion of life-long haematopoietic progenitors." Nat Cell Biol 24(10): 1475-1486.

Gazit R, et al. (2014). “Fgd5 identifies hematopoietic stem cells in the murine bone marrow”. J Exp Med.211(7):1315-31.

Geddis, A. E. (2010). "Megakaryopoiesis." Semin Hematol 47(3): 212-219.

Gekas, C., et al. (2010). "Hematopoietic stem cell development in the placenta." Int J Dev Biol 54(6-7): 1089-1098.

Gerritsen, J. S. and F. M. White (2021). "Phosphoproteomics: a valuable tool for uncovering molecular signaling in cancer cells." Expert Rev Proteomics 18(8): 661-674.

Gery, S., et al. (2009). "Lnk inhibits myeloproliferative disorder-associated JAK2 mutant, JAK2V617F." J Leukoc Biol 85(6): 957-965.

Gilfillan, S., et al. (1993). "Mice lacking TdT: mature animals with an immature lymphocyte repertoire." Science 261(5125): 1175-1178.

Gilfillan, A. M. and M. A. Beaven (2011). "Regulation of mast cell responses in health and disease." Crit Rev Immunol 31(6): 475-529.

Glotzbach, J. P., et al. (2011). "An information theoretic, microfluidic-based single cell analysis permits identification of subpopulations among putatively homogeneous stem cells." PLoS One 6(6): e21211.

Greenfield, G., et al. (2021). "Molecular pathogenesis of the myeloproliferative neoplasms." Journal of Hematology & Oncology 14(1).

Greenfield, G., et al. (2018). "The ruxolitinib effect: understanding how molecular pathogenesis and epigenetic dysregulation impact therapeutic efficacy in myeloproliferative neoplasms." Journal of Translational Medicine 16.

Goodell, M. A., et al. (1996). "Isolation and functional properties of murine hematopoietic stem cells that are replicating in vivo." J Exp Med 183(4): 1797-1806.

Gou, P. H., et al. (2022). "Insights into the Potential Mechanisms of JAK2V617F Somatic Mutation Contributing Distinct Phenotypes in Myeloproliferative Neoplasms." International Journal of Molecular Sciences 23(3).

Goyama, S., et al. (2015). "Xenograft models for normal and malignant stem cells." Blood 125(17): 2630-2640.

Guan, X., et al. (2017). "Safety and Efficacy of Megakaryocytes Induced from Hematopoietic Stem Cells in Murine and Nonhuman Primate Models." Stem Cells Transl Med 6(3): 897-909.

Guo, G., et al. (2013). "Mapping cellular hierarchy by single-cell analysis of the cell surface repertoire." Cell Stem Cell 13(4): 492-505.

Guo, S., et al. (2010). "MicroRNA miR-125a controls hematopoietic stem cell number." Proc Natl Acad Sci U S A 107(32): 14229-14234.

Haas, S., et al. (2015). "Inflammation-Induced Emergency Megakaryopoiesis Driven by Hematopoietic Stem Cell-like Megakaryocyte Progenitors." Cell Stem Cell 17(4): 422-434.

Haas, S., et al. (2018). "Causes and Consequences of Hematopoietic Stem Cell Heterogeneity." Cell Stem Cell 22(5): 627-638.

Hall, T. D., et al. (2022). "Murine fetal bone marrow does not support functional hematopoietic stem and progenitor cells until birth." Nat Commun 13(1): 5403.

Hallal, M., et al. (2017). "Characterization of Kinase Activity By Phosphoproteomics in Myeloid Cell Lines for Identification of Driving Oncogenic Pathways." Blood 130(Supplement 1): 2515-2515.

Hamanaka, S., et al. (2013). "Generation of transgenic mouse line expressing Kusabira Orange throughout body, including erythrocytes, by random segregation of provirus method." Biochem Biophys Res Commun 435(4): 586-591.

Hamey, F. K. and B. Gottgens (2019). "Machine learning predicts putative hematopoietic stem cells within large single-cell transcriptomics data sets." Exp Hematol 78: 11-20.

Han, Y. C., et al. (2010). "microRNA-29a induces aberrant self-renewal capacity in hematopoietic progenitors, biased myeloid development, and acute myeloid leukemia." J Exp Med 207(3): 475-489.

Hardy, R. R. and K. Hayakawa (1991). "A developmental switch in B lymphopoiesis." Proc Natl Acad Sci U S A 88(24): 11550-11554.

Harrison, D. E., et al. (1989). "Numbers and functions of transplantable primitive immunohematopoietic stem cells. Effects of age." J Immunol 142(11): 3833-3840.

Hasselbalch, H. C. and M. E. Bjorn (2015). "MPNs as Inflammatory Diseases: The Evidence, Consequences, and Perspectives." Mediators Inflamm 2015: 102476.

Heinrich, M. C., et al. (1993). "Constitutive expression of steel factor gene by human stromal cells." Blood 82(3): 771-783.

Hernandez-Valladares, M., et al. (2020). "The Implementation of Mass Spectrometry-Based Proteomics Workflows in Clinical Routines of Acute Myeloid Leukemia: Applicability and Perspectives." Int J Mol Sci 21(18).

Herr, L. M., et al. (2024). "Replication stress as a driver of cellular senescence and aging." Commun Biol 7(1): 616.

Hervieu, C., et al. (2021). "The Role of Cancer Stem Cells in Colorectal Cancer: From the Basics to Novel Clinical Trials." Cancers (Basel) 13(5).

Hidalgo, I., et al. (2022). "Bmi1 induction protects hematopoietic stem cells against pronounced long-term hematopoietic stress." Exp Hematol 109: 35-44.

Hitchcock, I. S., et al. (2008). "YRRL motifs in the cytoplasmic domain of the thrombopoietin receptor regulate receptor internalization and degradation." Blood 112(6): 2222-2231.

Hitchcock, I. S., et al. (2021). "The thrombopoietin receptor: revisiting the master regulator of platelet production." Platelets 32(6): 770-778.

Holmfeldt, P., et al. (2016). "Correction: Functional screen identifies regulators of murine hematopoietic stem cell repopulation." J Exp Med 213(11): 2525

Ho, T. T., et al. (2017). "Autophagy maintains the metabolism and function of young and old stem cells." Nature 543(7644): 205-210.

Ho, Y. H., et al. (2019). "Remodeling of Bone Marrow Hematopoietic Stem Cell Niches Promotes Myeloid Cell Expansion during Premature or Physiological Aging." Cell Stem Cell 25(3): 407-418 e406.

Hoffman, W., et al. (2016). "B Cells, Antibodies, and More." Clin J Am Soc Nephrol 11(1): 137-154.

Holinstat, M. (2017). "Normal platelet function." Cancer Metastasis Rev 36(2): 195-198.

Honey, K. (2005). “Notch balances self-renewal and differentiation.” Nat Rev Immunol 5, 184.

Hordyjewska, A., et al. (2015). "Characteristics of hematopoietic stem cells of umbilical cord blood." Cytotechnology 67(3): 387-396.

Hormaechea-Agulla, D., et al. (2021). "Chronic infection drives Dnmt3a-loss-of-function clonal hematopoiesis via IFNgamma signaling." Cell Stem Cell 28(8): 1428-1442 e1426.

Horton, P. D., et al. (2021). "Biomechanical Regulation of Hematopoietic Stem Cells in the Developing Embryo." Curr Tissue Microenviron Rep 2(1): 1-15.

How, J., et al. (2019). "Mutant calreticulin in myeloproliferative neoplasms." Blood 134(25): 2242-2248.

Huang, E. J., et al. (1992). "Differential expression and processing of two cell associated forms of the kit-ligand: KL-1 and KL-2." Mol Biol Cell 3(3): 349-362.

Huang, W., et al. (2019). "Regulatory networks in mechanotransduction reveal key genes in promoting cancer cell stemness and proliferation." Oncogene 38(42): 6818-6834.

Huang, X., et al. (2007). "Hematopoietic stem cells: generation and self-renewal." Cell Death Differ 14(11): 1851-1859.

Hughes, C. S., et al. (2019). "Single-pot, solid-phase-enhanced sample preparation for proteomics experiments." Nat Protoc 14(1): 68-85.

Hughes, J. M., et al. (2015). "C/EBPalpha-p30 protein induces expression of the oncogenic long non-coding RNA UCA1 in acute myeloid leukemia." Oncotarget 6(21): 18534-18544.

Ikuta, K., et al. (1990). "A developmental switch in thymic lymphocyte maturation potential occurs at the level of hematopoietic stem cells." Cell 62(5): 863-874.

Irannejad, R., et al. (2013). "Conformational biosensors reveal GPCR signalling from endosomes." Nature 495(7442): 534-538.

Ishibashi, T., et al. (2016). "ESAM is a novel human hematopoietic stem cell marker associated with a subset of human leukemias." Exp Hematol 44(4): 269-281 e261.

Islam, M., et al. (2017). "Microfluidic Sorting of Cells by Viability Based on Differences in Cell Stiffness." Sci Rep 7(1): 1997.

Itkin, T., et al. (2016). "Distinct bone marrow blood vessels differentially regulate haematopoiesis." Nature 532(7599): 323-328.

Ito, K., et al. (2004). "Regulation of oxidative stress by ATM is required for self-renewal of haematopoietic stem cells." Nature 431(7011): 997-1002.

Ito, K., et al. (2006). "Reactive oxygen species act through p38 MAPK to limit the lifespan of hematopoietic stem cells." Nat Med 12(4): 446-451.

Ito, K. and T. Suda (2014). "Metabolic requirements for the maintenance of self-renewing stem cells." Nat Rev Mol Cell Biol 15(4): 243-256.

Itokawa, N., et al. (2022). "Epigenetic traits inscribed in chromatin accessibility in aged hematopoietic stem cells." Nat Commun 13(1): 2691.

Iwasaki, H., et al. (2005). "Distinctive and indispensable roles of PU.1 in maintenance of hematopoietic stem cells and their differentiation." Blood 106(5): 1590-1600.

Jacobson, L. O., et al. (1951). "Recovery from radiation injury." Science 113(2940): 510-511.

Jaiswal, S., et al. (2014). "Age-related clonal hematopoiesis associated with adverse outcomes." N Engl J Med 371(26): 2488-2498.

Jassinskaja, M., et al. (2017). "Comprehensive Proteomic Characterization of Ontogenic Changes in Hematopoietic Stem and Progenitor Cells." Cell Rep 21(11): 3285-3297.

Jassinskaja, M., et al. (2021). "Ontogenic shifts in cellular fate are linked to proteotype changes in lineage-biased hematopoietic progenitor cells." Cell Rep 34(12): 108894.

Jassinskaja, M., et al. (2023). "Resolving the hematopoietic stem cell state by linking functional and molecular assays." Blood 142(6): 543-552.

Jassinskaja, M. and J. Hansson (2022). "The Opportunity of Proteomics to Advance the Understanding of Intra- and Extracellular Regulation of Malignant Hematopoiesis." Front Cell Dev Biol 10: 824098.

Johnson, C. S., et al. (2024). "Adaptation to ex vivo culture reduces human hematopoietic stem cell activity independently of cell cycle." Blood.

Jordan, C. T. and I. R. Lemischka (1990). "Clonal and systemic analysis of long-term hematopoiesis in the mouse." Genes Dev 4(2): 220-232.

Joshi, P. M., et al. (2010). "Caenorhabditis elegans as a model for stem cell biology." Dev Dyn 239(5): 1539-1554.

Kamminga, L. M., et al. (2006). "The Polycomb group gene Ezh2 prevents hematopoietic stem cell exhaustion." Blood 107(5): 2170-2179.

Karlmark, K. R., et al. (2012). "Monocytes in health and disease - Minireview." Eur J Microbiol Immunol (Bp) 2(2): 97-102.

Karpova, D., et al. (2019). "Mobilized peripheral blood: an updated perspective." F1000Res 8.

Keller, G., et al. (1985). "Expression of a foreign gene in myeloid and lymphoid cells derived from multipotent haematopoietic precursors." Nature 318(6042): 149-154.

Kempf, J. M., et al. (2021). "Loss-of-function mutations in the histone methyltransferase EZH2 promote chemotherapy resistance in AML." Sci Rep 11(1): 5838.

Kent, D. G., et al. (2008a). "Steel factor coordinately regulates the molecular signature and biologic function of hematopoietic stem cells." Blood 112(3): 560-567.

Kent, D. G., et al. (2008b). "Regulation of hematopoietic stem cells by the steel factor/KIT signaling pathway." Clin Cancer Res 14(7): 1926-1930.

Kent, D. G., et al. (2009). "Prospective isolation and molecular characterization of hematopoietic stem cells with durable self-renewal potential." Blood 113(25): 6342-6350.

Khoury, J. D., et al. (2022). "The 5th edition of the World Health Organization Classification of Haematolymphoid Tumours: Myeloid and Histiocytic/Dendritic Neoplasms." Leukemia 36(7): 1703-1719.

Kiel, M. J., et al. (2005). "SLAM family receptors distinguish hematopoietic stem and progenitor cells and reveal endothelial niches for stem cells." Cell 121(7): 1109-1121.

Kim, I., et al. (2007). "Sox17 dependence distinguishes the transcriptional regulation of fetal from adult hematopoietic stem cells." Cell 130(3): 470-483.

Kim, P. G., et al. (2016). "Interferon-alpha signaling promotes embryonic HSC maturation." Blood 128(2): 204-216.

Kimura, S., et al. (1998). "Hematopoietic stem cell deficiencies in mice lacking c-Mpl, the receptor for thrombopoietin." Proc Natl Acad Sci U S A 95(3): 1195-1200.

Klauke, K., et al. (2013). "Polycomb Cbx family members mediate the balance between haematopoietic stem cell self-renewal and differentiation." Nat Cell Biol 15(4): 353-362.

Klimmeck, D., et al. (2012). "Proteomic cornerstones of hematopoietic stem cell differentiation: distinct signatures of multipotent progenitors and myeloid committed cells." Mol Cell Proteomics 11(8): 286-302.

Knapp, D. J., et al. (2017). "Distinct signaling programs control human hematopoietic stem cell survival and proliferation." Blood 129(3): 307-318.

Kohli, L. and E. Passegue (2014). "Surviving change: the metabolic journey of hematopoietic stem cells." Trends Cell Biol 24(8): 479-487.

Kondo, M., et al. (1997). "Identification of clonogenic common lymphoid progenitors in mouse bone marrow." Cell 91(5): 661-672.

Koide, S., et al. (2022). "CD244 expression represents functional decline of murine hematopoietic stem cells after in vitro culture." iScience 25(1): 103603.

Kondo, M. (2010). "Lymphoid and myeloid lineage commitment in multipotent hematopoietic progenitors." Immunol Rev

Koschmieder, S., et al. (2016). "Myeloproliferative neoplasms and inflammation: whether to target the malignant clone or the inflammatory process or both." Leukemia 30(5): 1018-1024.

Kovtonyuk, L. V., et al. (2016). "Inflamm-Aging of Hematopoiesis, Hematopoietic Stem Cells, and the Bone Marrow Microenvironment." Front Immunol 7: 502.

Kristiansen, T. A., et al. (2016). "Cellular Barcoding Links B-1a B Cell Potential to a Fetal Hematopoietic Stem Cell State at the Single-Cell Level." Immunity 45(2): 346-357.

Kristiansen, T. A., et al. (2022). "Developmental cues license megakaryocyte priming in murine hematopoietic stem cells." Blood Adv.

Krystel-Whittemore, M., et al. (2015). "Mast Cell: A Multi-Functional Master Cell." Front Immunol 6: 620.

Kucinski, I., et al. (2024). "A time- and single-cell-resolved model of murine bone marrow hematopoiesis." Cell Stem Cell 31(2): 244-259 e210.

Kulak, N. A., et al. (2014). "Minimal, encapsulated proteomic-sample processing applied to copy-number estimation in eukaryotic cells." Nat Methods 11(3): 319-324.

Kumar, S. and H. Geiger (2017). "HSC Niche Biology and HSC Expansion Ex Vivo." Trends Mol Med 23(9): 799-819.

Kunisaki, Y., et al. (2013). "Arteriolar niches maintain haematopoietic stem cell quiescence." Nature 502(7473): 637-643.

Kuranda, K., et al. (2011). "Age-related changes in human hematopoietic stem/progenitor cells." Aging Cell 10(3): 542-546.

La Motte-Mohs, R. N., et al. (2005). "Induction of T-cell development from human cord blood hematopoietic stem cells by Delta-like 1 in vitro." Blood 105(4): 1431-1439.

Lansbergen, G., et al. (2006). "CLASPs attach microtubule plus ends to the cell cortex through a complex with LL5beta." Dev Cell 11(1): 21-32.

Laurenti, E., et al. (2015). "CDK6 levels regulate quiescence exit in human hematopoietic stem cells." Cell Stem Cell 16(3): 302-313.

Laurenti, E. and B. Gottgens (2018). "From haematopoietic stem cells to complex differentiation landscapes." Nature **553**(7689): 418-426.

LeBien, T. W. and T. F. Tedder (2008). "B lymphocytes: how they develop and function." Blood 112(5): 1570-1580.

Lee, H. J., et al. (2013). "Biomechanical force in blood development: extrinsic physical cues drive pro-hematopoietic signaling." Differentiation 86(3): 92-103.

Lee, Y., et al. (2017). "Extrinsic regulation of hematopoietic stem cells in development, homeostasis and diseases." Wiley Interdiscip Rev Dev Biol 6(5).

Lemieux, M. E., et al. (1995). "Characterization and purification of a primitive hematopoietic cell type in adult mouse marrow capable of lymphomyeloid differentiation in long-term marrow "switch" cultures." Blood 86(4): 1339-1347.

Lendeckel, U., et al. (2022). "Macrophages: shapes and functions." ChemTexts 8(2): 12.

Lennartsson, J. and L. Ronnstrand (2012). "Stem cell factor receptor/c-Kit: from basic science to clinical implications." Physiol Rev 92(4): 1619-1649.

Lessard, J. and G. Sauvageau (2003). "Bmi-1 determines the proliferative capacity of normal and leukaemic stem cells." Nature 423(6937): 255-260.

Levy, G., et al. (2020). "MPL mutations in essential thrombocythemia uncover a common path of activation with eltrombopag dependent on W491." Blood 135(12): 948-953.

Lewis, K., et al. (2021). "Fetal liver hematopoiesis: from development to delivery." Stem Cell Res Ther 12(1): 139.

Li, B., et al. (2016). "Colony-forming unit cell (CFU-C) assays at diagnosis: CFU-G/M cluster predicts overall survival in myelodysplastic syndrome patients independently of IPSS-R." Oncotarget 7(42): 68023-68032.

Li, H., et al. (2021). "Biomechanical cues as master regulators of hematopoietic stem cell fate." Cell Mol Life Sci 78(16): 5881-5902.

Li, Y., et al. (2014). "Inflammatory signaling regulates embryonic hematopoietic stem and progenitor cell production." Genes Dev 28(23): 2597-2612.

Li, Y., et al. (2020). "Single-Cell Analysis of Neonatal HSC Ontogeny Reveals Gradual and Uncoordinated Transcriptional Reprogramming that Begins before Birth." Cell Stem Cell 27(5): 732-747 e737.

Li, Y. and J. A. Magee (2021). "Transcriptional reprogramming in neonatal hematopoietic stem and progenitor cells." Experimental Hematology 101-102: 25-33.

Liang, Y., et al. (2021). "Fully Automated Sample Processing and Analysis Workflow for Low-Input Proteome Profiling." Anal Chem 93(3): 1658-1666.

Liu, M., et al. (2013). "Human long-term culture initiating cell assay." Methods Mol Biol 946: 241-256.

Liu, Y., et al. (2016). "On the Dependency of Cellular Protein Levels on mRNA Abundance." Cell 165(3): 535-550.

Lo Celso, C., et al. (2009). "Live-animal tracking of individual haematopoietic stem/progenitor cells in their niche." Nature 457(7225): 92-96.

Lo Celso, C. and D. T. Scadden (2011). "The haematopoietic stem cell niche at a glance." J Cell Sci 124(Pt 21): 3529-3535.

Lopez-Otin, C., et al. (2013). "The hallmarks of aging." Cell 153(6): 1194-1217.

Lu, R., et al. (2011). "Tracking single hematopoietic stem cells in vivo using high-throughput sequencing in conjunction with viral genetic barcoding." Nat Biotechnol 29(10): 928-933.

Ludin, A., et al. (2014). "Reactive oxygen species regulate hematopoietic stem cell self-renewal, migration and development, as well as their bone marrow microenvironment." Antioxid Redox Signal 21(11): 1605-1619.

Luinenburg, D. G., et al. (2021). "Persistent expression of microRNA-125a targets is required to induce murine hematopoietic stem cell repopulating activity." Exp Hematol 94: 47-59 e45.

Luo, Y., et al. (2018). "M1 and M2 macrophages differentially regulate hematopoietic stem cell self-renewal and ex vivo expansion." Blood Adv 2(8): 859-870.

Lv, Y., et al. (2024). "Small molecule drug discovery targeting the JAK-STAT pathway." Pharmacol Res 204: 107217.

Macaulay, I. C., et al. (2016). "Single-Cell RNA-Sequencing Reveals a Continuous Spectrum of Differentiation in Hematopoietic Cells." Cell Rep 14(4): 966-977.

Maiato, H., et al. (2003). "Human CLASP1 is an outer kinetochore component that regulates spindle microtubule dynamics." Cell 113(7): 891-904.

Malouf, C., et al. (2021). "miR-130b and miR-128a are essential lineage-specific codrivers of t(4;11) MLL-AF4 acute leukemia." Blood 138(21): 2066-2092.

Manesia, J. K., et al. (2015). "Highly proliferative primitive fetal liver hematopoietic stem cells are fueled by oxidative metabolic pathways." Stem Cell Res 15(3): 715-721.

Mansell, E., et al. (2021). "Mitochondrial Potentiation Ameliorates Age-Related Heterogeneity in Hematopoietic Stem Cell Function." Cell Stem Cell 28(2): 241-256 e246.

Mansson, R., et al. (2007). "Molecular evidence for hierarchical transcriptional lineage priming in fetal and adult stem cells and multipotent progenitors." Immunity 26(4): 407-419.

Mantel, C. R., et al. (2015). "Enhancing Hematopoietic Stem Cell Transplantation Efficacy by Mitigating Oxygen Shock." Cell 161(7): 1553-1565.

Manz, M. G., et al. (2001). "Dendritic cell potentials of early lymphoid and myeloid progenitors." Blood 97(11): 3333-3341.

Masuda, S., et al. (2013). "In vitro generation of platelets through direct conversion: first report in My Knowledge (iMK)." Cell Res 23(2): 176-178.

Mayani, H. (2016). "The regulation of hematopoietic stem cell populations." F1000Res 5.

McCulloch, E. A., et al. (1964). "Spleen-Colony Formation in Anemic Mice of Genotype Ww." Science 144(3620): 844-846.

McCulloch, E. A., et al. (1965). "The cellular basis of the genetically determined hemopoietic defect in anemic mice of genotype Sl-Sld." Blood 26(4): 399-410.

McGrath, K. E., et al. (2015). "Distinct Sources of Hematopoietic Progenitors Emerge before HSCs and Provide Functional Blood Cells in the Mammalian Embryo." Cell Rep 11(12): 1892-1904.

McKerrell, T., et al. (2015). "Leukemia-associated somatic mutations drive distinct patterns of age-related clonal hemopoiesis." Cell Rep 10(8): 1239-1245.

McKinney-Freeman, S., et al. (2012). "The transcriptional landscape of hematopoietic stem cell ontogeny." Cell Stem Cell 11(5): 701-714.

Mellman, I. and G. Warren (2000). "The road taken: past and future foundations of membrane traffic." Cell 100(1): 99-112.

Mejia-Ramirez, E. and M. C. Florian (2020). "Understanding intrinsic hematopoietic stem cell aging." Haematologica 105(1): 22-37.

Mendez-Ferrer, S., et al. (2010). "Mesenchymal and haematopoietic stem cells form a unique bone marrow niche." Nature 466(7308): 829-834.

Metayer, C., et al. (2016). "Childhood Leukemia: A Preventable Disease." Pediatrics 138(Suppl 1): S45-S55.

Metcalf, D. (2008). "Hematopoietic cytokines." Blood 111(2): 485-491.

Mercier, F. E., et al. (2016). "Single Targeted Exon Mutation Creates a True Congenic Mouse for Competitive Hematopoietic Stem Cell Transplantation: The C57BL/6-CD45.1(STEM) Mouse." Stem Cell Reports 6(6): 985-992.

Merlinsky, T. R., et al. (2019). "Unfolding the Role of Calreticulin in Myeloproliferative Neoplasm Pathogenesis." Clinical Cancer Research 25(10): 2956-2962.

Mikkola, H. K., et al. (2005). "Placenta as a site for hematopoietic stem cell development." Experimental Hematology 33(9): 1048-1054.

Miller, C. L. and C. J. Eaves (1997). "Expansion in vitro of adult murine hematopoietic stem cells with transplantable lympho-myeloid reconstituting ability." Proc Natl Acad Sci U S A 94(25): 13648-13653.

Mirshekar-Syahkal, B., et al. (2014). "Concise review: From greenhouse to garden: the changing soil of the hematopoietic stem cell microenvironment during development." Stem Cells 32(7): 1691-1700.

Mitchell, E., et al. (2022). "Clonal dynamics of haematopoiesis across the human lifespan." Nature 606(7913): 343-350.

Mochizuki-Kashio, M., et al. (2011). "Dependency on the polycomb gene Ezh2 distinguishes fetal from adult hematopoietic stem cells." Blood 118(25): 6553-6561.

Mohamad, S. F. and M. L. Capitano (2023). "Utilizing CyTOF to Examine Hematopoietic Stem and Progenitor Phenotype." Methods Mol Biol 2567: 113-126.

Mohrin, M., et al. (2015). "Stem cell aging. A mitochondrial UPR-mediated metabolic checkpoint regulates hematopoietic stem cell aging." Science 347(6228): 1374-1377.

Moignard, V., et al. (2013). "Characterization of transcriptional networks in blood stem and progenitor cells using high-throughput single-cell gene expression analysis." Nat Cell Biol 15(4): 363-372.

Moore, K. A., et al. (1997). "In vitro maintenance of highly purified, transplantable hematopoietic stem cells." Blood 89(12): 4337-4347.

Moran-Crusio, K., et al. (2011). "Tet2 loss leads to increased hematopoietic stem cell self-renewal and myeloid transformation." Cancer Cell 20(1): 11-24.

Morcos, M. N. F., et al. (2020). "Continuous mitotic activity of primitive hematopoietic stem cells in adult mice." J Exp Med 217(6).

Morrison, S. J., et al. (1995). "The purification and characterization of fetal liver hematopoietic stem cells." Proc Natl Acad Sci U S A 92(22): 10302-10306.

Morrison, S. J. and D. T. Scadden (2014). "The bone marrow niche for haematopoietic stem cells." Nature 505(7483): 327-334.

Mohyeldin, A., et al. (2010). "Oxygen in stem cell biology: a critical component of the stem cell niche." Cell Stem Cell 7(2): 150-161.

Muller-Sieburg, C. E., et al. (1986). "Isolation of two early B lymphocyte progenitors from mouse marrow: a committed pre-pre-B cell and a clonogenic Thy-1-lo hematopoietic stem cell." Cell 44(4): 653-662.

Muller-Sieburg, C. E., et al. (2002). "Deterministic regulation of hematopoietic stem cell self-renewal and differentiation." Blood 100(4): 1302-1309.

Muller-Sieburg, C. E., et al. (2004). "Myeloid-biased hematopoietic stem cells have extensive self-renewal capacity but generate diminished lymphoid progeny with impaired IL-7 responsiveness." Blood 103(11): 4111-4118.

Multhoff, G., et al. (2011). "Chronic inflammation in cancer development." Front Immunol 2: 98.

Murphy, M. J., et al. (2005). "More than just proliferation: Myc function in stem cells." Trends Cell Biol 15(3): 128-137.

Myers, K. C., et al. (2020). "Clinical features and outcomes of patients with Shwachman-Diamond syndrome and myelodysplastic syndrome or acute myeloid leukaemia: a multicentre, retrospective, cohort study." Lancet Haematol 7(3): e238-e246.

Nakamura, Y., et al. (2010). "Isolation and characterization of endosteal niche cell populations that regulate hematopoietic stem cells." Blood 116(9): 1422-1432

Nakauchi, H., et al. (2001). "Quantitative assessment of the stem cell self-renewal capacity." Ann N Y Acad Sci 938: 18-24; discussion 24-15.

Nangalia, J. and A. R. Green (2017). "Myeloproliferative neoplasms: from origins to outcomes." Blood 130(23): 2475-2483.

Nemeth, M. J., et al. (2007). "Wnt5a inhibits canonical Wnt signaling in hematopoietic stem cells and enhances repopulation." Proc Natl Acad Sci U S A 104(39): 15436-15441.

Nestorowa, S., et al. (2016). "A single-cell resolution map of mouse hematopoietic stem and progenitor cell differentiation." Blood 128(8): e20-31.

Nilsson, S. K., et al. (2005). "Osteopontin, a key component of the hematopoietic stem cell niche and regulator of primitive hematopoietic progenitor cells." Blood 106(4): 1232-1239.

Nombela-Arrieta, C. and L. E. Silberstein (2014). "The science behind the hypoxic niche of hematopoietic stem and progenitors." Hematology Am Soc Hematol Educ Program 2014(1): 542-547.

Norddahl, G. L., et al. (2011). "Accumulating mitochondrial DNA mutations drive premature hematopoietic aging phenotypes distinct from physiological stem cell aging." Cell Stem Cell 8(5): 499-510.

North, T. E., et al. (2009). "Hematopoietic stem cell development is dependent on blood flow." Cell 137(4): 736-748.

Notta, F., et al. (2011). "Isolation of single human hematopoietic stem cells capable of long-term multilineage engraftment." Science 333(6039): 218-221.

Ogawa, M., et al. (1991). "Expression and function of c-kit in hemopoietic progenitor cells." J Exp Med 174(1): 63-71.

Ogawa, M., et al. (1997). "In vitro expansion of hematopoietic stem cells." Stem Cells 15 Suppl 1: 7-11; discussion 12.

Oguro, H., et al. (2013). "SLAM family markers resolve functionally distinct subpopulations of hematopoietic stem cells and multipotent progenitors." Cell Stem Cell 13(1): 102-116.

Ohta, H., et al. (2007). "Near-maximal expansions of hematopoietic stem cells in culture using NUP98-HOX fusions." Experimental Hematology 35(5): 817-830.

Okada, S., et al. (1992). "In vivo and in vitro stem cell function of c-kit- and Sca-1-positive murine hematopoietic cells." Blood 80(12): 3044-3050.

Okuda, T., et al. (1996). "AML1, the target of multiple chromosomal translocations in human leukemia, is essential for normal fetal liver hematopoiesis." Cell 84(2): 321-330.

Oliinyk, D., et al. (2024). "microPhos: a scalable and sensitive platform for high-dimensional phosphoproteomics." Mol Syst Biol 20(8): 972-995.

Oostendorp, R. A., et al. (2002). "Stromal cell lines from mouse aorta-gonads-mesonephros subregions are potent supporters of hematopoietic stem cell activity." Blood 99(4): 1183-1189.

Orecchioni, M., et al. (2017). "Single-cell mass cytometry and transcriptome profiling reveal the impact of graphene on human immune cells." Nat Commun 8(1): 1109.

Orkin, S. H. and L. I. Zon (2008). "Hematopoiesis: an evolving paradigm for stem cell biology." Cell 132(4): 631-644.

Osawa, M., et al. (1996). "Long-term lymphohematopoietic reconstitution by a single CD34-low/negative hematopoietic stem cell." Science 273(5272): 242-245.

Ottersbach, K., et al. (2010). "Ontogeny of haematopoiesis: recent advances and open questions." Br J Haematol 148(3): 343-355.

Ottersbach, K. and E. Dzierzak (2005). "The murine placenta contains hematopoietic stem cells within the vascular labyrinth region." Dev Cell 8(3): 377-387.

Parekh, C. and G. M. Crooks (2013). "Critical differences in hematopoiesis and lymphoid development between humans and mice." J Clin Immunol 33(4): 711-715.

Park, I. K., et al. (2003). "Bmi-1 is required for maintenance of adult self-renewing haematopoietic stem cells." Nature 423(6937): 302-305.

Paul, F., et al. (2015). "Transcriptional Heterogeneity and Lineage Commitment in Myeloid Progenitors." Cell 163(7): 1663-1677.

Pawliuk, R., et al. (1996). "Evidence of both ontogeny and transplant dose-regulated expansion of hematopoietic stem cells in vivo." Blood 88(8): 2852-2858.

Petit-Cocault, L., et al. (2007). "Dual role of Mpl receptor during the establishment of definitive hematopoiesis." Development 134(16): 3031-3040.

Petriv, O. I., et al. (2010). "Comprehensive microRNA expression profiling of the hematopoietic hierarchy." Proc Natl Acad Sci U S A 107(35): 15443-15448.

Pich, O., et al. (2022). "Discovering the drivers of clonal hematopoiesis." Nat Commun 13(1): 4267.

Pietras, E. M., et al. (2016). "Chronic interleukin-1 exposure drives haematopoietic stem cells towards precocious myeloid differentiation at the expense of self-renewal." Nat Cell Biol 18(6): 607-618.

Pimanda, J. E., et al. (2007). "Gata2, Fli1, and Scl form a recursively wired gene-regulatory circuit during early hematopoietic development." Proc Natl Acad Sci U S A 104(45): 17692-17697.

Pimkova, K., et al. (2022). "Quantitative analysis of redox proteome reveals oxidation-sensitive protein thiols acting in fundamental processes of developmental hematopoiesis." Redox Biol 53: 102343.

Pinho, S., et al. (2018). "Lineage-Biased Hematopoietic Stem Cells Are Regulated by Distinct Niches." Dev Cell 44(5): 634-641 e634.

Pinho, S. and P. S. Frenette (2019). "Haematopoietic stem cell activity and interactions with the niche." Nat Rev Mol Cell Biol 20(5): 303-320.

Ploemacher, R. E., et al. (1991). "Use of limiting-dilution type long-term marrow cultures in frequency analysis of marrow-repopulating and spleen colony-forming hematopoietic stem cells in the mouse." Blood 78(10): 2527-2533.

Pogozheva, I. D., et al. (2023). "Structural modeling of cytokine-receptor-JAK2 signaling complexes using AlphaFold Multimer." bioRxiv.

Popescu, D. M., et al. (2019). "Decoding human fetal liver haematopoiesis." Nature 574(7778): 365-371.

Pretini, V., et al. (2019). "Red Blood Cells: Chasing Interactions." Front Physiol 10: 945.

Psaila, B., et al. (2016). "Single-cell profiling of human megakaryocyte-erythroid progenitors identifies distinct megakaryocyte and erythroid differentiation pathways." Genome Biol **17**: 83.

Purton, L. E. and D. T. Scadden (2007). "Limiting factors in murine hematopoietic stem cell assays." Cell Stem Cell 1(3): 263-270.

Qian, H., et al. (2007). "Critical role of thrombopoietin in maintaining adult quiescent hematopoietic stem cells." Cell Stem Cell 1(6): 671-684.

Ramos, C. A., et al. (2006). "Evidence for diversity in transcriptional profiles of single hematopoietic stem cells." PLoS Genet 2(9): e159.

Raskov, H., et al. (2021). "Cytotoxic CD8(+) T cells in cancer and cancer immunotherapy." Br J Cancer 124(2): 359-367.

Remberger, M., et al. (2020). "The CD34(+) Cell Dose Matters in Hematopoietic Stem Cell Transplantation with Peripheral Blood Stem Cells from Sibling Donors." Clin Hematol Int 2(2): 74-81.

Reya, T., et al. (2003). "A role for Wnt signalling in self-renewal of haematopoietic stem cells." Nature 423(6938): 409-414.

Rhodes, K. E., et al. (2008). "The emergence of hematopoietic stem cells is initiated in the placental vasculature in the absence of circulation." Cell Stem Cell 2(3): 252-263.

Rix, B., et al. (2022). "Markers for human haematopoietic stem cells: The disconnect between an identification marker and its function." Front Physiol 13: 1009160.

Roch, A., et al. (2015). "Brief Report: Single-Cell Analysis Reveals Cell Division-Independent Emergence of Megakaryocytes From Phenotypic Hematopoietic Stem Cells." Stem Cells 33(10): 3152-3157.

Rodrigues, C. P., et al. (2020). "Epigenetic Regulators as the Gatekeepers of Hematopoiesis." Trends Genet.

Rossi, D. J., et al. (2005). "Cell intrinsic alterations underlie hematopoietic stem cell aging." Proc Natl Acad Sci U S A 102(26): 9194-9199.

Rossi, D. J., et al. (2007). "Deficiencies in DNA damage repair limit the function of haematopoietic stem cells with age." Nature 447(7145): 725-729.

Rowe, R. (2016a). "Developmental regulation of myeloerythroid progenitor function by the Lin28b-let-7-Hmga2 axis." The Journal of experimental medicine 213(8): 1497–1512.

Rowe, R. et al. (2016b). "Engineering Hematopoietic Stem Cells: Lessons from Development." Cell Stem Cell 18(6): 707-720.

Sacma, M., et al. (2019). "Haematopoietic stem cells in perisinusoidal niches are protected from ageing." Nat Cell Biol 21(11): 1309-1320.

Sagoo, P. and H. B. Gaspar (2023). "The transformative potential of HSC gene therapy as a genetic medicine." Gene Ther 30(3-4): 197-215.

Sakurai, M., et al. “Chemically defined cytokine-free expansion of human haematopoietic stem cells.” Nature 615, 127–133 (2023).

Sanjuan-Pla, A., et al. (2013). "Platelet-biased stem cells reside at the apex of the haematopoietic stem-cell hierarchy." Nature 502(7470): 232.

Saravia, J., et al. (2019). "Helper T cell differentiation." Cell Mol Immunol 16(7): 634-643.

Sarson-Lawrence, K. T. G., et al. (2024). "Cryo-EM structure of the extracellular domain of murine Thrombopoietin Receptor in complex with Thrombopoietin." Nat Commun 15(1): 1135.

Sauvageau, G., et al. (2004). "In vitro and in vivo expansion of hematopoietic stem cells." Oncogene 23(43): 7223-7232.

Schaub, F. X., et al. (2010). "Clonal analysis of TET2 and JAK2 mutations suggests that TET2 can be a late event in the progression of myeloproliferative neoplasms." Blood 115(10): 2003-2007.

Schiroli, G., et al. (2024). "Cell of origin epigenetic priming determines susceptibility to Tet2 mutation." Nat Commun 15(1): 4325.

Schofield, R. (1978). "The relationship between the spleen colony-forming cell and the haemopoietic stem cell." Blood Cells 4(1-2): 7-25.

Schulte, R., et al. (2015). "Index sorting resolves heterogeneous murine hematopoietic stem cell populations." Exp Hematol 43(9): 803-811.

Schutte, J., et al. (2016). "An experimentally validated network of nine haematopoietic transcription factors reveals mechanisms of cell state stability." Elife 5: e11469.

Seet, C. S., et al. (2017). "Generation of mature T cells from human hematopoietic stem and progenitor cells in artificial thymic organoids." Nat Methods 14(5): 521-530.

Seita, J., et al. (2007). "Lnk negatively regulates self-renewal of hematopoietic stem cells by modifying thrombopoietin-mediated signal transduction." Proc Natl Acad Sci U S A 104(7): 2349-2354.

Seita, J. & Weissman, I. L.(2010) “Hematopoietic stem cell: self-renewal versus differentiation.” Wiley Interdiscip. Rev. Syst. Biol. Med. 2, 640–53.

Sekulovic, S., et al. (2011). "Ontogeny stage-independent and high-level clonal expansion in vitro of mouse hematopoietic stem cells stimulated by an engineered NUP98-HOX fusion transcription factor." Blood 118(16): 4366-4376.

Sell, S. (2005). "Leukemia: stem cells, maturation arrest, and differentiation therapy." Stem Cell Rev 1(3): 197-205.

Shah, H., et al. (2021). "Behind the scenes with basophils: an emerging therapeutic target." Immunother Adv 1(1): ltab008.

Shah, M. T. V., et al. (2021). "Allogeneic stem cell transplant for patients with myeloproliferative neoplasms in blast phase: improving outcomes in the recent era." British Journal of Haematology 193(5): 1004-1008.

Sharma, S. and G. Gurudutta (2016). "Epigenetic Regulation of Hematopoietic Stem Cells." Int J Stem Cells 9(1): 36-43.

Shi, H., et al. (2021). "Bias in RNA-seq Library Preparation: Current Challenges and Solutions." Biomed Res Int 2021: 6647597.

Shin, J. Y., et al. (2014). "High c-Kit expression identifies hematopoietic stem cells with impaired self-renewal and megakaryocytic bias." J Exp Med 211(2): 217-231.

Shivdasani, R. A., et al. (1995). "Absence of blood formation in mice lacking the T-cell leukaemia oncoprotein tal-1/SCL." Nature 373(6513): 432-434.

Sieburg, H. B., et al. (2006). "The hematopoietic stem compartment consists of a limited number of discrete stem cell subsets." Blood 107(6): 2311-2316.

Sigurdsson, V., et al. (2016). "Bile Acids Protect Expanding Hematopoietic Stem Cells from Unfolded Protein Stress in Fetal Liver." Cell Stem Cell 18(4): 522-532.

Signer, R. A., et al. (2014). "Haematopoietic stem cells require a highly regulated protein synthesis rate." Nature 509(7498): 49-54.

Simon, L., et al. (2020). "High frequency of germline RUNX1 mutations in patients with RUNX1-mutated AML." Blood 135(21): 1882-1886.

Solar, G. P., et al. (1998). "Role of c-mpl in early hematopoiesis." Blood 92(1): 4-10.

Soyfer, E. M. and A. G. Fleischman (2023). "Myeloproliferative neoplasms - blurring the lines between cancer and chronic inflammatory disorder." Front Oncol 13: 1208089.

Spangrude, G. J., et al. (1988). "Purification and characterization of mouse hematopoietic stem cells." Science 241(4861): 58-62.

Spencer Chapman, M., et al. (2023). "Clonal selection of hematopoietic stem cells after gene therapy for sickle cell disease." Nat Med 29(12): 3175-3183.

Specht, H., et al. (2021). "Single-cell proteomic and transcriptomic analysis of macrophage heterogeneity using SCoPE2." Genome Biol 22(1): 50.

Sellar, R. S., et al. (2022). "Degradation of GSPT1 causes TP53-independent cell death in leukemia while sparing normal hematopoietic stem cells." J Clin Invest 132(16).

Stevens, A. M., et al. (2017). "Interleukin-6 levels predict event-free survival in pediatric AML and suggest a mechanism of chemotherapy resistance." Blood Adv 1(18): 1387-1397.

Stoddart, A., et al. (2016). "Retroviral insertional mutagenesis identifies the del(5q) genes, CXXC5, TIFAB and ETF1, as well as the Wnt pathway, as potential targets in del(5q) myeloid neoplasms." Haematologica 101(6): e232-236.

Suda, J., et al. (1984). "Analysis of differentiation of mouse hemopoietic stem cells in culture by sequential replating of paired progenitors." Blood 64(2): 393-399.

Suda, T., et al. (2011). "Metabolic regulation of hematopoietic stem cells in the hypoxic niche." Cell Stem Cell 9(4): 298-310.

Sudo, K., et al. (2000). "Age-associated characteristics of murine hematopoietic stem cells." J Exp Med 192(9): 1273-1280.

Sudo, K., et al. (2021). "Polyvinyl alcohol hydrolysis rate and molecular weight influence human and murine HSC activity ex vivo." Stem Cell Res 56: 102531.

Sun, D., et al. (2014). "Epigenomic profiling of young and aged HSCs reveals concerted changes during aging that reinforce self-renewal." Cell Stem Cell 14(5): 673-688.

Sutherland, H. J., et al. (1990). "Functional characterization of individual human hematopoietic stem cells cultured at limiting dilution on supportive marrow stromal layers." Proc Natl Acad Sci U S A 87(9): 3584-3588.

Tadokoro, Y., et al. (2018). "Spred1 Safeguards Hematopoietic Homeostasis against Diet-Induced Systemic Stress." Cell Stem Cell 22(5): 713-725 e718.

Takubo, K., et al. (2010). "Regulation of the HIF-1alpha level is essential for hematopoietic stem cells." Cell Stem Cell 7(3): 391-402.

Tefferi, A. and A. Pardanani (2015). "Myeloproliferative Neoplasms A Contemporary Review." Jama Oncology 1(1): 97-105.

Thomas, E. D., et al. (1957). "Intravenous infusion of bone marrow in patients receiving radiation and chemotherapy." N Engl J Med 257(11): 491-496.

Thomas, E. D., et al. (1959). "Supralethal whole body irradiation and isologous marrow transplantation in man." J Clin Invest 38(10 Pt 1-2): 1709-1716.

Tiercy, J. M. (2016). "How to select the best available related or unrelated donor of hematopoietic stem cells?" Haematologica 101(6): 680-687.

Till, J. E. and C. E. McCulloch (1961). "A direct measurement of the radiation sensitivity of normal mouse bone marrow cells." Radiat Res 14: 213-222.

Till, J. E., et al. (1964). "A Stochastic Model of Stem Cell Proliferation, Based on the Growth of Spleen Colony-Forming Cells." Proc Natl Acad Sci U S A 51(1): 29-36.

Tiwari, A., et al. (2013). "Ex vivo expansion of haematopoietic stem/progenitor cells from human umbilical cord blood on acellular scaffolds prepared from MS-5 stromal cell line." J Tissue Eng Regen Med 7(11): 871-883.

Tracey, L. J., et al. (2021). "CyTOF: An Emerging Technology for Single-Cell Proteomics in the Mouse." Curr Protoc 1(4): e118.

Triana, S., et al. (2021). "Single-cell proteo-genomic reference maps of the hematopoietic system enable the purification and massive profiling of precisely defined cell states." Nat Immunol 22(12): 1577-1589.

Tsutsumi, N., et al. (2023). "Structure of the thrombopoietin-MPL receptor complex is a blueprint for biasing hematopoiesis." Cell 186(19): 4189-4203 e4122.

Tucci, F., et al. (2022). "A systematic review and meta-analysis of gene therapy with hematopoietic stem and progenitor cells for monogenic disorders." Nat Commun 13(1): 1315.

van den Brink, M. R., et al. (2015). "Immune reconstitution following stem cell transplantation." Hematology Am Soc Hematol Educ Program 2015: 215-219.

Vanner, R., et al. (2023). "Somatic TET2 Mutations Prime the Immune System for Response to Immune Checkpoint Blockade." Blood 142(Supplement 1): 2689-2689.

Vannini, N., et al. (2016). "Specification of haematopoietic stem cell fate via modulation of mitochondrial activity." Nat Commun 7: 13125.

van Os, R., et al. (2004). "Stem cell assays: something old, something new, something borrowed." Stem Cells 22(7): 1181-1190.

van Wilgenburg, B., et al. (2013). "Efficient, long term production of monocyte-derived macrophages from human pluripotent stem cells under partly-defined and fully-defined conditions." PLoS One 8(8): e71098.

Van Zant, G., et al. (1990). "Genotype-restricted growth and aging patterns in hematopoietic stem cell populations of allophenic mice." J Exp Med 171(5): 1547-1565.

Vasilatou, D., et al. (2010). "The role of microRNAs in normal and malignant hematopoiesis." Eur J Haematol 84(1): 1-16.

Velten, L., et al. (2017). "Human haematopoietic stem cell lineage commitment is a continuous process." Nat Cell Biol 19(4): 271-281.

Vivier, E., et al. (2011). "Innate or adaptive immunity? The example of natural killer cells." Science 331(6013): 44-49.

von Zastrow, M. and A. Sorkin (2021). "Mechanisms for Regulating and Organizing Receptor Signaling by Endocytosis." Annu Rev Biochem 90: 709-737.

Vorobjeva, N. V. and B. V. Chernyak (2020). "NETosis: Molecular Mechanisms, Role in Physiology and Pathology." Biochemistry (Mosc) 85(10): 1178-1190.

Wallace, L. and E. A. Obeng (2023). "Noncoding rules of survival: epigenetic regulation of normal and malignant hematopoiesis." Front Mol Biosci 10: 1273046.

Walter, D. *et al.* Exit from dormancy provokes DNA-damage-induced attrition in haematopoietic stem cells. *Nature* 520, 549–552 (2015).

Wang, H., et al. (2024). "Clonal hematopoiesis driven by mutated DNMT3A promotes inflammatory bone loss." Cell.

Wang, L. D., et al. (2016). "Phosphoproteomic profiling of mouse primary HSPCs reveals new regulators of HSPC mobilization." Blood 128(11): 1465-1474.

Wang, S., et al. (2019). "Enhancement of LIN28B-induced hematopoietic reprogramming by IGF2BP3." Genes Dev 33(15-16): 1048-1068.

Whitesides, G. M. (2006). "The origins and the future of microfluidics." Nature 442(7101): 368-373.

Wilkinson, A. C., et al. (2019). "Long-term ex vivo haematopoietic-stem-cell expansion allows nonconditioned transplantation." Nature 571(7763): 117-121.

Wilkinson, A. C., et al. (2020). "Haematopoietic stem cell self-renewal in vivo and ex vivo." Nat Rev Genet 21(9): 541-554.

Wilkinson, A. C. and B. Gottgens (2013). "Transcriptional regulation of haematopoietic stem cells." Adv Exp Med Biol 786: 187-212.

Wilmes, S., et al. (2020). "Mechanism of homodimeric cytokine receptor activation and dysregulation by oncogenic mutations." Science 367(6478): 643-652.

Wilson, A., et al. (2004). "c-Myc controls the balance between hematopoietic stem cell self-renewal and differentiation." Genes Dev 18(22): 2747-2763.

Wilson, N. K., et al. (2010). "Gfi1 expression is controlled by five distinct regulatory regions spread over 100 kilobases, with Scl/Tal1, Gata2, PU.1, Erg, Meis1, and Runx1 acting as upstream regulators in early hematopoietic cells." Mol Cell Biol 30(15): 3853-3863.

Wilson, N. K., et al. (2011). "Transcriptional regulation of haematopoietic transcription factors." Stem Cell Res Ther 2(1): 6.

Wilson, N. K., et al. (2015). "Combined Single-Cell Functional and Gene Expression Analysis Resolves Heterogeneity within Stem Cell Populations." Cell Stem Cell 16(6): 712-724.

Winter, S., et al. (2024). "Clonal hematopoiesis and its impact on the aging osteo-hematopoietic niche." Leukemia 38(5): 936-946.

Wojtowicz, E. E., et al. (2016). "Ectopic miR-125a Expression Induces Long-Term Repopulating Stem Cell Capacity in Mouse and Human Hematopoietic Progenitors." Cell Stem Cell 19(3): 383-396.

Wong, N. K., et al. (2018). "Long non-coding RNAs in hematological malignancies: translating basic techniques into diagnostic and therapeutic strategies." J Hematol Oncol 11(1): 131.

Woolthuis, C. M. and C. Y. Park (2016). "Hematopoietic stem/progenitor cell commitment to the megakaryocyte lineage." Blood 127(10): 1242-1248.

Xie, M., et al. (2014). "Age-related mutations associated with clonal hematopoietic expansion and malignancies." Nat Med 20(12): 1472-1478.

Xie, S. Z., et al. (2019). "Sphingolipid Modulation Activates Proteostasis Programs to Govern Human Hematopoietic Stem Cell Self-Renewal." Cell Stem Cell 25(5): 639-653 e637.

Xu, C., et al. (2018). "Stem cell factor is selectively secreted by arterial endothelial cells in bone marrow." Nat Commun **9**(1): 2449.

Xu, M. J., et al. (1998). "Stimulation of mouse and human primitive hematopoiesis by murine embryonic aorta-gonad-mesonephros-derived stromal cell lines." Blood 92(6): 2032-2040.

Yamamoto, R., et al. (2013). "Clonal analysis unveils self-renewing lineage-restricted progenitors generated directly from hematopoietic stem cells." Cell 154(5): 1112-1126.

Yamamoto, R., et al. (2018a). "Changing concepts in hematopoietic stem cells." Science 362(6417): 895-896.

Yamamoto, R., et al. (2018b). "Large-Scale Clonal Analysis Resolves Aging of the Mouse Hematopoietic Stem Cell Compartment." Cell Stem Cell 22(4): 600-607 e604.

Yamazaki, K. and T. D. Allen (1990). "Ultrastructural morphometric study of efferent nerve terminals on murine bone marrow stromal cells, and the recognition of a novel anatomical unit: the "neuro-reticular complex"." Am J Anat 187(3): 261-276.

Yamazaki, S., et al. (2006). "Cytokine signals modulated via lipid rafts mimic niche signals and induce hibernation in hematopoietic stem cells." EMBO J 25(15): 3515-3523.

Yamazaki, S. and H. Nakauchi (2014). "Bone marrow Schwann cells induce hematopoietic stem cell hibernation." Int J Hematol b(6): 695-698.

Yan, X. J., et al. (2011). "Identification of outcome-correlated cytokine clusters in chronic lymphocytic leukemia." Blood 118(19): 5201-5210.

Yang, Y., et al. (2016). "Integrated Biophysical and Biochemical Signals Augment Megakaryopoiesis and Thrombopoiesis in a Three-Dimensional Rotary Culture System." Stem Cells Transl Med 5(2): 175-185.

Ye, M., et al. (2013). "C/EBPa controls acquisition and maintenance of adult haematopoietic stem cell quiescence." Nat Cell Biol 15(4): 385-394.

Yoshiji, H., et al. (2023). "Safety and effectiveness of lusutrombopag in patients who have chronic liver disease with thrombocytopenia and undergoing invasive procedures: Real-world post-marketing surveillance in Japan." Hepatol Res 53(11): 1105-1116.

Yousefi, M., et al. (2017). "Hierarchy and Plasticity in the Intestinal Stem Cell Compartment." Trends Cell Biol 27(10): 753-764.

Yu, V. W. C., et al. (2017). "Epigenetic Memory Underlies Cell-Autonomous Heterogeneous Behavior of Hematopoietic Stem Cells." Cell 168(5): 944-945.

Yu, W. M., et al. (2013). "Metabolic regulation by the mitochondrial phosphatase PTPMT1 is required for hematopoietic stem cell differentiation." Cell Stem Cell 12(1): 62-74.

Yuan, Y., et al. (2004). "In vivo self-renewing divisions of haematopoietic stem cells are increased in the absence of the early G1-phase inhibitor, p18INK4C." Nat Cell Biol 6(5): 436-442.

Zanna, M. Y., et al. (2021). "Review of Dendritic Cells, Their Role in Clinical Immunology, and Distribution in Various Animal Species." Int J Mol Sci 22(15).

Zaro, B. W., et al. (2020). "Proteomic analysis of young and old mouse hematopoietic stem cells and their progenitors reveals post-transcriptional regulation in stem cells." Elife 9.

Zink, F., et al. (2017). "Clonal hematopoiesis, with and without candidate driver mutations, is common in the elderly." Blood 130(6): 742-752.

Zhang, C. C. and H. A. Sadek (2014). "Hypoxia and metabolic properties of hematopoietic stem cells." Antioxid Redox Signal 20(12): 1891-1901.

Zhang, C. C. and H. F. Lodish (2005). "Murine hematopoietic stem cells change their surface phenotype during ex vivo expansion." Blood 105(11): 4314-4320.

Zhang, S. and S. Pinho (2023). "Untangling the role of KIT ligand in HSC regulation." Blood 142(19): 1581-1582.

Zhu, Y., et al. (2018). "Nanodroplet processing platform for deep and quantitative proteome profiling of 10-100 mammalian cells." Nat Commun 9(1): 882.

Zohren, F., et al. (2012). "The transcription factor Lyl-1 regulates lymphoid specification and the maintenance of early T lineage progenitors." Nat Immunol 13(8): 761-769.